Exponential Asymptotics & Free-Surface Flows

PHILIPPE H. TRINH
Balliol College
Oxford

A thesis submitted for the degree of
Doctor of Philosophy
July 2010

ABSTRACT

When traditional linearised theory is used to study free-surface flows past a surface-piercing object or over an obstruction in a stream, the geometry of the object is usually lost, having been assumed small in one or several of its dimensions. In order to preserve the nonlinear nature of the geometry, asymptotic expansions in the low-Froude or low-Bond limits can be derived, but here, the solution invariably predicts a waveless free-surface at every order. This is because the waves are in fact, exponentially small, and thus *beyond-all-orders* of regular asymptotics; their formation is a consequence of the divergence of the asymptotic series and the associated Stokes Phenomenon.

In this thesis, we will apply exponential asymptotics to the study of two new problems involving nonlinear geometries. In the first, we examine the case of free-surface flow over a step including the effects of both gravity and surface tension. Here, we shall see that the availability of multiple singularities in the geometry, coupled with the interplay of gravitational and cohesive effects, leads to the discovery of a remarkable new set of solutions.

In the second problem, we study the waves produced by bluff-bodied ships in low-Froude flows. We will derive the analytical form of the exponentially small waves for a wide range of hull geometries, including single-cornered and multi-cornered ships, and then provide comparisons with numerical computations. A particularly significant result is our confirmation of the thirty-year old conjecture by Vanden-Broeck & Tuck (1977) regarding the impossibility of waveless single-cornered ships.

ACKNOWLEDGEMENTS

"The student of mathematics", Ernst Mach† once described, "often finds it hard to throw off the uncomfortable feeling that his science, in the person of his pencil, far surpasses him in intelligence". "In a great measure," he continued, "it is really the intelligence of other people that confronts us…"

In writing this thesis, from day to day, I found myself wrestling with this very feeling of diffidence and humility. The theory of asymptotic approximations and divergent series had been previously laid brick-by-brick by the greats of generations past—from Leonhard Euler and Pierre-Simon Laplace, to George Gabriel Stokes and Henri Poincaré; these intellectual giants, I confronted within the confines of dusty textbooks and ancient articles. They were, however, somehow never as *tangible* as the modern giants from which I constantly drew inspiration and guidance. And so to this distinguished list, I am compelled to add the following names:

Professor Jonathan Chapman, my supervisor, who is to me, unparallel in both mathematical ability and insight.

> *Jon*: Despite our many tussles on the rules and regulations of colons and capitalisation, exclamation marks(!) and literary theatrics, I recognise that coming to work with you at Oxford has, and will always have, a profound effect on my future. I hope that we will continue to argue about such trivialities in the many years to come, and that you will continue to inspire and guide me.

Professors Sam Howison and Michael Ward, two great mathematical pillars who, on July 23 2010, stood side-by-sude, ever so tall and ever so imposing, as my internal and external thesis examiners (respectively).

> *Sam & Michael*: This thesis is shaped by your collective wisdom and insight; I'm grateful you were both there to mark the end of my schooling and the beginning of my career.

And finally, Professor Jean-Marc Vanden-Broeck, whose immeasurable expertise on the topic of free-surface flows became a wonderful source of information as I navigated the pitfalls of research.

> *Jean-Marc*: I vividly remember sitting in your office foe nearly six hours once, hearing you speak about the great *zoo* of solutions which can be found in the gravity-capillary problem (*c.f.* Figure 1.1 on p. 5). Every facet of this thesis is coloured, in some way or another, by your pioneering work.

† Popular Scientific Lectures (Chicago, 1920), p. 196

SHORT CONTENTS

CONTENTS

PREFACE

> *The construction and acceptance of the theory of divergent series is another striking example of the way in which mathematics has grown…it demonstrates how far mathematicians have come to recognize that mathematics is man-made. The definitions of summability are not the natural notion of continually adding more and more terms...they are artificial.*
>
> —MORRIS KLINE, (1972)

Today, some of the most exciting scientific advances are made at the boundaries between fundamentally different theories of the universe—from classical mechanics to quantum mechanics, geometrical optics to wave optics, viscous flow to inviscid flow, and so on. The difficulty, however, is that the transition from one physical theory to the next occurs in a *singular* limit; as such, we must take great care in recognising the subtle and unexpected effects that often occurs in their study. This thesis, broadly speaking, is about these very effects.

Now as mathematicians, we know that the study of such singular problems typically leads to the solution, S, being represented as an asymptotic expansion,

$$S = \sum_{n=0}^{\infty} \epsilon^n S_n,$$

which depends on the limit of the small parameter, ϵ, tending to zero. But the limit that ϵ *tends* to zero differs qualitatively from when ϵ is *equal* to zero, and difficulties arise; the series S is divergent and consequently, by the Stokes Phenomenon, exponentially small terms can suddenly appear or disappear as the series is continued past critical lines in the complex plane. The resolution of the original problem often hinges on the effects of these tiny terms, but because such *beyond-all-orders* features are invisible to a traditional ϵ-power series, special techniques called *exponential asymptotics* (or asymptotics beyond-all-orders) must be used for their detection.

For those of you who have yet to encounter these cryptic properties of asymptotics, then the above paragraph likely resembles *hocus-pocus* rather than rigorous mathematics! The truth is, the use of divergent expansions did indeed spark one of the great controversies of mathematics, and the concept has painstakingly traversed the great rungs of public opinion, from sour dissension (Niels Abel famously wrote that "divergent series are the invention of the devil, and it is shameful to base on them any demonstration whatsoever") to acknowledgment and acceptance. Today, the use of divergent expansions is widespread in the applied sciences, and moreover, exponential asymptotics has emerged as a field of its own, a direct consequence of parallel developments in no less than nine interrelated fields of mathematics, physics, and engineering (Boyd, 1999).

Although the birth of these beyond-all-orders techniques may be attributed to the early investigations of Stieltjes (1886) and Stokes (1902), it was not until later applications to physically relevant problems that the theory flourished; some of these inspirational problems include Kruskal and Segur's (1991) work on the crystal growth problem, work on the viscous fingering problem in Hele-Shaw cells (*e.g.* in Combescot et al. 1986, 1988; Chapman 1999), and work on the exponentially-small waves of the fifth-order Korteweg-de Vries equation (*e.g.* in Combescot et al. 1988; Grimshaw & Joshi 1995). This thesis, however, is most directly motivated by the methods pioneered by Chapman and Vanden-Broeck (2002; 2006) for applying exponential asymptotics to the study of low-speed water waves disturbed by an obstruction.

The material in this thesis naturally splits between two problems, one about gravity-capillary theory, and the other about waveless ships. Because of the sharp distinction, every effort has been made to structure the thesis so as to allow selective reading; effectively, you may choose to begin your journey with the gravity-capillary waves of Chapter 1, or instead, you may join me in search of the fabled waveless ships of Chapter 3. The techniques that underly each work, as well as the relevant literature, are introduced separately and independently at the beginning of each of these chapters, and final remarks are made in Chapter 5.

Whichever path you choose, I dare say that together, we shall see some truly marvellous things in the world that lies *beyond-all-orders*. The study of exponential asymptotics will bring us from the real world, through the imaginary plane of existence, and back to the real; it will show us how divergent expansions—nonsensical in the conventional sense—can be refined for further information; it will reveal waves where there were none; and it will allow us to stare, unwavering and unafraid, into the abyss of the infinity, and to emerge with new insights. The problems and work that lies herein has served to enchant my mind and spirit over the last few years. I can only hope that it will do the same for you.

Theoretical predictions *of* new gravity-capillary waves

PART I: LINEAR THEORY

I

We begin this thesis with a very simple example which nevertheless illustrates the sombre gravitas surrounding the theory of water waves: consider the well-known problem of progressive free-surface waves that propagate without change of form. In the case of gravity waves, it was the classic work of Stokes (1847b; 1880) that first postulated the existence of periodic waves and presented a perturbation procedure for their computation. The great question of convergence of these series solutions had been more-or-less answered by Nekrasov (1921), Levi-Civita (1925), and Krasovskii (1960), and moreover, their unfortunate instabilities later discovered by Lighthill (1965), Benjamin (1967), Benjamin & Feir (1967), and Whitham (1967). Although open questions about Stokes waves still remain (Toland, 1996), we generally have a firm foothold for the theory. Even better, the equivalent problem for pure capillary waves in deep water was completely resolved by Crapper (1957), who produced an exact closed-form solution in terms of elementary functions. This was followed by the solutions for the finite-depth case by Kinnersley (1976), and so the pure capillary problem is also sufficiently well resolved.

This leaves the combined theory of gravity-capillary waves where unfortunately, Stokes' series expansions are no longer sufficient. For a taste of the formidable nature of the problem, the reader need only refer to the work of Schwartz & Vanden-Broeck (1979), which contains a systematic attempt to analyse numerical solutions of the nonlinear problem. From the combined results of about 400 numerical solutions, Schwartz and Vanden-Broeck demonstrated that the entirety of classes of possible solutions to the gravity-capillary problem is a remarkably complicated affair; there are certainly an infinite number of families, but the particular details of each one, as well as the unknown possibilities of others remains a mystery to this day.

Perhaps, then, the lesson we shall retain as we go on to explore the theory of gravity-capillary waves is the following: adding even a small amount of surface tension to an otherwise innocuous gravity wave can have an inherently nonlinear effect on the solutions. *Caveat viator!*

1.1 INTRODUCTION

Our interest in the gravity-capillary problem lies not with the case of freely propagating waves elucidated in the previous section, but rather with the more complicated scenario of gravity-capillary waves *induced* by interactions with objects in a stream. Here, the first significant theory was proposed by Lord Rayleigh (1883), whose chief source of inspiration had been the earlier experiments of Scott Russell (1844) and Thomson (1871). As Lord Rayleigh (1883) himself explains:

> *When a small obstacle, such as a fishing line, is [...] held stationary in moving water, the surface is covered with a beautiful wave-*

> *pattern, fixed relatively to the obstacle. On the up-stream side the wavelength is short, and, as Thomson has shown, the force governing the vibrations is principally cohesion. On the down-stream side the waves are longer, and are governed principally by gravity.*

Rayleigh supposed that the fluid could be assumed to be two-dimensional, inviscid, incompressible, and irrotational, and that the effects of the fishing line could be approximated by the application of a small pressure distribution to a single point on the free-surface (as might be produced by a small jet of air). Then, by linearising for small-amplitude waves and for a weakly-applied pressure distribution, the method of Fourier Transforms produces an approximation of the upstream capillary waves and downstream gravity waves. As Rayleigh remarked, the theory is particularly successful in predicting that those particular wave patterns can only exist when the speed of the stream is somewhat faster than 23 centimetres per second, a restriction that had been suggested by the experiments of Thomson.

Since Lord Rayleigh's seminal work, however, mathematical analyses of the general gravity-capillary problem have led to the realisation that, while the study of gravity-only or capillary-only flows are themselves rich in difficulties, the combination of both effects presents a much more formidable challenge. Following Rayleigh's work, Harrison (1909), Wilton (1915), and Kamesvara Rav (1920) each published approximate (but limited) solutions to the problem of symmetrical two-dimensional periodic waves moving without change of form in deep liquid. Afterwards, progress in the theory of gravity-capillary waves appears to have been largely stagnant, at least until the latter half of the twentieth century when an explosion of experimental, numerical, and theoretical findings appears in the literature.

For the theory of finite-depth gravity-capillary waves, the Froude number F, representing the ratio between inertial and gravitational forces, and the Bond number B, representing the ratio between gravitational and surface tension forces, are the two crucial parameters in the problem. In Figure 1.1, we have illustrated a few of the different kinds of solutions that might be expected when studying even the simplest problems incorporating both effects. Generally, we can expect qualitatively similar types of behaviours even for differently-arranged flows (finite or infinite depth, perturbed by a submerged object or a pressure distribution, *etc.*), so we will continue to refer to Figure 1.1, even for the case of Rayleigh's solution (for example), which is technically only applicable for infinite-depth flows.

The figure contains several key regions of interest, regions that are primarily separated by the critical dispersion curve $F = F_m$, the line $B = 1/3$, and the line $F = 1$ dividing subcritical and supercritical flows; we will address these bifurcations later in the text, and they are also described in Appendix 1.A. For the moment, let us note that if we begin with Rayleigh's original applied-pressure problem, then solutions like the one in (d) may appear, but only in the region below $F = F_m$. In addition to Rayleigh's work, Forbes (1983) and Grandison & Vanden-Broeck (2006) have also studied this problem of capillary-upstream, gravity-downstream waves, but for flows

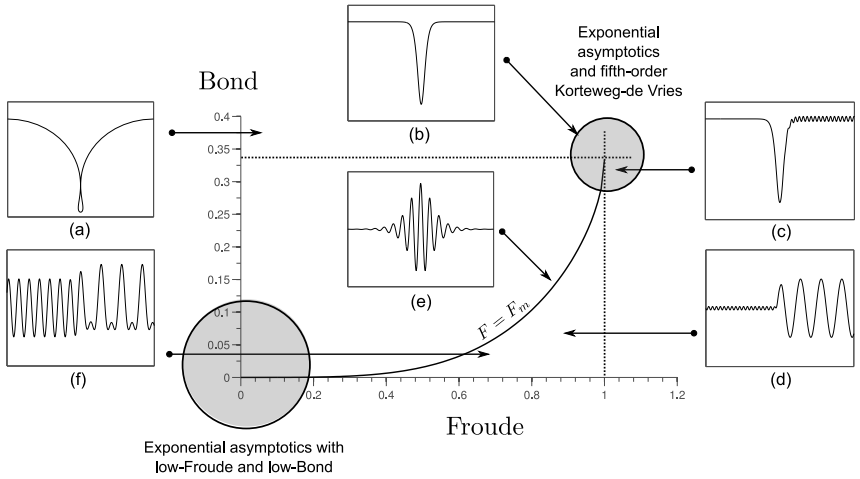

Figure 1.1: Many types of gravity-capillary waves can be found when studying steady finite-depth flows, perhaps over a localised bump or over a pressure distribution placed near the surface. Possible solutions include profiles with (a) trapped bubbles, (b) solitary waves, (c) generalised solitary waves, (d) capillary waves upstream and gravity waves downstream, (e) localised wavepackets, and (f) Wilton ripples. The circled region in the lower-left, corresponding to low-Froude and low-Bond flows has been largely ignored and we aim to study this asymptotic limit.

over a semi-circular obstruction. The latter two studies solve the full nonlinear equations numerically, but the requirement of imposing an *a priori* unknown radiation condition far upstream still represents a serious numerical difficulty. Within the region below the dispersion curve, it is also possible to find solutions (f) exhibiting the so-called *Wilton Ripples* phenomenon (Wilton, 1915), the result of resonant interactions when a capillary and gravity wave have commensurate phase speeds. Indeed, solutions with these secondary ripples have been computed numerically for the waves generated by a moving pressure distribution (Vanden-Broeck, 2002), and have also been seen in nature (Schooley, 1960).

If the Froude number is instead held fixed, and the Bond number is increased, then as we approach the critical dispersion curve, the solution set bifurcates. In particular, Rayleigh's result is singular as this curve is approached, and the system may bifurcate into one of many possible solutions in the form of envelope solitary waves (e), where an appropriate model is the forced Nonlinear Schrödinger Equation. If the Bond number is increased further and past $B = 1/3$, then the solutions take the form of classical solitary waves (b) and can then be approximated by a forced Korteweg-de Vries Equation. Within all these regions, there is occasionally the possibility of non-uniqueness, and a single point in (F, B) space often does correspond to multiple solutions, for which only one represents a perturbation from the uniform flow; for example, solutions can exhibit trapped bubbles (a), representing a perturbation from Crapper's (1957) exact solution of the unforced pure-capillary problem. These issues have been investigated for the case of flow induced by an applied pressure distribution by many authors, including Vanden-Broeck & Dias (1992), Dias & Vanden-Broeck (1993), Dias et al. (1996), and Maleewong et al. (2005a,b).

Finally, the historically controversial region just to the right of the line $F = 1$ exists as a warning sign to those who remain unaware of the importance of exponentially small terms in singular problems. The earliest numerical simulations of this region, computed from the full nonlinear equations, were performed by Hunter & Vanden-Broeck (1983). What they

discovered was that when the Bond number is greater than $1/3$, the solution ressembles the classical depression solitary wave of (b); but if the Bond number is instead less than $1/3$, the numerical solutions are bedeviled by small-scale oscillations near the tails (c). These dimpled solutions could not be explained at the time, and their significance was quickly glossed over.

However, in the years that followed, a series of papers by Hunter & Scheurle (1988), Pomeau et al. (1988), Beale (1991), and Sun (1991) established the notion of nonlocal (or generalised) solitary waves—essentially, a solitary wave coupled with exponentially small oscillations near the tails. Near the point $F = 1$, $B = 1/3$, the water waves are governed by the fifth-order Korteweg-de Vries Equation, for which recent standardised techniques in exponential asymptotics can be applied (Grimshaw, 2010; Trinh, 2010). The unique history and ultimately, the resolution of the fifth-order Korteweg-de Vries Equation is well documented and described in Boyd (1998).

What do we plan to accomplish?

There are two areas which still require much work: what is the nature of gravity-capillary waves over more general topographies that *cannot* be considered small (such as over a large step in a channel or past any full-bodied obstruction) and in particular, what analytical and numerical work can be done in the regime where the Froude and Bond numbers tend to zero.

The crucial idea is that in the zero-Froude and zero-Bond solution, the free-surface is replaced by a rigid wall, with the full geometry of the obstruction preserved in the solution. Thus, asymptotic approximations for low-Froude and low-Bond numbers allows us to directly relate the generation of waves to the shape of the obstruction. This is in marked contrast to more traditional linear approximations which depend on an asymptotic limit of small obstructions.

The difficulty in the low-Froude, low-Bond approximations, however, is that each of them represents a singular limit. At ever-decreasing Froude and Bond numbers, we would still expect waves to appear on the free-surface, but it is easy to check that the approximation at every single order in the asymptotic hierarchy yields a waveless solution. The waves are, in fact, exponentially small and thus *beyond-all-orders* of traditional asymptotics.

In this chapter, we will study the problem of flow over a rectangular step, but rather than performing the full low-Froude, low-Bond analysis for $\mathcal{O}(1)$ geometries, we first linearise for asymptotically small steps. With this assumption, the analysis can proceed in two equivalent ways. We may first regard the Froude and Bond numbers as fixed and $\mathcal{O}(1)$, and solve using Fourier Transforms, after which we take $F, B \to 0$. Alternatively, we may take $F, B \to 0$ immediately after the initial linearisation, and then make use of our methods in exponential asymptotics.

Our goals are twofold. First, we wish to compare and contrast the method of Fourier transforms with the method of exponential asymptotics. Do concepts like the Stokes Phenomenon and optimal truncation become

more transparent using one approach over the other? Second, we wish to show how exponential asymptotics can be applied to the simpler linearised equations of the small-step problem. In the chapters to follow, we will work with the full nonlinear equations; this first excursion, then, provides a smooth transition to the more advanced techniques that underly the subsequent work.

1.2 ILLUSTRATION OF THE GENERAL METHODOLOGY

We shall begin with a simple explanation of the Stokes Phenomenon using the complex Airy function, as given by the integral

$$\mathrm{Ai}(z) = \frac{1}{2\pi i}\int_C e^{f(w)}\,dw, \tag{1.1}$$

with

$$f(w) = -\frac{w^3}{3} + zw, \tag{1.2}$$

where $z \in \mathbb{C}$ and C is a contour which tends from $\infty e^{5\pi i/3}$ to $\infty e^{2\pi i/3}$. The standard technique of approximation is to deform C along paths of steepest *descent*; then in the limit that $|z| \to \infty$, the dominant contribution of $\mathrm{Ai}(z)$ must comes from the critical points of $f(w)$ (Bender & Orszag, 1978). Since these saddle points are given by $w_0 = \pm\sqrt{z}$, the lines of steepest descent are then prescribed by

$$\Im[f(w)] = \Im[f(w_0)] \quad \text{and} \quad \Re[f(w)] \leq \Re[f(w_0)]\,. \tag{1.3}$$

We assume that any branch cuts involved will be along the positive real axis, and first begin approximating (1.1) with $\theta \equiv \mathrm{Arg}(z) = 0$. As illustrated in Figure 1.2a, C should be chosen to pass through the saddle point at $w_0 = -z$; a standard computation shows that the contribution from this point is

$$\mathrm{Ai}(z) \sim \mathcal{A}e^{-\frac{2}{3}z^{3/2}}, \quad \text{with} \quad \mathcal{A} = \left[\frac{1}{2z^{1/4}\sqrt{\pi}}\right]. \tag{1.4}$$

As we analytically continue z, note that for $\theta \in [0, 2\pi/3)$, the topology of the integration contour remains the same, and so (1.4) continues to hold throughout. However at $\theta = 2\pi/3$, the descending contour from $-|z|e^{i\theta/2}$ passes *through* the other saddle point at $|z|e^{i\theta/2}$, shown in Figure 1.2c. Thus, immediately thereafter, the approximation must include an exponentially small contribution, and we can write this transition as

$$\mathcal{A}e^{-\frac{2}{3}z^{3/2}} \xrightarrow{\theta=2\pi/3} \mathcal{A}e^{-\frac{2}{3}z^{3/2}} + i\mathcal{A}e^{\frac{2}{3}z^{3/2}}. \tag{1.5}$$

The cycle repeats. At $\theta = \pi$, shown in Figure 1.2d, the previously subdominant contribution becomes the same size as the original term; it continues increasing in size until reaching peak dominance at $\theta = 4\pi/3$, where Figure 1.2e indicates the switching-off of the term in (1.4).

The *Stokes Phenomenon* is the name given to this sudden appearance or disappearance of exponentially small terms as an asymptotic expansion varies

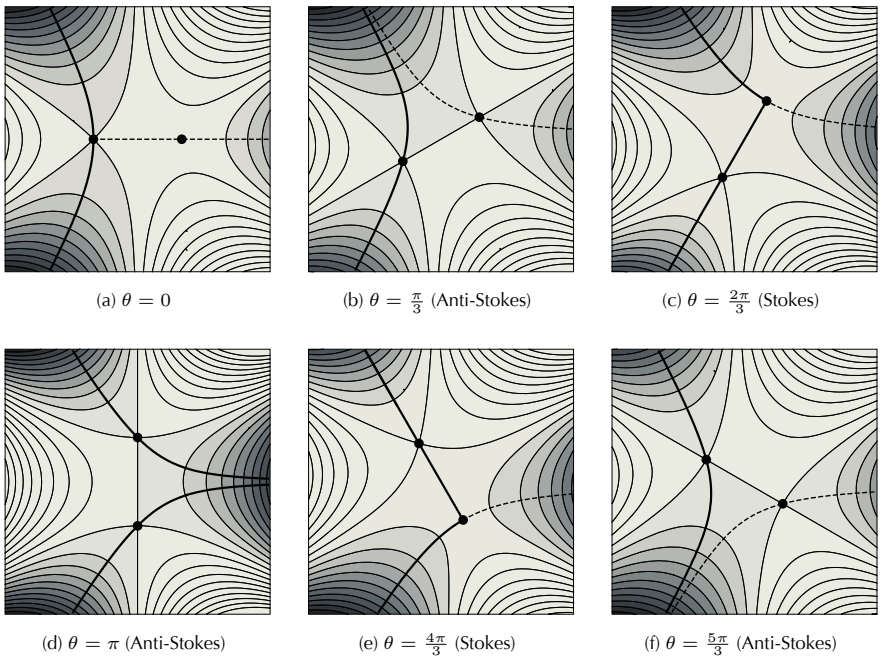

(a) $\theta = 0$ (b) $\theta = \frac{\pi}{3}$ (Anti-Stokes) (c) $\theta = \frac{2\pi}{3}$ (Stokes)

(d) $\theta = \pi$ (Anti-Stokes) (e) $\theta = \frac{4\pi}{3}$ (Stokes) (f) $\theta = \frac{5\pi}{3}$ (Anti-Stokes)

Figure 1.2: These figures illustrate the right contours to use when applying the method of steepest descents to the integral (1.1). The contour should begin at $\infty e^{5\pi i/3}$ and end at $\infty e^{2\pi i/3}$. The saddle points are marked as nodes, and the thin lines are constant contours of $\Re[f(w) - f(-z)]$, with dark regions corresponding to valleys. The thick solid line(s) indicate the correct contours to follow. Dashed line(s) also indicate steep paths from the saddles that are ultimately unused. There are Stokes lines at $\theta = 0, 2\pi/3, 4\pi/3$ and the Anti-Stokes lines at $\theta = \pi/3, \pi, 5\pi/3$. The branch cut is along $\theta = 0$.

in the complex plane. It occurs at *Stokes lines*, in this case, $\theta = 2\pi/3$ and $4\pi/3$, where one saddle point reaches peak dominance with respect to another; and this stands in contrast to *Anti-Stokes lines*, here, $\theta = \pi/3$ and $5\pi/3$, where both contributions are of the same order. This counter-intuitive phenomenon occupied Stokes (1847a, 1864) at various points throughout his life (and most memorably, he described the transition as causing the inferior term to emerge *"as it were into a mist"*). For him, it was a great mystery how the Airy function could suddenly change from oscillatory to exponential behaviour upon moving from the negative to the positive along the real axis, but this, we have easily explained using our powerful techniques of steepest descents.

A much more challenging task—and certainly one which better illustrates the *"aroma of paradox and audacity"* surrounding the Stokes Phenomenon (Hardy, 1949)—is to retrieve the same result, this time without using the integral representation of (1.1). Indeed, most physically relevant problems begin with a differential equation, so we could imagine beginning instead with the Airy Equation:

$$\frac{d^2y}{dz^2} = zy, \tag{1.6}$$

for which $\mathrm{Ai}(z)$ is one of two linearly independent solutions. In the limit that $|z| \to \infty$, a WKB approach allows a derivation of the two expansions,

$$y_1 \sim \mathcal{A}e^{-\frac{2}{3}z^{3/2}} \sum_{n=0}^{\infty} (-1)^n a_n, \tag{1.7}$$

$$y_2 \sim \mathcal{A}e^{\frac{2}{3}z^{3/2}} \sum_{n=0}^{\infty} a_n, \tag{1.8}$$

with coefficients

$$a_n = \frac{1}{(36z^{3/2})^n}\,\frac{\Gamma(3n+\frac{1}{2})}{n!\Gamma(n+\frac{1}{2})}, \tag{1.9}$$

and now, without an interpretation in terms of integration contours, we are left to wonder how the Stokes Phenomenon can possibly be predicted from the expressions in (1.7)–(1.9).

The key to resolving this problem, and indeed the entire foundation of exponential asymptotics, rests upon our understanding of aymptotic divergence—its causes and its consequences. We first take note that the leading-order behaviour of (1.4) contains a singularity at $z = 0$, despite the fact that any solution of (1.6) is an entire function. We have thus chosen a rather ill-behaved representation of a perfectly well-behaved solution, and so it is not surprising that we soon run into trouble. From the differential equation, we see that at each order, a_n, is determined by twice differentiating the previous order, a_{n-1}, so that as more and more terms are included, the effect of the singularity grows. As $n \to \infty$, the late terms of (1.9) must diverge in the form of a factorial over power, with

$$a_n \sim \frac{\Gamma(n)}{2\pi(\frac{4}{3}z^{3/2})^n}. \tag{1.10}$$

For fixed z, the error of the asymptotic approximation decreases as more terms are included, but then upon reaching its minimum (the *optimal truncation point*), the error diverges to infinity. This is shown in Figure 1.3.

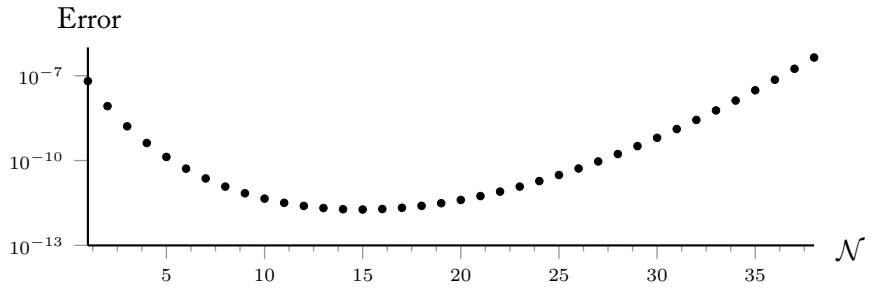

Figure 1.3: The error of the $\mathcal{N}^{\text{th}}$ partial sum of eqn (1.7) at $z = 5$. The *optimal truncation* point, where the error is the smallest (in fact, exponentially small), usually occurs at the point where subsequent terms of the series are of the same size. Here, it is at $\mathcal{N} = \lceil \frac{4}{3}|z|^{3/2} \rceil = 15$.

In fact, what we have just described is not only restricted to the Airy expansion, but is symptomatic of most singular approximations. Because the late terms of an expansion mainly depends on the generic influence of its nearest singularities, the form of the divergence obeys a beautiful universality. We have already demonstrated two of the implications, and a third, addressing the locations of the Stokes lines, is provided by Dingle (1973). Together, they form the three maxims of singular asymptotic expansions, and are listed in Table 1.1.

For example, in the case of the Airy expansions of (1.7)–(1.8), the third maxim implies that Stokes lines can be found at

$$\Im[\chi_1] = \Im[\chi_2] \quad \text{and} \quad \Re[-\chi_1] \geq \Re[-\chi_2], \tag{1.11}$$

where the exponential with argument $-\chi_1 = -\frac{2}{3}z^{3/2}$ switches on the exponential with argument $-\chi_2 = \frac{2}{3}z^{3/2}$. This condition then yields the

MAXIM	PROPERTY
1 · Divergence	The late terms of a singular asymptotic expansion diverge as a factorial over power expression (Darboux's Theorem).
2 · Truncation	Optimal truncation is at the point where subsequent terms in the series are approximately equal in size. Here, the error is exponentially small.
3 · Stokes lines	Stokes lines can be prescribed by: i) those locations where successive late terms of an asymptotic series are equal in phase, or ii) those locations for which the series (including its multipliers) attains peak exponential dominance over its associated function.

Table 1.1: The divergence of a typical singular asymptotic expansion only depends on the generic influence of its closest singularities, and therefore, most expansions will share these three universal properties. Throughout the thesis, we will often make use of these facts.

previously discovered Stokes line at $\theta = 2\pi/3$. The $\theta = 4\pi/3$ Stokes line is also given by the same condition (1.11), but with χ_1 and χ_2 switching roles. Dingle's condition, then, is akin to the steepest descent rules of (1.3), but establishes a general fact about series expansions, rather than integrals. Note that we often discuss asymptotic expansions in the limit of some small parameter, $\epsilon \to 0$; for the Airy equation (1.6), we could have equally introduced a new scaling, $Z = \epsilon^{2/3} z$, and studied the same problem for fixed Z and $\epsilon \to 0$.

In any case, once the three maxims of Table 1.1 have been used to characterise the behaviour of the asymptotic divergence and prescribe the locations of the Stokes lines, then the switching-on of the subdominant series (1.8) can be explicitly seen by examining the remainder when the dominant series (1.7) is optimally truncated. If we write

$$y(z) = \mathcal{A} e^{-\frac{2}{3}z^{3/2}} \sum_{n=0}^{\mathcal{N}-1} (-1)^n a_n + R_{\mathcal{N}}, \tag{1.12}$$

then, once substituted into eqn (1.6), this leaves an expression involving $R_{\mathcal{N}}$ and the remnant $n = \mathcal{N} - 1$ term of the series expansion:

$$\frac{d^2 R_{\mathcal{N}}}{dz^2} - z R_{\mathcal{N}} + \frac{d^2}{dz^2}\left[\mathcal{A} e^{-\frac{2}{3}z^{3/2}} (-1)^{\mathcal{N}-1} a_{\mathcal{N}-1}\right] = 0, \tag{1.13}$$

which can be alternatively written as

$$\frac{d^2 R_{\mathcal{N}}}{dz^2} - z R_{\mathcal{N}} = -z \mathcal{A} e^{-\frac{2}{3}z^{3/2}} (-1)^{\mathcal{N}} a_{\mathcal{N}}. \tag{1.14}$$

We know that $R_{\mathcal{N}} = y_2$ solves the homogeneous left-hand side of eqn (1.14), so in order to solve the full equation, we could try setting $R_{\mathcal{N}} = \mathcal{S}(z) i y_2$, where we would expect $\mathcal{S}(z)$ to vary from zero to a constant across the Stokes line at $\theta = 2\pi/3$ (in fact, it turns out that $\mathcal{S}(z) \sim 1$, *c.f.* eqn 1.5). The optimal truncation point tends to infinity as $z \to \infty$, so we re-write the right-hand side of eqn (1.14) using the late terms (1.10). Once this is done, the equation can be re-scaled near the Stokes line and $\mathcal{S}(z)$ derived.

The crucial idea behind this methodology is that (1.14) establishes a relationship between the Stokes Phenomenon and the late terms of the

asymptotic series. In effect, our procedure allows us to *decode* the tails of the divergent expansion and retrieve the previously hidden terms. Although Stokes originally believed the transition to be *discontinuous*, Berry (1989) demonstrated that for finite z, the switching-on of the exponential occurs *smoothly*. The approach we have just described, however, derives the same result by optimal truncation and Stokes-line smoothing, following the methodology of Olde Daalhuis et al. (1995) and Chapman et al. (1998).

Having now discussed the importance of the Stokes Phenomenon and the general ideas of exponential asymptotics, we can address how we intend to apply the same methods to the study of the gravity-capillary problem of this chapter.

1.2.1 The gravity-capillary methodology

Consider flow over a rectangular step in a channel. From the introduction, we know that for subcritical ($F < 1$) flows linearised theory predicts two regions of interest. In Region I and below the critical dispersion curve of Figure 1.9, we expect flows with capillary waves upstream and gravity waves downstream, while in Region II and above the dispersion curve, we expect localised solitary waves. As we will show in Section 1.4, the key difference between Type I and II solutions is the type of residue contributions that are collected in the Fourier inversion process: Region I solutions have four real residues (representing two real wavenumbers) while Region II solutions have four complex residues. However, this phenomenon can also be interpreted using exponential asymptotics, and we now give a taste of the underlying ideas of Section 1.5.

When the free-surface, described by the fluid speed $q(\phi)$, and streamline angle $\theta(\phi)$, as functions of the potential ϕ, is expanded into an asymptotic series in powers of the Froude and Bond numbers, then we find that the expansions of q and θ are waveless to every order. The exponentially small waves on the free-surface must instead be interpreted as arising from when the solution is analytically continued across critical *Stokes lines*.

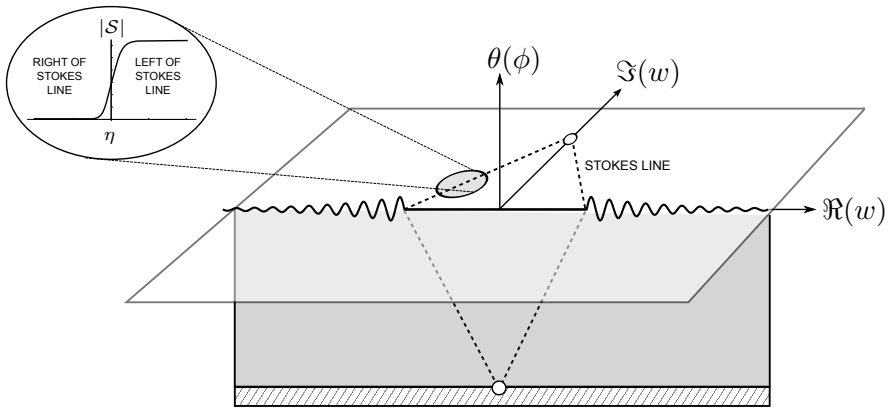

Figure 1.4: The *physical* solutions of interest is θ, the angle of the free-surface as a function of the potential $\phi \in \mathbb{R}$. Although this solution is perfectly well-defined, its asymptotic representation is divergent in some limit $\epsilon \to 0$ and contains a singularity in its analytic continuation (shown as a perpendicular plane, $\phi = w \in \mathbb{C}$). In the *physical* potential plane (shown shaded), this singularity corresponds to the source representing the linearised step. By re-scaling near the singularity and optimally truncating, we will be able to observe the smooth switching-on of the exponentially small terms (top-left) as Stokes lines are crossed.

Of course, the velocity $qe^{-i\theta}$ is entirely well-behaved on the free-surface, but its analytic continuation contains a singularity corresponding to the sharp

rise in the step. To study this issue, we complexify the free-surface, sending $\phi \mapsto \overline{\phi} + i\overline{\psi} = \overline{w} \in \mathbb{C}$ and $qe^{-i\theta} \mapsto \overline{q}e^{-i\overline{\theta}} = d\overline{w}/d\overline{z} \in \mathbb{C}$. This is represented by the perpendicular plane (out of the page) in Figure 1.4. However, because of the nature of complex variables, we may continue to identify these new complexified variables $\overline{w}$ and $d\overline{w}/d\overline{z}$, with the usual quantities of w (the complex potential) and dw/dz (the complex velocity). Thus, we may speak of the *corner of the step generating a wave*, but we are actually referring to the singularity in the analytic continuation identifiable with the step, rather than the step itself!

Once we have located these singularities, then we can expect Stokes lines to emerge from each one, across which the Stokes Phenomenon necessitates the switching-on of exponentially small waves. Afterwards, by the process of optimal truncation and Stokes smoothing, we can explicitly derive the form of the waves that switch on. This is our general plan of attack.

1.3 MATHEMATICAL FORMULATION

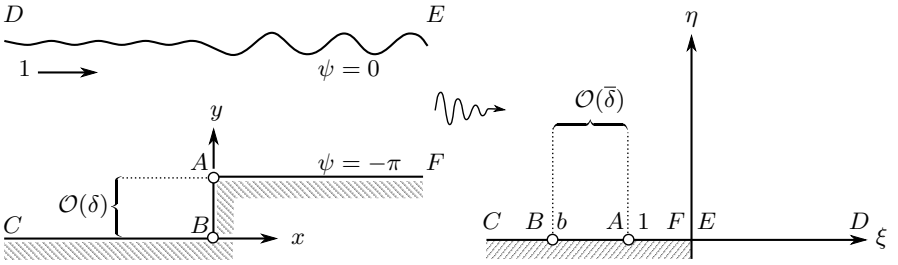

Figure 1.5: The flow in the physical xy-plane (left) is first mapped to the potential $w = \phi + i\psi$ plane, then again mapped to the upper half $\zeta = \xi + i\eta$ plane (right) using $\zeta = e^{-w}$. Later, the analysis will proceed by assuming that the height of the step is small.

Consider steady two-dimensional potential flow of an incompressible fluid over a rectangular step in a channel. Far upstream, the flow is uniform with constant velocity U and the height of the channel is L. We first non-dimensionalise the velocity with U and the length with L/π. Then, if the fluid velocity is $\mathbf{u} = (u, v) = \nabla\phi$, the potential satisfies Laplace's equation,

$$\nabla^2\phi = 0. \tag{1.15}$$

On all boundaries, we have the kinematic condition,

$$\frac{\partial\phi}{\partial n} = 0, \tag{1.16}$$

and on the free surface, Bernoulli's equation gives

$$\frac{F^2}{2}\Big(|\nabla\phi|^2 - 1\Big) + y = -B\kappa, \tag{1.17}$$

where $F = U/\sqrt{gL}$ is the Froude number defined for gravitational constant g; $B = \sigma/(\rho g L^2)$ is the Bond number defined according to the surface tension parameter σ and density ρ; and κ is the curvature, defined to be positive if the center of curvature lies in the fluid region.

We then define the complex potential by $w = \phi + i\psi$, where ψ is the streamfunction, and conformally map the flow from the physical plane to the

strip between $\psi = -\pi$ and $\psi = 0$. A second transformation with $w \mapsto \zeta = \xi + i\eta = e^{-w}$ is then used to map the potential plane to the upper half $\zeta-$plane. The stagnation and corner points of the step are mapped to $\zeta = -1$ and $\zeta = -b$, respectively, and we can prescribe the step by $y = \delta f(x) = \delta H(x)$ where $H(x)$ is the Heaviside function and $\delta \ll 1$. These physical and ζ-planes are shown in Figure 1.5.

The flow can now be handled more easily by formulating the problem in terms of the hodograph variables, $\log(dw/dz) = \log q - i\theta$, where q is the speed of the flow and θ is the angle the streamines make with the x-axis. Then by Cauchy's Theorem, it can be shown that

$$\log q = -\frac{1}{\pi}\int_{-\infty}^{\infty} \frac{\theta(\xi')}{\xi' - \xi}\, d\xi'. \tag{1.18}$$

Reposing the potential problem in terms of this integral formulation is a standard technique, but we will give a full derivation of (1.18) for the more interesting case of ship waves in Chapter 3.

Bernoulli's equation (1.17) can also be transformed into a more convenient form by differentiating with respect to the arclength parameter s (increasing in the flow direction), and using

$$\frac{d}{ds} = \frac{d\phi}{ds}\frac{d}{d\phi} = q\frac{d}{d\phi}.$$

Then after rearranging, Bernoulli's equation becomes

$$F^2\left[q^2\frac{dq}{d\phi}\right] - B\left[q^2\frac{d^2\theta}{d\phi^2} + q\frac{dq}{d\phi}\frac{d\theta}{d\phi}\right] = -\sin\theta. \tag{1.19}$$

Note that in the usual treatment of linearised flow in a channel (*cf.* Lamb 1932 and King & Bloor 1987, 1990) the problem is typically nondimensionalised so that the channel depth is 1, which ultimately changes the definition of the Froude and Bond numbers. Our decision to nondimensionalise with a depth of π is consistent with the choice of Chapman & Vanden-Broeck (2006).

1.4 CLASSICAL LINEARISED THEORY FOR SMALL STEPS

Linearised solutions for flow over a slight bottom topography have been treated for the case of gravity waves in the classic text of Lamb (1932) as well in King & Bloor (1987, 1990). For the case of gravity-capillary waves, Forbes (1983) performed the analysis for flow over a semi-circular obstruction (using the Joukowski map), but surprisingly, a similar analysis does not seem to have been done for the case of flow over a step.

First, so as to distinguish the free-surface and boundary, we use the following notation: if $\xi > 0$ and hence we are positioned on the free-surface, then we let $\xi = e^{-\phi}$ and $\theta(\xi) = \theta_f(\phi)$, where ϕ varies between ∞ and $-\infty$; otherwise, if $\xi < 0$ and we are positioned on the channel bottom, then we let $\xi = -e^{-\phi}$ and $\theta(\xi) = \theta_b(\phi)$, where now ϕ varies between $-\infty$ and ∞. The

boundary integral (1.18), evaluated along $\xi > \infty$, can first be written as

$$-\frac{1}{\pi}\int_{-\infty}^{\infty} \frac{\theta(\xi')}{\xi' - \xi} d\xi' = -\frac{1}{\pi}\left[\int_{-\infty}^{\infty} \frac{\theta_f(s)}{1 - e^{-(\phi - s)}} ds - \int_{-\infty}^{\infty} \frac{\theta_b(t)}{1 + e^{-(\phi - t)}} dt\right]$$
$$\equiv P_f(\phi)$$

with $\phi \in (-\infty, \infty)$. $P_f(\phi)$ can then be written as a sum of convolutions

$$P_f(\phi) = -\frac{1}{\pi}\Big[(\theta_f * k_+)(\phi) - (\theta_b * k_-)(\phi)\Big], \tag{1.20}$$

where

$$k_\pm(\sigma) = \frac{1}{1 \mp e^{-\sigma}}, \tag{1.21}$$

and the convolution product is defined by

$$(g * h)(\phi) \equiv \int_{-\infty}^{\infty} g(s) \cdot h(\phi - s)\, ds. \tag{1.22}$$

To linearise θ for small steps, we set

$$\theta = \delta\theta^{(1)} + \delta^2\theta^{(2)} + \dots \tag{1.23}$$

so that for $\xi > 0$ and along the free-surface, $q(\xi) = \exp\{P_f(\phi)\} = 1 + \mathcal{O}(\delta)$ from eqn (1.18). Then at $\mathcal{O}(\delta)$ we get:

$$\theta_b^{(1)} = f'(\phi), \tag{1.24}$$

$$F^2 \frac{dP_f^{(1)}}{d\phi} - B\frac{d^2\theta_f^{(1)}}{d\phi^2} = -\theta_f^{(1)}, \tag{1.25}$$

and now, (1.25) can be written as

$$-\frac{F^2}{\pi}\frac{d}{d\phi}\Big[(\theta * k_+)(\phi) - (f' * k_-)(\phi)\Big] - B\frac{d^2\theta}{d\phi^2} = -\theta. \tag{1.26}$$

In this final equation, we have replaced the notation of $\theta_f^{(1)}$ with θ, so long as it remains clear that we are only interested in the first approximation, evaluated along the free-surface.

1.4.1 Fourier integrals

We will define the Fourier Transform of a function, $f(x)$ as

$$\mathscr{F}[f] \equiv \frac{1}{\sqrt{2\pi}} \int_{-\infty}^{\infty} f(x) e^{-ikx}\, dx.$$

Taking the transform of eqn (1.26) gives

$$-\frac{F^2}{\pi}(-ik)\Big[\mathscr{F}[\theta]\mathscr{F}[k_+] - \mathscr{F}[f']\mathscr{F}[k_-]\Big] - B(ik)^2\mathscr{F}[\theta] = -\mathscr{F}[\theta],$$

and we can use the fact that

$$\mathscr{F}[k_+] = \frac{\pi i}{\tanh \pi k} \quad \text{and} \quad \mathscr{F}[k_-] = \frac{\pi i}{\sinh \pi k}, \tag{1.27}$$

and rearrange to get

$$\mathscr{F}[\theta] = \frac{kF^2}{kF^2 \cosh \pi k - \sinh \pi k (Bk^2 - 1)} \int_{-\infty}^{\infty} f'(t) e^{-ikt} \, dt. \tag{1.28}$$

Inversion then gives the form of the free-surface:

$$\theta = \frac{F^2}{2\pi} \int_{-\infty}^{\infty} \frac{k}{g(k) \cosh \pi k} \left[\int_{-\infty}^{\infty} f'(t) e^{ik(t-\phi)} \, dt \right] dk, \tag{1.29}$$

where

$$g(k) = kF^2 - \tanh(\pi k)(Bk^2 + 1) \tag{1.30}$$

is the dispersion relation and we will go on to define the inversion contour more specifically in the next section. The different root arrangements of the dispersion relation and their relationships with the various solutions mentioned in the introduction are expounded in Appendix 1.A, but briefly, there are two types of poles: the first type lies entirely on the imaginary axis and affects the free-surface only near the origin $\phi = 0$. Setting $k = \pm\beta_0, \pm\beta_1, \ldots$, where $\beta_i \in \mathbb{R}$, we see that these poles are given by solving the equation

$$\frac{\tan(\pi\beta_n)}{\beta_n} = \frac{F^2}{1 - B\beta_n^2}, \tag{1.31}$$

for $n \in \mathbb{Z}^+$. The second type of pole corresponds to the wavenumbers of the gravity-capillary waves; if we let $k = \pm k_0, \pm k_1$ be these wavenumbers and order them according to their behaviours as determined in Region I (of Figure 1.9 on page 30), then $\pm k_0$ corresponds to gravity waves and $\pm k_1$ to capillary waves, with $0 < k_0 < k_1$. However, if the Froude and Bond numbers are chosen to lie in Region II (of Figure 1.9 on page 30), then the four residues are entirely complex, and we identify the poles in the lower-half plane with k_0 and $-\overline{k_0}$, and the poles in the upper-half plane with k_1 and $-\overline{k_1}$. The reasons for this will become clear in the next section.

We make note of two points: first, (1.29) could have also have been derived by linearising the potential formulation in the physical plane; second, the following properties of $g(k)$ and $g'(k)$ will be useful in the sections to follow:

$$g(-k) = -g(k) \qquad g'(-k) = g'(k) \tag{1.32}$$

$$g(\overline{k}) = \overline{g(k)} \qquad g'(\overline{k}) = \overline{g'(k)} \tag{1.33}$$

1.4.2 Fourier inversion

At this point, we will now substitute the expression $f(t) = H(t)$ for the geometry of the step into (1.29), giving

$$\theta = \frac{F^2}{2\pi} \int_{-\infty}^{\infty} \frac{k e^{-ik\phi}}{g(k) \cosh(\pi k)} \, dk. \tag{1.34}$$

First, let us perform the Fourier inversion for solutions in Region I, so with four real wavenumbers; the contour is illustrated in Figure 1.6.

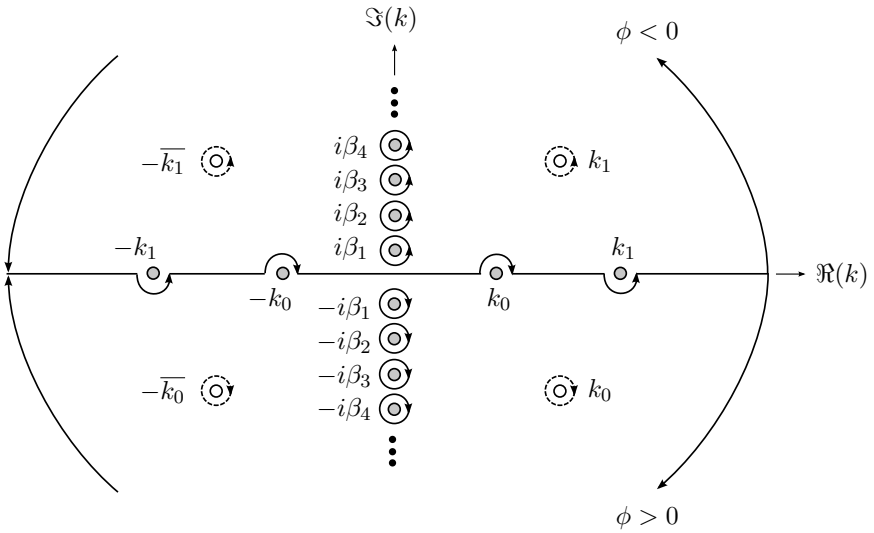

Figure 1.6: When there are four real wavenumbers, the Fourier inversion of eqn (1.34) is done so that for $\phi > 0$, the gravity residues ($k = \pm k_0$) are collected, whereas for $\phi < 0$, the capillary residues ($k = \pm k_1$) are collected. If there are four complex wavenumbers, then the residues in the upper and lower-half plane are similarly collected, in the orientation prescribed by the dotted lines.

The integral in (1.34) suffers from the presence of the four poles along the real axis, and this is a symptom of the unnatural steady-state problem (Stoker, 1957; Debnath, 1994). We must re-define the integration contour along the real k-axis, taking in account the correct radiation conditions far upstream and far downstream from the disturbance. Suppose that $\phi > 0$. Then in this case, we deform the contour into the lower-half k-plane, where the integrand tends to zero as $k \to -i\infty$. In the limit that $\phi \to \infty$, we want to preserve only gravity waves, and so we only collect the residues from $k = \pm k_0$. Similarly, if $\phi < 0$, then we still deform into the upper-half k-plane, but the path is chosen so that the residues $k = \pm k_1$ are collected as $\phi \to -\infty$.

With this in mind, we may write the Fourier integral (1.34) as

$$\theta = \frac{F^2}{2\pi}\int_{-\infty}^{\infty}\frac{G(k)}{g(k)}\,dk = \begin{cases} \left[\oint_{+k_0} + \oint_{-k_0} + \sum_{n=1}^{\infty}\oint_{-i\beta_n}\right]\dfrac{G(k)}{g(k)}\,dk & \phi > 0 \\ \left[\oint_{+k_1} + \oint_{-k_1} + \sum_{n=1}^{\infty}\oint_{+i\beta_n}\right]\dfrac{G(k)}{g(k)}\,dk & \phi > 0, \end{cases} \tag{1.35}$$

where $G(k) = ke^{-ik\phi}/\cosh(\pi k)$ and the integral-shorthand represents contour integrals around the indicated poles. Note that we have also included the residue contribution from $k = i\beta_0 = 0$ since this is simply zero. Then for solutions in Region I and for $\phi > 0$, we have

$$\theta = \frac{F^2}{2\pi}\left[-2\pi i\mathrm{Res}\left\{\frac{G(k)}{g(k)}, k = k_0\right\} - 2\pi i\mathrm{Res}\left\{\frac{G(k)}{g(k)}, k = -k_0\right\} - 2\pi i\sum_{n=1}^{\infty}\mathrm{Res}\left\{\frac{G(k)}{g(k)}, k = -i\beta_n\right\}\right].$$

The poles are simple roots of $g(k)$ so using Properties (1.32)-(1.33), we can write

$$\begin{aligned}\theta &= -F^2 i\left[\frac{G(k_0)}{g'(k_0)} + \frac{G(-k_0)}{g'(k_0)}\right] - F^2 i\sum_{n=1}^{\infty}\frac{G(-i\beta_n)}{g'(-i\beta_n)}\\ &= -F^2 i\left[\frac{k_0 e^{-ik_0\phi}}{g'(k_0)\cosh(\pi k_0)} - \frac{k_0 e^{ik_0\phi}}{g'(k_0)\cosh(\pi k_0)}\right] - F^2 i\sum_{n=1}^{\infty}\frac{(-i\beta_n)e^{i\beta_n|t-\phi|}}{\cos(\pi\beta_n)g'(i\beta_n)}\\ &= F^2\left[\frac{-2k_0}{g'(k_0)\cosh(\pi k_0)}\right]\sin k_0\phi - F^2\sum_{n=1}^{\infty}\left[\frac{\beta_n}{\cos(\pi\beta_n)g'(i\beta_n)}\right]e^{-\beta_n\phi}.\end{aligned} \tag{1.36}$$

Region I solutions with $\phi < 0$ are also handled similarly, giving

$$\theta = F^2\left[\frac{2k_1}{g'(k_1)\cosh(\pi k_1)}\right]\sin k_1\phi - F^2\sum_{n=1}^{\infty}\left[\frac{\beta_n}{\cos(\pi\beta_n)g'(i\beta_n)}\right]e^{\beta_n\phi}. \tag{1.37}$$

Solutions in Region II, with only complex residues can also be derived, but there is a more convenient expression for (1.36) and (1.37), which allows for the possibility of complex values of k. If we write a general residue as $k = k^* \in \mathbb{C}$, then the solution can be expressed as

$$\begin{aligned}\theta_\pm = F^2\left[\frac{\pm 2|k^*|e^{\Im(k^*)\phi}}{|g'(k^*)\cosh(\pi k^*)|}\right]\sin\Big(\Re(k^*)\phi - \mathrm{Arg}(k^*) + \mathrm{Arg}(\tau)\Big)\\ - F^2\sum_{n=1}^{\infty}\left[\frac{\beta_n}{\cos(\pi\beta_n)g'(i\beta_n)}\right]e^{-\beta_n|\phi|},\end{aligned} \tag{1.38}$$

where we have set

$$\tau \equiv \mathrm{Arg}[g'(k^*)\cosh(\pi k^*)],$$

and the $\pm$ signs in (1.38) are associated with $\phi \lessgtr 0$, respectively. The residue k^* should have $\Re(k^*) > 0$, and for gravity $(-)$ waves, we set $k^* = k_0$ while for capillary $(+)$ waves, we set $k^* = k_1$. Note that from these expressions for θ, the (re-scaled) free-surface can then be computed from

$$y \sim \delta\int^x \theta(s)\,ds,$$

and moreover, in the limit that $\phi \to \pm\infty$, the contributions from $k = \mp i\beta_n$ of eqn (1.38) tend to zero, leaving only the the contributions from the residues at $k = \pm k_0, \pm k_1$.

1.4.3 Taking the Low-Froude and low-Bond limits

The key result of the previous section, eqn (1.38), provides the form of the gravity-capillary waves over a small step. However, we are more interested in the nature of this approximation as the Froude and Bond numbers tend to zero, so we let $F = \beta\epsilon$ and $B = \beta\tau\epsilon^2$, where $\epsilon \ll 1$. This particular scaling for F and B is chosen so that a power of ϵ is associated with each derivative of the dependent variables of (1.17)—thus ϵ for the $\nabla\phi$, and ϵ^2 for

the curvature κ. The reason for this choice will become clear later when we perform the exponential asymptotic analysis (it can also be seen by examining the limiting scaling of the dispersion curve in Figure 1.9).

With this choice for the Froude and Bond numbers, a balance of terms in eqn (1.30) tells us that $k \sim \mathcal{O}(1/\epsilon)$. Since $\tanh(\pi k) \sim 1$ for $\Re(k) > 0$, we can write eqn (1.86) as

$$\beta\tau(\epsilon k)^2 - \beta(\epsilon k) + 1 \sim 0,$$

where we only consider the roots with $\Re(k) > 0$. Then we have the fact that

$$k_\pm \sim \frac{D_\pm}{\epsilon}, \tag{1.39}$$

where $D_\pm$ is defined by

$$D_\pm \equiv \frac{1 \pm \sqrt{\Delta}}{2\tau}, \tag{1.40}$$

with Δ defined by

$$\Delta \equiv 1 - \frac{4\tau}{\beta}. \tag{1.41}$$

The negative sign of eqn (1.39) corresponds to gravity waves ($k_- = k_0$) and the positive sign to capillary waves ($k_+ = k_1$), and the condition that both wavenumbers are real is equivalent to $\Delta > 0$ or $\tau < \beta/4$. In fact, this also indicates that the critical dispersion curve $F = F_m$ in Figure 1.1 and Figure 1.9 tends to the curve $B = F^2/4$ as $F \to 0$. Now, using eqns (1.39) and (1.40) in (1.87), we can show that

$$g'(k_\pm) \sim \mp\beta\epsilon\sqrt{\Delta}, \tag{1.42}$$

and noting that

$$\cosh(\pi k_\pm) \sim \cosh\left(\frac{\pi}{\epsilon}D_\pm\right) = \frac{1}{2}\left(e^{-\pi D_\pm/\epsilon} + e^{\pi D_\pm/\epsilon}\right) \sim \frac{e^{\pi D_\pm}/\epsilon}{2},$$

we then have the low-Froude, low-Bond approximation from (1.38),

$$\theta_\pm \sim \frac{4\delta}{\epsilon}\left|\frac{D_\pm}{\sqrt{\Delta}}\right| \exp\left[-\frac{\pi\Re(D_\pm)}{\epsilon} + \frac{\Im(D_\pm)\phi}{\epsilon}\right] \times \sin\left\{-\frac{\Re(D_\pm)\phi}{\epsilon} - \frac{\pi\Im(D_\pm)}{\epsilon} + \mathrm{Arg}(D_\pm) - \frac{\mathrm{Arg}(\Delta)}{2}\right\}, \tag{1.43}$$

where we have multiplied the first-order approximation by δ. This completes our determination of the gravity-capillary waves, and we now move on to retrieve a similar result using exponential asymptotics.

1.5 EXPONENTIAL ASYMPTOTICS

In the classical linearisation method of the previous section, we derived the small-step formula (1.38) for $F, B \sim \mathcal{O}(1)$, only to afterwards take the low-Froude, low-Bond limits. In the method of exponential asymptotics, we will instead take the $F, B \to 0$ limit *immediately* after the initial linearisation.

As explained in our overview of the methodology, we want to complexify the free boundary variables (ξ, ϕ, q, θ), which is simply equivalent to replacing the variables by their (2D) complex analogue. Analytically continuing the boundary integral (1.18) into the upper-half ξ-plane gives,

$$\log q - i\theta = -\frac{1}{\pi}\int_{-\infty}^{0} \frac{\theta(\xi')}{\xi' - \zeta}\, d\xi' + \mathscr{H}[\theta(\zeta)], \tag{1.44}$$

where we have relabeled $\xi \mapsto \zeta$ and $\mathscr{H}$ denotes a Hilbert transform operator on the free-surface, $\xi' \geq 0$:

$$\mathscr{H}[\theta(\zeta)] = -\frac{1}{\pi}\int_{0}^{\infty} \frac{\theta(\xi')}{\xi' - \zeta}\, d\xi'. \tag{1.45}$$

Complexifying the dynamic condition (1.19) also gives

$$\beta\epsilon\left[q^2\frac{dq}{dw}\right] - \beta\tau\epsilon^2\left[q^2\frac{d^2\theta}{dw^2} + q\frac{dq}{dw}\frac{d\theta}{dw}\right] = -\sin\theta, \tag{1.46}$$

with a relabeling of $\phi \mapsto w$, and where we have used the scalings for the Froude and Bond numbers given in Section 1.4.3. The expressions in (1.44)–(1.46) then provide an equation for the complexified free-surface, and this was illustrated using the perpendicular plane in Figure 1.4. Of course, at the end of the analysis, we must also remember to add any solutions from analytic continuation into the *lower*-half ζ-plane.

Assuming that the step is small, and letting $b = 1 + \overline{\delta}$, where $\overline{\delta} \ll 1$, then linearising around the uniform stream gives

$$q = 1 + \overline{\delta}q' + \mathcal{O}(\overline{\delta}^2) \qquad \text{and} \qquad \theta = \overline{\delta}\theta' + \mathcal{O}(\overline{\delta}^2). \tag{1.47}$$

Then (1.44) gives to leading order in $\overline{\delta}$ (dropping primes)

$$q - i\theta = \frac{1}{2(\zeta + 1)} + \mathscr{H}[\theta(\zeta)]. \tag{1.48}$$

The dynamic condition in (1.19) gives to leading order in $\overline{\delta}$ (also dropping primes)

$$\beta\epsilon\frac{dq}{dw} - \beta\tau\epsilon^2\frac{d^2\theta}{dw^2} = -\theta,$$

and using the fact that $\zeta = e^{-w}$, then

$$\frac{d}{dw} = -\zeta\frac{d}{d\zeta}, \qquad \frac{d^2}{dw^2} = \zeta\frac{d}{d\zeta} + \zeta^2\frac{d^2}{d\zeta^2},$$

and the linearised dynamic condition becomes

$$\beta\epsilon\zeta\frac{dq}{d\zeta} + \beta\tau\epsilon^2\left[\zeta^2\frac{d^2\theta}{d\zeta^2} + \zeta\frac{d\theta}{d\zeta}\right] = \theta. \tag{1.49}$$

1.5.1 *Outer problem*

We first write the solutions of eqns (1.48) and (1.49) as a regular asymptotic expansion:

$$\theta = \sum_{n=0}^{\infty} \epsilon^n \theta_n \quad \text{and} \quad q = \sum_{n=0}^{\infty} \epsilon^n q_n, \tag{1.50}$$

which gives at leading order,

$$\theta_0 = 0, \tag{1.51}$$

$$q_0 = \frac{1}{2(\zeta+1)}, \tag{1.52}$$

while at $\mathcal{O}(\epsilon^n)$ for $n \geq 1$, we have

$$q_n = i\theta_n + \mathscr{H}[\theta_n(\zeta)] \tag{1.53}$$

$$\beta\zeta \frac{dq_{n-1}}{d\zeta} + \beta\tau \left[\zeta^2 \frac{d^2\theta_{n-2}}{d\zeta^2} + \zeta \frac{d\theta_{n-2}}{d\zeta} \right] = \theta_n. \tag{1.54}$$

Now the leading-order solution q_0 in (1.52) has a singularity in the analytic continuation of the free-surface, $\zeta = -1$, which corresponds to the linearised step. But we see by eqns (1.53)–(1.54) that at each subsequent order, q_n is determined by the first and second derivatives of q_{n-1} and q_{n-2}, respectively. Thus, each subsequent order must add to the power of the early singularity, so that in the limit that $n \to \infty$, the effect of this early singularity dominates the behaviour of the late-order terms; q_n, then, will diverge like a factorial over power:

$$q_n \sim \frac{Q\Gamma(n+\gamma)}{\chi^{n+\gamma}}, \tag{1.55}$$

with γ constant, Q and χ as functions of ζ, and with $\chi(-1) = 0$; of course, the same process leads to a similar expression for θ_n:

$$\theta_n \sim \frac{\Theta\Gamma(n+\gamma)}{\chi^{n+\gamma}}. \tag{1.56}$$

At this point, we can profit from yet another simplification: as $n \to \infty$, and when ζ is taken near the Stokes line (which we will soon derive), the integral in (1.53) is found to be exponentially subdominant to the other terms of the same equation. Essentially, this occurs because $|\chi|$ is smallest near the singularity, $\zeta = -1$, and grows along the Stokes line as it tends towards the free-surface, upon which the integral is evaluated. This simplification was used in Chapman & Vanden-Broeck (2002, 2006) and is discussed in detail for the more interesting case of ship waves in Chapter 3; in any case, the assumption can simply be checked *a posteriori* after obtaining the correct form of χ. From (1.53) then, we have

$$q_n \sim i\theta_n, \tag{1.57}$$

valid as $n \to \infty$. Using this simplification, the $\mathcal{O}(\epsilon^n)$ terms are then given by (1.54), with

$$\beta\zeta \frac{dq_{n-1}}{d\zeta} - \beta\tau i \left[\zeta^2 \frac{d^2 q_{n-2}}{d\zeta^2} + \zeta \frac{dq_{n-2}}{dw} \right] \sim -iq_n. \tag{1.58}$$

Substitution of the ansatz in (1.55) into (1.58) gives to leading order as $n \to \infty$:

$$(\beta\tau i\zeta^2)\left(\frac{d\chi}{dw}\right)^2 + (\beta\zeta)\frac{d\chi}{dw} - i = 0, \tag{1.59}$$

or

$$\frac{d\chi}{d\zeta} = -i\left[\frac{\beta \pm \sqrt{\beta^2 - 4\beta\tau}}{2\beta\tau}\right]\left(-\frac{1}{\zeta}\right)\frac{d\chi}{d\zeta} = iD_{\pm}\left(\frac{1}{\zeta}\right), \tag{1.60}$$

with $D_{\pm}$ as in (1.40). Requiring that $\chi(-1) = 0$, we then have

$$\chi = iD_{\pm}\log(-\zeta)\,. \tag{1.61}$$

Proceeding to next order in (1.58), we also have

$$\frac{dQ}{dw}\left[\beta\zeta i - 2\beta\tau\zeta^2\frac{d\chi}{dw}\right] = Q\left[\beta\tau\frac{d\chi}{dw} + \beta\tau\zeta^2\frac{d^2\chi}{dw^2}\right]$$

and substituting the equation for χ in (1.61) zeros the right-hand side of the above expression; therefore $Q = \text{constant} = \Lambda$. Finally, to determine the constant γ, we note that in order to match the the leading order solution in eqn (1.52) with the ansatz of eqn (1.55), we need $\gamma = 1$.

Before we go on to discuss the implications of these late-order terms, let us us inspect the late-orders singulant χ. From Dingle (1973), and the third maxim of Section 1.2, we know that Stokes lines must emerge from the singularity at $\zeta = -1$, and are prescribed by locations where successive terms in the expansions of θ and q have the same phase, *i.e.* where

$$\Im(\chi) = 0 \qquad \text{and} \qquad \Re(\chi) \geq 0.$$

Stokes lines lie in the space corresponding to the complexified free surface, but as discussed in Section 1.2.1, each point in this imaginary plane can be identified with a point in the lower-half complex potential plane corresponding to physical space; here, the Stokes lines are given by the curves $w = \gamma(s) \in \mathbb{C}$ with

$$\gamma(s) = \begin{cases} si & \text{if } \Delta > 0 \text{ and for } s \in \left[-\pi, 0\right] \\ s + i\left[\dfrac{\Re(D_{\pm})}{\Im(D_{\pm})}s - \pi\right] & \text{if } \Delta < 0 \text{ and for } |s| \in \left[0, \pi\dfrac{\Im(D_{\pm})}{\Re(D_{\pm})}\right]. \end{cases} \tag{1.62}$$

Consider the case that $\Delta > 0$. As shown in Figure 1.7, both the capillary and gravity Stokes lines coalesce along the imaginary ψ axis, and we would thus expect for waves to switch-on as the free-surface is analytically continued across the origin—gravity waves downstream and capillary waves upstream. This transition is denoted by $[Bs \to C]$ or $[Bs \to G]$, describing the action of the base solution (1.50) switching on a capillary or gravity wave, respectively.

However, in inferring the behaviour of the Stokes contributions as Δ is decreased from $\Delta > 0$ to $\Delta < 0$, we must take great care in selecting the correct branch of the various square roots if we wish to continue to identify

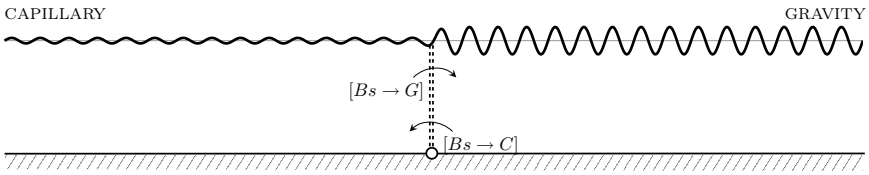

Figure 1.7: In Region I with $\Delta > 0$, both capillary and gravity Stokes lines emerge from $w = -i\pi$ and intersect the origin. Across this point, we expect a gravity wave to switch-on downstream and a capillary wave to switch-on upstream.

the same negative sign in $D_\pm$ to gravity waves and the same positive sign to capillary waves. A much easier mechanism is to see *a posteriori* which side the exponentials are decaying or growing and to assign the appropriate wave to the decaying region; we comment on this shortly in Section 1.5.3 once we have derived the form of the exponentials. For the moment, however, it is sufficient to claim that as Δ decreases from positive to negative values, the previously coalescent Stokes lines split, with the capillary-associated line moving upstream and the gravity-associated line moving downstream; this is shown in Figure 1.8. As the free-surface is analytically continued across these critical lines, we would again expect small waves to switch on, only now the waves decay in the far field.

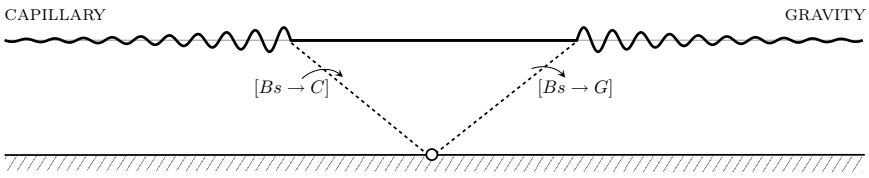

Figure 1.8: In Region II with $\Delta < 0$, the capillary Stokes line moves upstream while the gravity Stokes line moves downstream. We again expect the switching-on of gravity and capillary waves, but because of the non-zero imaginary component of χ, the waves are now exponentially decaying as they tend to infinity.

In the next section, we will explicitly show how the Stokes Phenomenon actually occurs and moreover, we will establish the connection between the resultant waves and the late-order terms of eqns (1.55) and (1.56).

1.5.2 Stokes smoothing

When an asymptotic expansion is truncated haphazardly, the error is generally algebraically small in ϵ; in order to observe the smooth switching-on of the waves as the Stokes line is crossed, we must instead truncate the expansions *optimally*, to where the error is exponentially small. To begin, we will truncate the asymptotic expansion in q:

$$q = \sum_{n=0}^{\mathcal{N}-1} \epsilon^n q_n + S_{\mathcal{N}}. \tag{1.63}$$

Note that the expansions and corresponding expressions for θ are also similarly done, but the fact that $q_n \sim i\theta_n$ from (1.57) allows us to work with only a single variable. Once the truncated sum (1.63) is substituted into eqns

(1.48) and (1.49), we get

$$\mathcal{L}(S_{\mathcal{N}};\epsilon) + \epsilon^{\mathcal{N}}\left[\beta\zeta q'_{\mathcal{N}-1} - \beta\tau i\left(\zeta^2 q''_{\mathcal{N}-2} + \zeta q'_{\mathcal{N}-2}\right)\right] - \epsilon^{\mathcal{N}+1}\beta\tau i\left[\zeta^2 q''_{\mathcal{N}-1} + \zeta q'_{\mathcal{N}-1}\right] = 0, \quad (1.64)$$

where primes denote differentiation in w and where the linear operator $\mathcal{L}$ is defined by

$$\mathcal{L}(S_{\mathcal{N}};\epsilon) = \epsilon\beta\zeta S'_{\mathcal{N}} - \epsilon^2\beta\tau i\left[\zeta^2 S''_{\mathcal{N}} + \zeta S'_{\mathcal{N}}\right] + iS_{\mathcal{N}}. \quad (1.65)$$

In (1.64), we can replace the $\mathcal{O}(\epsilon^{\mathcal{N}})$ bracketed quantities with the right-hand side of eqn (1.58), giving

$$\mathcal{L}(S_{\mathcal{N}};\epsilon) \sim \epsilon^{\mathcal{N}}\left[iq_{\mathcal{N}} + \epsilon\beta\tau i\zeta^2 q''_{\mathcal{N}-1}\right]. \quad (1.66)$$

It is easily verified that $Qe^{-\chi/\epsilon}$ is a solution of the homogeneous equation $\mathcal{L}(\bullet;\epsilon) = 0$, and so to solve the inhomogeneous equation, we let $\mathcal{S} = \mathcal{S}(w)$ be the *Stokes smoothing* parameter, which we expect to smoothly vary from zero to a constant across the Stokes line; then we set

$$\begin{aligned} S_{\mathcal{N}} &= \mathcal{S}\left[Qe^{-\chi/\epsilon}\right], \\ S'_{\mathcal{N}} &= \mathcal{S}\left[Qe^{-\chi/\epsilon}\right]' + \mathcal{S}'\left[Qe^{-\chi/\epsilon}\right], \\ S''_{\mathcal{N}} &= \mathcal{S}\left[Qe^{-\chi/\epsilon}\right]'' + 2\mathcal{S}'\left[-\frac{\chi'}{\epsilon}Qe^{-\chi/\epsilon} + Q'e^{-\chi/\epsilon}\right] + \mathcal{S}''Qe^{-\chi/\epsilon}. \end{aligned}$$

When this ansatz for the remainder is substituted into the left-hand side of (1.66), we are only left with terms involving derivatives in $\mathcal{S}$ at leading order:

$$\mathcal{L}(S_{\mathcal{N}};\epsilon) \sim \epsilon\, Qe^{-\chi/\epsilon}\left[\beta\zeta + 2\beta\tau i\zeta^2\chi'\right]\frac{d\mathcal{S}}{dw},$$

and switching to differentiation in χ and using eqn (1.59) to change the bracketed quantities, we then have

$$\mathcal{L}(S_{\mathcal{N}};\epsilon) \sim \epsilon\, Qe^{-\chi/\epsilon}\left[i + \beta\tau i\zeta^2(\chi')^2\right]\frac{d\mathcal{S}}{d\chi}. \quad (1.67)$$

Since we are interested in the limit that ϵ tends to zero, where the optimal truncation point, $\mathcal{N}$, tends to infinity, we can substitute the late-orders ansatz of (1.55) into the right-hand side of (1.66), giving

$$\mathcal{L}(R_{\mathcal{N}};\epsilon) \sim \frac{\epsilon^{\mathcal{N}}Q\Gamma(\mathcal{N}+\gamma)}{\chi^{\mathcal{N}+\gamma}}\left[i + \beta\tau i\zeta^2(\chi')^2\frac{\epsilon(\mathcal{N}+\gamma+1)}{\chi}\right]. \quad (1.68)$$

The optimal truncation point is at $\mathcal{N} \sim \lceil|\chi|/\epsilon\rceil$ (where adjacent terms in the expansion are roughly equal), so we will let $\chi = re^{i\vartheta}$ and thus set $\mathcal{N} = r/\epsilon + \rho$ where $\rho \in [0,1)$. Stirling's formula then gives

$$\Gamma(\mathcal{N}+\gamma) = \Gamma(r/\epsilon+\rho+\gamma) \sim \sqrt{2\pi}e^{-r/\epsilon}\left(\frac{r^{\mathcal{N}+\gamma}}{\epsilon^{\mathcal{N}}}\right)\frac{r^{-1/2}}{\epsilon^{\gamma-1/2}}.$$

Changing the derivatives to

$$\frac{d}{d\chi} = -\frac{e^{-i\vartheta}}{r}\frac{d}{d\vartheta}$$

gives from (1.67) and (1.68),

$$\frac{d\mathcal{S}}{d\vartheta}\left[i+\beta\tau i\zeta^2(\chi')^2\right] \sim \frac{\sqrt{2\pi r}}{\epsilon^{\gamma+1/2}}\left[i+\beta\tau i\zeta^2(\chi')^2\frac{1}{e^{i\vartheta}}\right]\left(e^{-i\vartheta}\right)^{\frac{r}{\epsilon}+\rho+\gamma} e^{\frac{r}{\epsilon}e^{i\vartheta}} e^{-\frac{r}{\epsilon}}.$$

The sum of the exponential factors on the right is exponentially small, except near the Stokes line $\vartheta = 0$. The critical scaling occurs with $\vartheta = \sqrt{\epsilon}\overline{\vartheta}$ and here,

$$\exp\left\{-\frac{r}{\epsilon}\left(1-\cos\vartheta\right)+i\left(\frac{r\sin\vartheta}{\epsilon}-\vartheta\left(\frac{r}{\epsilon}+\rho+\gamma+1\right)+\frac{\pi}{2}\right)\right\}$$
$$\sim \exp\left\{-\frac{r\overline{\vartheta}^2}{2}+\frac{\pi i}{2}+\mathcal{O}(\sqrt{\epsilon})\right\}.$$

In total then, we have the local change in the Stokes switching as

$$\frac{d\mathcal{S}}{d\overline{\vartheta}} \sim \frac{\sqrt{2\pi r}i}{\epsilon^{\gamma}}\exp\left(-\frac{r\overline{\vartheta}^2}{2}\right). \tag{1.69}$$

We now integrate this expression across the Stokes line from upstream, or $\overline{\vartheta} = \infty$ (indicated with a $+$ below), to downstream, or $\overline{\vartheta} = -\infty$ (indicated with a $-$ below). The apparent jump in the remainder is then

$$\left[S_{\mathcal{N}}\right]_{+}^{-} \sim -\frac{2\pi i Q}{\epsilon^{\gamma}}e^{-\chi/\epsilon},$$

and thus across the Stokes line, the terms

$$q_{\text{exp}}^{\pm} \sim -\frac{4\pi}{\epsilon^{\gamma}}\Im\left[Qe^{-\chi_{\pm}/\epsilon}\right], \tag{1.70}$$
$$\theta_{\text{exp}}^{\pm} \sim -\frac{4\pi}{\epsilon^{\gamma}}\Im\left[\Theta e^{-\chi_{\pm}/\epsilon}\right], \tag{1.71}$$

are switched on and where, to derive the above expressions, we have included the contribution from analytic continuation into the lower-half plane (or simply, the complex conjugate of the contribution from the upper-half plane). Formulae (1.70) and (1.71) thus provide us with the important connection between the exponentially small waves and the late-order terms (1.55).

In terms of θ, we will denote the Stokes switching procedure as

$$\sum_n \epsilon^n\theta_n \xrightarrow[[Bs\to C]]{} \sum_n \epsilon^n\theta_n + \theta_{\text{exp}}^{+}$$
$$\sum_n \epsilon^n\theta_n \xrightarrow[[Bs\to G]]{} \sum_n \epsilon^n\theta_n + \theta_{\text{exp}}^{-},$$

either indicating that the base series has switched on a capillary wave $[Bs \to C]$ or that the base series has switched on a gravity wave $[Bs \to G]$. Note that

because the Stokes smoothing proceeded from upstream to downstream, we will eventually need to negate the jump corresponding to the capillary wave.

We can finally return to our assertion in Section 1.5.1 about the selection of the branches of the various square roots and their association to the gravity or capillary waves. Examining (1.61) and (1.71), we see that since we need gravity waves to decay downstream, then for $\Delta < 0$, in order to continue identifying the negative sign of $D_\pm$ to gravity waves, we need

$$\Re(\chi_-) = -\Im(D_-)\log(\zeta) + \pi\Re(D_-)$$

to be *growing* as $\zeta \to 0^+$. This implies that we need $\Im(D_-)$ to be positive. Thus for $\Delta < 0$, we want the secondary branch of the square root $\sqrt{\Delta}$, in order to continue identifying χ_- with gravity waves and χ_+ with capillary waves. With these subtle details in mind, we see that the Stokes lines in Figure 1.8 with χ_+ and χ_- are indeed associated with capillary and gravity waves, respectively.

1.5.3 Determining Λ and the waves

The final step is to determine the unknown pre-factor $Q = \Lambda$ of eqn (1.71); to do this, we solve for the leading-order solution near the singularity $\zeta = -a$ and match with the late-orders expression of eqn (1.55), which is only valid far away from the singularity.

Near the singularity, however, a similar argument to the one used in deriving (1.57) can be applied to simplify the problem. From (1.48), we would like to evaluate

$$q_{\text{inner}}(w) - i\theta_{\text{inner}}(w) = \frac{1}{2(\zeta+1)} + \mathscr{H}[\theta_{\text{outer}}(\zeta)] \tag{1.72}$$

as $\zeta \to -1$ and where the indices help to remind us where the functions q and θ are being evaluated. The left-hand side is evaluated *near* the singularity and thus involves the exact expressions for $q(w)$ and $\theta(w)$ in the inner limit. However, the integrand on the right hand side is integrated over the free-surface, far away from the singularity, thus it involves only the *outer* expansion of $\theta(w)$. But we know that substituting the outer expansion into the right-hand side of eqn (1.72) leads to

$$q_{\text{inner}}(w) - i\theta_{\text{inner}}(w) = q_0 + \epsilon\mathscr{H}[\theta_1(\zeta)] + \epsilon^2\mathscr{H}[\theta_2(\zeta)] + \mathcal{O}(\epsilon^3),$$

and since the integrals are all finite for ζ off the axis, the expansion on the right continues to be well-ordered near the singularity. Thus the leading-order inner solution satisfies

$$q - i\theta \sim \frac{1}{2(\zeta+1)},$$

so that

$$\theta \sim \frac{i}{2(\zeta+1)} - iq,$$
$$\frac{d\theta}{d\zeta} \sim \frac{-i}{2(\zeta+1)^2} - i\frac{dq}{d\zeta},$$
$$\frac{d^2\theta}{d\zeta^2} \sim \frac{i}{(\zeta+1)^3} - i\frac{d^2q}{d\zeta^2}.$$

Substituting these expressions for θ into eqn (1.49) and simplifying gives

$$\beta\epsilon\zeta\frac{dq}{d\zeta} + \beta\tau\epsilon^2\left[-i\zeta^2\frac{d^2q}{d\zeta^2} - i\zeta\frac{dq}{d\zeta} - \frac{i\zeta}{2(\zeta+1)^2} + \frac{i\zeta^2}{(\zeta+1)^3}\right] = \frac{i}{2(\zeta+1)} - iq. \tag{1.73}$$

The scalings for the inner region are given by examining the region where $\epsilon^n q_n \sim q_0$, and so let $\zeta + 1 = i\epsilon\eta$ and $q = -i\overline{q}/(2\epsilon)$. Using

$$\frac{d}{d\zeta} = \frac{1}{i\epsilon}\frac{d}{d\eta},$$

we then have from eqn (1.73):

$$\begin{aligned}\beta\epsilon(-1)\left(\frac{1}{i\epsilon}\right)\left(\frac{-i}{2\epsilon}\right)\overline{q}' \\ + \beta\tau\epsilon^2\Bigg[-i(-1)^2\left(\frac{1}{i\epsilon}\right)^2\left(\frac{-i}{2\epsilon}\right)\overline{q}'' - i(-1)\left(\frac{1}{i\epsilon}\right)\left(\frac{-i}{2\epsilon}\right)\overline{q}' \\ - \frac{i(-1)}{2(i\epsilon\eta)^2} + \frac{i(-1)^2}{(i\epsilon\eta)^3}\Bigg] = \frac{i}{2}\frac{1}{(i\epsilon\eta)} - i\left(\frac{-i}{2\epsilon}\right)\overline{q},\end{aligned}$$

and, after simplifying, this gives

$$\frac{\beta}{2\epsilon}\overline{q}' + \frac{\beta\tau}{\epsilon}\left[\frac{1}{2}\overline{q}'' - \frac{1}{\eta^3} + \mathcal{O}(\epsilon)\right] = \frac{1}{2\epsilon\eta} - \frac{1}{2\epsilon}\overline{q},$$

so that the equation for the leading-order inner solution is

$$\beta\overline{q}' + \beta\tau\left[\overline{q}'' - \frac{2}{\eta^3}\right] = \frac{1}{\eta} - \overline{q}. \tag{1.74}$$

By comparing with the form of the outer ansatz (1.55), we expect that in the limit that the inner solution tends to the outer region, it must also diverge like a factorial over power. If we expand

$$\overline{q} = \sum_{n=0}^{\infty}\frac{A_n\Gamma(n+1)}{\eta^{n+1}},$$

as $\eta \to \infty$, this gives from (1.74),

$$\begin{aligned}-\sum_{n=1}^{\infty}\frac{A_{n-1}(n)\Gamma(n)}{\eta^{n+1}} + \beta\tau\left[\sum_{n=2}^{\infty}\frac{A_{n-2}(n+1)n\Gamma(n+1)}{\eta^{n+1}} - \frac{2}{\eta^3}\right] \\ = \frac{1}{\eta} - \sum_{n=0}^{\infty}\frac{A_n\Gamma(n+1)}{\eta^{n+1}}.\end{aligned}$$

In the limit that $\eta \to \infty$, the first three orders give

$$1 - A_0 = 0 \qquad \Rightarrow \qquad A_0 = 1, \tag{1.75}$$

$$-\beta A_0 \Gamma(1) = -A_1 \Gamma(2) \qquad \Rightarrow \qquad A_1 = \beta, \tag{1.76}$$

$$-2\beta A_1 + \beta\tau[2A_0 - 2] = -2A_2 \qquad \Rightarrow \qquad A_2 = \beta^2, \tag{1.77}$$

while for $n \geq 3$,

$$A_n = \beta(A_{n-1} - \tau A_{n-2})\,. \tag{1.78}$$

Using $D_\pm$ from (1.40), we can show that the solution of the recurrence relation in (1.78) is

$$A_n = \frac{1}{\sqrt{\Delta}}\left\{\left(\frac{1}{D_-}\right)^n - \left(\frac{1}{D_+}\right)^n\right\} \tag{1.79}$$

with Δ given by (1.41). In order to perform the matching between inner and outer expansions, we first note that

$$\chi_\pm = -iD_\pm \log(-\zeta) \sim iD_\pm(\zeta + 1) = -D_\pm \epsilon\eta, \tag{1.80}$$

and then matching is done by applying Van Dyke's (1975) rule. The n^{th} term of the outer solution (n.t.o), written in inner variables and re-expanded to one term (1.t.i) is

$$q \xrightarrow{\text{(n.t.o)}} \epsilon^n q_n \sim \frac{\epsilon^n \Lambda\Gamma(n+1)}{\chi^{n+1}} \xrightarrow{\text{(1.t.i)}} \frac{(-1)^{n+1}\Lambda\Gamma(n+1)}{\epsilon D_\pm^{n+1}\eta^{n+1}} \tag{1.81}$$

where we have used the inner limits of χ from eqn (1.80). Similarly, the leading-order term of the inner region (1.t.i), re-expanded to the n^{th} term in the outer limit (n.t.o) has

$$q \xrightarrow{\text{(1.t.i)}} \frac{-i}{2\epsilon}\overline{q} \xrightarrow{\text{(n.t.o)}} -\frac{i}{2\epsilon}\frac{A_n\Gamma(n+1)}{\eta^{n+1}},$$

and using the exact solution of the recurrence relation in (1.79) requires

$$\Lambda_\pm = \pm\frac{i}{2}\frac{D_\pm}{\sqrt{\Delta}}. \tag{1.82}$$

This completes our determination of all the components of the high-order terms of (1.55), as well as the exponentials switched-on across Stokes lines from (1.70)–(1.71).

Indeed, from (1.57), we know that $\Theta = -iQ = -i\Lambda_\pm$, and thus, from the expressions in (1.82),

$$\Theta = -i\Lambda = \frac{\pm 1}{2}\left|\frac{D_\pm}{\sqrt{\Delta}}\right| \exp\left[i\left(\operatorname{Arg}(D_\pm) - \frac{\operatorname{Arg}(\Delta)}{2}\right)\right].$$

The singulant, χ, in eqn (1.61), can be written as

$$\chi_\pm = \Big[\pi\Re(D_\pm) + \Im(D_\pm)\log\zeta\Big] + i\Big[\pi\Im(D_\pm) - \Re(D_\pm)\log\zeta\Big]$$

where the branch of the logarithm is chosen to correspond to analytic continuation into the upper-half plane. Thus, remembering to reverse the sign of the capillary waves, we see from eqns (1.71) and (1.82) that the form of the waves are given by

$$\theta_\pm \sim \frac{2\pi\bar{\delta}}{\epsilon}\left|\frac{D_\pm}{\sqrt{\Delta}}\right| \exp\left[-\frac{\pi\Re(D_\pm)}{\epsilon}+\frac{\Im(D_\pm)\phi}{\epsilon}\right] \times \sin\left\{-\frac{\Re(D_\pm)\phi}{\epsilon}-\frac{\pi\Im(D_\pm)}{\epsilon}+\mathrm{Arg}(D_\pm)-\frac{\mathrm{Arg}(\Delta)}{2}\right\}, \quad (1.83)$$

after having multiplied by $\bar{\delta}$ (since we chose to drop primes following the expansion of eqn 1.47). A simple flux argument gives $\pi\bar{\delta} = 2\delta$, relating the step height in the physical and potential planes, and so we see that indeed the waves from the standard Fourier analysis (1.43) are the same as the waves from the exponential asymptotics (1.83).

1.6 DISCUSSION

What is the connection between the treatment of the low-Froude, low-Bond problem using traditional Fourier methods and our new methods in exponential asymptotics?

For both the Fourier method and the exponential asymptotics, the free-surface waves given in (1.43) and (1.83) are produced by deforming a path of integration through the relevant singularities—*explicitly* in Fourier-space for the former, and *implicitly* in the analytically continued domain for latter. We find, however, that when we use exponential asymptotics, concepts like the Stokes Phenomenon and optimal truncation can be clearly interpreted, but if one only see the problem through Fourier-tinted glasses, then these equivalent notions remain well obfuscated.

Consider the case that $\Delta > 0$. The analysis by exponential asymptotics clearly indicates that the formation of the gravity and capillary waves occurs upon crossing the point $\phi = 0$ on the free-surface, and this is reflected in the integration contour in the Fourier plane, which runs in the upper-half k-plane upstream, but switches into the lower-half k-plane downstream. However, for $\Delta < 0$, the exponential asymptotics clearly show that the capillary and gravity waves only appear on *either side* of the point $\phi = 0$. In particular, this seems to imply that for a small region near $\phi = 0$, the integration contour within Fourier space does not include the complex residue contributions of the four poles—*there are no waves after all!* The connection between the optimal truncation and Stokes smoothing procedure with the standard linearised Fourier theory as $\epsilon \to 0$ is no longer clear.

How does the infinitude of complex poles in the Fourier plane relate to the optimally truncated asymptotic solution? From (1.53), the low-Froude, low-Bond solution has

$$\theta = -\beta\epsilon\delta\left[\frac{\zeta}{(\zeta+1)^2}\right] + \mathcal{O}(\epsilon^2), \quad (1.84)$$

and this expression must be related to the infinite summation of the residues along the positive or negative imaginary axis of eqn (1.38), which we write as

$$\theta = -\beta\epsilon\delta \sum_{n=0}^{\infty} \left[\frac{\beta_n}{\cos(\pi\beta_n) g'(i\beta_n)} \right] e^{-\beta_n \phi} + \mathcal{O}(e^{-\chi/\epsilon}), \tag{1.85}$$

having multiplied by the size of the step δ. As $\epsilon \to 0$, the complex roots $\pm i\beta_n$ can be found by setting $\beta_n = n + d$ so that from eqn (1.31) we find

$$\pi d + \frac{1}{3}(\pi d)^3 + \mathcal{O}(d^5) = \beta^2\epsilon^2(n+d)\left[1 + \beta\tau\epsilon^2(n+d)^2 + \mathcal{O}(\epsilon^4, d^4)\right],$$

and d can be expanded as a (regular) perturbation series in powers of ϵ. Now if we substitute $\beta_n \sim n$ back into eqn (1.85), we find

$$\theta = -\beta\epsilon\delta \sum_{n=0}^{\infty} (-1)^{n+1} n\zeta^n + \mathcal{O}(\epsilon^2),$$

after making the substitution $\zeta = e^{\phi}$. In fact, we may truncate this sum at $n = \mathcal{N}$ with

$$\sum_{n=0}^{\mathcal{N}} (-1)^{n+1} n\zeta^n = \left[\frac{\zeta}{(\zeta+1)^2} \right] \left\{ 1 - (-\zeta)^{\mathcal{N}} + \mathcal{N}(-\zeta)^{\mathcal{N}} + (-1)^{\mathcal{N}} \mathcal{N} \zeta^{\mathcal{N}+1} \right\}.$$

Then selecting $\mathcal{N} \sim \log\epsilon / \log\zeta$, we have

$$\theta = -\beta\epsilon\delta \left[\frac{\zeta}{(\zeta+1)^2} \right] + \mathcal{O}(\epsilon^2).$$

What we have thus shown is that by adding $\mathcal{N}$ of the residues along the imaginary axis, we can reconstruct the *exact* form of the leading-order term of the asymptotic approximation (1.84) using only the leading order behaviour of β_n. For a general term of the optimally truncated approximation (1.63), we would need to also truncate the expansion of each residue,

$$\beta_n = \beta_n^{(0)} + \epsilon\beta_n^{(1)} + \epsilon^2\beta_n^{(2)} + \ldots,$$

and then add up a further truncated sum from eqn (1.85) in order to retrieve the precise form. But because this involves a composite function of many truncated sums, the full process is likely to be excessively complicated.

Ultimately, however, the bridge between Fourier analysis and exponential asymptotics becomes less important as we move on to study the nonlinear problem, where only the latter method is applicable. In the next chapter, we will show how exponential asymptotics can be used without first linearising for small obstructions, thus providing an asymptotic approximation valid for $\mathcal{O}(1)$ geometries. There, we shall see that the availability of multiple singularities in the geometry, coupled with the interplay of gravitational and cohesive effects, leads to the discovery of a remarkable set of new gravity-capillary waves.

For the finite-depth flow in a channel of height π, the dispersion relation and its derivative can be written as

$$g(k) = kF^2 - \tanh(\pi k)(Bk^2+1), \tag{1.86}$$
$$g'(k) = F^2 - \operatorname{sech}^2(\pi k)(Bk^2+1) - \tanh(\pi k)(2kB). \tag{1.87}$$

The nature of the zeros of the dispersion relation provide a classification of the linearised solutions in the (F, B) plane. For all values of F and B, $k = 0$ is a root of (1.86), but it plays no role unless $F = 1$. There are an infinite number of purely imaginary roots at $k = \pm i\beta_0, \pm i\beta_1, \ldots$, but these are generally unimportant (*cf.* Section 1.4.2). The relevant regions in the linear classification are shown in Figure 1.9.

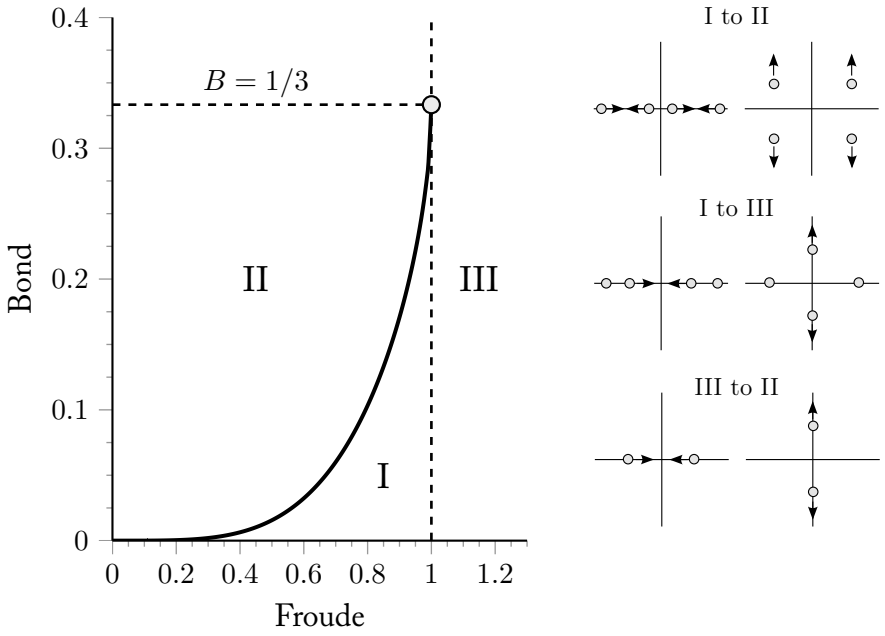

Figure 1.9: The three regions in (F, B) space which distinguish the linearised solutions are shown on the left. The transitions between the different regions can be understood by following the movements of the four (possibly repeated) wavenumbers in the complex complex k-plane, shown on the right.

First, consider Region I of the (F, B) plane. Here, the dispersion relation has four real roots: $k = \pm k_0$ and $k = \pm k_1$ where $0 < k_0 < k_1$; clearly, k_0 corresponds to the gravity waves and k_1 to the capillary waves and physically, we would expect capillary waves upstream and gravity waves downstream, and this subcritical region is the one relevant to Rayleigh's (1883) fishing-pole problem.

As $B \to 0$, $\pm k_1 \to \pm\infty$ and only the gravity waves remain. Alternatively, if we hold F fixed and increase B, then the roots coalesce at a critical value (corresponding to the dispersion curve $F = F_m$) and for B still larger, they split, forming four complex roots; here, we would expect localised solitary solutions. Physically, this bifurcation point corresponds to point where the group velocity of the wave equals the phase velocity, so that $k_0 = k_1 = k^*$ and critical dispersion curve $F = F_m$ is then defined by solving $g(k^*) = g'(k^*) = 0$.

Next, suppose we begin again in Region I, hold B fixed, and increase F. Then we find that the two gravity roots coalesce at the origin, and then

split, moving upwards and downwards on the imaginary axis. This bifurcation describes the more complex phenomena of the exponentially radiating waves of the fifth-order Korteweg-de Vries Equation.

Finally, if we begin in Region III with $B > 1/3$, and hold B fixed whilst decreasing F, we transition back to Region II. This corresponds to having the two capillary roots coalescing near the origin, and then splitting onto the imaginary axis.

PART II: NONLINEAR THEORY

2.1 INTRODUCTION

2

In the last chapter, we showed how techniques in exponential asymptotics could be used to derive the surface waves for flow over a small step; there, the geometry was replaced by a single source, from which gravity and capillary Stokes lines emerged, and an analysis of the associated Stokes Phenomenon revealed the smooth switching-on of exponentially small terms. In this chapter, we shall see how the same methods can be adopted to the study of waves induced by obstructions that *cannot* be considered small. For these *nonlinear* geometries, multiple singularities may exist, and this, combined with the competing effects of gravity and surface tension, leads to a much richer variety of possible surface waves.

2.2 MATHEMATICAL FORMULATION

We will briefly recapitulate the relevant equations, which parallel the ones presented in Sections 1.3 and 1.5 of Part I, but this time allowing for the possibility of flows over more general geometries. Consider steady, two-dimensional potential flow of an incompressible fluid with upstream velocity U, and a prescribed length scale L. The flow is non-dimensionalised with characteristic scales of U and L/π for the velocity and lengths, respectively, and the physical $z = x + iy$ plane is mapped to the complex potential $w = \phi + i\psi$ plane, then mapped again to the upper-half $\zeta = \xi + i\eta$ plane. The free-surface is then given by

$$\log q = -\frac{1}{\pi}\int_{-\infty}^{\infty} \frac{\theta(\xi')}{\xi' - \xi}\, d\xi', \tag{2.1}$$

$$\beta\epsilon\left[q^2\frac{dq}{d\phi}\right] - \beta\tau\epsilon^2\left[q^2\frac{d^2\theta}{d\phi^2} + q\frac{dq}{d\phi}\frac{d\theta}{d\phi}\right] = -\sin\theta, \tag{2.2}$$

where $F^2 = \beta\epsilon$ is the square of the Froude number, $B = \beta\tau\epsilon^2$ is the Bond number, and for hodograph variables $\log(dw/dz) = \log q - i\theta$, where q is the fluid speed and θ is the angle the streamlines make with the x-axis. This set-up is presented in Figure 2.1.

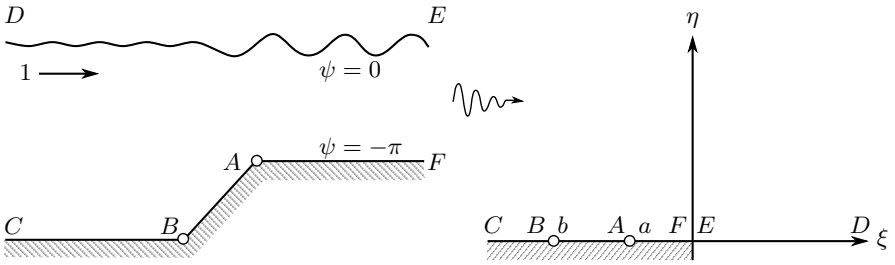

Figure 2.1: We consider a typical flow over an obstruction. The flow in the physical xy-plane (left) is first mapped to the potential $w = \phi + i\psi$ plane, then again mapped to the upper-half $\zeta = \xi + i\eta$ plane (right). For flow in a channel, the latter map is given by $\zeta = e^{-w}$.

Our analysis must then be extended to the complexification of the free-surface (originally, q and θ for $\xi \in \mathbb{R}^+$). Complexifying the free-surface into

the upper-half ξ-plane and relabeling $\xi \mapsto \zeta$ and $\phi \mapsto w$ gives

$$\log q - i\theta = -\frac{1}{\pi}\int_{-\infty}^{0} \frac{\theta(\xi')}{\xi' - \zeta}\, d\xi' + \mathscr{H}[\theta(\zeta)], \tag{2.3}$$

$$\epsilon\left[q^2\frac{dq}{dw}\right] - \epsilon^2\tau\left[q^2\frac{d^2\theta}{dw^2} + q\frac{dq}{dw}\frac{d\theta}{dw}\right] = -\frac{1}{\beta}\sin\theta. \tag{2.4}$$

where $\mathscr{H}$ denotes the Hilbert transform operator on the semi-infinite interval $\xi \geq 0$ which corresponds to the free-boundary, *i.e.*

$$\mathscr{H}[\theta(\zeta)] = -\frac{1}{\pi}\int_{0}^{\infty} \frac{\theta(\xi')}{\xi' - \zeta}\, d\xi'. \tag{2.5}$$

2.2.1 The step flow

The methodology developed throughout this chapter is applicable to most general non-surface-piercing geometries, which are defined by imposing the value of θ along the negative ζ axis. With minimal modification, it can also be applied to surface-piercing obstructions (such as for a ship), the only significant difficulty being the assumptions-to-make near the point of contact. Thus for a significant portion of the analysis to follow, we will not constrain ourselves to choosing any one particular geometry.

However, for concreteness and illustration, we will often take as an example the step in a channel, with $\zeta = e^{-w}$, and

$$\theta = \begin{cases} 0 & \text{for } \zeta < -b \\ \sigma\pi & \text{for } \zeta \in (-b, -a) \\ 0 & \text{for } \zeta \in (-b, 0) \end{cases} \tag{2.6}$$

where $0 < a < b$. We will always imagine a stepping *up* (from left-to-right), with b associated with the stagnation point, a associated with the corner, and therefore $0 < \sigma < 1$. In the next section, we will see that at zero Froude and Bond numbers, the leading-order solution is provided by substituting the above values for θ along $\zeta < 0$, as well as $\theta = 0$ for $\zeta > 0$ into the boundary integral equation (2.3), giving

$$q \sim \left(\frac{\zeta + b}{\zeta + a}\right)^{\sigma} \qquad \text{and} \qquad \theta = 0 + \mathcal{O}(\epsilon), \tag{2.7}$$

which is often termed the *rigid-wall flow*, as it is equivalent to replacing the free-surface by the rigid wall, $\theta = 0$.

2.3 Asymptotic approximation

Substituting the usual perturbation expansion,

$$\theta = \sum_{n=0}^{\infty} \epsilon^n \theta_n \quad \text{and} \quad q = \sum_{n=0}^{\infty} \epsilon^n q_n \tag{2.8}$$

into eqns (2.3) and (2.4) yields at $\mathcal{O}(1)$,

$$\theta_0 = 0, \tag{2.9}$$

$$\log q_0 = \left(\frac{\zeta + b}{\zeta + a}\right)^{\sigma}, \tag{2.10}$$

and at $\mathcal{O}(\epsilon)$,

$$q_0^2 \frac{dq_0}{dw} = -\frac{1}{\beta}\theta_1, \tag{2.11}$$

$$\frac{q_1}{q_0} - i\theta_1 = \mathscr{H}[\theta_1(\zeta)]. \tag{2.12}$$

The leading order expressions in (2.9)–(2.10) simply correspond to the zero-Froude, zero-Bond solution, which is equivalent to replacing the free-surface by a rigid wall, as discussed for eqn (2.7). The full expressions for the higher $\mathcal{O}(\epsilon^n)$ terms are prohibitively complicated, but we will mainly be concerned with the limit $n \to \infty$ and so we may proceed as follows.

The complexification of the leading-order free surface, $q_0(w)$ will typically contain singularities, identifiable with singularities in the flow-domain, such as those corresponding to corners or stagnation points. However, because all the higher-order problems are linear, no new singularities can be introduced and thus, for all n, the singular points of $q_n(w)$ must be those *same* points as for $q_0(w)$.

Now if we examine the dynamic condition (2.4), we can see that each successive term of the asymptotic approximation will require the derivative of the previous term. Thus if q_n contains a singularity of the form $1/(w-w^*)^n$, q_{n+1} will contain a singularity of the form $n/(w-w^*)^{n+1}$. Then as $n \to \infty$, we can expect the late terms to behave like factorial over power, or

$$\theta_n \sim \frac{\Theta(w)\Gamma(n+\gamma)}{\chi(w)^{n+\gamma}} \quad \text{and} \quad q_n \sim \frac{Q(w)\Gamma(n+\gamma)}{\chi(w)^{n+\gamma}}. \tag{2.13}$$

With this ansatz in mind, we can now pinpoint the necessary terms required at $\mathcal{O}(\epsilon^n)$. In the limit that $n \to \infty$, terms like $q_m q_n$ for m finite dominate terms with smaller indices in n, such as $q_m q_{n-1}$. Moreover, differentiating a term increases the order (in n) by 1, so a term like $\epsilon dq_{n-1}/dw$ is of the same order as q_n. This behaviour is also easily seen in terms of the Gamma function, with for example,

$$\frac{dq_n}{dw} \sim -\frac{Q\Gamma(n+\gamma+1)}{\chi^{n+\gamma+1}}\left(\frac{d\chi}{dw}\right) + \frac{dQ}{dw}\frac{\Gamma(n+\gamma)}{\chi^{n+\gamma}},$$

and

$$\frac{d^2q_n}{dw^2} \sim \frac{Q\Gamma(n+\gamma+2)}{\chi^{n+\gamma+2}}\left(\frac{d\chi}{dw}\right)^2 - \frac{\Gamma(n+\gamma+1)}{\chi^{n+\gamma+1}}\left(Q\frac{d^2\chi}{dw^2} + 2\frac{dQ}{dw}\frac{d\chi}{dw}\right) + \frac{d^2Q}{dw^2}\frac{\Gamma(n+\gamma)}{\chi^{n+\gamma}}.$$

The relevant terms at $\mathcal{O}(\epsilon^n)$ of the boundary integral equation (2.3) are thus

$$\frac{q_n}{q_0} - \frac{q_{n-1}q_1}{q_0^2} + \ldots - i\theta_n = \mathscr{H}[\theta_n(\zeta)],$$

for $n \geq 2$. As was explained in the discussion leading up to eqn (1.57) in the previous chapter, as $n \to \infty$, the terms on the right-hand side of this equation are exponentially subdominant to those on the left. Thus,

$$\theta_n \sim -i\frac{q_n}{q_0} + \frac{iq_1q_{n-1}}{q_0^2} + \ldots \quad \text{as } n \to \infty, \tag{2.14}$$

or,

$$q_n \sim iq_0\theta_n + i\theta_{n-1}q_1 + \ldots \quad \text{as } n \to \infty. \tag{2.15}$$

As for Bernoulli's Equation (2.4), we will use eqn (2.15) to replace q_n with θ_n, after which the relevant terms at $\mathcal{O}(\epsilon^n)$ are

$$\overbrace{\left[iq_0^3\right]\theta'_{n-1} - \left[\tau q_0^2\right]\theta''_{n-2} + \left[\frac{1}{\beta}\right]\theta_n}^{\text{first and second order as } n\to\infty}$$
$$+ \underbrace{\left[3iq_0^2q_0'\right]\theta_{n-1} + \left[3iq_0^2q_1 - \tau q_0q_0'\right]\theta'_{n-2} - \left[2\tau q_0q_1\right]\theta''_{n-3}}_{\text{second order as } n\to\infty} = 0. \tag{2.16}$$

Using the ansatz (2.13) in the above equation, we have at leading order as $n \to \infty$,

$$-iq_0^3\chi' - \tau q_0^2(\chi')^2 + \frac{1}{\beta} = 0, \tag{2.17}$$

which is simply solved to give

$$\frac{d\chi}{dw} = -i\left[\frac{q_0^2 \pm \sqrt{\Delta}}{2\tau q_0}\right], \tag{2.18}$$

where

$$\Delta = q_0^4 - A \qquad \text{and} \qquad A = \frac{4\tau}{\beta}. \tag{2.19}$$

Remember that $\chi(w)$ is the portion of the ansatz (2.13) that expresses the singularities of the higher order terms. Since $\chi(w^*) = 0$ for one of these singularities, w^*, we may express

$$\chi_\pm = -i\int_{w^*}^{w}\left[\frac{q_0^2 \pm \sqrt{\Delta}}{2\tau q_0}\right]\, d\varphi, \tag{2.20}$$

and we expect to find a series of terms like (2.13) corresponding to each singularity of q_0. By taking the limit $\tau \to 0$ and comparing with Chapman and Vanden-Broeck (2002; 2006), we see that the positive sign corresponds to capillary waves and the negative sign to gravity waves. Now returning to the dynamic condition (2.16) and with the ansatz, we find at next order in n:

$$\left[iq_0^3\right]\Theta' - \left[\tau q_0^2\right]\left\{-2\chi'\Theta' - \chi''\Theta\right\} + \left[3iq_0^2q_0'\right]\Theta$$
$$+ \left[3iq_0^2q_1 - \tau q_0q_0'\right]\left\{-\chi'\Theta\right\} - \left[2\tau q_0q_1\right]\left\{(\chi')^2\Theta\right\} = 0. \tag{2.21}$$

We may write this as

$$\frac{\Theta'}{\Theta} = -\frac{1}{4}\frac{\Delta'}{\Delta} \pm \frac{\Delta'}{2\sqrt{\Delta(\Delta+A)}} + \frac{iq_1}{2\tau}\left\{1 \pm \frac{\Delta+2A}{\sqrt{\Delta(\Delta+A)}}\right\}, \tag{2.22}$$

or after integrating,

$$\Theta = \frac{\left(\sqrt{\Delta+A}+\sqrt{\Delta}\right)^{\pm 1}\Lambda}{\Delta^{1/4}} \times \exp\left[\frac{i}{2\tau}\int_{w^\star}^{w} q_1\left\{1 \pm \frac{\Delta+2A}{\sqrt{\Delta(\Delta+A)}}\right\}\, d\varphi\right], \tag{2.23}$$

where Λ is a constant and we may begin the integration at any arbitrary point $w = w^\star$ where the integral is defined (often w^* is a natural choice for $w^\star$, but the integral may not exist at w^*). Taking the limit of $\tau \to 0$ and the negative sign gives

$$\Theta = -\frac{\Lambda i}{2q_0^3}\exp\left[-3i\int_{w^\star}^{w}\frac{q_1}{q_0^4}\, d\varphi\right],$$

which differs from Chapman & Vanden-Broeck (2006) by a factor of a half (*i.e.* our Λ is their 2Λ). Finally, eqn (2.15), allows us to relate Q with Θ, and

$$Q \sim iq_0\Theta. \tag{2.24}$$

2.4 Optimal truncation and Stokes line smoothing

The underlying divergence of the asymptotic expansions will cause the *Stokes Phenomenon* to occur: as the complexified asymptotic solution crosses a critical line (the *Stokes line*), a small exponential switches on.

Now, because the switching-on of the exponential is almost always via an error function (Berry, 1989), as in eqn (1.69), the optimal truncation and Stokes smoothing procedure will be very similar to the one we performed in Chapter 1. To begin, we *truncate* the asymptotic series at $n = \mathcal{N}$ so that

$$\theta = \sum_{n=0}^{\mathcal{N}-1}\epsilon^n\theta_n + R_{\mathcal{N}} \qquad \text{and} \qquad q = \sum_{n=0}^{\mathcal{N}-1}\epsilon^n q_n + S_{\mathcal{N}}, \tag{2.25}$$

where the remainders are related by eqn (2.15) and thus

$$\frac{S_{\mathcal{N}}}{q_0} - \frac{\epsilon q_1 S_{\mathcal{N}}}{q_0^2} - \frac{\epsilon^{\mathcal{N}} q_1 q_{\mathcal{N}-1}}{q_0^2} + \ldots = iR_{\mathcal{N}}. \tag{2.26}$$

We will substitute the truncated sums (2.25) into Bernoulli's Equation (2.4) and in doing so, we will see two separate types of terms, the ones involving only q_n and θ_n, and the ones involving the remainders, $R_{\mathcal{N}}$ and $S_{\mathcal{N}}$.

Let us first study the terms involving the remainders. The remainder $S_{\mathcal{N}}$ can be written in terms of $R_{\mathcal{N}}$ by (2.26) and after making this substitution, we are particularly interested in the leading-order terms, which are indicated by factors of $R_{\mathcal{N}}$, $\epsilon R'_{\mathcal{N}}$, and $\epsilon^2 R''_{\mathcal{N}}$, and second-order terms, which are indicated

by factors of $\epsilon R_{\mathcal{N}}$, $\epsilon^2 R'_{\mathcal{N}}$, and $\epsilon^3 R''_{\mathcal{N}}$. The relevant terms from Bernoulli's Equation are then given by the linear operator defined by

$$\mathcal{L}(R_{\mathcal{N}};\epsilon) = \left[iq_0^3\right]\epsilon R'_{\mathcal{N}} - \left[\tau q_0^2\right]\epsilon^2 R''_{\mathcal{N}} + \left[\frac{1}{\beta}\right]R_{\mathcal{N}} + \left[3iq_0^2 q_0'\right]\epsilon R_{\mathcal{N}} + \left[3iq_0^2 q_1 - \tau q_0 q_0'\right]\epsilon^2 R'_{\mathcal{N}} - \left[2\tau q_0 q_1\right]\epsilon^3 R''_{\mathcal{N}}, \quad (2.27)$$

which is exactly the same form as the left of our eqn (2.16). We then introduce the Stokes smoothing parameter, $\mathcal{S} = \mathcal{S}(w)$, and set

$$\begin{aligned} R_{\mathcal{N}} &= \mathcal{S}\left[\Theta e^{-\chi/\epsilon}\right], \\ R'_{\mathcal{N}} &= \mathcal{S}\left[\Theta e^{-\chi/\epsilon}\right]' + \mathcal{S}'\left[\Theta e^{-\chi/\epsilon}\right], \\ R''_{\mathcal{N}} &= \mathcal{S}\left[\Theta e^{-\chi/\epsilon}\right]'' + 2\mathcal{S}'\left[\Theta e^{-\chi/\epsilon}\right]' + \mathcal{S}''\left[\Theta e^{-\chi/\epsilon}\right]. \end{aligned}$$

We know that the WKB ansatz $\Theta e^{-\chi/\epsilon}$ solves $\mathcal{L}(\bullet;\epsilon)$, so only terms involving derivatives of $\mathcal{S}$ will be left. After some computation, we find to leading order,

$$\mathcal{L}(R_{\mathcal{N}};\epsilon) \sim \epsilon\Theta e^{-\chi/\epsilon}\frac{d\mathcal{S}}{dw}\left[iq_0^3 + 2\tau q_0^2\chi'\right],$$

and writing

$$\frac{d\mathcal{S}}{dw} = \chi'\frac{d\mathcal{S}}{d\chi}$$

and using eqn (2.17) gives

$$\mathcal{L}(R_{\mathcal{N}};\epsilon) \sim \epsilon\Theta e^{-\chi/\epsilon}\frac{d\mathcal{S}}{d\chi}\left[\frac{1}{\beta} + \tau q_0^2(\chi')^2\right].$$

Now let us turn to the terms involving q_n and θ_n: when the truncated sum in (2.25) is substituted into (2.4), terms of $\mathcal{O}(\epsilon^{\mathcal{N}-1})$ will automatically be satisfied, and this process leaves us only with the remnant $\mathcal{O}(\epsilon^{\mathcal{N}})$ contributions from the inertial terms, as well as the $\mathcal{O}(\epsilon^{\mathcal{N}})$ and $\mathcal{O}(\epsilon^{\mathcal{N}+1})$ contributions from the surface-tension terms; this, we may write as

$$\begin{aligned} \epsilon^{\mathcal{N}}\left[q_0^2\frac{dq_{\mathcal{N}-1}}{dw} + \ldots\right] - \epsilon^{\mathcal{N}}\tau\left[q_0^2\frac{d^2\theta_{\mathcal{N}-2}}{dw^2} + \ldots\right] - \epsilon^{\mathcal{N}+1}\tau\left[q_0^2\frac{d^2\theta_{\mathcal{N}-1}}{dw^2} + \ldots\right] \\ = \epsilon^{\mathcal{N}}\left[-\frac{\theta_{\mathcal{N}}}{\beta} + \ldots\right] - \epsilon^{\mathcal{N}+1}\tau\left[q_0^2\frac{d^2\theta_{\mathcal{N}-1}}{dw^2} + \ldots\right], \quad (2.28) \end{aligned}$$

and thus in total we have

$$\mathcal{L}(R_{\mathcal{N}};\epsilon) \sim \epsilon^{\mathcal{N}}\left(\frac{\theta_{\mathcal{N}}}{\beta} + \epsilon\tau q_0^2\frac{d^2\theta_{\mathcal{N}-1}}{dw^2}\right). \quad (2.29)$$

Since we are interested in the limit $\epsilon \to 0$ when $\mathcal{N} \to \infty$, we can substitute the late-orders ansatz of (2.13) into the right-hand side of (2.29), giving

$$\mathcal{L}(R_{\mathcal{N}};\epsilon) \sim \frac{\epsilon^{\mathcal{N}}\Theta\Gamma(\mathcal{N}+\gamma)}{\chi^{\mathcal{N}+\gamma}}\left(\frac{1}{\beta} + \tau q_0^2(\chi')^2\frac{\epsilon(\mathcal{N}+\gamma+1)}{\chi}\right),$$

The optimal truncation point is at $\lceil |\chi|/\epsilon \rceil$, so we will write $\chi = re^{i\vartheta}$ and thus $\mathcal{N} = r/\epsilon + \rho$ where $\rho \in [0,1)$. Stirling's formula then gives

$$\Gamma\Big(\mathcal{N}+\gamma\Big) = \Gamma\Big(r/\epsilon+\rho+\gamma\Big) \sim \sqrt{2\pi}e^{-r/\epsilon}\left(\frac{r^{\mathcal{N}+\gamma}}{\epsilon^{\mathcal{N}}}\right)\frac{r^{-1/2}}{\epsilon^{\gamma-1/2}}.$$

Writing

$$\frac{d}{d\chi} = -\frac{e^{-i\vartheta}}{r}\frac{d}{d\vartheta},$$

then we have,

$$\frac{d\mathcal{S}}{d\vartheta}\left[\frac{1}{\beta}+\tau q_0^2(\chi')^2\right] \sim \frac{\sqrt{2\pi r}}{\epsilon^{\gamma+1/2}}\left[\frac{1}{\beta}+\frac{\tau q_0^2(\chi')^2}{e^{i\theta}}\right]\left(e^{-i\vartheta}\right)^{r/\epsilon+\rho+\gamma} e^{re^{i\vartheta}/\epsilon}e^{-r/\epsilon}.$$

The exponential factor on the right is exponentially small, except near the Stokes line $\vartheta = 0$, where the critical scaling occurs with $\vartheta = \sqrt{\epsilon}\overline{\vartheta}$, and here,

$$\exp\left\{-\frac{r}{\epsilon}\Big(1-\cos\vartheta\Big)+i\left(\frac{r\sin\vartheta}{\epsilon}-\vartheta\Big(\frac{r}{\epsilon}+\rho+\gamma+1\Big)+\frac{\pi}{2}\right)\right\} \sim \exp\left\{-\frac{r\overline{\vartheta}^2}{2}+\frac{\pi i}{2}+\mathcal{O}(\sqrt{\epsilon})\right\}.$$

In total then

$$\frac{d\mathcal{S}}{d\overline{\vartheta}} \sim \frac{\sqrt{2\pi r i}}{\epsilon^{\gamma}}\exp\left(-\frac{r\overline{\vartheta}^2}{2}\right),$$

and we have recovered the typical error function expression for the Stokes multiplier, $\mathcal{S}$. We now integrate this expression across the Stokes line from upstream, or $\overline{\vartheta} = \infty$ (indicated with a $+$ below), to downstream, or $\overline{\vartheta} = -\infty$ (indicated with a $-$ below). The apparent jump in the remainder is then

$$\Big[R_{\mathcal{N}}\Big]_+^- \sim -\frac{2\pi i\Theta}{\epsilon^{\gamma}}\exp\Big[-\frac{\chi}{\epsilon}\Big], \tag{2.30}$$

with a similar exponentially small correction to q given by

$$\Big[S_{\mathcal{N}}\Big]_+^- \sim -\frac{2\pi i Q}{\epsilon^{\gamma}}\exp\Big[-\frac{\chi}{\epsilon}\Big]. \tag{2.31}$$

Remember that to finalise the analysis, we need to also complexify the free boundary into the lower-half plane. This analogous process yields the functional complex conjugates of (2.31) and (2.30), and thus the *total* contribution along the free-surface is twice the real parts of (2.31) and (2.30),

$$q_{\text{exp}} \sim -\frac{4\pi}{\epsilon^{\gamma}}\Im\Big(Qe^{-\chi/\epsilon}\Big) \tag{2.32}$$

$$\theta_{\text{exp}} \sim -\frac{4\pi}{\epsilon^{\gamma}}\Im\Big(\Theta e^{-\chi/\epsilon}\Big). \tag{2.33}$$

It will be convenient for us to also write $\chi = \chi_1 + i\chi_2$, splitting its real and imaginary parts; then eqn (2.32) can be placed in the form

$$q_{\text{exp}} \sim \left[\frac{4\pi|Q(\zeta)|e^{-\frac{\chi_1}{\epsilon}}}{\epsilon^{\gamma}}\right]\Im\Big[e^{i\left(-\frac{\chi_2}{\epsilon}+\text{Arg}[Q(\zeta)]+\pi\right)}\Big]. \tag{2.34}$$

Lastly, we will re-introduce our notation for the switching-on mechanism, which was used in Part I. We will write, for example,

$$\sum_n \epsilon^n q_n \xrightarrow[[Bs\to C]]{\text{Stag.}} \sum_n \epsilon^n q_n + q_{\text{exp}}$$
$$\sum_n \epsilon^n q_n \xrightarrow[[Bs\to G]]{\text{Corn.}} \sum_n \epsilon^n q_n + q_{\text{exp}},$$

and the arrow notation with, for example, $\xrightarrow[[Bs\to C]]{\text{Stag.}}$ should be read as "the base series turns on a capillary wave as the Stokes line from the stagnation point is crossed".

2.5 INNER LIMITS OF χ AND STOKES LINES

In the low-Froude, low-Bond limit, we can think of the exponentially small free-surface waves as having been generated by singularities in the flow-domain. For example, in the case of the step (eqn 2.7), both the corner $\zeta = -a$, and stagnation point $\zeta = -b$ can be linked to the creation of waves. In Section 2.6, we will see that there is another type of singularity which is responsible for generating waves, *turning points*, which have no direct physical interpretation in terms of the geometry, but rather, correspond to locations where the capillary and gravity wavenumbers coalesce (as at the minimum of the linear dispersion curve). In this section, we will study the former type of singularity; we will consistently refer to the latter singularities as *turning points*, leaving a discussion of their effects for Section 2.6.

Now in general, we will be interested in the behaviour of the outer solutions, derived in Section 2.3, as we tend towards a general flow-field singularity, $w = w^*$. Thus, the nature of the solutions q_0 (and thus q_n) will depend on the *type* of singularity found.

Near singularities, $w - w^* = \text{const} \times (z - z^*)^\kappa$ for some κ. In the case of stagnation points, $\kappa = 2$, while for corner singularities, $\kappa = \pi/\nu$, where ν is the in-fluid angle of the corner. In the analytic continuation of the free boundary, we have

$$\frac{dw}{dz} \sim q_0 e^{-i\theta_0} = q_0 = c(z - z^*)^{\kappa-1} = c(w - w*)^{(\kappa-1)/\kappa}, \tag{2.35}$$

where c is constant, and thus the speed of the flow in the outer region is given by

$$q \sim c(w - w^*)^\alpha \equiv cW^\alpha \tag{2.36}$$

as $w \to w^*$, where $\alpha = (\kappa-1)/\kappa$ and we have defined the shifted coordinate, W. We will come back to this expression again and again, and it will be convenient for us to go between the three coordinate systems, z, w, and ζ near the point of interest. We will write ζ^* as the corresponding singularity

in ζ and then using the fact that $\zeta = e^{-w}$, we have

$$\begin{aligned} w - w^* &\sim \left[\frac{-1}{\zeta^*}\right](\zeta - \zeta^*), \\ z - z^* &\sim \left[\frac{-1}{c\alpha}\right](w - w^*)^{1-\alpha}, \\ z - z^* &\sim \left[\frac{(-1)^{-\alpha}}{c\alpha\zeta^{*1-\alpha}}\right](\zeta - \zeta^*)^{1-\alpha}, \end{aligned}$$

for the case of flow over a step. Using (2.18) and the limiting form for q_0 in (2.36), we see that $\chi(w)$ must exhibit different limiting behaviours as $w \to w^*$, depending on which sign of the square root is chosen and whether α is positive or negative. Simplification yields

$$\chi \sim \begin{cases} \left[\dfrac{\mp 1}{c\sqrt{\beta\tau}(1-\alpha)}\right] W^{1-\alpha} \equiv X_1^{\pm} W^{1-\alpha} & \text{for } \alpha > 0 \\ \left[\dfrac{-i}{c^3\beta(1-3\alpha)}\right] W^{1-3\alpha} \equiv X_2\, W^{1-3\alpha} & \text{for gravity and } \alpha < 0 \\ \left[\dfrac{-ic}{\tau(\alpha+1)}\right] W^{\alpha+1} \equiv X_3\, W^{\alpha+1} & \text{for capillary and } \alpha < 0 \end{cases} \tag{2.37}$$

as $W \to 0$, where we have defined the constants X_1, X_2, and X_3 for later use. Note that the $\mp$ sign in the first line is due to the fact that $\pm\sqrt{\Delta} = \pm\sqrt{q_0^4 - A} \sim \mp i\sqrt{A}$ because the argument of Δ is negative as the critical point is approached from above.

For $\alpha < 0$, the choice of the negative sign for the square root leads to gravity waves, whereas the positive sign is associated with capillary waves; this is clear from the appearance of either β (gravity) or τ (capillary) in the coefficients of χ, but can also be understood by taking the zero capillary limit of $\tau \to 0$, and noticing that the capillary root in (2.17) disappears to infinity, leaving us with only the gravity root.

For all values of $\alpha \in (-1, 1)$, the zeros of χ in (2.37) represent singularities in the analytically continued domain, and are thus accompanied by Stokes lines. However, the existence of a Stokes line does not guarantee the appearance of surface waves; indeed there are cases where the associated Stokes line fails to intersect the free-surface, as well as cases where the line lies on a different Riemann sheet altogether—these issues are examined in the next section.

2.5.1 Stokes line analysis

In this section we derive necessary conditions for a Stokes line to emerge from a singularity on the relevant Riemann sheet. Whether such a line actually encounters the free-surface ($\zeta \in \mathbb{R}^+$) is a global function of the leading-order flow and in general, must be checked by evaluating the integral in (2.20).

We begin with the corner analysis. From (2.7), then, we know that $\alpha =$

$-\sigma \in (-1, 0)$ and $c \in \mathbb{R}^+$, and in the notation of (2.37),

$$\chi \sim \left\{ \begin{array}{ll} |X_2| e^{-\pi i/2} W^{1-3\alpha} & \text{for gravity} \\ |X_3| e^{-\pi i/2} W^{\alpha+1} & \text{for capillary} \end{array} \right\} \quad \text{as } W \to 0. \tag{2.38}$$

Thus the condition that χ is real and positive along Stokes lines requires $W^{1-3\alpha}$ (gravity) and $W^{\alpha+1}$ (capillary) to be imaginary and positive. Let us write $\mathrm{Arg}(W) = \vartheta_{\text{grav}}$ for the local angle of a gravity Stokes line and $\mathrm{Arg}(W) = \vartheta_{\text{cap}}$ for the local angle of a capillary Stokes line. Taking the first solution from the positive W-axis yields the pair

$$\vartheta_{\text{grav}} = \frac{\pi}{2(1-3\alpha)} \qquad \text{and} \qquad \vartheta_{\text{cap}} = \frac{\pi}{2(\alpha+1)}.$$

As α decreases from 0 to -1, the gravity Stokes line simply increases from $\theta_g = \pi/2$ to $\pi/8$. However, for the same range in α, θ_c begins at $\pi/2$ and reaches π at $\alpha = -1/2$. For values of α smaller than this one, the Stokes line lies in the lower-half plane and is thus ignored[†]. By taking the local analysis to next order, it can be shown that if the Stokes line leaves along the boundary (as in the case for $\alpha = -1/2$), then it must remains on the boundary until it (potentially) encounters another critical point.

[†] Here, we ignore the possibility of a Stokes line emerging from the lower-half plane and crossing into the upper-half plane. These and other *global* issues are further discussed in the final discussion at the end of this chapter.

For the case of the stagnation point, $\alpha \in (0, 1)$ and $c = |c| e^{-\pi i \sigma}$, and thus

$$\chi_\pm \sim \mp |X_1| e^{\pi i \sigma} W^{1-\sigma}, \qquad \text{as } W \to 0.$$

The requirement for a Stokes line is then

$$\vartheta_{\text{grav}} = \pi \left(\frac{2k - \sigma}{1 - \sigma} \right) \quad \text{and} \quad \vartheta_{\text{cap}} = \pi \left(\frac{2k - 1 - \sigma}{1 - \sigma} \right),$$

for $k \in \mathbb{Z}$. For gravity waves, there are no relevant Stokes lines lying in the upper-half plane. For capillary waves, the only relevant value of k is 1, which shows that there exists a Stokes line along $\theta = \pi$ for all shapes. However, a secondary analysis to next order in w shows that the Stokes line which initially tends along $\theta = \pi$ lifts off the boundary.

To summarise, given a step-up obstruction with initial inclination σ, the following occurs: first, the stagnation point, $\zeta = -b$ *always* produces a capillary Stokes line; second, the corner, $\zeta = -a$ *always* produces a gravity Stokes line, but only produces a capillary Stokes line if $\sigma > 1/2$. Table 2.1 provides an illustration of our local Stokes line analysis.

2.6 TURNING POINTS AND THEIR STOKES LINES

As given in eqn (2.19), the turning points are found at

$$\Delta = q_0^4 - A = q_0^4 - \frac{4\tau}{\beta} = 0, \tag{2.39}$$

and represent locations where the exponentially small gravity waves are of the same order as the capillary waves. Like the Airy equation studied in the previous chapter, these points can lead to one wave switching on another.

Local Power α	Grav. Stokes ϑ_{grav}	Cap. Stokes ϑ_{cap}	Sketch
-1	$\frac{\pi}{8}$	none	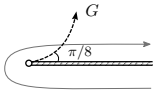
$\left(-1, \frac{1}{2}\right)$	$\left(\frac{\pi}{8}, \frac{\pi}{5}\right)$	none	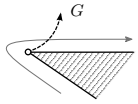
$-\frac{1}{2}$	$\frac{\pi}{5}$	π	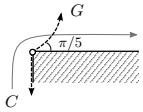
$\left(-\frac{1}{2}, 0\right)$	$\left(\frac{\pi}{5}, \frac{\pi}{2}\right)$	$\left(\pi, \frac{\pi}{2}\right)$	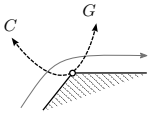
0	$\frac{\pi}{2}$	$\frac{\pi}{2}$	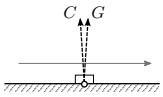
$\left(0, 1\right)$	none	π	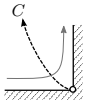

Table 2.1: This table indicates the local angle of a Stokes line as it emerges from a singularity for which the complex velocity behaves like $dw/dz \sim$ constant $\times$ $(w - w^*)^\alpha$. Note that at $\alpha = 0$, there is no singularity, so the corresponding entry instead refers to the limiting process as $\alpha \to 0$ from above.

However, in solving $\Delta = 0$, there is the potential for a great deal of confusion since we may be dealing with the inversion of complicated composite functions with branch cuts. The general rule is that, if we write $q_0 = \mathcal{Z}^\sigma$, then when we solve $\Delta(\mathcal{Z}) = 0$, we must then make sure that (a) $\mathcal{Z}$ remains on the same branch originally defined (that is, q_0 remains real and positive on $\zeta \in \mathbb{R}^+$) and (b) We remain in the upper half ζ plane. The solution to (2.39) is then

$$(\mathcal{Z}^\sigma)^4 = A \Rightarrow \mathcal{Z} = |A|^{1/4\sigma} e^{2\pi i k/4\sigma}, \quad \text{for } k \in \mathbb{Z}. \tag{2.40}$$

It is not quite correct to ignore the order of operations and take powers of powers, as different orders can result in certain solutions falling on different branches. Depending on the choice of σ, then, there may be an infinitude of possible solutions (particularly if σ is irrational!). However, we can write (2.40) as so and check the validity of the roots *a posteriori*.

Again, we take the step flow corresponding to eqn (2.7) as an example. Then we may write

$$\zeta = \frac{a\mathcal{Z} - b}{1 - \mathcal{Z}},$$

where we have chosen the branch cut in ζ to lie along $(-b, -a)$, and so the corresponding cut in $\mathcal{Z}$ is taken along the negative real axis. There are three solutions of immediate importance, which we denote as $\zeta = \zeta_0, \zeta_{-1}$, and ζ_1, corresponding to $k = 0, -1$, and 1 in eqn (2.40), respectively, and we study their motions as A and σ vary.

First consider the real solution, ζ_0, and any $\sigma \in (0,1)$. The evolution of the turning point as A is increased from zero to infinity is depicted in the smaller illustrations of Figure 2.3, labeled from ❶ to ❻. In particular, ζ_0 goes through the following stages:

A	Evolution of the turning point, ζ_0
0	Lies directly on the stagnation point, $\zeta_0 = -b$
$\big(0,1\big)$	Decreases along the negative real axis to negative infinity
$\big(1,(b/a)^{4\sigma}\big)$	Decreases along the positive real axis towards to the origin
$\big((b/a)^{4\sigma},\infty\big)$	Decreases along the negative real axis towards the corner, $\zeta = -a$

Next, let us consider the complex solutions ζ_{-1} and ζ_1. These solutions correspond to the first nontrivial roots of eqn (2.40) rotated from the positive axis. Again, we begin at $A = 0$, where all the solutions coalesce at the stagnation point, $\zeta = -b$. For fixed $\sigma \in (1/2,1)$ and as A varies from in $[0,\infty)$, the roots ζ_1 vary along families of arcs between $\zeta = -b$ and $\zeta = -a$ in the upper-half plane, with a mirror image for ζ_{-1} in the lower-half plane. These arcs are shown in the uppermost illustration of Figure 2.2.

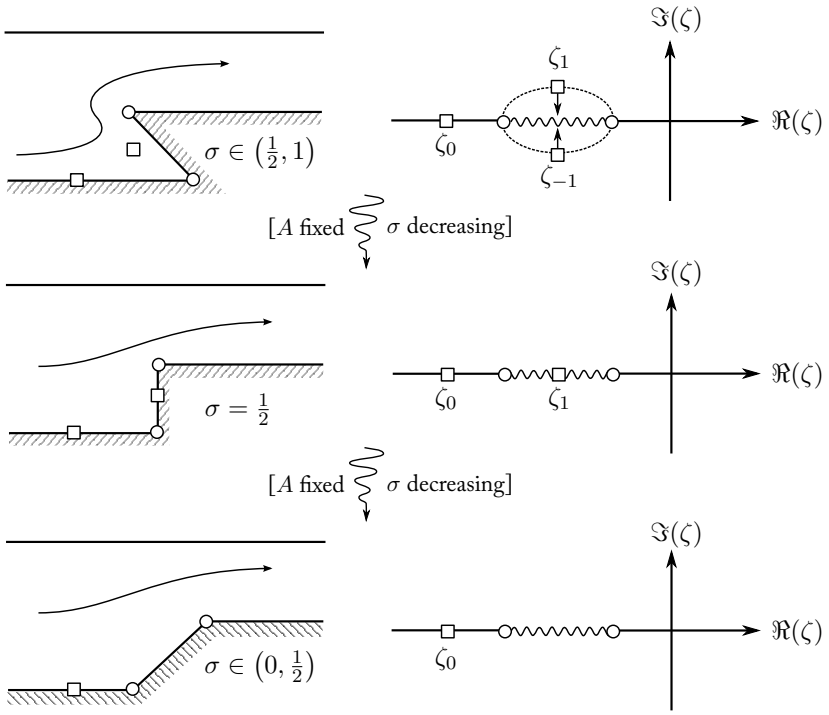

Figure 2.2: Evolution of the turning points (square nodes) for fixed A and decreasing σ (from top to bottom). Only the turning points along the axis and in the upper-half plane are relevant, though we have illustrated the lower-half plane as well. There may be many other of turning points lying on other (irrelevant) Riemann sheets. As usual, the singularities at $\zeta = -b$ and $\zeta = -a$ are illustrated by circular nodes.

As σ decreases to $1/2$, these arcs flatten onto the branch cut, so that at $\sigma = 1/2$, ζ_1 lies on the axis, whereas ζ_{-1} has moved onto another branch. If σ is then decreased to less than $1/2$, then both ζ_1 and ζ_{-1} are now on irrelevant sheets. The next birth of a turning point from eqn (2.40) with $k = \pm 2$ requires $\sigma \geq 1$, so we have covered all the possible cases.

In summary, there are two relevant turning points for $\sigma \in (1/2,1)$ (one real, one complex), two relevant turning points for $\sigma = 1/2$ (both real), and only one turning point for $\sigma \in (0,1/2)$ (real). The evolution of the turning

points as A and σ vary is also depicted in Figure 2.2. In all these cases, it is easy to see that the turning points are *simple* and so $\Delta \sim \mathcal{O}(\zeta - \zeta_T)$ near the points. In the next section, we will show how one wave may turn on another across Stokes lines which originate from these turning points.

2.6.1 Inner analysis and reduction to the Airy Equation

It is crucial to note that the locations of the turning points provide a classification of all the different types of solutions. They are important for two reasons: first, a turning point which lies on the free surface, as in the case for $A > 1$, produces a change in one or both gravity and capillary waves from constant-amplitude to decaying; second, turning points also possess Stokes lines and can thus lead to the birth of new exponentials. The locations of these Stokes lines are given by

$$[G \to C]: \qquad \Im[\chi_-] = \Im[\chi_+] \quad \text{and} \quad \Re[-\chi_-] \geq \Re[-\chi_+], \tag{2.41}$$

$$[C \to G]: \qquad \Im[\chi_+] = \Im[\chi_-] \quad \text{and} \quad \Re[-\chi_+] \geq \Re[-\chi_-], \tag{2.42}$$

comparable to conditions (1.11) for the Airy function. From eqn (2.24), the exponentials produced by the wave-generating singularities, $\zeta = \zeta^*$, can be written as

$$q_{\text{exp}} \sim \frac{2\pi i Q_\pm(\zeta)}{\epsilon^\gamma} \exp\left[-\frac{1}{\epsilon}\int_{\zeta^*}^{\zeta^T} \frac{d\chi_\pm}{d\zeta'}\, d\zeta'\right] \exp\left[-\frac{1}{\epsilon}\int_{\zeta_T}^{\zeta} \frac{d\chi_\pm}{d\zeta'}\, d\zeta'\right], \tag{2.43}$$

where $\zeta = \zeta_T$ corresponds to a turning point. From (2.23) and (2.24), it can be easily verified that $Q_\pm \sim B_\pm/(\zeta - \zeta_T)^{1/4}$ near the turning point, where $B_\pm$ are constants. Thus, if we let

$$\frac{d\chi}{d\zeta} = S_1(\zeta) \pm S_2(\zeta),$$

then in fact,

$$q_{\text{exp}} \sim \exp\left[-\frac{1}{\epsilon}\int_{\zeta_T}^{\zeta} S_1(\zeta')\, d\zeta'\right] \times \frac{G_\pm(\zeta)}{(\zeta - \zeta_T)^{1/4}} \exp\left[\mp\frac{1}{\epsilon}\int_{\zeta_T}^{\zeta} S_2(\zeta')\, d\zeta'\right],$$

where $G_\pm(\zeta)$ is defined in the obvious way from (2.43). Crucially then, we see that by scaling out the first exponential in the above expression, and taking $\zeta \to \zeta_T$, where $G_\pm$ is constant, then we recover the standard exponentials near first-order turning-point problems (*c.f.* Bender & Orszag 1978); consequently, the points $\zeta = \zeta_T$ where $S_2(\zeta_T) = 0$ likely correspond to locations where subdominant exponentials may switch on. To see this in more detail, we shall study the inner region near $\zeta = \zeta_T$.

Like in Section 1.5.3 of the last chapter, the boundary integral (2.3) can be considerably simplified away from the free-surface. In this case, we would like to evaluate

$$\log q_{\text{inner}}(w) + i\theta_{\text{inner}}(w) = \log q_0 + \mathscr{H}[\theta_{\text{outer}}(\zeta)]. \tag{2.44}$$

as $\zeta \to \zeta_T$ and where the indices help to remind us where the functions q and θ are being evaluated. The left-hand side is evaluated *near* the turning point and thus involves the exact expressions for $q(w)$ and $\theta(w)$ in the inner limit. However, the integrand on the right hand side is integrated over the free surface, far away from the singularity, thus it involves only the *outer* expansion for $\theta(w)$. But we know that substituting the outer expansion into the right-hand side of eqn (2.44) leads to

$$\log q_{\text{inner}}(w) + i\theta_{\text{inner}}(w) = \log q_0 + \epsilon \mathscr{H}[\theta_1(\zeta)] + \epsilon^2 \mathscr{H}[\theta_2(\zeta)] + O(\epsilon^3),$$

and since the integrals are all finite for ζ off the axis, the expansion remains well-ordered near the turning point. The leading-order inner solution, then, is found by setting $\log q - i\theta \sim \log q_0$ and thus we may substitute

$$\sin\theta = \frac{e^{i\theta} - e^{-i\theta}}{2i} = \frac{1}{2i}\left(\frac{q}{q_0} - \frac{q_0}{q}\right)$$

into eqn (2.4), giving

$$\beta\epsilon\left[iq_0 q^3 \frac{dq}{dw}\right] - \beta\tau\epsilon^2\left[q_0 q^2 \frac{d^2q}{dw^2} - \frac{d^2q_0}{dw^2}q^3 + \left(\frac{dq_0}{dw}\right)^2 \frac{q^3}{q_0} - \frac{dq_0}{dw}q^2\frac{dq}{dw}\right] = \frac{1}{2}\left(q_0^2 - q^2\right).$$

If we let

$$q = q_0 + \exp\left[-\frac{1}{\epsilon}\int_{\zeta_T}^{\zeta} S_1(\zeta')\, d\zeta'\right] u(\zeta),$$

then, to leading order, the differential equation is given by

$$\epsilon^2 u'' = R(\zeta) u,$$

where

$$R(\zeta) = S_2^2(\zeta) = -\frac{\left[\beta^2 q_0^4 - 4\beta\tau\right]}{4\beta^2\tau^2 q_0^2} = -\frac{\Delta}{4\beta^2\tau^2 q_0^2} \sim C_R(\zeta - \zeta_T), \quad (2.45)$$

with C_R constant. This last statement holds because $\zeta = \zeta_T$ is a simple turning point, and consequently, we see that locally, u is simply determined by the standard Airy equation (after a re-scaling of ζ). We already know that the two WKB solutions are given by

$$u \sim \frac{C}{(\zeta - \zeta_T)^{1/4}} \exp\left[\mp\frac{1}{\epsilon}\int_{\zeta_T}^{\zeta} S_2(\zeta')\, d\zeta'\right]$$

where D is a constant. By taking the inner limit of the outer exponentials, we see that $D = G_{\pm}(\zeta_T)$ and thus, according to the Airy connection formulae in (1.5), the transition of $u(\zeta)$ across the Stokes line satisfies

$$u \sim \frac{G_{\pm}(\zeta_T)}{(\zeta - \zeta_T)^{1/4}} \exp\left[\mp\frac{1}{\epsilon}\int_{\zeta_T}^{\zeta} S_2(\zeta')\, d\zeta'\right]$$
$$\longmapsto \frac{G_{\pm}(\zeta_T)}{(\zeta - \zeta_T)^{1/4}} \exp\left[\mp\frac{1}{\epsilon}\int_{\zeta_T}^{\zeta} S_2(\zeta')\, d\zeta'\right] + i\frac{G_{\pm}(\zeta_T)}{(\zeta - \zeta_T)^{1/4}} \exp\left[\pm\frac{1}{\epsilon}\int_{\zeta_T}^{\zeta} S_2(\zeta')\, d\zeta'\right]. \quad (2.46)$$

In terms of the outer variables, q, this shows that as we analytically continue across a Stokes line emanating from a turning point at $\zeta = \zeta_T$, the already existing exponential switches on a wave satisfying the transition rule:

$$q_{\text{exp}} \sim -\frac{2\pi i Q_{\pm}(\zeta)}{\epsilon^{\gamma}} \exp\left[-\frac{1}{\epsilon}\int_{\zeta^*}^{\zeta} \frac{d\chi_{\pm}}{d\zeta'}\, d\zeta'\right]$$
$$\longmapsto q_{\text{exp}} + i\left[-\frac{2\pi i Q_{\mp}(\zeta)}{\epsilon^{\gamma}}\right]\left[\frac{B_{\pm}}{B_{\mp}}\right] \exp\left[-\frac{1}{\epsilon}\int_{\zeta^*}^{\zeta_T} \frac{d\chi_{\pm}}{d\zeta'}\, d\zeta'\right] \exp\left[-\frac{1}{\epsilon}\int_{\zeta^T}^{\zeta} \frac{d\chi_{\mp}}{d\zeta'}\, d\zeta'\right]. \quad (2.47)$$

The expressions in (2.46) and (2.47) are written based on the assumption that $C_R \in \mathbb{R}^+$ in (2.45) and that we are analytically continuing the solution across Stokes lines in a counter-clockwise direction, with the origin at the turning point. If, for example, $C_R \in \mathbb{R}^-$, then the transitions will need to be negated. This will be made clear in the following section.

2.7 NEW CLASSES OF SOLUTIONS

In this section, we will show how the theory we have developed thus far can be applied to derive new classes of gravity-capillary waves for the rectangular step studied in Part I.

The notation we use is the following: first, we label the waves associated with the stagnation point, the corner, the turning point ζ_0, and the turning point ζ_1, as S, C, T_1, and T_2, respectively. The underline, $\underline{T_1}$ is used to distinguish when the first turning point lies on bottom boundary and the overline, $\overline{T_1}$ when it lies on the free-surface. Solution-types are then distinguished by a sequence of labels, indicating the path as we analytically continue across the free-surface from left to right (in the downstream direction). Also, it is sufficient for us to work with the waves generated by analytic continuation into the upper-half plane only, rather than both the upper and lower-half planes.

For example, a sequence like $\underline{T_1} \cdot T_2 \cdot C \cdot G$ corresponds to crossing (from left-to-right and downstream) (i) the Stokes line from $\underline{T_1}$ ($\underline{T_1}$-line), (ii) the Stokes line from T_2 (T_2-line), (iii) the capillary Stokes line from the stagnation point (C-line), and (iv) the gravity Stokes line from the corner (G-line). And another example: a sequence like $C \cdot \overline{T_1} \cdot G$ corresponds to crossing the C-line, crossing the $\overline{T_1}$ point on the free-surface, and then crossing the G-line. Next, we will write

$$X_{\text{grav}} = -\frac{1}{\epsilon}\int_{-a}^{\zeta} \frac{d\chi_+}{d\zeta'} d\zeta' \qquad \text{and} \qquad X_{\text{cap}} = -\frac{1}{\epsilon}\int_{-b}^{\zeta} \frac{d\chi_-}{d\zeta'} d\zeta'.$$

Any waves turned on can then be expressed relative to these expressions. The pre-factor for the exponentials we will denote by a calligraphic letter with a subscript for the associated singularity and a superscript for the upper limit of integration (if applicable). For example, we will write $\mathcal{C}_C e^{X_{\text{grav}}}$ to denote a gravity wave with amplitude $\mathcal{C}_C$ turned on by crossing the Stokes line from

the corner. Similarly, an expression like $(\mathcal{A}_S + \mathcal{B}_S)^{\overline{T_1}} e^{X_{\text{grav}}}$ corresponds to the gravity wave turned on when a (capillary) wave with two combined pre-factors crosses the $\overline{T_1}$ turning point. So the new wave amplitude can be derived by finding the amplitude of the $(\mathcal{A}_S + \mathcal{B}_S) e^{X_{\text{cap}}}$ wave near the turning point, and multiplying by i (from the Airy transition). Our choice of notation and their associated expressions will be made clear in the many examples and figures to follow.

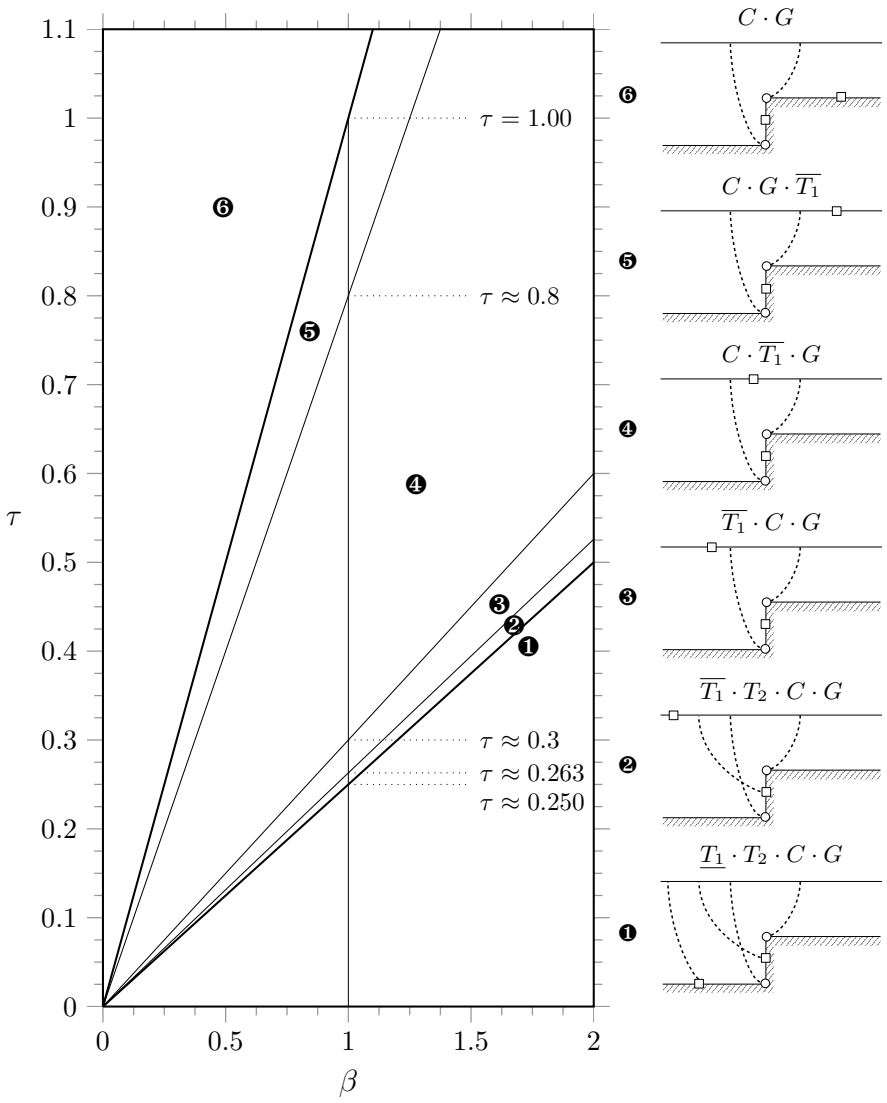

Figure 2.3: Our Stokes line analysis indicates that there are six regimes of interest for flow over a rectangular step, as shown here in the $\beta\tau$-plane. Linearised theory predicts only two (❶ and ❻), but here we see that in considering the nonlinearity of the step, other scenarios are possible (❷ to ❺); these new regimes lie within a strip bounded by $A = 1$ and $A = (b/a)^2$, which thickens for larger and larger steps. The arrangement of the Stokes lines, as well as our naming convention is shown on the right. Circular and square nodes are used to represent singularities and turning points, respectively, and only Stokes lines that intersect the free-surface are shown.

In any case, the movement of the turning points (as described in Section 2.6) provides us with *six* different regions of interest in the β-τ, or Froude-Bond plane. These regions are shown in Figure 2.3. Note that the extremum solutions ❶ and ❻ correspond to the standard linearised solutions. This figure then shows that the usual dispersion 'line' differentiating the linearised solutions actually contains a *series* of solutions ❷ to ❺; the line's thickness and these new solutions are a manifestation of the nonlinearity (and largeness) of the step. As the step-height tends to zero (or as $\beta, \tau \to 0$), the line thickness tends to zero and we recover the standard linearised solutions.

In order to derive the correct wave expressions on the free-surface for each of these six types, we will analytically continue across the free-surface (from left-to-right or right-to-left depending on what is more convenient), beginning with a wave that satisfies the radiation condition (zero gravity waves upstream and zero capillary waves downstream). Upon reaching the end, we again apply the radiation conditions, and this process provides us with a complete set of fully-determined waves. A similar process of analytic continuation was used in the work of Chapman (2002) for the study of transition to turbulence in Couette flow.

2.7.1 Region ❶

Consider the case of $A < 1$. For most (larger) values of τ, as we analytically continue across the free-surface, the sequence of events is $\underline{T_1} \cdot T_2 \cdot C \cdot G$, which involves the T_2 Stokes line crossing the C Stokes line. In fact, for extremely small values of τ, the lines may not actually cross, and so the sequence is $\underline{T_1} \cdot C \cdot T_2 \cdot G$; however, both cases are equivalent because, as we shall see, the turning points do not have an effect on the eventual solution. If we start with an arbitrary upstream capillary wave $\mathcal{A}_S e^{X_{\text{cap}}}$, then the sequence of events is as follows:

$$\begin{aligned}
\mathcal{A}_S e^{X_{\text{cap}}} &\xrightarrow[[G\to C]]{\underline{T_1}} \mathcal{A}_S e^{X_{\text{cap}}} \\
&\xrightarrow[[G\to C]]{T_2} \mathcal{A}_S e^{X_{\text{cap}}} \\
&\xrightarrow[[Bs\to C]]{\text{Stag.}} (\mathcal{A}_S + \mathcal{B}_S) e^{X_{\text{cap}}} \\
&\xrightarrow[[Bs\to G]]{\text{Corn.}} (\mathcal{A}_S + \mathcal{B}_S) e^{X_{\text{cap}}} + \mathcal{C}_C e^{X_{\text{grav}}}.
\end{aligned}$$

There are no capillary waves downstream, so $\mathcal{A}_S + \mathcal{B}_S = 0$, and the final solution has

$$\mathcal{A}_S e^{X_{\text{cap}}} \xrightarrow[[Bs\to C]]{\text{Stag.}} 0 \xrightarrow[[Bs\to G]]{\text{Corn.}} \mathcal{C}_C e^{X_{\text{grav}}},$$

where the pre-factors are given by the standard relations of (2.31):

$$\mathcal{A}_S = \frac{2\pi i Q_-}{\epsilon^{\gamma_S}} \quad \text{and} \quad \mathcal{C}_C = -\frac{2\pi i Q_+}{\epsilon^{\gamma_C}} \tag{2.48}$$

with $Q_\pm$ computed from (2.23) and (2.24). For the rectangular step, $\gamma_S = 0$ and $\gamma_C = 6/5$, which we will show in Section 2.8.

In some problems, the intersection of Stokes lines can lead to the birth of new Stokes lines (see for example, Howls et al. 2004); this phenomenon can be detected by analytically continuing around the intersection point and seeing if the solution returns to its original value. In this case, we see that the T_2 line remains inactive regardless of the direction of approach, and so the intersection of the two Stokes lines is not a concern. In the end, the free-surface is simply akin to the standard linearised solution with capillary waves upstream and gravity waves downstream, but now, with a wave-free region near the center. This is shown in Figure 2.4.

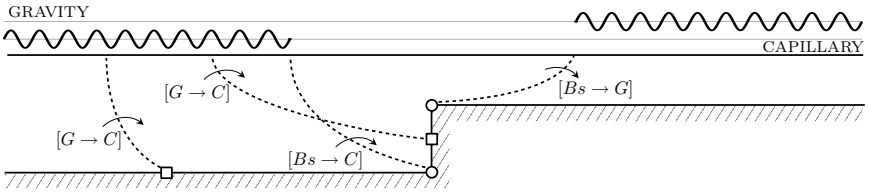

Figure 2.4: Region ❶ with $\underline{T_1} \cdot T_2 \cdot C \cdot G$. The Stokes lines from the turning points remain inactive and we recover the standard linearised solutions with capillary waves upstream and gravity waves downstream.

2.7.2 *Region* ❷

As τ is increased and β held steady, the $\underline{T_1}$ turning point moves upstream along the solid boundary and reaches $-\infty$ at $A = 1$. Solutions in region ❷ have $A > 1$ and the turning point $\overline{T_1}$ has now moved onto the free-surface and travels downstream as τ is further increased. The turning point on the free-surface also implies that upstream waves will now decay, but downstream waves will remain constant. Again, we will start with an arbitrary upstream capillary wave $\mathcal{A}_S e^{X_{\text{cap}}}$, and then the sequence of events is:

$$\begin{aligned}
\mathcal{A}_S e^{X_{\text{cap}}} &\xrightarrow[[G\leftrightarrow C]]{\overline{T_1}} \mathcal{A}_S e^{X_{\text{cap}}} + i\mathcal{A}_S^{T_1} e^{X_{\text{grav}}} \\
&\xrightarrow[[G\to C]]{T_2} (\mathcal{A}_S + \mathcal{A}_S^{T_2}) e^{X_{\text{cap}}} + i\mathcal{A}_S^{T_1} e^{X_{\text{grav}}} \\
&\xrightarrow[[Bs\to C]]{\text{Stag.}} (\mathcal{A}_S + \mathcal{A}_S^{T_2} + \mathcal{B}_S) e^{X_{\text{cap}}} + i\mathcal{A}_S^{T_1} e^{X_{\text{grav}}} \\
&\xrightarrow[[Bs\to G]]{\text{Corn.}} (\mathcal{A}_S + \mathcal{A}_S^{T_2} + \mathcal{B}_S) e^{X_{\text{cap}}} + (i\mathcal{A}_S^{T_1} + \mathcal{C}_C) e^{X_{\text{grav}}}.
\end{aligned}$$

In the first line, the $\overline{T_1}$ transition follows directly from (2.47), but in the second line, the T_2 transition has a negated $(-i \cdot i)$ coefficient—this is because crossing the Stokes line in the downstream direction is equivalent to analytically continuing the Airy functions in the clockwise direction. Again, $\mathcal{C}_C$ is given by (2.48). Moreover, since there are no capillary waves downstream and $\mathcal{B}_S$ is provided by the jump condition in (2.31), then

$$\mathcal{B}_S = \mathcal{A}_S + \mathcal{A}_S^{T_2} = -\frac{2\pi i Q_+}{\epsilon^{\gamma_S}}. \tag{2.49}$$

Let us write $\mathcal{A}_S = -\overline{\mathcal{A}_S} 2\pi i Q_+(\zeta)/\epsilon^{\gamma_S}$. Then by (2.47), the pre-factor of the first gravity wave switched on is

$$\mathcal{A}_S^{T_1} = \overline{\mathcal{A}_S}\left[-\frac{2\pi i Q_-(\zeta)}{\epsilon^{\gamma_S}}\right]\left[\frac{B_+^{T_1}}{B_-^{T_1}}\right]\exp\left[-\frac{1}{\epsilon}\left\{\int_{-b}^{T_1}\frac{d\chi_+}{d\zeta'}\,d\zeta' + \int_{T_1}^{-a}\frac{d\chi_-}{d\zeta'}\,d\zeta'\right\}\right], \tag{2.50}$$

where $Q_\pm(\zeta_{T_1}) \sim B_\pm^{T_1}/(\zeta - \zeta_{T_1})^{1/4}$ and we have added the second integral in the exponential so as to express all waves relative to $e^{X_{\text{grav}}}$. By the same procedure, we can now compute the second turning-point switching as

$$\mathcal{A}_S^{T_2} = \overline{\mathcal{A}_S}\left[-\frac{2\pi i Q_+(\zeta)}{\epsilon^{\gamma_S}}\right]\left[\frac{B_+^{T_1}}{B_-^{T_1}}\right]\left[\frac{B_-^{T_2}}{B_+^{T_2}}\right]\exp\left[-\frac{H}{\epsilon}\right], \tag{2.51}$$

where

$$H = \left(\int_{-b}^{T_1} + \int_{T_2}^{-a}\right) \frac{d\chi_+}{d\zeta'}\, d\zeta' + \left(\int_{T_1}^{-a} + \int_{-a}^{T_2}\right) \frac{d\chi_-}{d\zeta'}\, d\zeta'. \tag{2.52}$$

Combining (2.49), (2.51), and (2.52), we then have

$$\overline{\mathcal{A}_S} = \left(1 + e^{-H/\epsilon}\left[\frac{B_+^{T_1}}{B_-^{T_1}}\right]\left[\frac{B_-^{T_2}}{B_+^{T_2}}\right]\right)^{-1},$$

and we have completely determined all the required pre-factors.

Therefore, far upstream we have a decaying capillary wave, while far downstream we have a constant gravity wave. Also, switched on after encountering the $\overline{T_1}$ turning point is a (doubly) exponentially small gravity wave, which continues downstream. Finally, there is an even smaller decaying capillary wave which has been turned on by the gravity wave across the T_2 line. This is illustrated in Figure 2.5, and in summary:

$$\begin{aligned}\mathcal{A}_S e^{X_{\text{cap}}} &\xrightarrow[[G\leftrightarrow C]]{\overline{T_1}} \mathcal{A}_S e^{X_{\text{cap}}} + i\mathcal{A}_S^{T_1} e^{X_{\text{grav}}} \xrightarrow[[G\to C]]{T_2} (\mathcal{A}_S - \mathcal{A}_S^{T_2}) e^{X_{\text{cap}}} + i\mathcal{A}_S^{T_1} e^{X_{\text{grav}}} \\ &\xrightarrow[[Bs\to C]]{\text{Stag.}} i\mathcal{A}_S^{T_1} e^{X_{\text{grav}}} \xrightarrow[[Bs\to G]]{\text{Corn.}} (i\mathcal{A}_S^{T_1} + \mathcal{C}_C) e^{X_{\text{grav}}}. \end{aligned} \tag{2.53}$$

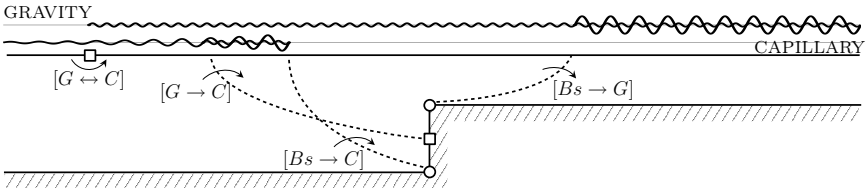

Figure 2.5: Region ❷ with $\overline{T_1} \cdot T_2 \cdot C \cdot G$. All four Stokes lines are now active, and so we have doubly and in fact, triply small waves turned on by crossing the $\overline{T_1}$ and T_2 lines. All waves decay upstream and are constant downstream.

2.7.3 *Region* ❸

The previous Region ❷ solutions are actually contained in an extremely small section of $\beta\tau$-space (as shown in Figure 2.3). The reason is that near $A = 1$, the location of the $\overline{T_1}$ turning point is

$$w \sim -\log\left(\frac{b-a}{A^{1/2}-1}\right),$$

and so it quickly tends to the origin, $\phi = 0$. However, once $\overline{T_1}$ has crossed the intersection point of the T_2 line and the free-surface, the region to the left of $\overline{T_1}$ is no longer a constant contour of $\Re(\chi'_+ - \chi'_-)$, so the T_2 line is rendered inactive (and tends to $-\infty$ without intersecting the free-surface). Once this occurs, we have passed into Region ❸; so again starting with an arbitrary upstream capillary wave $\mathcal{A}_S e^{X_{\text{cap}}}$, the sequence of events is now:

$$\begin{aligned}\mathcal{A}_S e^{X_{\text{cap}}} &\xrightarrow[[G\leftrightarrow C]]{\overline{T_1}} \mathcal{A}_S e^{X_{\text{cap}}} + i\mathcal{A}_S^{T_1} e^{X_{\text{grav}}} \\ &\xrightarrow[[Bs\to C]]{\text{Stag.}} (\mathcal{A}_S + \mathcal{B}_S) e^{X_{\text{cap}}} + i\mathcal{A}_S^{T_1} e^{X_{\text{grav}}} \\ &\xrightarrow[[Bs\to G]]{\text{Corn.}} (\mathcal{A}_S + \mathcal{B}_S) e^{X_{\text{cap}}} + (i\mathcal{A}_S^{T_1} + \mathcal{C}_C) e^{X_{\text{grav}}}. \end{aligned}$$

We need $\mathcal{B}_S = -\mathcal{A}_S$. Relation (2.48) provides the expressions for $\mathcal{A}_S$ and $\mathcal{C}_C$, and moreover, (2.50) with $\overline{\mathcal{A}_S} = 1$ gives the expression for $\mathcal{A}_S^{T_1}$. The final result is

$$\mathcal{A}_S e^{X_{\text{cap}}} \xrightarrow[[G\leftrightarrow C]]{\overline{T_1}} \mathcal{A}_S e^{X_{\text{cap}}} + i\mathcal{A}_S^{T_1} e^{X_{\text{grav}}} \xrightarrow[[Bs\to C]]{\text{Stag.}} i\mathcal{A}_S^{T_1} e^{X_{\text{grav}}} \xrightarrow[[Bs\to G]]{\text{Corn.}} (i\mathcal{A}_S^{T_1} + \mathcal{C}_C) e^{X_{\text{grav}}}.$$

Thus the only difference between the solutions in Region ❷ and ❸ is a very small (and in fact, subdominant) capillary wave. This is shown in Figure 2.6.

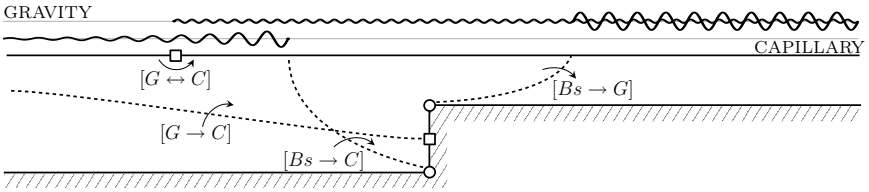

Figure 2.6: Region ❸ with $\overline{T_1} \cdot C \cdot G$. Once the $\overline{T_1}$ point has proceeded far enough downstream, the T_2 line is rendered inactive. The only difference between solutions in ❷ and ❸ is that in the former, there exists a second subdominant capillary wave.

2.7.4 *Region* ❹

For A still larger, $\overline{T_1}$ eventually crosses the intersection point of the C line and the free-surface, and then the sequence is then $C \cdot \overline{T_1} \cdot G$. If we start with an arbitrary upstream capillary wave $\mathcal{A}_S e^{X_{\text{cap}}}$, then the chain of events follows

$$\begin{aligned}
\mathcal{A}_S e^{X_{\text{cap}}} &\xrightarrow[[Bs\to C]]{\text{Stag.}} (\mathcal{A}_S + \mathcal{B}_S) e^{X_{\text{cap}}} \\
&\xrightarrow[[G\leftrightarrow C]]{\overline{T_1}} (\mathcal{A}_S + \mathcal{B}_S) e^{X_{\text{cap}}} + i(\mathcal{A}_S + \mathcal{B}_S)^{T_1} e^{X_{\text{grav}}} \\
&\xrightarrow[[Bs\to G]]{\text{Corn.}} (\mathcal{A}_S + \mathcal{B}_S) e^{X_{\text{cap}}} + (i(\mathcal{A}_S + \mathcal{B}_S)^{T_1} + \mathcal{C}_C) e^{X_{\text{grav}}}.
\end{aligned}$$

Again, we cannot have capillary waves downstream, so $\mathcal{B}_S = -\mathcal{A}_S$ and the coefficients are given by (2.48). The final result is illustrated in Figure 2.7 and given by

$$\mathcal{A}_S e^{X_{\text{cap}}} \xrightarrow[[Bs\to C]]{\text{Stag.}} 0 \xrightarrow[[Bs\to G]]{\text{Corn.}} \mathcal{C}_C e^{X_{\text{grav}}}.$$

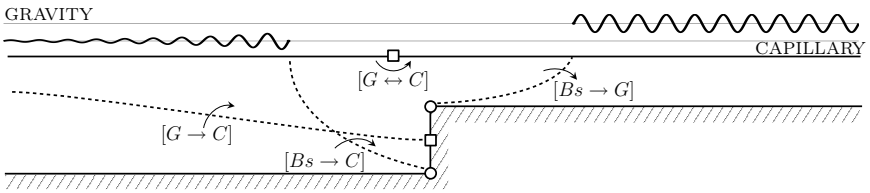

Figure 2.7: Region ❹ with $C - \overline{T_1} \cdot G$. The $\overline{T_1}$ has been rendered inactive, and solutions simply contain a decaying capillary wave and a constant gravity wave.

2.7.5 *Region* ❺

Eventually, $\overline{T_1}$ passes the intersection of the G line and the free-surface, and so downstream waves will also decay. For these cases, it is easier to

analytically continue from downstream to upstream. If we start with an arbitrary downstream gravity wave $\mathcal{C}_C e^{X_{\text{grav}}}$, the sequence follows

$$\begin{aligned}
\mathcal{C}_C e^{X_{\text{grav}}} &\xleftarrow[[G\leftrightarrow C]]{\overline{T_1}} -i\mathcal{C}_C^{T_1} e^{X_{\text{cap}}} + \mathcal{C}_C e^{X_{\text{grav}}} \\
&\xleftarrow[[Bs\to G]]{\text{Corn.}} -i\mathcal{C}_C^{T_1} e^{X_{\text{cap}}} + (\mathcal{C}_C + \mathcal{D}_C) e^{X_{\text{grav}}} \\
&\xleftarrow[[Bs\to C]]{\text{Stag.}} (-i\mathcal{C}_C^{T_1} + \mathcal{A}_S) e^{X_{\text{cap}}} + (\mathcal{C}_C + \mathcal{D}_C) e^{X_{\text{grav}}}.
\end{aligned}$$

The negated coefficient of the first line is due to crossing the Stokes line in the direction of right to left. We impose the requirement that there are no gravity waves downstream, so $\mathcal{D}_C = -\mathcal{C}_C$, and the values $\mathcal{A}_S$ and $\mathcal{C}_C$ are given in (2.48). From (2.47), the pre-factor of the smaller capillary wave is

$$\mathcal{C}_C^{T_1} = \left[-\frac{2\pi i Q_+(\zeta)}{\epsilon^{\gamma_C}}\right]\left[\frac{B_+^{T_1}}{B_-^{T_1}}\right]\exp\left[-\frac{1}{\epsilon}\left\{\int_{-b}^{\zeta_{T_1}}\frac{d\chi_+}{d\zeta'}\,d\zeta' + \int_{-a}^{\zeta_{T_1}}\frac{d\chi_-}{d\zeta'}\,d\zeta'\right\}\right], \tag{2.54}$$

The final result is shown in Figure 2.8 and given by (from left to right):

$$\begin{aligned}
(i\mathcal{C}_C^{T_1} + \mathcal{A}_S) e^{X_{\text{cap}}} &\xrightarrow[[Bs\to C]]{\text{Stag.}} i\mathcal{C}_C^{T_1} e^{X_{\text{cap}}} \\
&\xrightarrow[[Bs\to G]]{\text{Corn.}} i\mathcal{C}_C^{T_1} e^{X_{\text{cap}}} + \mathcal{C}_C e^{X_{\text{grav}}} \xrightarrow[[G\leftrightarrow C]]{\overline{T_1}} \mathcal{C}_C e^{X_{\text{grav}}}.
\end{aligned}$$

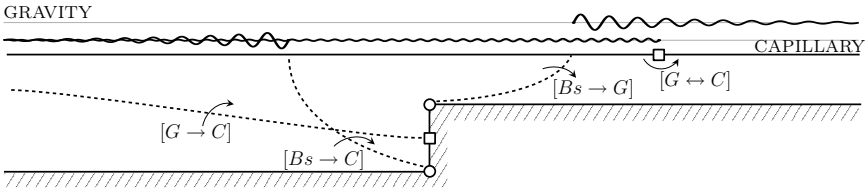

Figure 2.8: Region ❺ with $C \cdot G \cdot \overline{T_1}$. These solutions mirror the solutions of Region ❸, but with *all* waves decaying in the far-field.

2.7.6 *Region* ❻

Finally, once $A = (b/a)^{1/2}$, the $\overline{T_1}$ point has reached $\phi = \infty$ and for larger values of A in Region ❻, it begins to moving from right-to-left along the downstream solid boundary. Again proceeding backwards, if we start with an arbitrary downstream gravity wave $\mathcal{C}_C e^{X_{\text{grav}}}$, then the sequence of events is simply

$$\mathcal{A}_S e^{X_{\text{cap}}} \xrightarrow[[Bs\to C]]{\text{Stag.}} 0 \xrightarrow[[Bs\to G]]{\text{Corn.}} \mathcal{C}_C e^{X_{\text{grav}}},$$

with the coefficients given by (2.48)

It is easy to check that for a capillary wave generated by the stagnation point, by the time it has reached the $\underline{T_1}$ point, it has become exponentially large rather than exponentially small, so in fact, the $\underline{T_1}$ line with $[C \to G]$ cannot be active and this removes any of the possibly troubling consequences of crossing Stokes lines. The result is shown in Figure 2.9

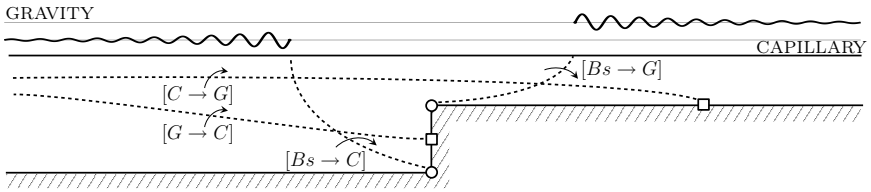

Figure 2.9: Region ❻ with $C \cdot G$. The solutions with decaying capillary waves upstream and decaying gravity waves downstream are analogous to the standard linearised solutions. The $[C \to C]$ line is inactive.

2.8 CALCULATING Λ

The value of Λ, which appears as a constant pre-factor in Q and Θ, is the missing piece of the puzzle. As in Section 1.5.3 of the preceding chapter, we will need to develop an inner solution valid near the singularity, where the gravity or capillary wave is now $\mathcal{O}(1)$, and then match this solution to the outer solution, given by the expansion in (2.8).

There are two cases to consider. From Section 2.5, we know that stagnation points with $q \sim c(w - w^*)^\alpha$ and $\alpha > 0$, possess only a single capillary Stokes line; we will study this case first and in Section 2.8.2. Here, the analysis is mostly straightforward and proceeds similarly to the capillary-only flows of Chapman & Vanden-Broeck (2002).

The second case is for the corner, with $\alpha < 0$, and we study this scenario in Section 2.8.3. Here, we will discover a surprising result: near the singularity, the gravity and capillary effects decouple within distinct layers. The application of exponential asymptotics then consists of traveling through three layers: an outer layer, where both gravity and capillary waves are exponentially small, a middle layer where the gravity waves are $\mathcal{O}(1)$, and the final, inner layer where the capillary waves are $\mathcal{O}(1)$. Because of the change in the structure of the solution as each layer is traversed, the properties (including the size) of the innermost layer can only be revealed once the analysis in the middle layer is complete. A depiction of this triple-layer procedure is shown in Figure 2.10.

Remember that for a rectangular step, the corner does not have a capillary Stokes line, so this triple-layer theory reduces to the usual two layers. In fact, we know from Table 2.1 that the triple-layer structure only emerges for the case of a step with $\sigma > 1/2$.

2.8.1 *Inner limits of Θ and Q*

In computing the limits of Θ and Q as $w \to w^*$, we will need to make use of q_1 from eqns (2.11) and (2.12):

$$q_1 = -i\beta q_0^3 q_0' + q_0 \mathscr{H}[\theta_1(w)].$$

The Hilbert transform is found by integrating along the free surface, where θ_1 is well-behaved and thus it too, is well-behaved and $\mathcal{O}(1)$ as $w \to w^*$. We will now substitute this expression into the form of Θ from eqn (2.23) for each of the cases delineated earlier.

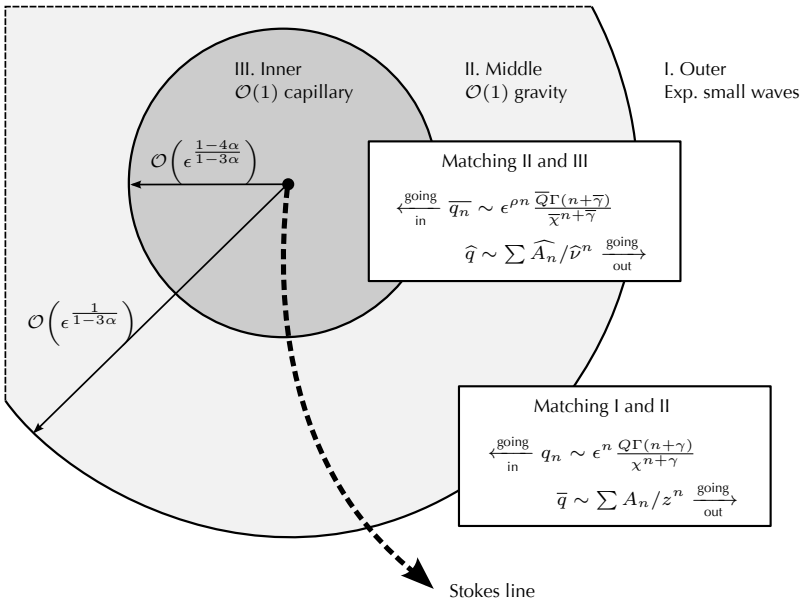

Figure 2.10: The triple layer problem occurs when a corner, with $\alpha < 0$, can generate both capillary and gravity waves. The solution proceeds from the outermost layer (where all the waves are exponentially small), through the middle layer(where the gravity waves are $\mathcal{O}(1)$, and finally into the inner layer, where the capillary waves are $\mathcal{O}(1)$. The exact size of the innermost layer can only be predicted once the analysis in the middle region is complete.

First, for $\alpha > 0$ it is easy to show that

$$\begin{aligned}
\Theta_\pm &= \left[\frac{(\sqrt{-A})^{\pm 1}}{(-A)^{1/4}} + \mathcal{O}(q_0^2)\right] \Lambda \exp\left\{\frac{i}{2\tau}\int_{w^*}^{w} q_1 \left[\frac{\pm A}{\sqrt{-A}q_0^2} + \mathcal{O}(1)\right]\, du\right\} \\
&= \left[\frac{(\sqrt{-A})^{\pm 1}}{(-A)^{1/4}} + \mathcal{O}(q_0^2)\right] \Lambda \exp\left\{\frac{\pm\beta A}{2\tau\sqrt{-A}}\int_{w^*}^{w} \left[q_0 q_0' + \frac{i}{\beta q_0}\mathscr{H}[\theta_1(u)] + \mathcal{O}(q_0^3 q_0')\right] du\right\} \\
&= \left[\frac{(\sqrt{-A})^{\pm 1}}{(-A)^{1/4}} + \mathcal{O}(q_0^2)\right] \Lambda \exp\left\{\frac{\pm\beta A}{4\tau\sqrt{-A}} q_0^2 + \mathcal{O}(W^{1-\alpha}) + \mathcal{O}(q_0^4)\right\} \\
&= \Lambda \frac{(\sqrt{-A})^{\pm 1}}{(-A)^{1/4}} + \mathcal{O}(q_0^2, W^{1-\alpha}).
\end{aligned} \tag{2.55}$$

Note that the terms involved in the Hilbert transform lead to a subdominant $\mathcal{O}(W^{1-\alpha})$ contribution, and the order notation $\mathcal{O}(a,b)$ is shorthand for $\mathcal{O}(\max\{a,b\})$ as $w \to w^*$. Next, for $\alpha < 0$ and the negative sign,

$$\begin{aligned}
\Theta_- &= \left[\frac{1}{2q_0^3} + \mathcal{O}(1/q_0^7)\right] \Lambda \exp\left\{\frac{i}{2\tau}\int_{w^*}^{w} q_1 \left[1 - \left(1 + \frac{3A}{2q_0^4} + \mathcal{O}(1/q_0^8)\right)\right]\, du\right\} \\
&= \left[\frac{1}{2q_0^3} + \mathcal{O}(1/q_0^7)\right] \Lambda \exp\left\{\frac{\beta}{2\tau}\int_{w^*}^{w} \left[-\frac{3Aq_0'}{2q_0} - \frac{3iA}{2\beta q_0^3}\mathscr{H}[\theta_1(u)] + \mathcal{O}(q_0'/q_0^5)\right]\, du\right\} \\
&= \left[\frac{1}{2q_0^3} + \mathcal{O}\left(\frac{1}{q_0^7}\right)\right] \Lambda \exp\left\{-\log\left[\frac{q_0(w)}{q_0(w^*)}\right]^3 - \frac{3i}{\beta}\int_{w^*}^{w} \frac{\mathscr{H}[\theta_1(u)]}{q_0^3}\, du + \mathcal{O}(1/q_0^4)\right\} \\
&= \frac{\Lambda}{q_0^6} \underbrace{\left[\frac{q_0^3(w^*)}{2} \exp\left(-\frac{3i}{\beta}\int_{w^*}^{w} \frac{\mathscr{H}[\theta_1(u)]}{q_0^3}\, du\right)\right]}_{C} \left\{1 + \mathcal{O}(1/q_0^4)\right\}.
\end{aligned} \tag{2.56}$$

On the other hand, for $\alpha < 0$ and the positive sign,

$$\begin{aligned}
\Theta_+ &= \left[2q_0 + \mathcal{O}(1/q_0^2)\right] \Lambda \exp\left[\frac{i}{2\tau}\int_{w^*}^{w} q_1 \left\{1 + \left(1 + \frac{3A}{2q_0^4} + \mathcal{O}(1/q_0^8)\right)\right\}\, du\right] \\
&= \left[2q_0 + \mathcal{O}(1/q_0^2)\right] \Lambda \exp\left[\frac{\beta}{2\tau}\int_{w^*}^{w} \left\{2q_0^3 q_0' + \frac{3Aq_0'}{2q_0} + \frac{2iq_0}{\beta}\mathscr{H}[\theta_1(u)] + \mathcal{O}(q_0'/q_0^5)\right\}\, dw\right] \\
&= \left[2q_0 + \mathcal{O}(1/q_0^2)\right] \Lambda \exp\left[\frac{\beta}{4\tau}q_0^4 + \log q_0^3 + \mathcal{O}(W^{\alpha+1}, 1/q_0^4)\right] \\
&= \Lambda q_0^4 \exp\left(\frac{\beta}{4\tau}q_0^4\right)\left\{1 + \mathcal{O}(W^{\alpha+1}, 1/q_0^4)\right\}. \qquad (2.57)
\end{aligned}$$

The blow-up for θ_+ in this last case (in contrast to the first two cases) is an apt warning of a different sort of behaviour, and we will see the implications of this shortly. However, in summary,

$$\Theta \sim \left\{\begin{array}{ll} \Lambda\dfrac{(\sqrt{-A})^{\pm 1}}{(-A)^{1/4}} & \text{for } \alpha > 0 \\ \dfrac{\Lambda C}{q_0^6} & \text{for } \alpha < 0 \text{ and gravity} \\ \Lambda q_0^4 \exp\left(\dfrac{\beta}{4\tau}q_0^4\right) & \text{for } \alpha < 0 \text{ and capillary} \end{array}\right\} \quad \text{as } w \to w^*, \qquad (2.58)$$

where C is the constant indicated in eqn (2.56). The limit for Q is now easily found from eqn (2.24). Thus as $n \to \infty$ and $w \to w^*$, we may summarise our findings as

$$\theta_n \sim \left\{\begin{array}{ll} \left[\Lambda\dfrac{(\sqrt{-A})^{\pm 1}}{(-A)^{1/4}}\right]\dfrac{\Gamma(n+\gamma_1)}{\left(X_1 W^{1-\alpha}\right)^{n+\gamma_1}} & \alpha > 0 \\ \left[\Lambda C\right]\dfrac{\Gamma(n+\gamma_2)}{q_0^6\left(X_2 W^{1-3\alpha}\right)^{n+\gamma_2}} & \alpha < 0 \text{ and gravity} \\ \left[\Lambda q_0^4 \exp\left(\dfrac{\beta}{4\tau}q_0^4\right)\right]\dfrac{\Gamma(n+\gamma_3)}{\left(X_3 W^{\alpha+1}\right)^{n+\gamma_3}} & \alpha < 0 \text{ and capillary} \end{array}\right. \qquad (2.59)$$

again, as $w \to w^*$. The constants γ_1, γ_2, and γ_3 are determined by ensuring that the late terms above match with the early terms. The case of $\alpha < 0$ and for capillary waves is clearly problematic due to the exponential, but we will later find that the expression for Θ in eqn (2.57) is in fact *invalid*—there is an intermediary layer so that blindly matching with the inner limit of the outer approximation, q_0, is incorrect.

The most straightforward value to determine is γ_2; using (2.24), (2.36), and setting $n = 0$ in (2.59) gives

$$\gamma_2 = \frac{-6\alpha}{1 - 3\alpha}. \qquad (2.60)$$

We have already discussed (in Section 2.6.1) how the two governing equations change as we tend towards a point not on the free-surface. We will repeat the analysis, but this time with the added precaution of keeping higher-order terms. Near the singularity, the dynamic condition remains unchanged, but the boundary integral equation is considerably simplified as the Hilbert Transform term $\mathscr{H}[\theta(\zeta)]$ now forms a regular series in ϵ. We then replace

$$i\theta \sim \log q - \alpha \log(w - w^*) - \log c + \mathcal{O}(\epsilon) \tag{2.61}$$

$$i\frac{d\theta}{dw} \sim \frac{dq}{dw}\frac{1}{q} - \frac{\alpha}{(w - w^*)} + \mathcal{O}(\epsilon) \tag{2.62}$$

$$i\frac{d^2\theta}{dw^2} \sim \frac{d^2q}{dw^2}\frac{1}{q} - \left(\frac{dq}{dw}\right)^2 \frac{1}{q^2} + \frac{\alpha}{(w - w^*)^2} + \mathcal{O}(\epsilon), \tag{2.63}$$

We may now substitute eqns (2.61)-(2.63) into the dynamic condition (2.4), yielding

$$\begin{aligned} \epsilon i q^2 q_w - \epsilon^2 \tau \left[q_{ww} q - q_w^2 + \left\{ \frac{\alpha}{(w - w^*)^2} + \mathcal{O}(\epsilon) \right\} q^2 + q_w^2 + \left\{ -\frac{\alpha}{w - w^*} + \mathcal{O}(\epsilon) \right\} q q_w \right] \\ = \frac{1}{2\beta} \left[\left(\frac{c(w - w^*)^\alpha}{q} \right) - \frac{q}{c(w - w^*)^\alpha} + \mathcal{O}(\epsilon) \left(\frac{q}{c(w - w^*)^\alpha} + \frac{c(w - w^*)^\alpha}{q} \right) \right]. \end{aligned} \tag{2.64}$$

This is the correct equation to use for analysis near the singularity.

2.8.2 *An isolated capillary singularity* ($\alpha > 0$)

We first note that the inner-limit for χ found in (2.37) had involved the following dominant balance from (2.18):

$$-\tau q_0^2 \left(\frac{d\chi}{dw}\right)^2 \sim \frac{1}{\beta},$$

or

$$\frac{d\chi_\pm}{dw} \sim \mp \frac{1}{\sqrt{\beta\tau} q_0},$$

as $w \to w^*$, and with the reversal of the signs due to the analytic continuation process, as discussed in the paragraph following eqn (2.18). χ is thus formed by a balance between the surface curvature (double-derivative) terms which are $\mathcal{O}(\epsilon^2)$, and gravitational terms which are $\mathcal{O}(1)$, both contained in Bernoulli's equation (2.4). As we tend towards the singularity, the late-order ansatz is dominated by its behaviour between terms coupled an $\mathcal{O}(\epsilon^2)$ apart, so q''_{n-2} and q_n, rather than the $\mathcal{O}(\epsilon)$ coupling between terms, q''_{n-2}, q'_{n-1}, and q_n of the *outer* ansatz.

Note that a similar type of mechanism was also observed in the study of Chapman & Vanden-Broeck (2002) for the study of capillary waves in low-Bond flows, but there, they found waves which were generated by a balance between inertial and surface-tension terms. In our case, we have waves which are initially generated between gravitational and surface-tension terms, but also involves inertial effects near the free-surface!

In preparation for the matching procedure, then, we can write the outer expansion of (2.8) as

$$q = \sum_{n=0}^{\infty} \epsilon^{2n} q_{2n} + \sum_{n=0}^{\infty} \epsilon^{2n+1} q_{2n+1}.$$

Then, the late-order ansatzes are provided by

$$q_{2n+k} \sim \frac{Q\Gamma(2n+\gamma_k)}{\chi^{2n+\gamma_k}}, \qquad \text{for } k = 0, 1.$$

where the expressions for χ and Q are still the same. In the inner region, we know (ignoring constant pre-factors) $\chi \sim \mathcal{O}(W^{1-\alpha})$ and $Q \sim \mathcal{O}(W^{\alpha})$, so matching powers we have

$$\begin{aligned} \gamma_0 &= 0, \\ \gamma_1 &= \left(\frac{1-3\alpha}{1-\alpha}\right). \end{aligned}$$

However, before studying the matching procedure, we mention a crucial simplification. In this problem, although there are two different ansatzes (matched with q_0 and q_1), the second ansatz is smaller than the first in the inner region, and so only the first dominant ansatz plays a role in determining Λ. To see this, we assume that $W \sim \epsilon^{1/(1-\alpha)}$ (the size of the inner region) and then

$$\epsilon^{2n+k} q_{2n+k} \sim \left\{ \begin{array}{ll} \mathcal{O}\left(\dfrac{\epsilon^{2n}\epsilon^{\frac{\alpha}{1-\alpha}}}{\epsilon^{2n}}\right) = \mathcal{O}\left(\epsilon^{\frac{\alpha}{1-\alpha}}\right) & \text{for } k = 0 \\ \mathcal{O}\left(\dfrac{\epsilon^{2n+1}\epsilon^{\frac{\alpha}{1-\alpha}}}{\epsilon^{\frac{1-3\alpha}{1-\alpha}}\epsilon^{2n}}\right) = \mathcal{O}\left(\epsilon^{\frac{3\alpha}{1-\alpha}}\right) & \text{for } k = 1 \end{array} \right\} \quad \text{as } w \to w^*, \tag{2.65}$$

so the late-order terms corresponding to the second ansatz are smaller within the inner region. With this in mind, we substitute

$$w - w^* = \epsilon^{\frac{1}{1-\alpha}}\nu \qquad \text{and} \qquad q = c\epsilon^{\frac{\alpha}{1-\alpha}}\nu^{\alpha}\widetilde{q}$$

into eqn (2.64). Then to leading order

$$-\tau c^2 \widetilde{q}^2 \left[-\alpha\eta^{2\alpha-2}\widetilde{q} + \alpha\eta^{2\alpha-1}\frac{d\widetilde{q}}{d\nu} + \eta^{2\alpha}\frac{d^2\widetilde{q}}{d\nu^2}\right] = \frac{1}{2\beta}\left[1 - \widetilde{q}^2\right].$$

We will write $\widetilde{X} = X_1^+$, which is taken from (2.37). Letting $z = \widetilde{X}^2\nu^{2(1-\alpha)}$ in the above equation and simplifying then gives

$$-\tau c^2 \widetilde{X}^2 \left[-\alpha\frac{\widetilde{q}^3}{z} + 2(\alpha-1)^2\left(\widetilde{q}^2\frac{d\widetilde{q}}{dz} + 2z\widetilde{q}^2\frac{d^2\widetilde{q}}{dz^2}\right)\right] = \frac{1}{2\beta}\left[1 - \widetilde{q}^2\right].$$

We now seek the series expansion of $\widetilde{q}$ as $z \to \infty$ by setting

$$\widetilde{q} = \sum_{n=0}^{\infty} \frac{A_n}{z^n},$$

which leads to the recurrence relation

$$A_n = \frac{1}{2A_0}\left\{2\beta\tau c^2\widetilde{X}^2\sum_{j=0}^{n-1}\sum_{k=0}^{n-j-1}\left[2k(2k+1)(\alpha-1)^2-\alpha\right]A_kA_jA_{n-j-k-1} - \sum_{k=1}^{n-1}A_kA_{n-k}\right\},$$

for $n \geq 1$, and where $A_0 = 1$ (we have eliminated $A_0 = -1$ from the requirement that the inner solution matches with q_0 as $z \to \infty$). We can re-write this last equation as

$$A_n = \sum_{j=0}^{n-1}\sum_{k=0}^{n-j-1}\left[4k\left(k+\frac{1}{2}\right) - \frac{\alpha}{(1-\alpha)^2}\right]A_kA_jA_{n-j-k-1} - \sum_{k=1}^{n-1}\frac{A_kA_{n-k}}{2}, \tag{2.66}$$

and now, Van Dyke's Rule can be used to match the inner and outer expansions. The rule stipulates that the n^{th} term outer approximation, written in inner variables and taking the leading-order term is the same as the leading-order inner-expansion, written in outer variables and taking the n^{th} term. Or more briefly, (1.t.i)(n.t.o) = (n.t.o)(1.t.i).

Taking n^{th} term outer approximation, written in inner variables, and keeping the first term gives

$$q = \sum_{n=0}^{\infty}\epsilon^{2n}q_{2n} \xrightarrow{(n.\text{t.o})} \epsilon^{2n}q_{2n} \sim \epsilon^{2n}\frac{iq_0\Theta_+\Gamma(2n)}{(\widetilde{X}W^{1-\alpha})^{2n}} \xrightarrow{(1.\text{t.i})} \epsilon^{\frac{\alpha}{1-\alpha}}\frac{ic\nu^\alpha\Theta\Gamma(2n)}{z^n},$$

while taking the leading-order inner approximation, and re-expanding to the n^{th} term gives

$$q \xrightarrow{(1.\text{t.i})} \epsilon^{\frac{\alpha}{1-\alpha}}c\nu^\alpha\widetilde{q} \xrightarrow{(n.\text{t.o})} \epsilon^{\frac{\alpha}{1-\alpha}}\frac{c\nu^\alpha A_n}{z^n}.$$

Matching the final two expressions gives

$$\Theta_+ = -i\left[\lim_{n\to\infty}\frac{iA_n}{\Gamma(2n)}\right],$$

and using the fact that $\Theta_+ \sim \Lambda(-A)^{1/4}$ from eqn (2.58) we have

$$\Lambda = \frac{1}{(-A)^{1/4}}\left[\lim_{n\to\infty}\frac{A_n}{\Gamma(2n)}\right].$$

This completes the determination of Λ for the case of $\alpha > 0$ and the capillary-only singularities.

2.8.3 *A gravity-capillary singularity* ($\alpha < 0$)

Remember that from the discussions surrounding Figure 2.10 that we expect a more complicated triple-layer structure near the singularities with $\alpha < 0$. Here, the correct scalings in the middle region are given by the asymptotic forms of q and χ as $w \to w^*$. We let

$$w - w^* = \epsilon^{\frac{1}{1-3\alpha}}\eta \qquad \text{and} \qquad q = \epsilon^{\frac{\alpha}{1-3\alpha}}c\eta^\alpha\overline{q}. \tag{2.67}$$

Substituting both these re-scaled variables into the equation for the middle-layer (2.64) gives

$$ic^3\overline{q}^3\left[\alpha\eta^{3\alpha-1}\overline{q}+\eta^{3\alpha}\frac{d\overline{q}}{d\eta}\right]-\epsilon^{\rho}\tau c^2\overline{q}^2\left[\eta^{2\alpha}\frac{d^2\overline{q}}{d\eta^2}+\alpha\eta^{2\alpha-1}\frac{d\overline{q}}{d\eta}\right] + E(\eta,\overline{q};\epsilon)=\frac{1}{2\beta}\left[1-\overline{q}^2\right], \quad (2.68)$$

where we have defined $\rho=-4\alpha/(1-3\alpha)$ and

$$E(\eta,\overline{q};\epsilon)=-\epsilon^{\rho}\tau c^2\overline{q}^2\left[\mathcal{O}\left(\epsilon^{\frac{3-3\alpha}{1-3\alpha}}\right)\eta^{2\alpha}\overline{q}+\mathcal{O}\left(\epsilon^{\frac{2-3\alpha}{1-3\alpha}}\right)\alpha\eta^{2\alpha-1}\overline{q} + \mathcal{O}\left(\epsilon^{\frac{2-3\alpha}{1-3\alpha}}\right)\eta^{2\alpha}\frac{d\overline{q}}{d\eta}\right]-\mathcal{O}(\epsilon)\frac{1}{2\beta}\left[\overline{q}^2+1\right]. \quad (2.69)$$

In this layer, we will need to do two things. First, we perform a Taylor Series expansion for the leading-order solution, $\overline{q}$, in order to match with the outer solution, q, in the limit that $\eta\to\infty$; second, we generate the high order terms $\overline{q_n}$ of this intermediate layer so that we may later match with the solutions in the innermost layer.

The key here is that $E(\eta,\overline{q};\epsilon)$, which is composed of terms of the Hilbert Transform taken in the inner limit, remains subdominant in the analysis to follow. This is akin to our analysis of the outer problem, for which we discovered that the integral terms are unimportant for both the determination of the outer-to-inner limits, as well as for late-orders expansion of q_n. Let us first begin with the middle-to-outer matching problem.

The middle-to-outer matching problem

Conveniently, this middle-to-outer matching problem is *identical* to the one studied in Chapman & Vanden-Broeck (2006), except with a general β instead of $\beta=1$. The leading order solution in the middle-layer is given by balancing the first and last brackets of eqn (2.68):

$$2\beta c^3 i\overline{q}^2\left[\alpha\eta^{3\alpha-1}\overline{q}+\eta^{3\alpha}\overline{q}'\right]=\left[-\overline{q}+\frac{1}{\overline{q}}\right]. \quad (2.70)$$

We may then let

$$z=|X_2|\eta^{1-3\alpha}=\frac{i\eta^{1-3\alpha}}{\beta c^3(1-3\alpha)},$$

with X_2 given by (2.37); this gives

$$-\frac{2\alpha\overline{q}^3}{z(1-3\alpha)}-2\overline{q}^2\frac{d\overline{q}}{dz}=-\overline{q}+\frac{1}{\overline{q}},$$

which is now identical to eqn (3.26) in Chapman & Vanden-Broeck. Following their results, the matching between the leading order approximation in this layer with the late terms of the outer approximation yields

$$\Lambda=\frac{c^{-3\gamma}e^{-\pi\gamma/2}}{2\beta^{\gamma-1}C(1-3\alpha)^{\gamma}}\lim_{n\to\infty}\frac{\phi_n}{\Gamma(n+\gamma)}, \quad (2.71)$$

where ϕ_n is provided by the recurrence relation,

$$\begin{aligned}\phi_0 &= 1,\\ \phi_n &= \sum_{m=0}^{n-1} \beta\left(m - \frac{2\alpha}{1-3\alpha}\right)\phi_m\phi_{n-m-1} \quad \text{for } n \geq 1,\end{aligned}$$

and we have only modified eqn (2.71) to take in account the factor of β.

Late-order terms and inner limits

We now substitute the asymptotic expansion,

$$\overline{q} = \sum_{n=0}^{\infty} \epsilon^{\rho n}\overline{q_n} \tag{2.72}$$

into eqn (2.68). Although there are terms in $E(\eta, \overline{q}; \epsilon)$ that contain powers of ϵ not of the form ρn, we can see that the first contribution of E occurs at $\mathcal{O}(\epsilon)$, which, for $\alpha \in (-1, 0)$ is subdominant to $\overline{q} \sim \overline{q_0} + \epsilon^\rho \overline{q}$. In other words, the expansion in eqn (2.72) is valid for *at least* the first two terms; coupling with the Hilbert Transforms does not occur until later.

Returning to (2.68) then, at $\mathcal{O}(1)$ this yields

$$c^3 i\overline{q_0}^3\left[\underbrace{\alpha\eta^{3\alpha-1}\overline{q_0}}_{①} + \underbrace{\eta^{3\alpha}\overline{q_0}'}_{②}\right] = \frac{1}{2\beta}\left[\underbrace{1}_{③} - \underbrace{\overline{q_0}^2}_{④}\right], \tag{2.73}$$

the same as (2.70). This time, however, instead of seeking the middle-to-outer limit ($\eta \to \infty$), we want the middle-to-inner limit ($\eta \to 0$). If we attempt a balance between ① and ③ in eqn (2.73) the first possibility is

$$\overline{q_0} \sim \pm\left(\frac{-1}{2\beta}\right)\left(\frac{1}{ci\alpha}\right)\eta^{\frac{1-3\alpha}{4}}. \tag{2.74}$$

However, there is also a possibility of a dominant balance in terms ① and ②. This yields

$$\overline{q_0} \sim \bar{c}\eta^{-\alpha} \tag{2.75}$$

where $\bar{c}$ is a constant. It is easily verified that both cases are possible by examining the remaining terms, but since $\alpha \in (-1, 0)$, the unforced solution (2.75) will dominate the other (2.74), assuming that $\bar{c} \neq 0$. We can verify that $\bar{c}$ is non-zero by letting $r(\eta) = (\overline{q_0}\eta^\alpha)^2$. Then r satisfies the equation

$$\frac{dr}{d\eta} = \frac{1}{\beta c^3}\left(\eta^{-\alpha} - \frac{\eta^\alpha}{r}\right), \tag{2.76}$$

where, remembering that $\overline{q_0} \to 1$ as $\eta \to \infty$, we would expect r to decay to zero as $\eta \to \infty$. Moreover, if a nontrivial solution does indeed exist, then using (2.75), we would have $r(0) = \bar{c}$. The eigenvalue problem for $\bar{c}$ can then be solved by using a shooting method on eqn (2.76): we begin with a sufficiently large value of c^* and solve the differential equation subject to the initial condition $r(0) = c^*$, but if the solution diverges, then the value of c^*

is decreased, while if the solution crosses $r = 0$, then the value is increased. Convergence, $c^* \to \overline{c}$ is fast for all interesting values of β and c and indeed, $\overline{c} \neq 0$. Thus, it is the asymptotic behaviour of eqn (2.75) that we want.

Proceeding now to $\mathcal{O}(\epsilon^\rho)$, we have

$$c^3 i\alpha\eta^{3\alpha-1}\left[4\overline{q_0}^3\overline{q_1}\right] + ic^3\eta^{3\alpha}\left[\overline{q_0}^3\frac{d\overline{q_1}}{d\eta} + 3\overline{q_0}^2\overline{q_1}\frac{d\overline{q_0}}{d\eta}\right] - \tau c^2\left[\eta^{2\alpha}\overline{q_0}^2\frac{d\overline{q_0}}{d\eta^2} + \alpha\eta^{2\alpha-1}\overline{q_0}^2\frac{d\overline{q_0}}{d\eta}\right] = -\frac{1}{\beta}\overline{q_0}\,\overline{q_1} \quad (2.77)$$

and we can reorganise this linear differential equation to be

$$\left[ic^3\left(4\alpha\eta^{3\alpha-1}\overline{q_0}^3 + 3\eta^{3\alpha}\overline{q_0}^2\frac{d\overline{q_0}}{d\eta}\right) + \frac{1}{\beta}\overline{q_0}\right]\overline{q_1} + \left[ic^3\eta^{3\alpha}\overline{q_0}^3\right]\frac{d\overline{q_1}}{d\eta} = \tau c^2\left[\eta^{2\alpha}\overline{q_0}^2\frac{d^2\overline{q_0}}{d\eta^2} + \alpha\eta^{2\alpha-1}\overline{q_0}^2\frac{d\overline{q_0}}{d\eta}\right]. \quad (2.78)$$

While this is complicated, we again only need the asymptotic form of $\overline{q_1}$. Using (2.75), we can show that

$$\frac{d\overline{q_1}}{d\eta} + \left(\frac{\alpha}{\eta}\right)\overline{q_1} \sim \left(\frac{-i\tau}{c\eta^{\alpha+2}}\right),$$

which can be solved to yield

$$\overline{q_1} \sim \left(\frac{i\alpha\tau}{c}\right)\frac{1}{\eta^{\alpha+1}}. \quad (2.79)$$

This completes our determination of the first two orders of the asymptotic series. Let us now begin the high-order analysis; like in Section 2.3, we will write down the $\mathcal{O}(\epsilon^{\rho n})$ terms of eqn (2.68), but in doing so, we will only need to keep the *two* highest order terms as $n \to \infty$; this is in anticipation of later substituting-in of the ansatz

$$\overline{q_n} \sim \frac{\overline{Q}\Gamma(n+\overline{\gamma})}{\overline{\chi}^{n+\overline{\gamma}}}, \qquad \text{as } n \to \infty \quad (2.80)$$

The relevant terms of eqn (2.68) are

$$\overbrace{\left[4i\alpha c^3\eta^{3\alpha-1}\overline{q_0}^3 + 3ic^3\eta^{3\alpha}\overline{q_0}^2\overline{q_0}' + \frac{1}{\beta}\overline{q_0}\right]}^{①}\overline{q_n} + \underbrace{\left[ic^3\eta^{3\alpha}\overline{q_0}^3\right]}_{②}\frac{d\overline{q_n}}{d\eta} + \underbrace{\left[3ic^3\eta^{3\alpha}\overline{q_0}^2\overline{q_1} - \tau c^2\alpha\eta^{2\alpha-1}\overline{q_0}^2\right]}_{③}\frac{d\overline{q_{n-1}}}{d\eta} + \underbrace{\left[-\tau c^2\eta^{2\alpha}\overline{q_0}^2\right]}_{④}\frac{d^2\overline{q_{n-1}}}{d\eta^2} + \underbrace{\left[-2\tau c^2\eta^{2\alpha}\overline{q_0 q_1}\right]}_{⑤}\frac{d^2\overline{q_{n-2}}}{d\eta^2} + \ldots = 0, \quad (2.81)$$

and again, we point out the fact that the term $E(\eta, \overline{q}; \epsilon)$ containing the Hilbert Transforms does not determine the form of the late-orders behaviour. This is because we would expect the behaviour of the late-order terms to be dominated by

$$E(\eta, \overline{q}; \epsilon) \sim -\epsilon^{\rho} \tau c^2 \overline{q}^2 \left[\mathcal{O}\left(\epsilon^{\frac{2-3\alpha}{1-3\alpha}} \right) \eta^{2\alpha} \frac{d\overline{q}}{d\eta} \right] - \mathcal{O}(\epsilon) \frac{\overline{q}^2}{2\beta}. \tag{2.82}$$

The term on the left with the derivative of $\overline{q}$ would be needed for the late-orders only if it was of comparable order to

$$-\epsilon^{\rho} \tau c^2 \overline{q}^2 \left[\alpha \eta^{2\alpha - 1} \frac{d\overline{q}}{d\eta} \right],$$

which is from the surface-tension terms of (2.68), and contributes at *second-order* as $n \to \infty$. However, $\frac{2-3\alpha}{1-3\alpha} > 1$ so this cannot be the case. Similar reasoning applies to the second term on the right of eqn (2.68). Terms like $\overline{q}$ contribute only at second-order as $n \to \infty$, and so $\mathcal{O}(\epsilon)\overline{q}^2$ is not relevant.

Returning to eqn (2.81) we now substitute the ansatz (2.80) and take the limit as $n \to \infty$. At leading order, only the terms from ② and ④ are involved and we have

$$\frac{d\overline{\chi}}{d\eta} \left(-② + ④ \cdot \frac{d\overline{\chi}}{d\eta} \right) = 0.$$

The solution with $d\overline{\chi}/d\eta = 0$ corresponds to the $\mathcal{O}(1)$ gravity waves studied in the previous section and we will instead focus on the other branch, which has

$$\frac{d\overline{\chi}}{d\eta} = \frac{②}{④} = \frac{ci\eta^{\alpha}\overline{q_0}}{-\tau}, \tag{2.83}$$

and in particular, we see that as $\eta \to 0$,

$$\overline{\chi} \sim \frac{c\bar{c}i}{-\tau}\eta. \tag{2.84}$$

At second order as $n \to \infty$, we have

$$\begin{aligned} \left(\frac{d\overline{Q}}{d\eta} \right) \frac{1}{\overline{Q}} &= \left[\frac{① - ③\left(\frac{d\overline{\chi}}{d\eta} \right) - ④\left(\frac{d^2\overline{\chi}}{d\eta^2} \right) + ⑤\left(\frac{d\overline{\chi}}{d\eta} \right)^2}{②} \right] \\ &= 2\left(\frac{d\overline{q_0}}{d\eta} \right) \frac{1}{\overline{q_0}} + \frac{2\alpha}{\eta} + \frac{ic\eta^{\alpha}\overline{q_1}}{\tau} - \frac{i\eta^{-3\alpha}}{\beta c^3 \overline{q_0}^2}, \end{aligned}$$

and thus

$$\overline{Q} = \overline{\Lambda}\overline{q_0}^2 \eta^{2\alpha} \exp\left[\int_{\eta^{\star}}^{\eta} \left(\frac{ics^{\alpha}\overline{q_1}(s)}{\tau} - \frac{is^{-3\alpha}}{\beta c^3 \overline{q_0}^2(s)} \right) ds \right], \tag{2.85}$$

where $\overline{\Lambda}$ is a constant. Now let us seek the limit of $\overline{Q}$ as $\eta \to 0$. If we use eqns (2.75) and (2.79), we can write

$$\begin{aligned} \overline{q_0} &= \bar{c}\eta^{-\alpha} + \mathcal{O}(\eta^{-\alpha+j}) \\ \overline{q_1} &= \left(\frac{i\alpha\tau}{c} \right) \eta^{-\alpha-1} + \mathcal{O}(\eta^{-\alpha-1+k}), \end{aligned}$$

where $j > 0$ and $k > 0$. Then

$$\begin{aligned}\overline{Q} &= \left[\bar{c}^2 + \mathcal{O}(\eta^j)\right]\overline{\Lambda}\exp\left\{\int_{\eta^\star}^{\eta}\left[-\frac{\alpha}{s} + \mathcal{O}(s^{k-1}) - \frac{is^{-3\alpha}}{\beta c^3\overline{q_0}^2(s)}\right]ds\right\} \\ &= \overline{\Lambda}\,\bar{c}\eta^{-\alpha}\underbrace{\left[\bar{c}\eta^{\star\alpha}\exp\left\{\int_{\eta^\star}^{\eta}\frac{-is^{-3\alpha}}{\beta c^3\overline{q_0}^2(s)}\,ds\right\}\right]}_{\overline{C}}\left\{1 + \mathcal{O}(\eta^j, \eta^k)\right\},\end{aligned}$$

where $\eta^\star$ is any arbitrary point where the integrand is defined, and in summary, then,

$$\overline{Q} \sim \overline{\Lambda C}\,\bar{c}\eta^{-\alpha} \sim \overline{\Lambda C}\overline{q_0}. \tag{2.86}$$

The last step is to determine the value of $\overline{\gamma}$. We substitute the inner limits of $\overline{\chi}$ and $\overline{Q}$ from (2.84) and (2.86) into the ansatz of (2.80), set $n = 0$, and require the behaviour to match that of $\overline{q_0}$ in (2.75); this shows that $\overline{\gamma} = 0$.

We have thus completed the late-orders analysis of the gravity-layer. The key aspect of our work in this section was to derive the properties of $\overline{\chi}$ and $\overline{Q}$ as $\eta \to 0$. Now armed with this correct behaviour, we can properly study the innermost layer.

2.8.4 The innermost layer with $\mathcal{O}(1)$ capillary waves

For the innermost region, eqn (2.84) suggests that the layer occurs when $\eta \sim \mathcal{O}(\epsilon^\rho)$ whereas eqn (2.75) suggests that $\overline{q} \sim \mathcal{O}(\eta^{-\alpha})$. Therefore we will let

$$\eta = \epsilon^{\frac{-4\alpha}{1-3\alpha}}\nu \qquad \text{and} \qquad \overline{q} = \bar{c}\eta^{-\alpha}\widehat{q}$$

where $\widehat{q}$ and ν indicate the re-scaled variables in the innermost layer. In terms of the original outer coordinates,

$$w - w^* = \epsilon^{\frac{1-4\alpha}{1-3\alpha}}\nu \tag{2.87}$$

and

$$q = c\bar{c}\epsilon^{\frac{\alpha}{1-3\alpha}}\widehat{q}, \tag{2.88}$$

and these scalings seem rather strange, as they have little relevance to the original *outer* approximations! The location and scalings of the innermost layer cannot simply be gleaned by studying the outermost series. We also note that with $\alpha < 0$,

$$\epsilon^{\frac{1}{1-3\alpha}} \gg \epsilon^{\frac{1-4\alpha}{1-3\alpha}},$$

so we are assured that the innermost layer is indeed smaller than the middle, gravity-dominated layer.

Recall that near the singularity, eqn (2.64) applies, so with $\alpha < 0$ and the new scalings in (2.87) and (2.88), we find that the left-hand side of the equation dominates the right, giving at leading order

$$c\bar{c}\left[\widehat{q}\frac{d\widehat{q}}{d\nu}\right] - \frac{\tau}{i}\left[\frac{d^2\widehat{q}}{d\nu^2} - \frac{\alpha}{\nu^2}\frac{d\widehat{q}}{d\nu} + \frac{\alpha}{\nu}\widehat{q}\right] = 0.$$

Integration then gives

$$\frac{(c\bar{c})}{2}\widehat{q}^2 - \tau\left[\frac{d\widehat{q}}{d\nu} - \frac{\alpha}{\nu}\widehat{q}\right] = \text{constant}.$$

Since we need $\widehat{q} \to 1$ as $\nu \to \infty$, the constant must be equal to $c\bar{c}/2$ and so

$$\frac{c\bar{c}}{2}\left[\widehat{q}^2 - 1\right] - \frac{\tau}{i}\left[\frac{d\widehat{q}}{d\nu} - \alpha\frac{\widehat{q}}{\nu}\right] = 0.$$

We will re-scale again, setting

$$\widehat{\nu} = \left(\frac{ic\bar{c}}{-\tau}\right)\nu$$

into the inner equation. Rearranging then gives

$$\frac{d\widehat{q}}{d\widehat{\nu}} + \frac{1}{2}\left[\widehat{q}^2 - 1\right] - \frac{\alpha\widehat{q}}{\widehat{\nu}} = 0. \tag{2.89}$$

Like our analysis of the leading-order gravity problem in the middle layer, we have thus reduced the nonlinear inner problem to a previous sub-case, this one from Chapman & Vanden-Broeck (2002) for the study of free-surface flows with only surface tension. Our (2.89) is identical to their (3.18) and represents a dominant balance between inertial and surface-tension terms contained in Bernoulli's Equation.

We can now proceed as usual and study the inner-to-middle limit of the solution $\widehat{q}$ by expanding

$$\widehat{q} = \sum_{n=0}^{\infty} \frac{\widehat{A_n}}{\widehat{\nu}^n},$$

as $\widehat{\nu} \to \infty$ and solving the resultant nonlinear recurrence relation. However, as shown in Chapman & Vanden-Broeck (2002), the exact solution of (2.89) can be given in terms of Bessel functions and in fact,

$$\widehat{A_n} \sim \frac{2}{\pi}\sin\left(\frac{\pi\alpha}{2}\right)\Gamma(n). \tag{2.90}$$

We can now apply the Van-Dyke matching procedure to the innermost and middle solutions. Taking n^{th} term middle approximation, written in inner variables, and keeping the first term gives

$$\overline{q} \xrightarrow{(n.\text{t.m})} \epsilon^{\rho n}\overline{q_n} \sim \epsilon^{\rho n}\frac{\overline{\Lambda C}\,\overline{q_0}\Gamma(n)}{\left[\left(\frac{ic\bar{c}}{-\tau}\right)\eta\right]^n} \xrightarrow{(1.\text{t.i})} \overline{\Lambda C}\,\overline{q_0}\frac{\Gamma(n)}{\widehat{\nu}^n},$$

while taking the leading-order inner approximation, and re-expanding to the n^{th} term gives

$$\overline{q} \xrightarrow{(1.\text{t.i})} \overline{q_0}\widehat{q} \xrightarrow{(n.\text{t.m})} \overline{q_0}\frac{\widehat{A_n}}{\widehat{\nu}^n}.$$

Finally, using (2.90), matching provides us with the result that

$$\overline{\Lambda} = \frac{1}{\overline{C}}\left[\lim_{n\to\infty}\frac{\widehat{A_n}}{\Gamma(n)}\right] = \frac{2}{\pi\overline{C}}\sin\left(\frac{\pi\alpha}{2}\right). \tag{2.91}$$

2.8.5 *Relating the inner, middle, and outer analyses*

The Stokes smoothing procedure of Section 2.4 shows that near the free surface, the waves are of the form

$$q_{\text{exp}} \sim -\frac{2\pi i}{\epsilon^{\gamma}} Q e^{-\chi/\epsilon}, \tag{2.92}$$

where we have only included the contribution from analytic continuation into the upper-half plane. For the case of gravity waves, we have already derived complete expressions for each of the components of the above equation, up the determination of a numerical constant Λ shown in Section 2.8.3. It thus remains to do the same for the capillary branch of the solutions. An analogous smoothing procedure to the one done in the outer layer (Section 2.4) gives a similar expression:

$$q_{\text{exp}} \sim -2\pi i q_0 \overline{Q} e^{-\overline{\chi}/\epsilon^{\rho}}, \tag{2.93}$$

valid in the middle region, and our goal is to thus relate (2.92) and (2.93) within the intermediary region between middle and outer layers.

First, beginning with the form of the outer solutions, from (2.24) and (2.57), we can write the inner limits of Q using the middle variables of (2.67). This gives

$$Q = i\Theta q_0 \sim \epsilon^{\frac{5\alpha}{1-3\alpha}} i\Lambda c^5 \eta^{5\alpha} \exp\left[\frac{\beta c^4 \eta^{4\alpha}}{4\tau\epsilon^{\rho}}\right]. \tag{2.94}$$

Similarly, written in inner variables, the outer χ behaves like

$$\frac{\chi}{\epsilon} \sim \frac{-ic\eta^{\alpha+1}}{\tau(\alpha+1)\epsilon^{\rho}}. \tag{2.95}$$

Now, turning to the middle solutions as they tend to the outer layer ($\eta \to \infty$), the leading-order term of (2.73) behaves like

$$\overline{q_0} = 1 - \frac{i\alpha c^3 \beta}{\eta^{1-3\alpha}}, \tag{2.96}$$

and from (2.83), this shows that

$$\frac{\overline{\chi}}{\epsilon^{\rho}} = \frac{1}{\epsilon^{\rho}} \int_{\eta\star}^{\eta} \left(\frac{ci\eta^{\alpha}}{-\tau}\right) \overline{q_0}(s)\, ds \sim \left[-\frac{ic\eta^{\alpha+1}}{\tau(\alpha+1)} - \frac{\beta c^4 \eta^{4\alpha}}{4\tau}\right] \frac{1}{\epsilon^{\rho}}. \tag{2.97}$$

The term on the left is simply the re-scaled inner limit of the outer χ, whereas the term on the right is the exponential factor in Q. Using the form of $\overline{q_0}$ in (2.96), with $\overline{Q}$ from (2.85), and the value of $\overline{\Lambda}$ in (2.91), we have

$$\overline{Q} = \frac{2\sin\left(\frac{\pi\alpha}{2}\right)\eta^{4\alpha}}{\pi} \left\{ \exp\left[\int_{\eta\star}^{\eta} \left(\frac{ics^{\alpha}\overline{q_1}(s)}{\tau} - \frac{is^{-3\alpha}}{\beta c^3}\right) ds\right] \frac{1}{\overline{C}} \right\}. \tag{2.98}$$

However, the procedure leading to the definition of $\overline{C}$ in (2.86) necessarily implies that the ratio between the exponential and $\overline{C}$ tends to 1 as $\eta \to \infty$. Combining the set of eqns (2.92) to (2.98) gives the final result that

$$\Lambda = -\frac{2i\epsilon^{\gamma+\rho}}{c^4\pi} \sin\left(\frac{\pi\alpha}{2}\right),$$

and so we have completely determined the capillary waves generated by the triple-layer singularity.

Now having reached the end of our work on the gravity-capillary problem, we have one final query: *do these new waves truly exist?*

Certainly, our theoretical predictions form the first attempt of exploring the previously unknown region of low-Froude and low-Bond numbers. Our results posit the existence of six different families of waves for flow over a step (❶–❻), revealing that the usual dispersion curve separating linear solutions ❶ and ❻ widens if we include the nonlinear nature of the geometry. While this structure is only valid at low Froude and low Bond numbers, it also sheds new light on the general complexity of gravity-capillary problem, which has been acknowledged in the past.

Many open questions remain, some of which may ultimately hold the key to detecting these new waves (or discounting their existence altogether!). Throughout this chapter, we have provided a clear analysis of the *local* issues of the gravity-capillary problem. We have shown, for example, how the emergence of a Stokes line depends on the local angle of the obstruction (Table 2.1); how the switching-on of waves near turning points can be predicted via an Airy-like transition (Section 2.6.1); or how the crucial pre-factor, Λ, can be solved-for by matching inner and outer solutions near the singularities of the asymptotic solution (Section 2.8). But what of the *global* properties of the Stokes lines?

In Section 2.7, while studying the Stokes lines for flow over a rectangular step, we encountered several subtle issues which were never completely resolved. For example, can a Stokes line emerge from a singularity along an irrelevant Riemann sheet, only to later return to the correct sheet and intersect the free-surface? Do the crossing of Stokes lines (Figure 2.4 and 2.9) produce any other unanticipated effects? It is well known that even the asymptotic analysis of 'toy' problems containing multiple singularities can lead to very complex Stokes line structures, and indeed, some of these issues have appeared elsewhere, and in the works of Berk et al. (1982), Howls et al. (2004), and Chapman & Mortimer (2005).

Early efforts by the author to detect these new waves by solving the nonlinear equations (2.1)–(2.2) have been unsuccessful. But this failure could mean very little; in the search for solutions of wave problems with non-trivial upstream conditions, the correct manner in applying the radiation condition is still an unsolved problem. The resultant solutions are heavily influenced by the chosen treatment of the far field and it is entirely possible that the inherent errors in current numerical treatments make it extremely difficult to differentiate between the structure of our new gravity-capillary waves. Do these waves truly exist? Our results say they do, and a discovery of such a solution, in nature or in the digital world, would be a triumphant success for our theory indeed.

Do waveless ships exist?

PART I: SINGLE-CORNERED SHIPS

3.1 INTRODUCTION

3

> *Whosoever commands the sea*
> *commands the trade;*
> *whosoever commands the trade of the world*
> *commands the riches of the world,*
> *and consequently the world itself.*
> —SIR WALTER RALEIGH, (1829)

The world of today may have changed a great deal since Raleigh's time, but the weight of his words have not: sea-faring ships continue to transport over ninety percent of the world's total trade (Brockel, 1982; Europa, 2009) and a reduction of their combined wave resistance would equate to great savings in fuel, time and, most importantly, money. It should thus come as no surprise that the tantalising idea of a waveless ship has fascinated the naval community for some time. Our interests, then, are simply stated: are waveless ships theoretically possible? If so, what restrictions must we placed on their design? If not, what can be done to minimise their production of waves?

Of course, when we refer to a waveless ship, we have a very specific regime in mind: that of potential flow (a standard assumption). Now in attempting to solve this problem, it becomes necessary to linearise the boundary conditions at the free surface, and as it concerns ship waves we generally have three ways of proceeding. The most standard and most well-developed method linearises the geometry of the ship by assuming that the hull is sufficiently small in one or several of its dimensions. For example, applying the thin-ship approximation leads to the well-known Mitchell integral, for which it has been shown that wave resistance can never vanish at any finite speed for ships of finite displacement (Kotik & Newman 1964 and Krein in Kostyukov 1968). But as remarked by Tuck (1991a):

> *This is not quite a closed issue. Mitchell's integral is only an approximation to the actual wave resistance, and, lacking any general or exact formula for the wavemaking properties of a ship, or any moving object near a free-surface, one cannot be quite sure that a similar result will hold for non-thin ships.*

Instead, if we wish to preserve the geometry of the ship in the approximation, an alternative linearisation can be performed by developing a solution valid as the Froude number tends to infinity. For these high-Froude problems, the flow detaches from the ship smoothly at leading order (zero gravity) and the free-surface is a free streamline. Spurred on by the initial numerical computations of Vanden-Broeck (1980), Madurasinghe & Tuck (1986) went on to discover waveless ships, an analysis which was later confirmed by the more detailed numerics of Farrow & Tuck (1995).

However, in discerning the effects of the ship's geometry on the resultant waves, the low-Froude limit is by far the more important and non-trivial choice. The reason is that the analysis near a blunt three-dimensional ship can be reduced to the study of the two-dimensional potential flow problem for which the ship is modeled as a semi-infinite body with constant draft (Dagan & Tulin, 1972). Ultimately, it is the low-Froude limit which truly models the ship-water interactions and for which the nonlinearity of the ship's geometry is taken into account.

The question we ask in this chapter and the following is then: do there exist waveless ships in the low-Froude limit? For example, are any of these ships waveless?

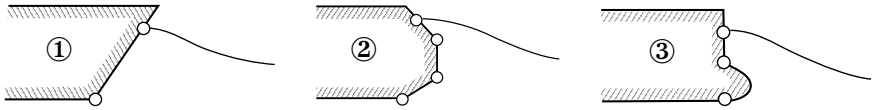

Figure 3.1: ① is the single-cornered ship, ② is the multi-cornered ship, ③ is the bulbous ship, and the flow tends from the left to the right.

Note that in the potential flow problem, a waveless solution past the stern (rear) of a ship is equivalent to a splashless solution at the bow (front) of a ship. Then, if the profiles in Figure 3.1 are indeed solutions, then they are equally valid for flow in either direction.

We know from previous chapters that there is an important difficulty: when an ideal fluid flows past a surface-piercing object or over an obstruction, waves are sometimes produced upstream or downstream of the disturbance. But in the low-speed limit, the traditional asymptotic series in powers of the Froude number fails to capture this phenomenon—in the context of ship-wave studies, this has been termed the *Low-Speed Paradox*, first mentioned by Ogilvie (1968). The waves are in fact, exponentially small (in the Froude number) and thus invisible to any traditional asymptotic analysis.

This formidable singular limit has been painfully problematic in regards to previous asymptotic and numerical treatments of the ship-wave problem. The fully nonlinear problem was first computed by Vanden-Broeck & Tuck (1977), and on the basis of numerical evidence, they conjectured that ship hulls with a single front face will always generate waves. Moreover, the earlier experimental work of Baba (1976) had indicated that a bulbous bow can eliminate, or at least reduce the splash at the bow of a ship. This prompted the discovery of seemingly waveless ships with bulbous profiles, first by Tuck and Vanden-Broeck (1984) and later confirmed by Madurasinghe (1988)—but again, only *numerically so*. Another surprising result was suggested by Yeung in (1991), whose recent numerics suggested that, for the single-cornered hull, there exists a critical Froude number below which no trailing waves are possible—in direct contrast to Vanden-Broeck & Tuck (1977)! Unfortunately, these last three results were refuted by the more comprehensive numerical study of Farrow & Tuck (1995); there, they wrote:

> *The free surface would at first sight appear to be waveless, but on closer examination of the numerical data, there are very small waves present and they have a steepness of* 1.5×10^{-3},

a comment they had made in reference to the bulbous profiles found in the work of Tuck & Vanden-Broeck (1984). Clearly, these are questions which cannot be easily answered using simple numerics. Indeed, in *Reminiscences and Reflections: Ship Waves, 1950–2000*, Tulin mentions two open problems:

> *The fundamental questions of whether such rising potential free-surface flows before bluff bodies exist [...] still remain open*,

and

> *Is it demonstrable [...] that continuous solutions will not exist in the limit of vanishing speed? Does this have anything to do with the inability of Tuck and his colleagues [...] to find a continuous solution in the two-dimensional bow wave case? Do nonbreaking flows exist at all for surface-piercing ship forms of arbitrary form and thickness, at any speed?*

The above encapsulates a brief summary of the last forty years of research on the *numerical* nonlinear ship problem, much of which stems from the seminal work of Vanden-Broeck & Tuck (1977). Unfortunately, moving along the same timeline, there was still much confusion as to the correct method of analysing the low-Froude limit. For example, there was still debate as to the correct method of linearising the Bernoulli free-surface conditions. The methods of this period were dependent on a linearisation of the free-surface, η, and potential, ϕ, about the zeroth order asymptotic approximation, and thus setting $\phi = \phi_0 + \phi'$ and $\eta = \eta_0 + \eta'$. Afterwards, this was substituted into Bernoulli's equation, and different authors chose to keep different terms, depending on what they each believed to be important in the preservation of the eventual wave-like structure of the solutions. In (1996), Raven lists *five* different linearisations offered in Newman (1976), Dawson (1977), Eggers (1981), Brandsma & Hermans (1985), and Nakos (1990).

Now, however, we know that resolving the Low-Speed Paradox is dependent on a clear understanding of asymptotic divergence—its causes and its consequences. The low-Froude limit is singular, and thus causes the leading-order solution to exhibit singularities in its analytic continuation, which eventually produces the divergence of the series. This divergence, in turn, is associated with the presence of exponentially small terms representing, in this case, our hidden free-surface waves. The essential correction to the aforementioned linearisation(s) is that the solution should be expanded about its optimally truncated expansion, rather than its first asymptotic approximation; otherwise, the perturbation η' will contain the $\mathcal{O}(\epsilon)$ error of the higher order terms, plus the exponentially small error of the hidden waves.

In this chapter, we will apply methods in exponential asymptotics and attempt a resolution of the problem of low-Froude flows past a single-cornered ship. We will show how the exponentially small waves arise when the solution crosses the Stokes line originating from the corner-singularity of the stern and in doing so, we will confirm the 1977 conjecture of Vanden-Broeck and Tuck concerning the impossibility of waveless single-cornered ships. Finally, we will provide sufficiently accurate numerical simulations which confirm our analytical predictions.

In the first chapter of this thesis, we used the Airy function to introduce many of the underlying techniques of exponential asymptotics. In this section, we provide another simple example which nevertheless illustrates the key ideas; ideas like asymptotic divergence, the Stokes Phenomenon, optimal truncation, and so on. In this way, readers already familiar with the previous chapters can freely move on to the next section, whereas readers who chose to forego gravity-capillary waves in favour of ship waves can profit from this independent survey.

The nature of the Stokes Phenomenon and its importance for the study of asymptotic expansions can be discussed by considering the differential equation

$$\frac{df}{dz} + f = \frac{\epsilon}{z} \qquad \text{with } f(z) \to 0 \text{ as } z \to -\infty, \tag{3.1}$$

and where we will first suppose z to be real and negative. In the limit that $\epsilon \to 0$, we can derive the full asymptotic expansion from this differential equation, giving

$$f(z) = \sum_{n=1}^{\infty} \epsilon^n \frac{(n-1)!}{z^n}. \tag{3.2}$$

For all (fixed) values of z and ϵ, the series in (3.2) clearly diverges, a result of the factorial growth of the numerator overpowering the entire expansion. We can plot the error between the exact value of $f(z)$ and the $\mathcal{N}^{\text{th}}$ partial sum of the expansion:

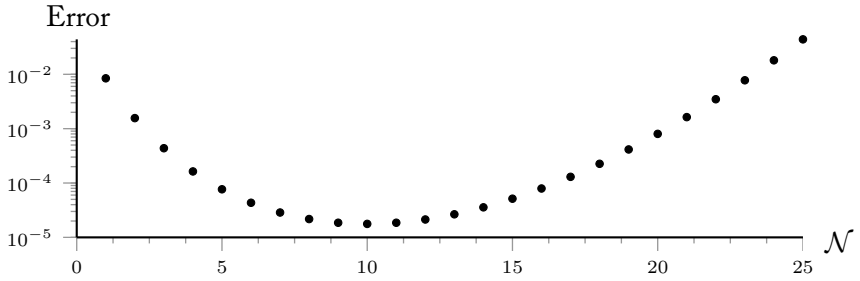

Figure 3.2: The error of the $\mathcal{N}^{\text{th}}$ partial sum of (3.2) for $z = -1$ and $\epsilon = 0.1$. The optimal truncation point, where the error is smallest, occurs at $N \sim |z|/\epsilon = 10$. This type of curve, which has the error decreasing to a minimum, then diverging to infinity, represents the typical behaviour for singular approximations.

This type of behaviour almost always accompanies singular asyptotic expansions and the point of least error, called the *optimal truncation point*, is generally found where adjacent terms in the expansion have the same magnitude—in this case, at $\mathcal{N} \sim |z|/\epsilon$ (*c.f.* Bender & Orszag 1978).

Now suppose that we return to (3.2) and allow z to be a complex number and moreover, we allow it to vary along a contour which begins at some point on the negative real axis, encircles the origin in a counter-clockwise fashion, and returns to the same point, but now from the upper-half imaginary plane. Of course, throughout this whole process, the asymptotic expansion (3.2) is seemingly indifferent to any change. But the integral formulation of $f(z)$ tells a different story. For here,

$$f(z) = e^{-z/\epsilon} \int_{-\infty}^{z/\epsilon} \frac{e^t}{t}\, dt, \tag{3.3}$$

and for z in the lower-half plane, the method of steepest descents allows a re-derivation of the asymptotic expansion (3.2) by expanding about the right endpoint at $t = z$. However, as z crosses the positive real axis, the path of steepest descent crosses the pole and we are required to add a contribution of size $2\pi i e^{-z/\epsilon}$ to the asymptotic expansion. That is, $f(z) \sim \epsilon/z$ in the forth quadrant, but $f(z) \sim \epsilon/z + 2\pi i e^{-z/\epsilon}$ in the first! This is shown in the following figure:

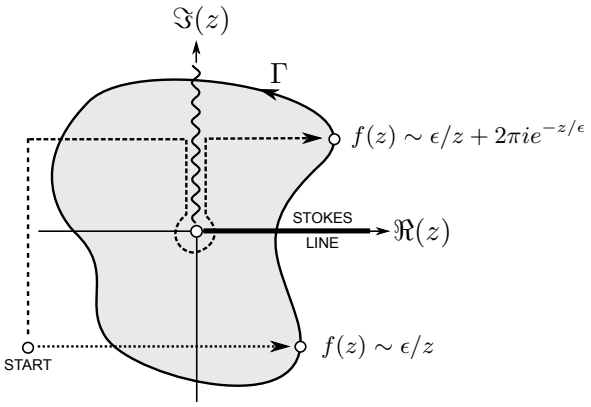

Figure 3.3: As z is analytically continued into the upper-half plane, the previous steepest descent contour (dotted) must include the addition of a pole contribution (dashed), and thus switches on an exponentially small term across the Stokes line. The oscillatory line indicates the branch cut.

The *Stokes Phenomenon* is the name given to this sudden appearance of exponentially small terms as a critical line is crossed. These *Stokes lines* must originate from singularities in the analytic continuation of the asymptotic solution and are a *necessary* consequence of the singular nature of the problem.

However, a more pressing question is in regards to the relationship between the Stokes Phenomenon, the asymptotic representation of $f(z)$ in (3.2), and the corresponding differential equation (3.1). In many problems, the integral formulation is unavailable (or simply too unwieldy); in this case, how can we re-derive the exponentially small contributions?

The key to answering this question—and thus leading to the theory of exponential asymptotics and asymptotics beyond all orders—is the idea that the information for the determination of the exponential is contained in the late terms of the asymptotic expansion (3.2). There are a number of ways to retrieve this seemingly hidden information, but we will focus on a method which uses optimal truncation and matched asymptotics, as developed in Olde Daalhuis et al. (1995) and Chapman et al. (1998).

We will quickly describe the process. First, the asymptotic expansion (3.2) is truncated at $n = \mathcal{N}$ and substituted into the differential equation (3.1), thus providing an equation for the remainder, $R_{\mathcal{N}}(z)$:

$$\epsilon \frac{dR_{\mathcal{N}}}{dz} + R_{\mathcal{N}} = \epsilon^{\mathcal{N}} \frac{(\mathcal{N}-1)!}{z^{\mathcal{N}}}. \tag{3.4}$$

When $\mathcal{N}$ is chosen to be the optimal truncation point, the remainder is *exponentially small* (rather than only algebraically small) and can be written as $R_{\mathcal{N}} = \mathcal{S}(z)e^{-z/\epsilon}$, where we expect $\mathcal{S}(z)$ to smoothly vary from zero to a constant across the Stokes line. Indeed a brief calculation shows that if

$z = re^{i\theta}$, then $\mathcal{S}(z)$ is given by

$$\mathcal{S}(z) = i\sqrt{2\pi}\int_{-\infty}^{\sqrt{r}\overline{\theta}} e^{-t^2/2}\,dt,$$

for a re-scaled variable $\overline{\theta} = \theta/\sqrt{\epsilon}$ near the critical line. Thus, as $\overline{\theta} \to \infty$, we have jumped across the Stokes line, and the apparent jump in $\mathcal{S}(z)$ is $[\mathcal{S}] \sim 2\pi i$. Note that the determination of the remainder in (3.4) relies upon knowledge of the late-order terms of the asymptotic expansion—hence the connection between the Stokes Phenomenon and the terms *beyond-all-orders*. This is the general methodology we follow in solving the ship problem.

Finally, we shall conclude this section by directing the reader to Figure 3.4, where we have illustrated and briefly described the key ideas behind our ship-wave analysis.

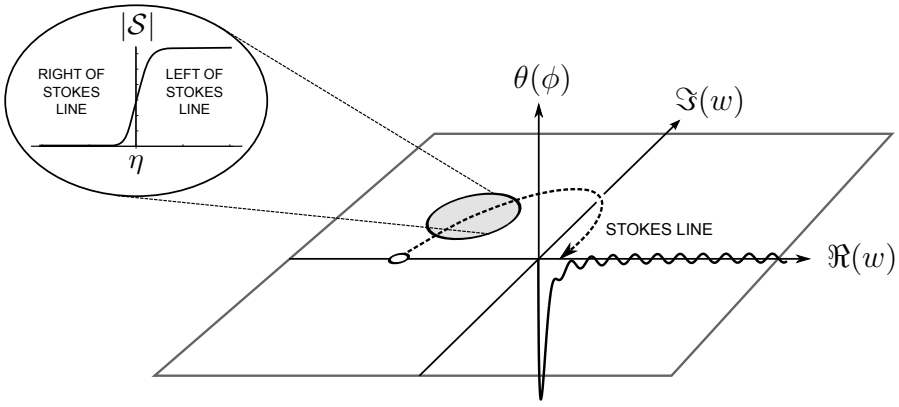

Figure 3.4: The *physical* solution of interest in the ship-wave problem is θ, the angle of the free-surface as a function of some real potential $\phi > 0$. Although this solution is perfectly well-defined, its asymptotic representation is divergent in some limit $\epsilon \to 0$ and contains a singularity in its analytic continuation (shown as a perpendicular plane, $\phi = w \in \mathbb{C}$). By re-scaling near the Stokes line and optimally truncating, we will be able to observe the smooth switching-on of the exponentially small terms (top-left).

3.3 MATHEMATICAL FORMULATION

Consider two-dimensional, steady, incompressible, irrotational, and inviscid flow past a semi-infinite body in the presence of gravity and with small Froude number. We will consider bodies consisting of a flat bottom ($y^* = -H, x^* < 0$) and a face oriented with an angle $\pi\sigma$ to the horizontal, with $0 < \sigma < 1$. There is a uniform stream of speed U as $x^* \to -\infty$, and we assume that the flow attaches to the stern at a stagnation point, $(x^*, y^*) = (0, 0)$. The set-up is shown in the figure below.

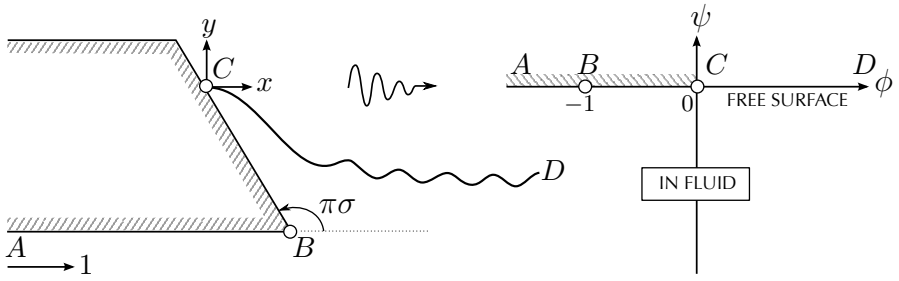

Figure 3.5: Nondimensional flow past a one-cornered ship is shown in the physical xy-plane (left) and the potential $w = \phi + i\psi$ plane (right).

Letting the fluid velocity be $\mathbf{u}^* = (u^*, v^*) = \nabla\phi^*$, the velocity potential, ϕ^*

then satisfies Laplace's Equation,

$$\nabla^2 \phi^* = 0. \tag{3.5}$$

There are two boundary conditions: on all boundaries, we have the kinematic condition

$$\frac{\partial \phi^*}{\partial n} = 0, \tag{3.6}$$

while on the free surface, we have the dynamic condition, provided by Bernoulli's Equation,

$$\frac{1}{2}\left(|\nabla \phi^*|^2 - U^2\right) + g y^* = 0. \tag{3.7}$$

At the moment, the problem in eqns (3.5) to (3.7) is posed in terms of the dimensional velocity potential $\phi^*(x^*, y^*)$. To non-dimensionalise the problem, we select a new potential, $\phi(x, y)$, which tends to the unit free stream, $\phi \to x$ as $x \to \infty$. To do that, we define the non-dimensional variables as

$$x = \left[x^* - \left(H + \frac{U^2}{2g}\right)\right]\frac{1}{L}, \qquad y = \left[y^* - \frac{U^2}{2g}\right]\frac{1}{L}, \qquad \phi = \frac{\phi^*}{UL}.$$

The length scale is chosen so that $L = K/U$ where $\phi^* = -K$ at the corner of the stern, and this places the corner at $\phi = -1$. Without loss of generality we choose to centre the system at the stagnation point, so $\phi = 0$ and thus, we arrive at the following non-dimensionalised equations:

$$\nabla^2 \phi = 0, \tag{3.8}$$

$$\frac{\partial \phi}{\partial n} = 0, \tag{3.9}$$

$$\frac{\epsilon}{2}|\nabla \phi|^2 + y = 0, \tag{3.10}$$

where $\epsilon = U^2/gL$ is related to the square of the draft-based Froude number and $\epsilon \ll 1$.

Unfortunately, formulated as a function of cartesian coordinates (x, y), the problem is rather difficult to approach—especially since the dynamic condition (3.10) must be applied to an *as-yet* unknown free-surface. In the simplifying *hodograph* formulation, we introduce the complex potential $w = \phi + i\psi$ and let $z = x + iy$; now both Laplace's equation (3.8) and the kinematic condition (3.9) are immediately satisfied, so long as we ensure the complex potential is analytic. We now define

$$q e^{-i\theta} \equiv \frac{dw}{dz} = u - iv, \tag{3.11}$$

so q is the speed of the flow and θ is the angle the streamline makes with the x-axis. Then if s is the arclength along the free-surface, then

$$\frac{dx}{ds} = \cos\theta, \qquad \frac{dy}{ds} = \sin\theta.$$

Differentiating Bernoulli's Equation (3.10) with respect to s now gives

$$\epsilon q \frac{dq}{ds} + \sin\theta = 0. \tag{3.12}$$

Since

$$\frac{dq}{ds} = \frac{d\phi}{ds}\frac{dq}{d\phi} = q\frac{dq}{d\phi}$$

we may write (3.12) as

$$\epsilon q^2 \frac{dq}{d\phi} + \sin\theta = 0, \tag{3.13}$$

where the free surface condition is now applied to the streamline $\psi = 0$ for $\phi > 0$.

To close the system, we will need one final equation, and for this, we examine the analyticity of the logarithm of the hodograph variable, given by $\log q - i\theta = \log dw/dz$. Remember that when $\epsilon = 0$, the free-surface is replaced by a rigid wall $y = 0$, and the flow is then equivalent to the flow in a channel (see for example, Milne-Thomson 1968). The problem then has the leading order solution

$$\theta = 0, \qquad q = \left(\frac{w}{w+1}\right)^{\sigma}. \tag{3.14}$$

The logarithm of the hodograph, $\log q - i\theta$, is analytic everywhere in the fluid ($\psi < 0$), but not continuous along the boundary at the stagnation point, $w = 0$, or the corner, $w = -1$. Because of this, consider instead the function

$$\Upsilon(w) = (\log q - i\theta) - \log\left(\frac{w}{w+1}\right)^{\sigma} \tag{3.15}$$

which removes the discontinuities at $w = 0$ and $w = -1$, and also vanishes at $\epsilon = 0$ and $\psi \to -\infty$. Since $\Upsilon(w)$ is now analytic everywhere in the lower half plane and continuous on the real axis, we can apply Cauchy's Theorem to $\Upsilon(w)$ on a path consisting of the streamline $\psi = 0$ and the semi-circle at $\psi = -\infty$,

$$\Upsilon(w) = -\frac{1}{2\pi i}\int_{-\infty}^{\infty} \frac{\Upsilon(\varphi)}{\varphi - w} d\varphi, \tag{3.16}$$

where w is located *off* the axis, where the integral is taken along the axis, and where the semi-circular contribution at infinity has disappeared since $\Upsilon \to 0$ as $\psi \to -\infty$. When we let w approach the axis, the integral then decomposes into a Cauchy Principal Value and a residue contribution,

$$\Upsilon(\phi - i0) = -\frac{1}{2\pi i}\left(\fint_{-\infty}^{\infty} + \int_{\frown}\right) \frac{\Upsilon(\varphi)}{\varphi - \phi} d\varphi. \tag{3.17}$$

Moving the residue to the left hand side and simplifying yields

$$\Upsilon(\phi - i0) = -\frac{1}{\pi i}\fint_{-\infty}^{\infty} \frac{\Upsilon(\varphi)}{\varphi - \phi} d\varphi, \tag{3.18}$$

and taking the real part of eqn (3.18) yields

$$\log q = \frac{1}{\pi} \fint_{-\infty}^{\infty} \frac{\theta(\varphi)}{\varphi - \phi} d\varphi, \tag{3.19}$$

i.e. the usual boundary integral result for two-dimensional free-surface flows. Steps (3.15) to (3.19) serves to verify that the discontinuity along the real axis does not cause any problems to the usual formula.

As in Chapman & Vanden-Broeck (2002, 2006), we want to complexify the free-boundary $\psi = 0$, so that we may examine the nature of $q(\phi)$ from eqn (3.14) as it is analytically continued into the complex ϕ plane.

Here, there is a fortuitous, though somewhat subtle simplification: when we complexify $\phi \mapsto \overline{\phi} + i\overline{\psi}$, we may identify this *new* complexified potential with the *old* potential $w = \phi + i\psi$, and thus each point in the complexified free boundary (illustrated as the perpendicular plane of Figure 3.4) can be identified with a point in the fluid region. Similarly, when we complexify q and θ, these new variables can be identified with the *old* complex potential $dw/dz = qe^{-i\theta}$, where here, q and θ are of course *real*. This subtle difference between the complexified free boundary and the fluid region must be kept in mind; we will complexify the free boundary both into the upper-half and lower-half ϕ planes—but of course, only the lower-half w plane contains actual fluid! This subtly was also discussed in Section 1.2 of the first chapter.

When we analytically continue the boundary integral (3.19) and the dynamic condition (3.13), this gives

$$\log q \pm i\theta = \frac{1}{\pi} \int_{-\infty}^{0} \frac{\theta(\varphi)}{\varphi - w}\, d\varphi + \mathscr{H}[\theta(w)], \tag{3.20}$$

$$\epsilon q^2 \frac{dq}{dw} + \sin\theta = 0, \tag{3.21}$$

where we have replaced the complexified ϕ by w and the $\pm$ signs correspond to analytic continuation in the upper and lower-half ϕ planes, respectively. We have also introduced the notation

$$\mathscr{H}[\theta(w)] = \frac{1}{\pi} \int_{0}^{\infty} \frac{\theta(\varphi)}{\varphi - w}\, d\varphi,$$

to represent the Hilbert transform of θ, integrated over the free-surface, $\varphi \geq 0$. For the next few sections, we will perform the asymptotic analysis of (3.20) and (3.21) for analytic continuation into the *upper*-half plane. Remember that in the end, we will need to perform the same analysis for continuation into the *lower*-half ϕ plane as well.

3.4 Asymptotic approximation

Substituting the usual perturbation expansion

$$\theta = \sum_{n=0}^{\infty} \epsilon^n \theta_n \quad \text{and} \quad q = \sum_{n=0}^{\infty} \epsilon^n q_n, \tag{3.22}$$

into eqns (3.20) and (3.21) yields at $\mathcal{O}(1)$,

$$\theta_0 = 0 \quad \text{on the free boundary, } \phi > 0, \tag{3.23}$$

$$\log q_0 = \frac{1}{\pi}\int_{-\infty}^{0} \frac{\theta_0(\varphi)}{\varphi - w}\, d\varphi. \tag{3.24}$$

Using the fact that $\theta = \pi\sigma$ on the real w-axis from -1 to 0, (3.20) gives

$$\log q_0 = \sigma \log\left(\frac{w}{w+1}\right) \Rightarrow q_0 = \left(\frac{w}{w+1}\right)^{\sigma}, \tag{3.25}$$

a fact we already know. Then at $\mathcal{O}(\epsilon)$, (3.20) and (3.21) yield

$$\theta_1 = -q_0^2 \frac{dq_0}{dw}, \tag{3.26}$$

$$\frac{q_1}{q_0} + i\theta_1 = \mathscr{H}[\theta_1(w)]. \tag{3.27}$$

The full expressions for the higher $\mathcal{O}(\epsilon^n)$ terms are more complicated, but since we are only concerned with the limit $n \to \infty$, we may proceed as follows: examine the leading order free surface, $q_0(w)$ in (3.25); the solution contains two singularities, identifiable with points in the flow-domain—one at the corner of the stern ($w = -1$) and the other at the stagnation point ($w = 0$). However, because all the higher-order problems are linear, no new singularities can be introduced and thus the singular points of $q_n(w)$ must be those *same* singularities as for $q_0(w)$.

For example, if we examine the dynamic condition in (3.21), we can see that each successive term of the asymptotic approximation will require the derivative of the previous term. Thus if q_n contains a singularity of the form $1/(w - w_0)^n$, q_{n+1} will contain a singularity of the form $n/(w - w_0)^{n+1}$; each new derivative adds a factor to the numerator and increases the strength of the singularity. Then as $n \to \infty$, we can expect the late terms to behave like factorial over power,

$$\theta_n \sim \frac{\Theta(w)\Gamma(n+\gamma)}{\chi(w)^{n+\gamma}} \quad \text{and} \quad q_n \sim \frac{Q(w)\Gamma(n+\gamma)}{\chi(w)^{n+\gamma}}. \tag{3.28}$$

With this ansatz in mind, we can now pinpoint the terms required at $\mathcal{O}(\epsilon^n)$. In the limit that $n \to \infty$, terms like $q_m q_n$ (for m finite) dominate terms with smaller indices in n, such as $q_m q_{n-1}$. Moreover, differentiating a term increases the order (in n) by 1, so a term like $\epsilon dq_{n-1}/dw$ is of the same order as q_n. The relevant terms at $\mathcal{O}(\epsilon^n)$ are:

$$\overbrace{\frac{q_n}{q_0} + i\theta_n}^{\text{first order}} - \overbrace{\frac{q_{n-1}q_1}{q_0^2}}^{\text{second order}} + \ldots = \overbrace{\mathscr{H}[\theta_n]}^{\text{exp. subdominant}}, \tag{3.29}$$

$$\underbrace{q_0^2 q'_{n-1}}_{\text{first order}} + \underbrace{2q_0 q'_{n-2} + 2q_0 q'_0 q_{n-1}}_{\text{second order}} + \ldots = \underbrace{-\cos(\theta_0)\theta_n}_{\text{first order}} + \ldots. \tag{3.30}$$

By recourse to Chapman and Vanden-Broeck (2006), we claim, at least for the moment, that the integral on the right-hand side of the boundary integral

equation (3.29) is exponentially subdominant to the terms on the left-hand side for large n. We address this claim a little later in Section 3.5.3, but for now, we will assume that

$$\theta_n \sim i\frac{q_n}{q_0} - \frac{iq_1q_{n-1}}{q_0^2} + \dots \qquad \text{as } n \to \infty, \tag{3.31}$$

or,

$$q_n \sim -iq_0\theta_n - i\theta_{n-1}q_1 + \dots \qquad \text{as } n \to \infty. \tag{3.32}$$

Finally, substituting (3.31) into the dynamic condition (3.30) and simplifying yields the final form of our $\mathcal{O}(\epsilon^n)$ expression:

$$\overbrace{\left[q_0^3 q'_{n-1} + iq_n\right]}^{\text{first/second order}} + \underbrace{\left[2q_0^2 q'_0 q_{n-1} + 3q_0^2 q_1 q'_{n-2}\right]}_{\text{second order}} + \dots = 0. \tag{3.33}$$

The factorial over power ansatz (3.28) can now be substituted into (3.33). As $n \to \infty$, the leading-order expression is

$$-q_0^3\frac{d\chi}{dw} + i = 0, \tag{3.34}$$

which is simply solved to yield

$$\chi = \int^w \frac{i}{q_0^3}\, d\varphi, \tag{3.35}$$

where we will choose the initial point of integration in the next section. At the next order in n, we find

$$q_0^3 Q' + 2Qq_0^2 q'_0 - 3Qq_0^2 q_1 \chi' = 0$$

or,

$$\frac{Q'}{Q} = -\frac{2q'_0}{q_0} + \frac{3iq_1}{q_0^4}, \tag{3.36}$$

and thus by the usual integration and simplification,

$$Q = \frac{\Lambda}{q_0^2}\exp\left(3i\int_{w\star}^w \frac{q_1}{q_0^4}\, d\varphi\right), \tag{3.37}$$

where Λ is a constant of integration and $w^\bigstar$ is any arbitrary point for which the integral exists. By the ansatz (3.28) and relation (3.31), we know that $\theta_n \sim iq_n/q_0$ and thus

$$\Theta = \frac{\Lambda i}{q_0^3}\exp\left(3i\int_{w\star}^w \frac{q_1}{q_0^4}\, d\varphi\right). \tag{3.38}$$

3.5 THE SINGULANT AND ITS STOKES LINES

In this section, we will use the expression (3.35) for the singulant, χ, to address three separate questions: (1) Must the stagnation point at the origin produce an exponentially small wave on the free-surface? (2) What necessary conditions are imposed on the corner of the hull in order for it to generate a wave? and (3) How can the boundary integral on the right-hand side of eqn (3.20) be shown to be exponentially subdominant to the residue contributions on the left?

3.5.1 *The stagnation point*

The nature of the free-surface near the stagnation point, $w = 0$, is a surprisingly complex problem. First, there is the issue of how the solution behaves near $w = 0$, that is to say, for fixed ϵ and within the inner region; the works of, for example, Dagan & Tulin (1972) and Vanden-Broeck & Tuck (1994) have examined some of these problems. Second, there is the question of how the solution near $w = 0$ interacts with the low-Froude expansion of (3.22) and in particular, what is its role (if any) in controlling the production of downstream waves. In regards to this latter question, Tuck (1991a) has provided a series of unanswered questions for simpler differential equations related to the full water wave equations in (3.20) and (3.21).

The local analysis near the stagnation point for ϵ fixed and $w \to 0$ is given in Appendix 3.A. There we show that

$$q \sim \begin{cases} \mathcal{O}(w^\sigma) & \text{if } \sigma \geq 1/3 \\ \mathcal{O}(w^{1/3}) & \text{if } \sigma < 1/3 \end{cases} \tag{3.39}$$

and

$$\theta \sim \theta_0 + \mathcal{O}(w^\kappa) \sim \begin{cases} 0 + \mathcal{O}(w^{3\sigma-1}) & \text{if } \sigma \geq 1/3 \\ \pi\left(\sigma - \frac{1}{3}\right) + \mathcal{O}(w^\varsigma) & \text{if } \sigma < 1/3 \end{cases} \tag{3.40}$$

where ς is a transcendental number given by solving (3.70). In words, then, (3.40) states that for hulls with $\sigma \geq 1/3$, the near-stagnation flow is the same as the rigid wall solution; but for hulls with $\sigma < 1/3$, the free-surface makes a $2\pi/3$ angle with the ship—very much like the cusp of a highest Stokes wave (Wehausen & Laitone, 1960).

Now we investigate the inner limit of the outer approximations. Consider first (3.27):

$$q_1 = -iq_0\theta_1 + \frac{q_0}{\pi}\int_0^\infty \frac{\theta_1}{\varphi - w}\, d\varphi.$$

In the case of $1/3 < \sigma < 1$, the integrand satisfies the Hölder condition on the interval $[0, \infty)$ and moreover, $\theta_1(0) = 0$. This guarantees that

$$\frac{1}{\pi}\int_0^\infty \frac{\theta_1}{\varphi - w}\, d\varphi \sim \frac{1}{\pi}\int_0^\infty \frac{\theta_1}{\varphi}\, d\varphi = \text{constant}$$

as $w \to 0$. Thus $q_1 \sim q_0$ as $w \to 0$ (the residue contribution $-iq_0\theta_1$ is lower order) and by induction $q_n \sim q_{n-1}$ for all n. In other words, for hulls with $\sigma > 1/3$, the singular nature of the origin does not magnify as n increases and hence there is no eventual divergence in the asymptotic series. In this case, then, there is no exponential contribution.

Now consider the case that $0 < \sigma < 1/3$. Here, the outer solution behaves like $q_0 \sim \mathcal{O}(w^\sigma)$ and consequently $\theta_1 \sim \mathcal{O}(w^{3\sigma-1})$ tends to infinity at the stagnation point. An inner layer is required where the solution has the behaviour of (3.71) as $w \to 0$. In any case, we can write

$$\mathscr{H}[\theta_1(w)] = \frac{-\sigma}{\pi}\int_0^\infty \frac{d\varphi}{\varphi^{1-3\sigma}(\varphi - w)} + \frac{\sigma}{\pi}\int_0^\infty \frac{-(\varphi+1)^{-1-3\sigma} + 1}{\varphi^{1-3\sigma}(\varphi - w)}\, d\varphi.$$

It is easy to verify that the rightmost integrand satisfies the Hölder condition on $[0, \infty)$ and is thus bounded and tending to a definite limit as $w \to 0$. The integral on the left contains a power singularity and thus by (Gakhov, 1966, p. 55), $\mathscr{H}[\theta_1(w)] \sim \mathcal{O}(w^{3\sigma-1})$. Inductively continuing this line of reasoning verifies that the growth of the integral term is indeed proportional to the growth of the residue term and thus,

$$q_n \sim \mathcal{O}(iq_0\theta_{n-1}) \qquad \text{as } n \to \infty.$$

This shows that for $\sigma \leq 1/3$, the singularity *does* cause the late-order outer terms to diverge and moreover, at a rate specified by the ansatz (3.28). Thus, the stagnation point must be accompanied by the Stokes Phenomenon and the switching-on of exponentials. Still, it is entirely possible that the accompanying Stokes line does not come to intersect the free-surface (other than at $w = 0$) and/or lies on a separate Riemann sheet altogether; *this is our conjecture*. And while the claim remains unproven, the numerical analysis of the problem in Section 3.7 provides compelling evidence in its favour. We will return to this issue in the discussion of Section 3.8.

3.5.2 The corner

The corner is the critical point which is responsible for the generation of waves. Since $\chi(-1) = 0$, we may write (3.35) as

$$\chi = i\int_{-1}^{w} \frac{1}{q_0^3}\, d\varphi = i\int_{-1}^{w} \left(\frac{\varphi+1}{\varphi}\right)^{3\sigma} d\varphi, \tag{3.41}$$

where the contour of integration can be taken along any path in the upper-half plane, *not* through $w = 0$. In fact, this expression can be exactly integrated in terms of special functions, and

$$\chi(w) = -i(-w)^{3\sigma} w^{-3\sigma} B\Big(-w; 1-3\sigma, 1+3\sigma\Big) + 3\sigma\pi\Big[1 + i\cot(3\sigma\pi)\Big] \tag{3.42}$$

where $B(x, y)$ is the Beta function. Near the corner,

$$q_0 \sim e^{\pi i\sigma}(w+1)^{-\sigma} \quad \text{and} \quad \chi \sim \left[\frac{ie^{-3\pi i\sigma}}{1+3\sigma}\right](w+1)^{1+3\sigma}$$

and from Dingle (1973), Stokes lines are expected whenever χ is purely real and positive. Thus, the first (and only relevant) Stokes line leaves the critical point at an angle of

$$\vartheta = \pi\left(\frac{3\sigma - 1/2}{1+3\sigma}\right),$$

arcs into the upper-half plane, and continues until it intersects the free-surface. This is shown in Figure 3.6. The intersection points are farthest when σ large and as $\sigma \to 0$, they tend towards the origin. In Section 3.6 and onwards, we will focus what happens when each of these Stokes lines is crossed.

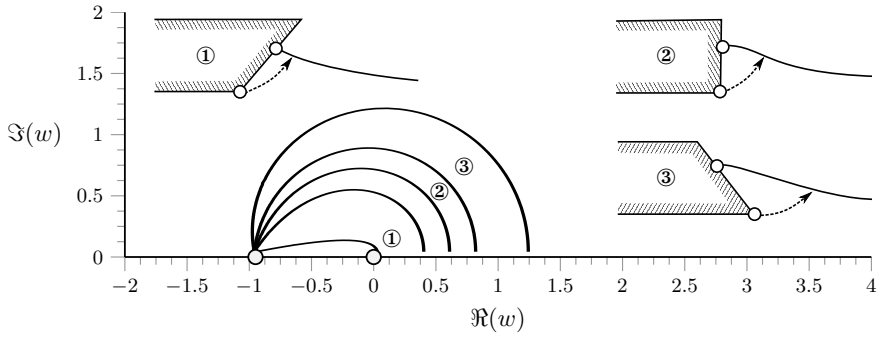

Figure 3.6: Stokes lines for various hulls, such ① $\sigma = 0.2$, ② $\sigma = 0.5$, and ③ $\sigma = 0.6$ (the tags are to the upper-right of their associated lines). The Stokes lines begin and end at $w = -1$ and are symmetrical about the real axis. Across the intersection of the Stokes line with $\Re(w) > 0$, we expect an exponential to switch on. Although they are an *imaginary* construct and lie on the analytically continued free-surface, they nevertheless share a correspondence with a line in the physical plane which begins at the corner and arcs towards the free-surface, as shown in the smaller sketches.

3.5.3 *Exponential subdominance of the integral*

In order to demonstrate the late-order subdominance of the boundary integral in (3.20), consider the case of $\sigma = 1/2$ (other values of σ are similarly done). Here, the Stokes line originating from the corner leaves at an angle of $2\pi/5$ in the potential plane, curves in an arc, and intersects the free surface at about $w = \phi_c \approx 0.635$. Along the real and positive w-axis, $\Re(\chi) = 3\pi/2$, which can be computed by the residue contribution of (3.41) at infinity or alternatively, by using (3.42).

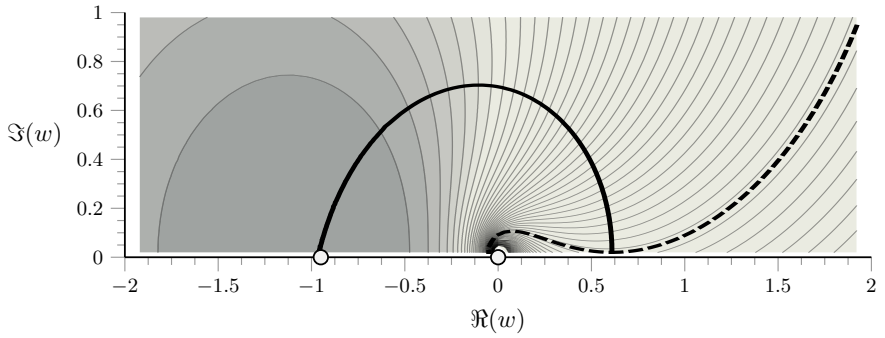

Figure 3.7: The light lines are contours for $|\chi(w)|$, with dark regions corresponding to small values. The thick black line corresponds to the Stokes line, and the dashed line to $|\chi(w)| = 3\pi/2$. Our Stokes line switching analysis is confined to the region above the dashed line, where the relevant exponentials are larger than anywhere along the free-surface.

In Figure 3.7, we plot the contours of $|\chi(w)|$, a thick line representing the Stokes line, as well as a dashed line for the contour $|\chi| = 3\pi/2$. Since $\chi(w)$ is an analytic function away from its singularities, the contour $|\chi| = 3\pi/2$ must necessarily intersect both the Stokes line and the real axis at the single point $w = \phi_c$. Moreover, along the real axis the point ϕ_c constitutes an absolute minimum. For the equation

$$\frac{q_n}{q_0} + i\theta_n - \frac{q_{n-1}q_1}{q_0^2} + \ldots = \mathscr{H}[\theta_n(w)],$$

when the ansatz (3.28) is used and the late terms sought, the integral will be evaluated on the real axis, where χ is larger than on anywhere along the Stokes line. Thus the right-hand side of the equation is negligible as $n \to \infty$. Essentially, its only effect is in altering the values of the early terms, q_0, q_1, q_2, and so on.

The subdominance of the boundary integral term which occurs in potential theory was also used for the analysis of the viscous fingering problem in

Hele-Shaw flows (see for example, Pomeau et al. 1988 and Chapman 1999) and was rigorously justified for that problem by Xie & Tanveer (2002).

3.6 INNER PROBLEM

In the previous sections, we derived the general form of the high order terms q_n and θ_n, up to the determination of certain unknown coefficients, namely Q, Θ, and γ. In this section, we will show how these coefficients can be determined by matching the high-order terms near the singularities in the flow field.

3.6.1 Inner limits of outer expansions

Before we begin studying the inner problem, let us take note of the behaviour of Q and Θ as we tend towards to the flow-field singularity, $w = -1$. Recall from eqns (3.37) and (3.38) that

$$Q = \frac{\Lambda}{q_0^2}\exp\left(3i\int_{w\star}^{w}\frac{q_1}{q_0^4}\,d\varphi\right) \quad \text{and} \quad \Theta = \frac{\Lambda i}{q_0^3}\exp\left(3i\int_{w\star}^{w}\frac{q_1}{q_0^4}\,d\varphi\right), \tag{3.43}$$

while from (3.27), q_1 is given by

$$q_1 = -iq_0\theta_1 + q_0\cdot\mathscr{H}[\theta_1(w)].$$

Using $\theta_1 = -q_0^2 dq_0/dw$ from (3.26), we have

$$q_1 = iq_0^3\frac{dq_0}{dw} + q_0\cdot\mathscr{H}[\theta_1(w)]. \tag{3.44}$$

Thus the exponential factor in the expressions for Q and Θ in (3.43) can be written as

$$\begin{aligned}\exp\left(3i\int_{w\star}^{w}\frac{q_1}{q_0^4}d\varphi\right) &= \exp\left(-3\int_{w\star}^{w}\frac{q_0'}{q_0}d\varphi\right)\times\exp\left(3i\int_{w\star}^{w}\frac{\mathscr{H}[\theta_1(\varphi)]}{q_0^3}\,d\varphi\right)\\ &= \frac{q_0^3(w^\bigstar)}{q_0^3(w)}\times\exp\left(3i\int_{w\star}^{w}\frac{\mathscr{H}[\theta_1(\varphi)]}{q_0^3}\,d\varphi\right).\end{aligned} \tag{3.45}$$

For this equation, the integrand is well behaved *near* the singularity at $w = -1$ and so

$$\exp\left(3i\int_{w\star}^{w}\frac{q_1}{q_0^4}\,d\varphi\right) \sim \frac{C}{q_0^3(w)},$$

where C is the constant,

$$C = q_0^3(w^\bigstar)\exp\left(3i\int_{w\star}^{-1}\frac{\mathscr{H}[\theta_1(\varphi)]}{q_0^3}\,d\varphi\right), \tag{3.46}$$

and thus the inner limits of the late terms of the outer expansion are

$$\theta_n \sim \frac{i\Lambda C}{q_0^6}\frac{\Gamma(n+\gamma)}{\chi^{n+\gamma}} \quad \text{and} \quad q_n \sim \frac{\Lambda C}{q_0^5}\frac{\Gamma(n+\gamma)}{\chi^{n+\gamma}}. \tag{3.47}$$

In order to select the constant γ, we require that the asymptotic behaviour of the late terms given in (3.28) to be consistent with the order of the singularities of q_0 and θ_0 as $w \to -1$. Equating powers, we need $-5\sigma - (1+3\sigma)\gamma = \sigma$ or

$$\gamma = \frac{6\sigma}{1+3\sigma}. \tag{3.48}$$

3.6.2 *Outer limit of inner expansions*

Let us begin by discussing how the two governing equations change as we tend towards the corner. Near the singularity, the dynamic condition (3.21) remains unchanged, but the boundary integral (3.20) can be considerably simplified. In this case, we would like to evaluate

$$\log q_{\text{inner}}(w) + i\theta_{\text{inner}}(w) = \mathscr{H}[\theta_{\text{outer}}(w)]. \tag{3.49}$$

as $w \to -1$ and where the indices help to remind us where the functions q and θ are being evaluated. The left-hand side is evaluated *near* the singularity and thus involves the exact expressions for $q(w)$ and $\theta(w)$ in the inner limit. However, the integrand on the right hand side is integrated over the free surface, far away from the singularity, thus it involves only the *outer* expansion for $\theta(w)$. But we know that substituting the outer expansion into the right-hand side of (3.49) leads to

$$\log q_{\text{inner}}(w) + i\theta_{\text{inner}}(w) = \log q_0 + \epsilon\mathscr{H}[\theta_1(w)] + O(\epsilon^2),$$

and since $\mathscr{H}[\theta]$ is well-behaved for w off the axis, this forms a well-ordered asymptotic expansion. The leading-order inner solution then, is equivalent to using $\log q + i\theta \sim \log q_0$ and we may thus substitute

$$\sin\theta = \frac{e^{i\theta} - e^{-i\theta}}{2i} \sim \frac{i}{2}\left(\frac{q}{q_0} - \frac{q_0}{q}\right)$$

into the dynamic condition (3.21), yielding

$$\epsilon q_0 q^3 \frac{dq}{dw} + \frac{i}{2}\left(q^2 - q_0^2\right) = 0. \tag{3.50}$$

The correct scaling to use is hinted by the inner limits of the outer approximations. In the inner region, we let

$$w = -1 + \epsilon^{1/1-3\alpha}\eta, \qquad q_0 \sim cw^{\alpha/(1-3\alpha)}, \qquad \text{and } q = ce^{\alpha/(1-3\alpha)}\eta^\alpha \overline{q}.$$

Then (3.50) becomes

$$2ic^3\overline{q}^2\left(\alpha\eta^{3\alpha-1} + \eta^{3\alpha}\frac{d\overline{q}}{d\eta}\right) = \overline{q} - \frac{1}{\overline{q}}, \tag{3.51}$$

which is identical to the inner equation of Chapman & Vanden-Broeck (2006), except for the negated right-hand side. We now let

$$z = \frac{i\eta^{1-3\alpha}}{c^2(1-3\alpha)}, \qquad \phi = \overline{q}^2, \qquad \text{and} \qquad \phi = \sum_{n=0}^{\infty}\frac{\phi_n}{z^n},$$

yielding a recurrence relation for the *outer limit of the leading-order inner* solution:

$$\phi_0 = 1, \qquad \phi_n = \sum_{m=0}^{n-1} \left(m - \frac{2\alpha}{1-3\alpha} \right) \phi_m \phi_{n-m-1}. \tag{3.52}$$

We match the leading-order inner limit of the n^{th} term of the outer expansion of q^2 and match with the outer limit of the n^{th} term of the leading-order inner expansion. This gives

$$\Lambda = \frac{c^{6-3\gamma} e^{i\pi\gamma/2}}{2C(1-3\alpha)} \times \underbrace{\lim_{n\to\infty} \frac{\phi_n}{\Gamma(n+\gamma)}}_{\Omega}. \tag{3.53}$$

The crucial limiting ratio of Ω only depends on the local power of the singularity, and numerical values for different ships are given Figure 3.8.

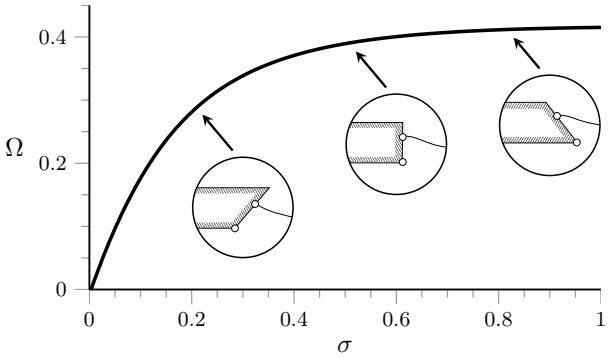

σ	Ω
0.1	0.1762854
0.2	0.2811203
0.3	0.3385194
0.4	0.3706919
0.5	0.3893600
0.6	0.4004895
0.7	0.4072291
0.8	0.4113096
0.9	0.4137380
1.0	0.4151100

Figure 3.8: Values of Ω for various hull forms. Ω is non-zero for all hull configurations, which is enough to guarantee that a wave of non-zero amplitude appears on the free-surface.

3.6.3 Stokes smoothing

Remember: the underlying divergence of the asymptotic expansions will cause the *Stokes Phenomenon* to occur and as the complexified asymptotic solution crosses a critical line (the *Stokes line*), a small exponential switches on. The details of the Stokes smoothing procedure are precisely the same as in Chapman & Vanden-Broeck (2006), and we will perform a similar analysis in full detail for the multi-cornered ships of the next chapter. Here, we will only summarise the key ideas.

In order to identify the exponentially small waves, we first *optimally truncate* the asymptotic series at $n = \mathcal{N}$ so that

$$\theta = \sum_{n=0}^{\mathcal{N}} \epsilon^n \theta_n + R_{\mathcal{N}} \qquad \text{and} \qquad q = \sum_{n=0}^{\mathcal{N}} \epsilon^n q_n + S_{\mathcal{N}}, \tag{3.54}$$

whereby the remainders are related by (3.31) and thus $S_{\mathcal{N}} \sim -iq_0 R_{\mathcal{N}}$. At the optimal truncation point, the remainder $S_{\mathcal{N}}$ is *exponentially small* (rather than only algebraically small) and can be written as $S_{\mathcal{N}}(w) = \mathcal{S}(w) Q e^{-\chi/\epsilon}$, where we expect $\mathcal{S}(w)$ to smoothly vary from zero to a constant across the Stokes line.

The procedure then is to re-scale near the Stokes line and examine the jump in the exponentially small remainder as the Stokes line is crossed from upstream (indicated with a $+$ below) to downstream (indicated with a $-$ below). The apparent jump in the remainder can be shown to be

$$\left[S_{\mathcal{N}}\right]_{+}^{-} \sim \frac{2\pi i Q}{\epsilon^{\gamma}} \exp\left[-\frac{\chi}{\epsilon}\right], \tag{3.55}$$

while the exponentially small correction to θ is,

$$\left[R_{\mathcal{N}}\right]_{+}^{-} \sim \frac{2\pi i \Theta}{\epsilon^{\gamma}} \exp\left[-\frac{\chi}{\epsilon}\right]. \tag{3.56}$$

To finalise the analysis, we need to also complexify the free boundary into the lower-half plane and this analogous process yields the functional complex conjugates of (3.55) and (3.56); thus, the *total* contribution along the free-surface is twice the real parts of (3.55) and (3.56),

$$q_{\text{exp}} \sim \frac{4\pi}{\epsilon^{\gamma}} \Im\left(Q e^{-\chi/\epsilon}\right), \tag{3.57}$$

$$\theta_{\text{exp}} \sim \frac{4\pi}{\epsilon^{\gamma}} \Im\left(\Theta e^{-\chi/\epsilon}\right). \tag{3.58}$$

These formulae provide a link between the terms that are switched-on across Stokes lines, and the late terms of the asymptotic series.

3.6.4 The simplified nonlinear problem

The attentive reader will have noticed the fact that the only effect of the Hilbert transform, $\mathscr{H}[\theta(w)]$, is to adjust the far-field waves by a non-zero, $\mathcal{O}(1)$ amount. In fact, if we were to simply *ignore* $\mathscr{H}[\theta]$, the only effects would be: (i) changing q_1 in (3.27), (ii) changing the computation of C in (3.46), and (iii) replacing the expression of Q in (3.37), valid everwhere, by its expression valid near the singularity.

Thus, the salient features of the problem can still be retained if we use $\log q \pm i\theta = \log q_0$ instead of (3.20), and this way, we can simplify the full problem in (3.20)–(3.21) to a simpler nonlinear differential equation in q. Analytic continuation into the upper-half plane then gives

$$\epsilon q_0 q^3 \frac{dq}{dw} + \frac{i}{2}(q^2 - q_0^2) = 0. \tag{3.59}$$

Tuck (1991a) also realised that the essential characteristics of the waveless ship problem could be encapsulated by a single, local differential equation (his example, however, was pedagogic in nature, whereas our approximation is justifiable). The one-cornered ship problem can thus be analysed more simply by studying (3.59) instead of the full problem, and this is briefly presented in Trinh et al. (2010); in fact, we shall use this simplified formulation to study the more difficult multi-cornered ship problem in the next chapter.

However, we now return to our study of the *full* problem in eqns (3.20) and (3.21), for which we have already completed the asymptotic analysis. In the next section, we will provide numerical validation of our beyond-all-orders predictions.

Precise computation of exponential smallness is hardly a trivial affair, but despite the fact that the quantities of interest are exceedingly small, many past workers have still managed to confirm *beyond-all-orders* predictions with numerical simulations. For example, by using a spectral basis supplemented by a function which mimics the far-field waves, Boyd (1991a) was able to compute the exponentially-small gravity-capillary waves of the fifth-order Korteweg-de Vries equation to over ten digits of accuracy. And although these methods were never applied to the full nonlinear water-wave equations, Chapman & Vanden-Broeck (2002, 2006) still comfortably computed small capillary and small gravity waves for the full problem using a second-order finite differences—this time to five or six digits of accuracy.

Unfortunately, as we shall see, the ship-wave problem presents numerous new challenges not encompassed by the previous numerical methods. These challenges arise because of the surface-piercing nature of the ship, which supplements the usual difficulties of resolving exponential smallness with the problem of now dealing with an essential singularity at the origin.

3.7.1 ALGORITHM A*: a simple method*

We first propose a very simple method based on the work in Chapman and Vanden-Broeck (2002; 2006), though many authors have used this method for computing two-dimensional nonlinear flows over obstructions (see for example Forbes (1983) for the case of gravity flow over a semi-circular cylinder, and King & Bloor (1990) for the case of flow over an arbitrary bed topography).

To begin, we first truncate the semi-infinite domain to a finite interval and introduce an equally spaced mesh for ϕ and its midpoints, with separation distance, $\Delta\phi$:

$$\begin{aligned} \phi_i &= (i-1)\Delta\phi && \text{for } i = 1, 2, \ldots, n, \\ \phi_i^m &= \frac{1}{2}\Big(\phi_i + \phi_{i+1}\Big) && \text{for } i = 1, 2, \ldots, n-1, \end{aligned}$$

Now, given an initial guess for the n unknowns, θ_i (evaluated at the points ϕ_i), values of $\tau = \log q$ at the $n-1$ midpoints are computed using

$$\tau_i^m = \sigma \log\left(\frac{\phi_i^m}{\phi_i^m + 1}\right) + \frac{1}{\pi}\fint_0^{\phi_{\max}} \frac{\theta}{\phi - \phi_i^m}\, d\phi \qquad \text{for } i = 1, 2, \ldots, n-1.$$

The principal value integral is computed by applying the trapezoidal rule with a summation over the mesh points ϕ_i; this use of equally spaced points and midpoints should allow us to neglect the singularity of the principal value without losing accuracy. Bernoulli's equation then provides a system of $n-1$ equations to solve:

$$F_i = \epsilon e^{3\tau_i^m} \left(\frac{d\tau^m}{d\phi_m}\right)_i + \sin\theta_i^m = 0 \qquad \text{for } i = 1, 2, \ldots, n-1, \tag{3.60}$$

where the derivatives $d\tau/d\phi$ are computed using second-order differences and θ_i^m denotes the value of θ at the midpoints. For the n^{th} equation, we assign the boundary condition

$$F_n = \theta_1 = \begin{cases} 0 & \text{if } \sigma \geq \frac{1}{3} \\ \pi\left(\sigma - \frac{1}{3}\right) & \text{if } \sigma < \frac{1}{3} \end{cases}, \tag{3.61}$$

and moreover, we replace the first equation with the condition that

$$F_1 = \theta_3 - \theta_0 - (\theta_2 - \theta_0)\left(\frac{\phi_3}{\phi_2}\right)^{\kappa} = \theta_3 - \theta_0 - (\theta_2 - \theta_0)2^{\kappa}. \tag{3.62}$$

where θ_0 and κ are as prescribed in 3.40. Conditions (3.61) and (3.62) then assure us that $\theta \sim \theta_0 + c\phi^{\kappa}$ for some constant c over the first three mesh points. Table 3.1 shows just how compact this code can be made when combined with the built-in nonlinear solver of the MATLAB environment. In the included example, we solve for the vertical $\sigma = 1/2$ hull at $\epsilon = 0.5$.

```
% Parameters and potential mesh
n = 1000; dw = 0.03; ep = 0.5; sigma = 1/2;
w = [0:n-1]*dw; wm = w(1:end-1) + dw/2;

% Solve the system and plot the solution
fwd = @(u)func(u, w, wm, n, ep, sigma, dw);
u = fsolve(fwd, zeros(1, n));
plot(wm, 1/2*(u(1:end-1) + u(end, 2:end));

function F = func(u, w, wm, n, ep, sigma, dw)
  tau = sigma*log(wm./(wm+1)); aux = [dw*ones(1,n-1) dw/2];
  for j = 1:n-1, tau(j) = tau(j) + 1/pi*sum(u.*aux./(w-wm(j))); end

  um = 1/2*(u(1:n-1)+u(2:n));
  dtau = 1/dw*[(tau(2)-tau(1)), ...
    (tau(3:n-1)-tau(1:n-3))/2.0, (tau(n-1)-tau(n-2))];

  F(1:n-1) = ep*exp(2*tau).*dtau + exp(-tau).*sin(um);
  F(n) = u(1);
```

Table 3.1: MATLAB code for the simple stern solver. This particular instance solves the $\sigma = 0.5$ stern at $\epsilon = 0.5$ with $n = 1000$ points and a discretisation distance of $\Delta\phi = 0.03$ (denoted dw in the code). It makes use of MATLAB's `fsolve` function for the solution of the algebraic equation denoted by `func`.

Solutions for the $\sigma = 20/48$ and $\sigma = 32/48$ hulls at $\epsilon = 0.8$ and $\epsilon = 0.4$, respectively are shown in Figure 3.9. It is important to note that the values shown are not from θ_i but rather, the midpoints θ_i^m; this is due to the fact that the central difference approach in the algorithm causes the original θ values to exhibit a sawtooth pattern between meshpoints—it is, after all, the *midpoints* which are used in the solution of (3.60). Notice from the lower figure that even for these relatively moderate values of ϵ, the downstream waves are already quite small. The algorithm is most effective for both moderate values of σ (near or greater than the vertical hull) and moderate wave amplitudes. Unfortunately, it proves to be ineffective for specific types of solutions, due to certain numerical difficulties, as we shall now discuss.

The first difficulty is that the method of computing singular integrals by trapezoidal integration over the midpoints is generally not as accurate as other comparable second-order methods, particularly when the singularity is allowed to approach one of the endpoints (see Noble & Beighton 1980). For increased accuracy, we need an alternative treatment of the boundary integral.

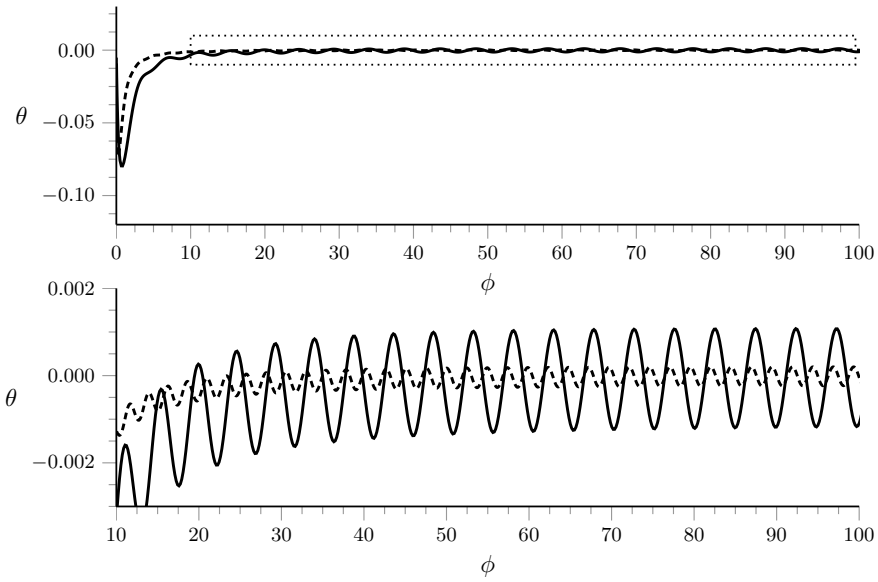

Figure 3.9: Solutions for $\sigma = 20/48$ at $\epsilon = 0.4$ (dashed) and $\sigma = 32/48$ at $\epsilon = 0.8$ (solid); these solutions were computed using ALGORITHM A with $n = 2000$ and $\Delta\phi = 0.05$ for the former hull, and $n = 1000$ and $\Delta\phi = 0.1$ for the latter. Zooming in (not shown) shows that the solution is ill-resolved near the stagnation point, but for a limited range of hulls, the algorithm is sufficient.

The second minor difficulty is that compared to the amplitude of the far-field waves, the algebraic decay of the core solution is extremely slow, at the rate of

$$\theta \sim \mathcal{O}\left(\frac{w^{3\sigma-1}}{(w+1)^{3\sigma+1}}\right),$$

as $\epsilon \to 0$ and $w \to \infty$. Wave amplitudes are measured by computing differences in numerical maxima and minima near $\phi_{\max}$, and increased accuracy can be achieved by averaging the small, locally linear shifts in the amplitudes. However, this slow algebraic decay is a symptom of the surface-piercing nature of the problem and still provides an additional loss of accuracy in comparison with problems for which the tails are generally exponentially decaying—as in the fifth-order Korteweg-de Vries problem discussed in Boyd (1991a), and also for gravity flows over a submerged obstruction studied in Chapman & Vanden-Broeck (2006).

Finally and most importantly, for values of σ near or less than $1/3$, the algorithm does a poor job of approximating the solution, particularly those containing wave amplitudes on the order of 10^{-3}. Examination of θ near the stagnation point shows that the numerical discretisation cannot cope with the essential singularity at the origin; unfortunately, as $\sigma \to 0$, the outer low-Froude solution becomes increasingly singular. The inherent errors in using an inappropriately spaced mesh swamp the computations and low-Froude solutions for σ small cannot be trusted.

In the next section, we will propose an alternative algorithm which focuses on minimising the errors produced by the stagnation point.

3.7.2 ALGORITHM B*: a comprehensive method*

The algorithm in this section is similar to the one presented in Farrow & Tuck (1995) but with a few key differences which allow for a better resolution of the near-stagnation flow.

The first change we implement is the use of a stretched grid in ϕ near the stagnation point. We need a mesh which can approximate the essential singularity at the origin, but which can also capture the almost-periodic waves downstream. For this, we define a stretched grid near the origin

$$\phi_i = \phi_0 + (\phi_c - \phi_0)\left(\frac{i-1}{m-1}\right)^{1/s} \quad \text{for } i = 1, 2, \ldots, m,$$

for some initial point ϕ_0, some *matchpoint* ϕ_c, a chosen number of mesh points m, and a value of s we will later specify. Afterwards, a downstream discretisation is chosen:

$$\phi_i = \phi_c + \Delta\phi_{\max}\left(\frac{i-1}{n-m-1}\right) \quad \text{for } i = m+1, 2, \ldots, n,$$

for a total of n of mesh points and a downstream spacing of $\Delta\phi_{\max}$. A better parameter to use for the latter is given by

$$K = \frac{2\pi\epsilon}{\Delta\phi_{\max}},$$

where K now indicates the number of mesh points per linear wavelength of the downstream waves. If the value of s is not too small, then we may select ϕ_c and m so that the last separation distance of the initial mesh, $\phi_m - \phi_{m-1}$, is equal to the spacing of the downstream mesh, $\Delta\phi_{\max}$; we refer to this as a *smoothed mesh*. However, if s is too small, then the growth of the initial mesh is too slow, and we generally need to manually choose suitable values of ϕ_c and m for each individual problem. The complete choice of parameters which fully determine the initial and downstream mesh is quite tricky and largely dependent on the choice of σ and ϵ. For solutions given in the figures, we let $\mathbf{B}(\sigma) = [n, \phi_0, K, m, \phi_c]$ denote a vector of parameter values, and write $\mathbf{B}(\sigma) = [n, \phi_0, K, *, *]$ if a *smoothed mesh* is used. In the next section, however, we will discuss which particular values work and which do not.

This time, we will look to solve

$$F_i = \frac{\epsilon}{3} q_0(\phi_i)^3 \exp\left[\frac{1}{\pi}\int_{\phi_1}^{\phi_n} \frac{\theta}{\varphi - \phi_i}\, d\varphi\right] + \int_{\phi_1}^{\phi_i} \sin\theta\, d\theta = 0, \tag{3.63}$$

for $i = 1, 2, \ldots, n$ and the principle advantage of dealing with (3.63) rather than its differentiated counterpart, (3.60), is that the lack of smoothness between the two meshes at $\phi = c$ can now be ignored.

Now we turn to the computation of the rightmost integral. We proceed as in Farrow & Tuck (1995), and split the integral as

$$\int_0^{\phi_i} \sin\theta\, d\varphi = \int_0^{\phi_{i-1}} \sin\theta\, d\varphi + \int_{\phi_{i-1}}^{\phi_i} \sin\theta\, d\varphi.$$

The second integral on the right is calculated by computing the quadratic interpolation of $\sin\theta$ over ϕ_{i-1}, ϕ_i, and ϕ_{i+1}, and integrating the quadratic

exactly (the use of the additional ϕ_{i+1} point is to ensure stability and accuracy of the method). Similarly, for the integral

$$\int_0^\infty \frac{\theta\, d\varphi}{\varphi - \phi_i} = \int_0^{\phi_{i-1}} \frac{\theta\, d\varphi}{\varphi - \phi_i} + \int_{\phi_{i-1}}^{\phi_{i+1}} \frac{\theta\, d\varphi}{\varphi - \phi_i} + \int_{\phi_{i+1}}^{\phi_{\max}} \frac{\theta\, d\varphi}{\varphi - \phi_i},$$

the first and last terms on the right-hand side can be computed using the trapezoid rule, whereas the singular term is calculated by fitting a quadratic through the points θ_{i-1}, θ_i, and θ_{i+1} and integrating exactly.

Next, let us turn to boundary conditions. The selection of the *number* and *type* of boundary conditions to impose is generally an *ad-hoc* issue. In general, we must worry about the solution remaining bounded at the last endpoint $\phi = \phi_{\max}$, and moreover, for it to have the correct behaviour as $\phi \to 0$. For the former condition, we find it sufficient to construct a quadratic interpolation through the three next-to-last mesh points, and require the last mesh point to satisfy this relation; that is,

$$F_n = \theta_n - \left(p_2\phi_n^2 + p_1\phi_n + p_0\right) = 0,$$

where p_0, p_1, and p_2 are the coefficients of the quadratic satisfying $p_2\phi_i^2 + p_1\phi_i + p_0 = \theta_i$ for $i = n-3, n-2$, and $n-1$.

The behavioural condition as $\phi \to 0$ is more difficult. For example, we could simply ignore the issue, and assume that our choice for the near-field discretisation would be sufficient for the solution to converge. Alternatively, we could impose the condition that the quadratically extrapolated value from the first three mesh points coincides with the correct value of θ at the origin. That is,

$$F_1 = \theta_0 - \left(p_2\phi_1^2 + p_1\phi_1 + p_0\right) = 0, \tag{3.64}$$

where p_2, p_1, and p_0 are the coefficients of the quadratic satisfying $p_2\phi_i^2 + p_1\phi_i + p_0 = \theta_i$ for $i = 1, 2$, and 3.

Another condition could be to require that

$$F_1 = \theta_2 - \theta_1\left(\frac{\phi_2}{\phi_1}\right)^\kappa = 0, \tag{3.65}$$

where κ is as prescribed in Section 3.5.1. Other possibilities include requiring $q(0) = 0$ using a condition akin to (3.64), or requiring that $q \sim \mathcal{O}(w^\sigma)$ if $\sigma \geq 1/3$ or $q \sim \mathcal{O}(w^{1/3})$ if $\sigma < 1/3$ using a condition akin to (3.65).

As a general rule of thumb, the conditions in eqns (3.64) and (3.64) both seem adequate and more-or-less equivalent in correctly resolving the behaviour near the stagnation point, provided the mesh is suitably chosen. With this in mind, we choose to use (3.64) as this does not require an input of κ. Examples of successfully computed solutions are given in Figure 3.10.

3.7.3 Numerical versus analytical results

In the end however, even with various *ad-hoc* changes to accommodate the numerical challenges of the surface-piercing and singular-integral aspects of

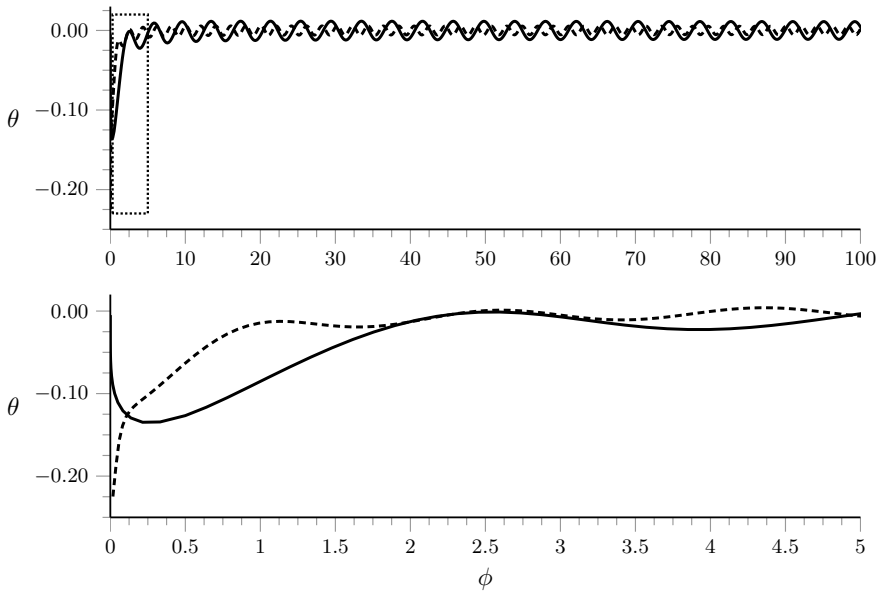

Figure 3.10: Solutions for $\sigma = 12/48$ at $\epsilon = 1/3$ (dashed) and $\sigma = 18/48$ at $\epsilon = 1/3$ (solid). These were computed using the stretched grids of ALGORITHM B and as shown in the lower figure, successfully produced well-resolved solutions near the stagnation point. Parameters used were: $\mathbf{B}(12/48) = [1450, 10^{-8}, 30, 20, .5]$ $\mathbf{B}(18/48) = [800, 10^{-8}, 30, 20, .5]$.

the problem, it is still difficult to understand how one change may affect the resultant wave amplitudes in contrast with another. Because our regime of interest involves exponentially small waves, small changes in not only the choice of boundary conditions, but also the number of mesh points to place in the both the initial and downstream mesh can have a significant impact on the eventual results.

We leave these questions concerning the construction of a truly robust and accurate numerical method for further research and instead focus on *sufficient* confirmation of our analytical results. Our numerical results are constructed by relying on a combination of all the techniques mentioned in the previous sections.

In general, there are five crucial parameters to choose when using ALGORITHM B. These include n, the total number of mesh points; m, the number of points in the stretched grid; ϕ_0, the first grid point; ϕ_c, the matchpoint between the two meshes; and finally K, the points per wavelength. For small ϵ, a small adjustment in one of these parameters can have a significant impact on the relative error of the solutions.

Let us begin with the easiest case: the $\sigma = 1/2$ hull is simplest to calculate because its waves are only moderately small, and its behaviour near the origin, only moderately singular. Here, ALGORITHM A provides accurate results for amplitudes down to roughly 10^{-4}. Afterwards, the more careful treatment of the stagnation point and quadrature schemes from ALGORITHM B can be used to extend these results down to around 10^{-6}.

There is a surprising requirement for numerical accuracy of hulls with σ larger than $1/2$. For these cases, the behaviour near the stagnation point is less singular and in fact, the increase in accuracy gained from ALGORITHM B over A is less significant. However, for smaller and smaller wave amplitudes, it becomes crucial to increase the number of points per wavelength; in the case of $\sigma = 5/8$, for example, accurate results can only be obtained for $\epsilon \approx 0.5$ with $K = 60$–90 points per wavelength. With this in mind, both

algorithms provide similar results, and because the simpler version is much more computationally efficient, we favour it for these larger values of σ.

The most challenging regime occurs when σ is small and particularly when $\sigma < 1/3$. In this case, it is crucial to correctly resolve the behaviour near the stagnation point. Here, the difficulty is that the solution exhibits two types of behaviours near the critical point: as ϵ tends to zero, the outer solution tends to negative infinity at the rate of $\theta \sim w^{3\sigma-1}$, which is a particularly *strong* blowup. However, the nonlinear inner region has $\theta \sim \theta_0 + w^{\varsigma}$, which behaves almost *linearly* for small σ. Worst still, the inner region is growing ever smaller and smaller, at the rate of $\epsilon^{1/1-3\sigma}$.

Consider the case of $\sigma = 14/48 \approx 0.2917$. In this problem, the outer solution roughly behaves like $\theta \sim w^{-0.13}$, whereas the nonlinear prediction is $\theta = \theta_0 + w^{0.39}$. These two behaviours are not wholly disparate. In this case, we may use ALGORITHM B with the choice of $s = \varsigma \approx 0.39$ for the initial mesh. The choice is then sufficiently singular to resolve the correct near-field behaviour and provide accurate results for wave amplitudes down to about 10^{-6}. Figure 3.11 is a blow-up of the stagnation point for solutions of this ship for various values of ϵ.

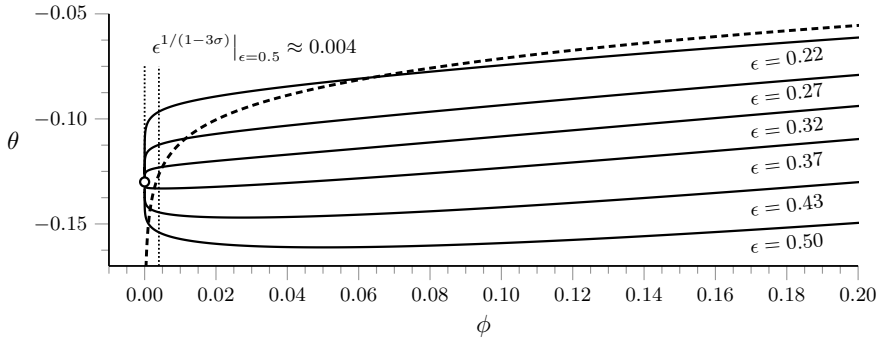

Figure 3.11: Solutions near the stagnation point for $\sigma = 14/48$ and for various values of ϵ. The leading-order asymptotic solution for $\epsilon = 0.22$ is the dashed line whereas the small node indicates the value $\theta_0 \approx -0.13$. Initially (for $\epsilon = 0.5$), there is a fairly clear inner region (marked on the figure). As $\epsilon \to 0$, this inner region grows smaller and smaller, making it increasingly difficult to resolve the inner-most solution. All computations use $\mathbf{B}(14/48) = [1000, 10^{-8}, 30, *, *]$.

Now consider the most challenging case: for $\sigma = 12/48 = 0.25$, the outer solution roughly behaves like $\theta \sim w^{-0.25}$, whereas the nonlinear prediction is $\theta = \theta_0 + w^{0.89}$. Choosing s from either approximation leads to trouble! Our *ad-hoc* solution is been to choose a value of s sufficiently small as to resolve the outer blow-up, but within reach of the true nonlinear behaviour—for example $s = 0.25$. Once solutions for this mesh have been computed, we may then slowly increase s while increasing m and examine the convergence of the solutions.

By patiently adjusting each of the values involved in the computations, we have been able to construct Figure 3.12, which plots numerical and asymptotic results for the hulls we have discussed, accurate to around five or six digits of accuracy. The slope of the semi-log trends are each matched to a particular hull, with the backward-facing hulls ($\sigma > 1/2$) producing smaller waves than the forward-facing hulls. The agreement between analytical and numerical results is very good, even over relatively large ranges of ϵ.

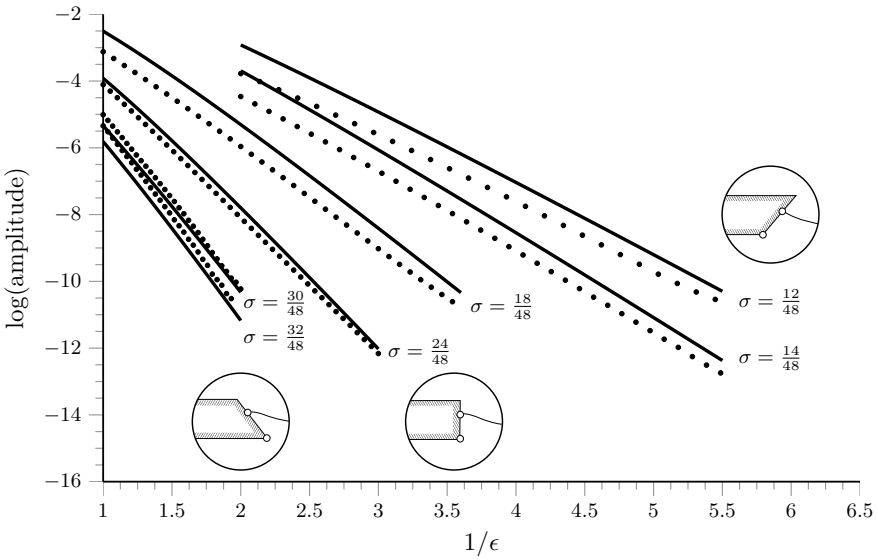

Figure 3.12: Downstream numerical (dots) and asymptotic (solid) wave amplitudes for a range of hull inclinations. At a given Froude number, the waves can be minimised by simply inclining the hull 'backwards'. The asymptotic predictions provide a good fit for a large range of Froude numbers. The $\sigma = 32/48$ computation was done using ALGORITHM A with $n = 1500$ and discretisation distance $E = 0.04$; the rest were done using ALGORITHM B. The following parameter values were used:
$\mathbf{B}(12/48) = [800, 10^{-8}, 30, 90, .3]$
$\mathbf{B}(14/48) = [1000, 10^{-8}, 30, *, *]$
$\mathbf{B}(18/48) = [800, 10^{-8}, 30, 50, .5]$
$\mathbf{B}(24/48) = [800, 10^{-5}, 30, 20, .5]$.

So in the end, do *waveless ships exist*?

For the one-cornered ship, the answer is quite clearly *'No!'* The Stokes line smoothing necessitates the existence of the non-zero wave on the free-surface. For stern flows, these waves must propagate downstream, while for bow flows, these waves grow to be of infinite amplitude near the hull. In particular, this implies that for such flows, the assumption that the flow attaches to the hull at a stagnation point is *false* (and indeed, it has been conjectured that the correct assumption must include an overturning splash near the bow, see Dias & Vanden-Broeck 1993 and Tuck 1994). Thus for the one-cornered hull, neither waveless sterns nor splashless bows are possible.

But there are still a handful of open questions, and many of these unresolved issues are significant for the wider study of general free-surface problems. One such issue, which we had previously encountered in Section 3.5.1, deals with the attachment between free-surface and ship when the inclination of the hull is less than $\pi/3$; here, does the stagnation point produce an exponentially small contribution on the surface? Our numerics seem to indicate that it does not, but this issue of *evanescent* waves near a free-surface singularity has already been highlighted as a particularly challenging problem (see Tuck 1991a,b), and we invite other researchers to address the issue.

Another open issue relates to the separation of our mathematical analysis into local and global approaches. For example, consider the late-order terms of Section 3.4, or consider the local emergence of the Stokes lines of Section 3.5.2, or the numerical solution of the recurrence relation of Section 3.6; all these results were derived using *local* properties of the problem—indeed, their analysis simply depends on the behaviour of the asymptotic solutions near the relevant singularities. In contrast, the *global* nature of the ship problem, which largely depends on the physical set-up, must be handled on a case-by-case basis. Are there less obvious Stokes line arrangements, not examined in this study, which produce different classes of solutions?

In discussing these global issues, we are naturally led to the following

question: *do waveless ships of a more general form exist?* Perhaps. One could imagine that for a general multi-cornered ship, the position of each corner could be strategically chosen so that the wave contribution due to each singularity adds to zero in the far-field—the entire body would then move without a wake. Addressing this issue is the task that awaits us in the next and final part of the thesis.

3.A (Appendix) Local behaviour near the stagnation point

In this section, we will derive the local behaviour of the free-surface near the stagnation point along the ship's hull. For the local behaviour, it is initially easier to work with cartesian coordinates as a function of the potential $z = z(w)$, and now, assuring analyticity of z (or w) is equivalent to satisfying the boundary integral equation; we may thus focus on Bernoulli's Equation, given by

$$\frac{\epsilon}{2}\left|\frac{dw}{dz}\right|^2 = -\eta, \qquad \text{on } w \in \mathbb{R}^+,$$

where we have shifted $\eta \mapsto \eta - \epsilon/2$ so that the origin is now at the stagnation point. Alternatively we can write this equation as

$$-\frac{2}{\epsilon}\Im[z]\left|\frac{dz}{dw}\right|^2 = 1, \qquad \text{on } w \in \mathbb{R}^+, \tag{3.66}$$

where the wall condition requires that

$$\sin(\pi\sigma)\left(\frac{dx}{dw}\right) - \cos(\pi\sigma)\left(\frac{dy}{dw}\right) = 0, \qquad \text{on } w \in (-1, 0). \tag{3.67}$$

Now, one way to proceed is to let

$$z(w) \sim \mathcal{A}w^\alpha + \mathcal{B}w^\beta$$

where $\mathcal{A}, \mathcal{B} \in \mathbb{C}$ and we are concerned with $w \to 0$. Tuck & Roberts (1997) instead consider $z = X(w) + iY(w)$ where they require $X, Y \in \mathbb{R}$ on $w \in \mathbb{R}^+$, but the two approaches are equivalent. We now have to split everything into real and imaginary parts and multiply out. If we write

$$z = \left[ae^{i\delta}\right]w^\alpha + \left[be^{i\rho}\right]w^\beta$$

where $\beta > \alpha$, and all the variables save for w are real, then we find two possible cases. First, if $\delta = 0$, then the requirement that z is real on $w \in \mathbb{R}^+$ is satisfied automatically, whereas the wall condition in (3.67) requires that $\alpha = 1 - \sigma$. Thus,

$$z(w) \sim aw^{1-\sigma} \Rightarrow \frac{dw}{dz} = qe^{-i\theta} \sim \mathcal{C}w^\sigma, \tag{3.68}$$

where the constants $\mathcal{C}$ and a cannot be determined purely by local means. The expression in (3.68) is simply the leading-order solution in the small ϵ limit.

Now suppose on the other hand that $\delta \neq 0$. Then we may write

$$\frac{dz}{dw} = \widehat{\mathcal{A}} e^{i\delta} w^{\alpha-1} + \widehat{\mathcal{B}} e^{i\rho} w^{\beta-1}$$

where we have denoted $\widehat{\mathcal{A}} = \alpha a$ and $\widehat{\mathcal{B}} = \beta b$. Then along the free-surface, we can write for $w = \phi > 0$,

$$\left|\frac{dz}{dw}\right|^2 = \widehat{\mathcal{A}}^2 \phi^{2\alpha-2} + \widehat{\mathcal{B}}^2 \phi^{2\beta-2} + 2\widehat{\mathcal{A}}\widehat{\mathcal{B}} \cos(\delta - \rho)\phi^{\alpha+\beta-2},$$

whereas

$$\Im(z) = \Im\Big[ae^{i\delta}\phi^{\alpha} + be^{i\rho}\phi^{\beta}\Big] = \Big[a\sin\delta\Big]\phi^{\alpha} + \Big[b\sin\rho\Big]\phi^{\beta}.$$

We may now write the free-surface condition in (3.66) as

$$\Big[a\sin\delta\cdot\phi^{\alpha} + b\sin\rho\cdot\phi^{\beta}\Big]\Big[\widehat{\mathcal{A}}^2\phi^{2\alpha-2} + \widehat{\mathcal{B}}^2\phi^{2\beta-2} + 2\widehat{\mathcal{A}}\widehat{\mathcal{B}}\cos(\delta-\rho)\phi^{\alpha+\beta-2}\Big] = \frac{\epsilon}{2}.$$

The leading-order dominant balance requires

$$a^3\alpha^2 \sin\delta \cdot \phi^{3\alpha-2} = -\frac{\epsilon}{2}, \tag{3.69}$$

so $\alpha = 2/3$ and the wall condition in (3.67) requires $\delta = \pi\sigma - \pi/3$. Finally, a can be determined by substituting these values into (3.69), yielding

$$a = \left[\frac{9\epsilon}{8\sin(\pi/3 - \pi\sigma)}\right]^{1/3}.$$

The next order in the free-surface equation is $\phi^{2\alpha+\beta-2}$, where

$$2\beta\sin(\pi\sigma - \pi/3)\cos(\pi\sigma - \pi/3 - \rho) + 2/3\sin\rho = 0,$$

and here, the wall condition requires that $\rho = \pi\sigma - \pi\beta - 1$; substituting this into the above gives

$$2\beta\sin(\pi\sigma - \pi/3)\cos(2\pi/3 + \pi\beta) + 2/3\sin(\pi\sigma - \pi\beta - 1) = 0. \tag{3.70}$$

The above expression provides a formula for the transcendental power, β and in fact, it can be shown that the series expansion for $z(w)$ with ϵ fixed and $w \to 0$ proceeds in transcendental powers after the first term. Nevertheless, along the free surface, we may write

$$\theta = \delta + \left(\frac{b}{a}\right)\phi^{\beta-\alpha}\left\{\frac{\sin\rho}{\cos\delta} - \tan\delta\cdot\frac{\cos\rho}{\cos\delta}\right\} + O\Big(\phi^{2\beta-2\alpha}\Big) = \delta + \mathcal{D}\phi^{\varsigma} \tag{3.71}$$

where we define the important power as $\varsigma = \beta - \alpha = \beta - 2/3$ and the constant $\mathcal{D}$ cannot be found by local means alone. Values of ς for various values hull inclinations are found in Table 3.2.

σ	ς	σ	ς
$9/48$	1.14125	$17/48$	0.33714
$10/48$	1.11395	$18/48$	0.32904
$11/48$	1.06034	$19/48$	0.32286
$12/48$	0.88890	$20/48$	0.31793
$13/48$	0.46525	$21/48$	0.31388
$14/48$	0.39466	$22/48$	0.31046
$15/48$	0.36526	$23/48$	0.30750
$16/48$	0.34835	$24/48$	0.30490

Table 3.2: Values of ς for various hull inclinations with $\sigma < 1/3$. With these values, we can compute the power in the quantity $\theta \sim \delta + \mathcal{D}\phi^{\varsigma}$, which determines the behaviour of the free-surface near the stagnation point.

3.B (Appendix) Computation of C in equation (3.46)

In this section, we will analytically derive $|C|$ and provide numerical computations for the argument of C. Without loss of generality, we will choose the initial point of integration $\varphi = w^{\bigstar}$ to lie on the positive real axis. There is a residue contribution at $\varphi = \infty$, so we will also let $\zeta' = 1/\varphi$. The integral becomes

$$C \sim q_0^3(w^{\bigstar}) \exp\left(-3i \int_{1/w^{\bigstar}}^{w^*} \frac{1}{\zeta'^2 q_0^3} \left[\frac{1}{\pi} \int_0^{\infty} \frac{\theta_1(t)}{t - 1/\zeta'} \, dt \right] \, d\zeta' \right).$$

where the singularity is $w^* = -1$ for the one-cornered ship. Now since we are only interested in the modulus of C, we note that for real ζ',

$$\Im\left[\frac{1}{\pi} \int_0^{\infty} \frac{\theta_1(t)}{t - 1/\zeta'} \, dt \right] = \begin{cases} 0 & \zeta' < 0 \\ \theta_1 & \zeta' > 0 \end{cases}$$

the residue being positive since we wish to remain in the upper-half φ plane during integration. Thus

$$\Re\left[-3i \int_{1/w^{\bigstar}}^{w^*} \frac{1}{\zeta'^2 q_0^3 \pi} \int_0^{\infty} \frac{\theta_1(t)}{t - 1/\zeta'} \, dt \, d\zeta' \right] = 3 \int_{1/w^{\bigstar}}^{0} \frac{\theta_1}{\zeta'^2 q_0^3} \, d\zeta' - 3 \operatorname{Res}\left\{ \frac{\frac{1}{q_0^3} \int_0^{\infty} \frac{\theta_1(t)}{t - 1/\zeta'} \, dt}{\zeta'^2}, \; \zeta' = 0 \right\}.$$

Setting $\theta_1 = -q_0^2 dq_0/dw$ by (3.27) and changing the first integral back to the w-plane yields

$$3 \int_{w^{\bigstar}}^{\infty} \frac{\theta_1}{q_0^3} \, d\varphi = 3 \int_{w^{\bigstar}}^{\infty} \frac{q_0'(\varphi)}{q_0(\varphi)} \, d\varphi = -3 \log q_0(w^{\bigstar}),$$

And the residue is

$$\operatorname{Res}\left\{ \frac{\frac{1}{q_0^3} \int_0^{\infty} \frac{\theta_1(t)}{t - 1/\zeta'} \, dt}{\zeta'^2}, \; \zeta = 0 \right\} = \operatorname{Res}\left\{ \frac{\frac{1}{q_0^3} \int_0^{\infty} -\theta_1(t) \, dt}{\zeta'}, \; \zeta' = 0 \right\} = \frac{1}{3}.$$

Thus

$$\Re\left[-3i\int_{w^\star}^{-1}\frac{1}{q_0^3\pi}\int_0^\infty\frac{\theta_1(t)}{t-\varphi}\,dt\,d\varphi\right]=-3\log q_0(w^\star)-1,$$

and so the magnitude of C is

$$|C|=\frac{1}{e}. \tag{3.72}$$

Note that this computation for $|C|$ does not depend on the particular form of q_0, only that it tends to 1 as $w\to\infty$. Thus, in the next chapter, we will be able to re-use this same value for $|C|$, even for different hull configurations.

The numerical computation of $\mathrm{Arg}(C)$ can be considerably simplified by using the exact expression for the inner integral,

$$\frac{1}{\pi}\int_0^\infty\frac{\theta_1(\varphi)}{\varphi-w}\,d\varphi=\frac{\sigma}{3\pi(1+w)}\left[\frac{1}{a}+\frac{3\pi\exp[-3\pi i\sigma]\csc(3\sigma\pi)}{w}\right.$$
$$\left.+\left(\frac{w}{w+1}\right)^{3\sigma}+3\Gamma(1-3\sigma)\,{}_2F_1(1,1,2-3\sigma,-2)\right]. \tag{3.73}$$

With this, (3.46) can now be computed by numerically integrating along a semi-circular arc in the upper-half plane from $w\in\mathbb{R}^+$ to $w_0=-1$. Figure 3.13 illustrates and lists the values of Arg C for different hull configurations.

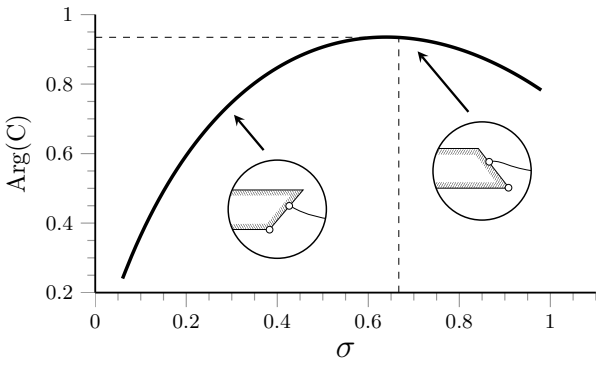

σ	Arg(C)
0.1	0.3647648
0.2	0.5945286
0.3	0.7470284
0.4	0.8469189
0.5	0.9066125
0.6	0.9330085
0.7	0.9301421
0.8	0.9003831
0.9	0.8450331

Figure 3.13: Numerically integrated values of Arg(C) for various hull forms. The value of σ where the argument reaches its maximum is likely $\sigma=2/3$, where it is approximately 0.9346.

PART II: MULTI-CORNERED SHIPS

4

4.1 INTRODUCTION

In the low-speed limit, a blunt ship modeled as two-dimensional semi-infinite body with a single corner *can never be made waveless*. This was the conclusion of the previous chapter. And while its truth has been more-or-less known since the late 1970s (Vanden-Broeck & Tuck 1977), previous numerical and analytical analyses of the problem were made difficult by the singular nature of the low-speed limit.

By now, we know that at low Froude (draft) numbers, the waves generated by a ship become exponentially small and are thus invisible to a regular asymptotic expansion. The ineffectiveness of traditional asymptotics in capturing the low-speed limit was first remarked by Ogilvie (1968) and later termed the *Low-Speed Paradox*; it is only by using special techniques in exponential asymptotics that we have been able to derive approximations to these hidden waves. More important, however, is the valuable insight that these approximations give: an explicit formula that relates the shape of the hull with the resultant waves in its wake.

In this chapter, we study the much more open-ended problem of waves produced by ships with piecewise-linear hulls. Little, if any, literature exists on the topic, perhaps for the simple reason that without analytical guidelines, one has great difficulty distinguishing between, for example, the wake of a *three*-cornered ship from that of a *five*-cornered ship. Numerical results can always be proffered, but the infinitude of hull and parameter choices make inferring from quantitative data nearly impossible. The only mention of such piecewise-linear hulls can be found in Farrow & Tuck (1995), for which a certain three-cornered ship is briefly studied.

This chapter will proceed as follows. First, we extend the previous analysis for the one-cornered hull to ships with multiple corners. An explicit expression for the wake of an arbitrary multi-cornered ship is given, and later, numerical computations for two-cornered hulls provide vindication of our analysis. Second, from these analytical results, we prove that certain classes of multi-cornered ships can never be made waveless. Finally, we address the more difficult problem of hull geometries which contain closely-spaced corners. The general methodology for their solutions is described, and analytical and numerical results are given for a specific case.

Our goal, then, is not to provide an all-inclusive theory encompassing the most general of multi-cornered ships, but rather, to provide an analytical roadmap for understanding how the waves that trail a ship depend upon its chosen geometry. In the end, we would like to be able to briefly scan each of the eight hulls presented in Figure 4.1 and—in a matter of seconds—answer the question: *are any of these ships waveless?*

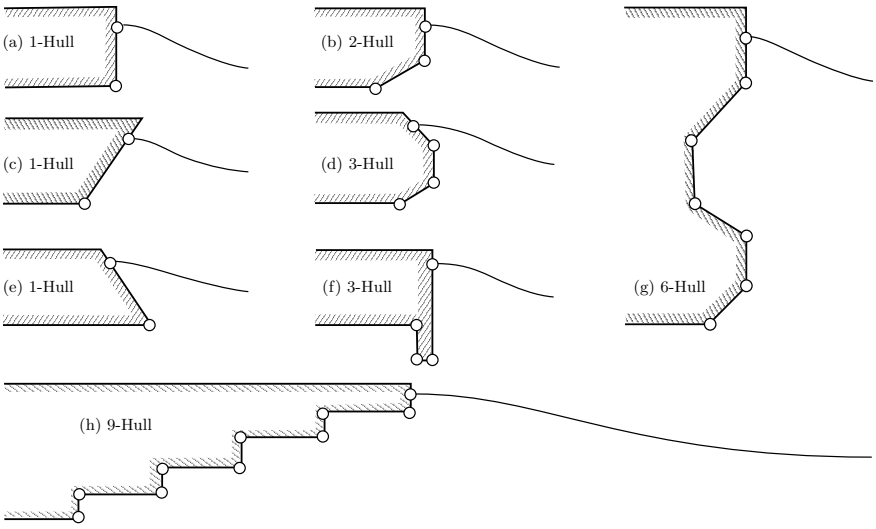

Figure 4.1: Are any of these ships waveless? In all cases, the flow is from left to right and nodes indicate singularities in the analytic continuation. A particularly fascinating case is the (f) 3-Hull, which was studied in Farrow & Tuck (1995) and for which the addition of a downward-pointing bulb was shown to dramatically reduce the wave resistance compared to a rectangular ship (a).

4.2 MATHEMATICAL FORMULATION

Consider steady, incompressible, irrotational, and inviscid flow in the presence of gravity and past a semi-infinite body consisting of a flat bottom and a piecewise linear front face. The non-dimensionalised problem can be reposed as a boundary-integral problem in the potential plane:

$$\log q = \frac{1}{\pi} \fint_{-\infty}^{\infty} \frac{\theta(\varphi)}{\varphi - \phi}\, d\phi \tag{4.1}$$

$$\epsilon q^2 \frac{dq}{d\phi} = -\sin\theta \qquad \text{on } \psi = 0, \tag{4.2}$$

where $\epsilon = U^3/gK$ is related to the square of the Froude draft number with upstream flow U, $\nabla\phi$ is the non-dimensionalised fluid velocity, $q = q(\phi, \psi)$ is the speed of the flow, and $\theta = \theta(\phi, \psi)$ is the angle the streamlines make with the x-axis. Moreover, we position the origin $\phi = 0$ so that it corresponds to the stagnation point at $(x, y) = (0, 0)$, and K is defined by

$$K = \sum_{i=1}^{N} K_i,$$

where the dimensionalised value at each of the corners is $\phi_i^* = -K_i$. In this way, if $\phi = a_i$ for $1 \leq i \leq N+1$ denote the corners in the non-dimensionalised problem we have the property that

$$\sum_{i=1}^{N} a_i = 1.$$

We will henceforth refer to the N-cornered piecewise-linear hull as an N-Hull and describe it by N angles

$$\theta_k = \sum_{j=1}^{k} \sigma_j,$$

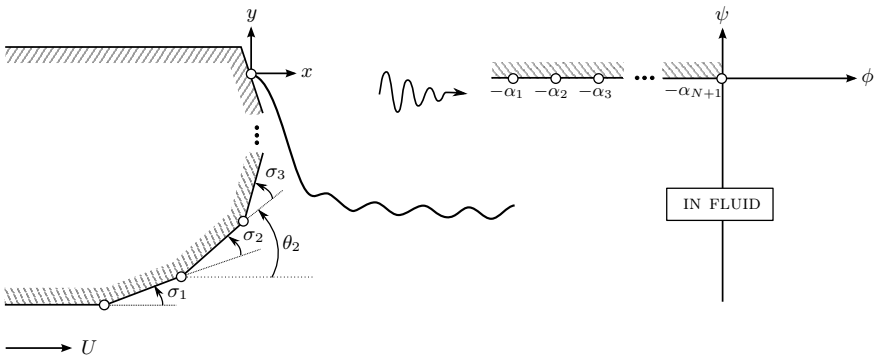

Figure 4.2: Flow past a piecewise-linear N-Hull. The N corners of divergent angles $\sigma_1, \sigma_2, \ldots, \sigma_N$ in the (x, y) plane (left) are mapped to $w = -\alpha_1, -\alpha_2, \ldots, -\alpha_N$ in the complex potential plane (right). The stagnation point is $w = \alpha_{N+1} = 0$ and typically, we non-dimensionalise the flow so that the first corner is set to $\alpha_1 = 1$.

for $\alpha_k < \phi < \alpha_{k+1}$ and $k = 1, \ldots, N+1$; more simply, the shape of the hull is then described by N *divergent* angles of σ_k, and this is depicted in Figure 4.2. Because the *zero*-Froude solution requires a horizontal attachment angle between the free surface and the hull, this also implies that

$$\theta_{N+1} = 0 \quad \text{or} \quad \sigma_{N+1} = -\sum_{j=1}^{N+1} \sigma_j. \tag{4.3}$$

We may then write the boundary integral over the negative real axis as

$$\frac{1}{\pi} \fint_{-\infty}^{0} \frac{\theta(w')}{w' - w}\, dw' = \log\left[\prod_{k=1}^{N+1} (w + a_k)^{-\sigma_k}\right] \equiv \log q_s(w). \tag{4.4}$$

As in the previous chapter, we will be interested in studying the analytic continuation of the free-surface and thus allowing $\phi + i0 \mapsto w$, $q(\phi, 0) \mapsto q(w)$, and $\theta(\phi, 0) \mapsto \theta(w)$ to be elements of a complex variable. Analytically continuing eqns (4.1) and (4.2) then gives

$$\log q \pm i\theta = \log q_s(w) + \mathscr{H}[\theta(w)] \tag{4.5}$$

$$\epsilon q^2 \frac{dq}{dw} = -\sin\theta, \tag{4.6}$$

where the $\pm$ signs correspond to analytic continuation in the upper and lower-half ϕ planes, respectively, and $\mathscr{H}$ denotes the Hilbert Transform operator on the semi-infinite line:

$$\mathscr{H}[\theta(w)] = \frac{1}{\pi} \int_0^\infty \frac{\theta(\varphi)}{\varphi - w}\, d\varphi.$$

In the following asymptotic analysis, we will analytically continue into the upper-half plane and find exponentially small terms switched on across Stokes lines. However, once the analysis is complete, a similar procedure must be performed in the lower-half plane as well.

4.3 Asymptotic approximation

The late-orders analysis proceeds almost identically to the one performed in the previous chapter, with the exception that each corner of the ship now has

the potential to produce a separate factorial over power ansatz to contribute to the divergence of the late terms. In this section, we quickly recapitulate the methodology of the previous work and provide the corresponding formulae for the multi-cornered ship.

4.3.1 Late-order terms

We begin as usual by calculating the regular asymptotic expansion of eqns (4.5) and (4.6) in the limit $\epsilon \to 0$ by letting

$$\theta = \sum_{n=0}^{\infty} \epsilon^n \theta_n \quad \text{and} \quad q = \sum_{n=0}^{\infty} \epsilon^n q_n. \tag{4.7}$$

The leading-order solution is the rigid-wall flow of eqn (4.4),

$$\theta_0 = 0, \tag{4.8}$$

$$q_0 = q_s = \prod_{k=1}^{N+1} (w + a_k)^{-\sigma_k}, \tag{4.9}$$

while the $\mathcal{O}(\epsilon)$ expression gives

$$\theta_1 = -q_0^2 \frac{dq_0}{dw}, \tag{4.10}$$

$$q_1 = -iq_0^3 \frac{dq_0}{dw} + q_0 \mathscr{H}[\theta_1(w)]. \tag{4.11}$$

Now the leading order solution possesses singularities at each of the corners, $w = -a_k$. Each subsequent order requires a single derivative of the previous order and thus we would expect that as $n \to \infty$, the asymptotic expansion (4.7) exhibits factorial over power divergence of the form:

$$\theta_n \sim \sum_{k \in \mathcal{K}} \frac{\Theta_k \Gamma(n + \gamma_k)}{\chi_k^{n+\gamma_k}} \quad \text{and} \quad q_n \sim \sum_{k \in \mathcal{K}} \frac{Q_k \Gamma(n + \gamma_k)}{\chi_k^{n+\gamma_k}}, \tag{4.12}$$

where γ_k is complex constant, Q_k and χ_k are functions of the complex potential w, and $\chi_k(-a_k) = 0$.

Here, $\mathcal{K} \subseteq \{1, 2, \ldots, N+1\}$ is the set of numbers that describes which corners have a sufficiently strong singularity so as to contribute to the eventual divergence of the asymptotic series. For most of the analysis, however, we can simply choose *one* of the corners of interest with $k \in \mathcal{K}$ and add each of the contributions at the end.

The singularities are located off the free surface, where the Hilbert Transform in (4.5) is evaluated and so, as justified in the previous chapter, $\mathscr{H}[\theta_n(w)]$ is exponentially subdominant to the terms on the left-hand side for large n. At $\mathcal{O}(\epsilon^n)$, the expression in (4.5) is equivalent to

$$\theta_n \sim i\frac{q_n}{q_0} - \frac{iq_1 q_{n-1}}{q_0^2} + \ldots \qquad \text{as } n \to \infty, \tag{4.13}$$

and substituted into (4.6), this gives the relevant terms at $\mathcal{O}(\epsilon^n)$:

$$\left[q_0^3 q'_{n-1} + i q_n\right] + \left[2q_0^2 q'_0 q_{n-1} + 3q_0^2 q_1 q'_{n-2}\right] + \ldots = 0. \tag{4.14}$$

Substituting the ansatz of (4.12) into (4.14) reveals at leading order as $n \to \infty$,

$$\frac{d\chi}{dw} = \frac{i}{q_0^3}, \tag{4.15}$$

which we can then write as

$$\chi_k = \int_{-a_k}^{w} \frac{i}{q_0^3}\, d\varphi. \tag{4.16}$$

At the next order in n we find also find

$$Q_k = \frac{\Lambda_k}{q_0^2} \exp\left[3i \int_{w^\star}^{w} \frac{q_1}{q_0^4}\, d\varphi\right], \tag{4.17}$$

for some arbitrary point $w^\star$ for which the integral is defined, and for some value of the constant Λ_k which must be determined by the method of matched asymptotics near the singularities.

4.3.2 Stokes lines, optimal truncation, and Stokes Smoothing

The Stokes lines for the flow past a multi-cornered ship are each virtually identical to the single Stokes line from a one-cornered ship, except now there may be more than one. These special lines are simply given by the prescription:

$$\Im[\chi_k(w)] = 0 \quad \text{and} \quad \Re[\chi_k(w)] \geq 0.$$

If we assume that $q_0 \sim c_k w^{\alpha_k}$ near $w = -a_k$, and thus $\alpha_k = -\sigma_k$ and

$$c_k = \prod_{\substack{j=1 \\ j\neq k}}^{N+1} (a_j - a_k)^{-\sigma_j},$$

then

$$\chi_k \sim \underbrace{\left[\frac{i}{c_k^3(1-3\alpha)}\right]}_{X_k} (w + a_k)^{1-3\alpha_k},$$

and for the remainder of this chapter, we will often make use of the coefficients c_k, X_k, and α_k in describing the local behaviour near the singularities. In any case, the condition that $\chi_k(-a_k) = 0$ thus requires that $1 - 3\alpha_k > 0$ or that $\sigma_k > -1/3$. In other words, for there to be a singularity, the local deviation of the corner must be greater than $-\pi/3$. This is a *necessary* (but not *sufficient*) condition for there to be a free-surface wave produced by the corner.

A stronger condition for the existence of a Stokes line emerging on the relevant Riemann sheet can be derived. Since $qe^{-i\theta} = u - iv$, we can write

$$\operatorname{Arg}(c_k) = \theta_k$$

for analytic continuation into the upper-half plane, where $\theta_k \in (-\pi, \pi)$ is the angle of the downstream hull as $w \to a_k^+$, measured from the positive x-axis (shown in Figure 4.2). If we write $\mathrm{Arg}(w + a_k) = \nu_k$, then Stokes lines must leave at angles of

$$\nu_k = \left(\frac{3\theta_k + 2k\pi - \pi/2}{1 + 3\sigma} \right), \tag{4.18}$$

for $k \in \mathbb{Z}$ and we then need $\nu \in (0, \pi)$ in order for the line to emerge in the upper-half plane. The general requirements for a Stokes line to intersect the free-surface is a global function of the leading-order flow, but for most hulls, condition (4.18) is adequate. In any case, we will let $\mathcal{J} \subseteq \mathcal{K}$ denote those corners which have Stokes lines crossing the free-surface.

As an example, consider Figure 4.3, which illustrates the Stokes lines for various N-hulls, from a simple 2-Hull to more elaborate ones including the 3-Hull of Farrow & Tuck (1995), a bulbous 6-Hull, as well as a step-like 9-Hull. With the exception of a single configuration, the condition that a Stokes line emerges into the upper-half plane is enough to guarantee that it intersects the free-surface. The exception is with the 3-Hull, for which the second singularity has a Stokes line emerging at an angle of $\nu_2 = 3\pi/5$, but the line does not later encounter the free-surface.

To derive the form of the exponentials that appear whenever a Stokes line intersects the free surface, we will need to optimally truncate the asymptotic expansions and smooth the Stokes line. We let

$$q = \sum_{n=0}^{\mathcal{N}-1} \epsilon^n q_n + S_{\mathcal{N}} \tag{4.19}$$

with a similar expression for the series for θ. When $\mathcal{N}$ is chosen to be the optimal truncation point, the remainder $R_{\mathcal{N}}$ is found to be exponentially small, and by re-scaling near the Stokes line, it can be shown that a wave of the following form switches on:

$$q_{\mathrm{exp},k} \sim \frac{2\pi i}{\epsilon^{\gamma_k}} Q_k \exp\left[-\frac{\chi_k}{\epsilon} \right]. \tag{4.20}$$

We must also include the addition of the complex conjugate of this wave due to the contributions from the analytic continuation into the lower-half plane, in which case the sum of the two contributions is

$$q_{\mathrm{exp},k} \sim \frac{4\pi}{\epsilon^{\gamma_k}} \Im\left\{ Q_k \exp\left[-\frac{\chi_k}{\epsilon} \right] \right\}, \tag{4.21}$$

with of course, only one of such expressions for every $k \in \mathcal{J}$.

Thus, for any given arbitrary N-hull with a geometry such that $\mathcal{J}$ is nonempty, the appearance of exponentially small waves is a *necessary consequence* of the divergent low-Froude problem; in order to check that such a ship can never be waveless, we need only verify that the sum of all the contributions incurred can never be zero.

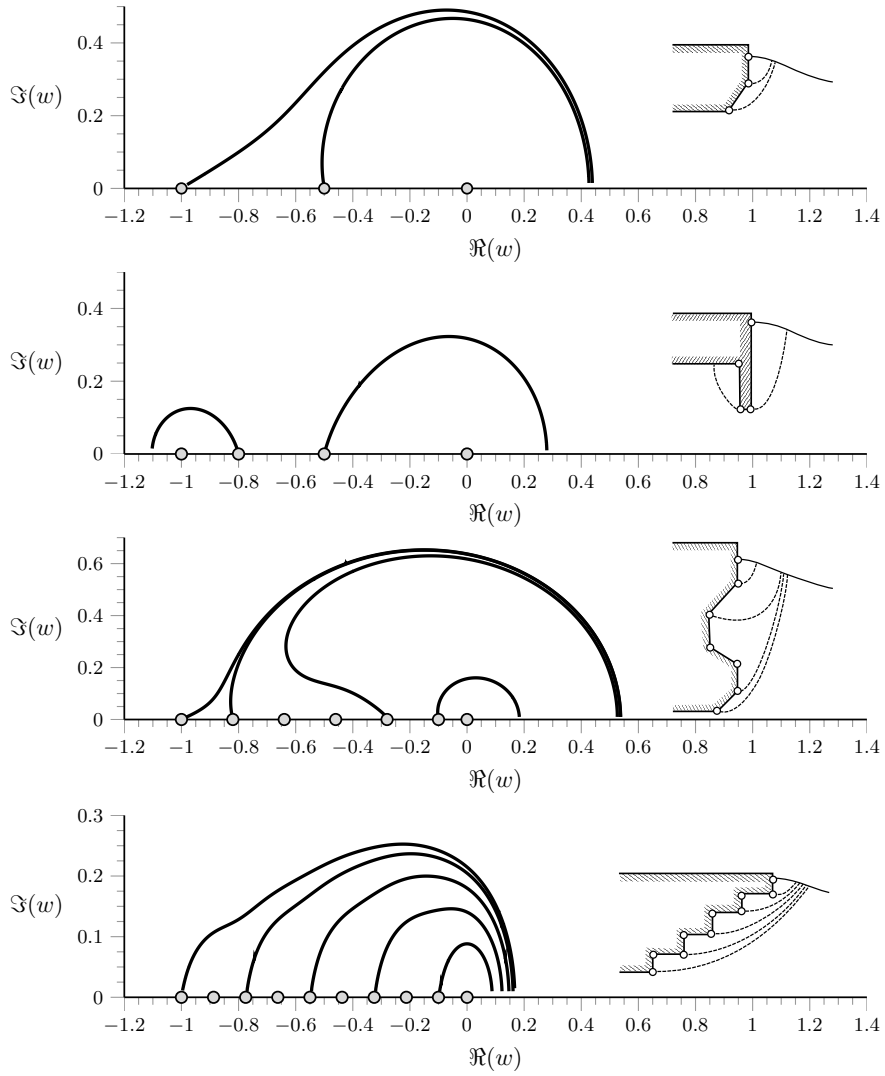

Figure 4.3: From top to bottom: Stokes lines for the 2-Hull, Farrow and Tuck's (1995) 3-Hull, the 9-Hull, and the 6-Hull shown before in Figure 4.2. For the 2-Hull and 6-Hull, the corner angles diverge at $\pm\pi/4$; for the remaining hulls, the corner angles are all rectangular.

4.3.3 Inner matching procedure and Λ_k

In order to compute Λ_k, we must solve for the leading-order solutions near the singularities in the flow field, and then match with the high-order terms of eqn (4.12). By re-scaling w and $q(w)$, and then solving for the leading-order inner solutions, specifying that as they tend outwards they must match with the outer solutions of (4.12), it can be shown that

$$\Lambda_k = \frac{c_k^{6-3\gamma_k} e^{i\pi\gamma_k/2}}{2C_k(1+3\sigma_k)^{\gamma_k}} \left[\lim_{n\to\infty} \frac{\phi_{n,k}}{\Gamma(n+\gamma_k)} \right], \tag{4.22}$$

where C_k is given by

$$C_k = q_0^3(w^\bigstar) \exp\left(3i \int_{w^\bigstar}^{-a_k} \frac{1}{q_0^3} \mathscr{H}[\theta_1(\varphi)]\, d\varphi \right), \tag{4.23}$$

and has $|C_k| = e^{-1}$ as shown in Appendix 3.B. The terms $\phi_{n,k}$ are given by

the recurrence relation,

$$\phi_{0,k} = 1, \tag{4.24}$$

$$\phi_{n,k} = \sum_{m=0}^{n-1}\left(m + \frac{2\sigma_k}{1+3\sigma_k}\right)\phi_m\phi_{n-m-1} \quad \text{for } n \geq 1. \tag{4.25}$$

We will often make reference to the limiting ratio in eqn (4.22), so we define the function:

$$\Omega_k \equiv \lim_{n\to\infty} \frac{\phi_{n,k}}{\Gamma(n+\gamma_k)}. \tag{4.26}$$

The constant Ω_k, which only depends on the local divergence of the k^{th} corner, is the same as the Ω which appears in eqn (3.53) of the previous chapter, and for which its values are given in Figure 3.8. Since $\Omega_k \neq 0$ for all choices of the local angle σ_k, Λ_k is also non-zero and this verifies that each of the $|\mathcal{J}|$ corners of an N-Hull must necessarily generate a non-zero wave on the free-surface.

4.3.4 Formulae for N-Hull waves

We now collect all the required formulae for computing the far-field waves of the N-Hull problem. First, in order to deal with the exponential factor in eqn (4.21), we notice that the integrand in

$$\chi_1 = \int_{-a_1}^{w} \frac{i}{q_0^3}\, d\varphi$$

is entirely real imaginary along $w \in (-\infty, -a_1)$ since the total angular deviation is zero from eqn (4.3). Since $q_0(w)$ is also real on $w \in (0,\infty)$, then for $w \in \mathbb{R}^+$, the real part of χ_1 must be given by the residue at $w = \infty$. If we make the substitution $\zeta = 1/w$, then

$$\begin{aligned} q_0\left(\frac{1}{\zeta}\right) &= \prod_{k=1}^{N+1}\left(\frac{1+\zeta a_k}{\zeta}\right)^{-\sigma_k} \\ &= \left(\prod_{k=1}^{N+1}\zeta^{\sigma_k}\right)\prod_{k=1}^{N+1}(1+\zeta a_k)^{-\sigma_k} \\ &= 1 + \zeta\sum_{k=1}^{N+1}(-\sigma_k a_k) + \mathcal{O}(\zeta^2), \end{aligned}$$

where the third line follows from the total angular deviation being zero. Therefore, it follows that

$$\Re\big[\chi_1(w)\big] = 3\pi\sum_{k=1}^{N}\sigma_k a_k, \tag{4.27}$$

for $w \in \mathbb{R}^+$, after using the fact that $a_{N+1} = 0$; this equation, however, is only true if χ' is integrable at $w = -a_1$, so for example, the 3-Hull in Figure 4.1(f) does not satisfy this condition. However, if (4.27) applies, then

by deforming the contour involved in computing χ_k so that it passes through $w = -a_1$, we can express

$$\Re\big[\chi_k(w)\big] = 3\pi \sum_{k=1}^{N} \sigma_k a_k + \Re\left[\int_{-a_k}^{-a_1} \frac{d\chi}{d\varphi}\, d\varphi\right],$$

again for $w \in \mathbb{R}^+$. Similarly, the imaginary parts can be expressed in terms of

$$\Im\big[\chi_k(w)\big] \sim \Im\big[\chi_1(w)\big] + \Im\left[\int_{-a_k}^{-a_1} \frac{d\chi}{d\varphi}\, d\varphi\right].$$

Now with Q_k given by eqn (4.17) and Λ_k given by eqns (4.22) and (4.26), we have from (4.21),

$$q_{\text{exp},k} \sim \frac{4\pi\Omega_k(\sigma_k)}{\epsilon^{\gamma_k} q_0^2(w)} \left[\frac{|c_k|^{6-3\gamma_k}}{2|C_k|(1+3\sigma_k)^{\gamma_k}}\right] \exp\left[-\frac{\Re[\chi_k]}{\epsilon}\right] \cos\left(-\frac{w}{\epsilon} + \Psi_k\right) \tag{4.28}$$

as $w \to \infty$, with the extra phase, Ψ_k, defined by

$$\Psi_k = -\frac{1}{\epsilon}\Im\Big[\chi_1(w)\Big] - \frac{1}{\epsilon}\Im\left[\int_{-a_k}^{-a_1} \frac{d\chi}{d\varphi}\, d\varphi\right] + (6-3\gamma_k)\text{Arg}(c_k) + \frac{\pi}{2}\gamma_k + \Im\left[-3\int_{-a_k}^{-a_1} \frac{\mathscr{H}[\theta_1(\varphi)]}{q_0^3}\, d\varphi\right]. \tag{4.29}$$

Then for each $k \in \mathcal{J}$, we add the waves together so that the total contribution as $w \to \infty$ is given by

$$q_{\text{exp}} \sim \sum_{k\in\mathcal{J}} q_{\text{exp},k}. \tag{4.30}$$

4.4 THE NON-EXISTENCE RESULT

Although the form of the individual and summed wave amplitudes in eqns (4.28) and (4.30) are complicated, many inferences on the question of existence of waveless N-Hulls can nevertheless be made by studying the individual components of (4.28). In this section, we will establish the non-existence of certain classes of waveless N-Hulls. First, let us establish the two easiest cases:

Result. *One or two cornered ships (1-Hulls or 2-Hulls) cannot be waveless.*

Proof. The wavelessness of the 1-Hull is clear from the previous chapter. The assertion is also easily proven for the case of a two-cornered ship. In the 2-Hull, if $|\mathcal{J}| = 1$, the argument is the same as for the 1-Hull. Otherwise, $|\mathcal{J}| = 2$, and both corners must produce waves. In order for phase cancellation to occur, each corner must be of the same angle $\sigma_k = \sigma$, otherwise the algebraic factor of ϵ^{γ_k} in eqn (4.28) would differ between the two waves. Moreover, the exponential factor $\exp[-\Re(\chi_k)/\epsilon]$ must be the same for each corner and thus, by deforming the path of integration, it must be the case that

$$\Re\left[\int_{-a_2}^{-a_1} \frac{i}{q_0^3}\, d\varphi\right] = 0 \tag{4.31}$$

However, the imaginary part of $1/q_0^3$ is non-zero and of a single sign between $w = -a_1$ and $w = -a_2$, so condition (4.31) can never be satisfied and waveless 2-Hulls are not possible. In words, then, what we have shown is that for a 2-Hull, the waves from one corner must exponentially dominate the waves from the other. □

Now we turn to the general N-Hull. Our proof for the non-existence of waveless hulls is similar to the above argument for the 2-Hull; the strategy is to reduce the wavelessness requirement to integral expressions between distinct corners of the ship. But before we do this, we impose the following three conditions on the geometry:

$$|\mathcal{J}| = N, \tag{4.32}$$

$$\sum_{j=1}^{N} \sigma_j < \frac{2\pi}{3}, \tag{4.33}$$

$$\sigma_j \text{ is strictly positive for } j = 1, 2, \ldots, N. \tag{4.34}$$

This means that the angle of each subsequent corner must diverge positively from the previous, that each corner generates a surface-intersecting Stokes line, and that the total deviation before the final stagnation point must be less than $2\pi/3$. In Figure 4.1, ships (a) through (e) satisfy this requirement, while ships (f) through (g) do not. At the end of this section, we will comment on the remaining types of N-Hulls.

First let us establish the crucial property of $d\chi/dw$ in eqn (4.15). The $N+1$ points at $w = \alpha_k$ separate the negative real axis into $N+1$ regions of interest which we define by

$$R_k = \Big\{ w : w \in (-\alpha_k, -\alpha_{k+1}) \Big\},$$

for $k = 0, 1, \ldots, N$, with $\alpha_0 = \infty$. It is clear that

$$\left| \frac{d\chi(w)}{dw} \right| \to \infty \quad \text{as } w \to \alpha_{N+1}, \tag{4.35}$$

$$\frac{d\chi(\alpha_k)}{dw} = 0 \text{ for } k = 1, \ldots, N, \tag{4.36}$$

$$\Im\left(\frac{d\chi}{dw}\right) \text{ is non-zero and of a single sign for } w \in R_k. \tag{4.37}$$

We will only need to establish the sign of the imaginary part of $d\chi/dw$. For $w \in R_k$, the argument of $1/q_0^3$ is

$$\mathcal{A}(k) \equiv \operatorname{Arg}\left(\frac{1}{q_0^3}\right) = \sum_{j=k+1}^{N+1} 3\pi\sigma_j,$$

where we restrict the arguments such that $0 < \mathcal{A}(k) \leq 2\pi$. Then by Properties (4.3) and (4.32), $\mathcal{A}(k)$ is a monotonically decreasing function as k advances from integer values of 0 to $N+1$. Moreover, there may exist a least

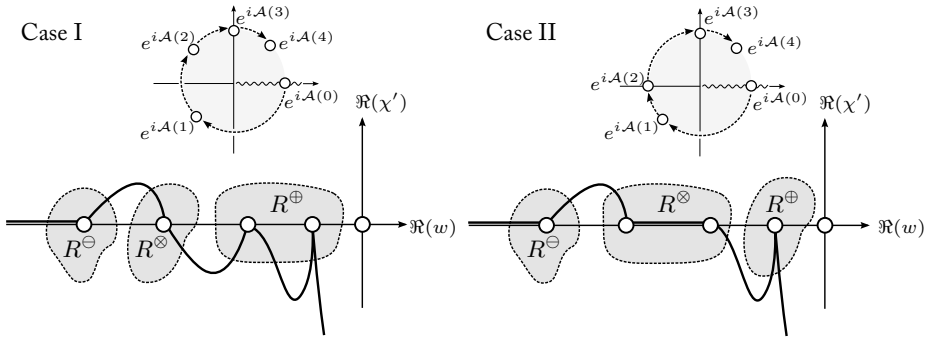

Figure 4.4: Notation used in the nonexistence results. The two plots at the bottom illustrate the function $\Re(\chi')$ along the real w-axis, while the two plots at the top illustrate the arguments $\mathcal{A}(k)$ as a function of the $k = 0, 1, 2, \ldots, N$ regions. These plots correspond to a 4-Hull.

value of $k = k^*$ such that $\mathcal{A}(k^*) \leq \pi$. We then describe the following three regions:

$$R^{\ominus} = \{-a_k : 1 \leq k < k^*\}$$
$$R^{\oplus} = \{-a_k : k^* \leq k < N\} \setminus R^{\otimes}$$
$$R^{\otimes} = \begin{cases} \{-\alpha_{k^*}\} & \text{if } \mathrm{Arg}(k^*) < \pi \quad \textbf{(Case I)} \\ \{-a_{k^*}, -a_{k^*+1}\} & \text{if } \mathrm{Arg}(k^*) = -\pi \quad \textbf{(Case II)} \end{cases}$$

In other words, $R^{\ominus}$, $R^{\oplus}$, $R^{\otimes}$ contains those points delimiting regions with negative, positive, and zero imaginary parts, respectively, and **Case I** and **II** correspond to configurations with $R^{\otimes}$ having one or two corners, respectively.

As examples, we can consider the 4-Hull with $\sigma_1 = 3/12$, $\sigma_2 = 2/12$, $\sigma_3 = 1/12$, and $\sigma_4 = 1/12$ in order to produce a **Case 1** configuration; or alternatively, we can use $\sigma_1 = 3/12$, $\sigma_2 = 1/12$, $\sigma_3 = 3/12$, and $\sigma_4 = 1/12$ in order to produce an example of a **Case II** configuration. Both of these examples satisfy Properties (4.32) to (4.34), and their qualitative behaviour is illustrated in Figure 4.4.

Result. *Given an N-Hull with the restrictions (4.32)–(4.34), if phase cancellation occurs, then it must do so between even-numbered groups of corners and in a pairwise manner.*

Proof. Suppose we select m corners with m odd and $m > 1$. Label these points $S = \{a_{b_j}\}$, with $j = 1, 2, \ldots, m$ and stipulate that the total wave contribution of the group cancels. By (4.21), each corner must generate a wave with an exponential factor of $\exp[-\Re(\chi_i)/\epsilon]$ where $\Re(\chi_i)$ is calculated by integrating (4.15). However by deforming the contours of integration, it must be the case that the real part of the integral between any member of S is zero,

$$\Re\left[\int_{-\alpha_j}^{-a_k} \frac{i}{q_0^3}\, d\varphi\right] = 0, \qquad \text{for } \alpha_j, a_k \in S$$

Now suppose that $S \cap R^{\otimes} \neq \emptyset$. Then clearly the real integral from any element in the intersection to any element of S in $R^{\ominus}$ or $R^{\oplus}$ is non-zero.

Alternatively, suppose that $S \cap R^{\otimes} = \emptyset$. Then since m is an odd-number, one of $R^{\oplus}$ or $R^{\ominus}$ must contain more points of S. Whichever group contains more points must then contain a non-zero real integral between at least two

members. Thus, this leaves us only with the possibility of even-numbered groups of corners producing total phase cancellation. Moreover, the process in which the selection is determined is in a pairwise manner, with one choosing one element from $R^{\oplus}$ to cancel with an element from $R^{\ominus}$ or between two elements in $R^{\otimes}$. □

Result. *Waveless N-hulls with the restrictions (4.32)–(4.34) do not exist.*

Proof. By the previous result, odd-numbered groupings of corners can never be waveless so it is clear that waveless N-Hulls are only possible if N is even. It is also clear that we need two points in $R^{\otimes}$, for otherwise the integral from the single member of $R^{\otimes}$ to its pair in $R^{\oplus}$ or $R^{\ominus}$ could not possibly be zero. Thus only **Case II** is admissible (and with the two points in $R^{\otimes}$ cancelling each other).

Now the construction of **Case II** implies that the sum of angles from the corners in $R^{\ominus} \cap R^{\otimes}$ is $\pi/3$. In order for there to be phase cancellation, the algebraic ϵ dependence must be the same for each pairwise matching of corners and so the sum of angles in $R^{\oplus} \cap R^{\otimes}$ must also be $\pi/3$. However, earlier we restricted the class of hulls to those with a maximum deviation of less than $2\pi/3$. Thus, N-Hulls with N an even number cannot occur either. □

The case of N-Hulls without restrictions (4.32)–(4.34) is much more open-ended and we have not managed to produced a proof of existence or non-existence. However, in specific cases, the wavelessness property can be easily dismissed.

For example, consider the 3-Hull in Figure 4.1(f), which is found in the work of Farrow & Tuck (1995) and for which the addition of a downward pointing bulb was shown to dramatically reduce the wave resistance compared to a rectangular ship. In this case, $|\mathcal{J}| = 1$ and $w = -a_3$ is the only relevant corner (as shown in Figure 4.3). The principal effect of the bulb, then, is to lower the usual singularity farther away from the free-surface, thus decreasing the amplitude of the surface waves. With this in mind, it is not surprising that the bulb reduces the wave resistance!

The wavelessness of the 6-Hull in Figures 4.1(g) and 4.3 can also be easily dismissed by noting that $|\mathcal{J}| = 4$, with three positively divergent corners ($\sigma_k > 0$), but only one negatively divergent one. Thus the waves from $w = -a_5$ must always exist on the free-surface. As a final example, consider the 9-Hull given in Figure 4.1(h), which has $|\mathcal{J}| = 1$ and the form

$$q_s = w^{\frac{1}{2}}(w+a_1)^{\frac{-1}{2}}(w+a_2)^{\frac{1}{2}}(w+a_3)^{\frac{-1}{2}}\ldots(w+a_9)^{\frac{-1}{2}}.$$

Examining $\Re[\chi']$, we see that it alternates between zero and negative values within the delineated intervals R_k. It is easy to conclude that the corner at $w = -a_1$ dominates all other contributions and so ship (h) cannot be waveless, either.

We now set out to numerically verify the asymptotic predictions of eqns (4.28)–(4.30). The easiest non-trivial application of the N-Hull theory of the preceeding sections is with $N = 2$. Henceforth, we will use the alternative description of a 2-Hull as a $[\sigma_1, \sigma_2]$-Hull in order to more conveniently describe a ship with divergent corner-angles σ_1 and σ_2 and with leading-order flow given by:

$$q_0 = \frac{w^{\sigma_1+\sigma_2}}{(w+a_1)^{\sigma_1}(w+a_2)^{\sigma_2}},$$

with $a_1 + a_2 = 1$. Far downstream, the waves generated by each corner have amplitude

$$A_k = \frac{4\pi\Omega_k^2(\sigma_k)}{\epsilon^{\gamma_k}}\left[\frac{|c_k|^{6-3\gamma_k}}{2|C|(1+3\sigma_k)^{\gamma_k}}\right]\exp\left[-\frac{\Re[\chi_k]}{\epsilon}\right],$$

for $k = 1, 2$ where

$$\Re(\chi_1) = 3\pi(\sigma_1 a_1 + \sigma_2 a_2), \tag{4.38}$$

$$\Re(\chi_2) = \Re(\chi_1) + \Re\left[\int_{-a_2}^{-a_1} \frac{i}{q_0^3}\, d\varphi\right], \tag{4.39}$$

and

$$c_1 = \left[\frac{\alpha_1^{\sigma_1+\sigma_2}}{(a_1-a_2)^{\sigma_2}}\right]e^{\pi\sigma_1 i} \qquad \gamma_1 = \frac{6\sigma_1}{1+3\sigma_1}$$

$$c_2 = \left[\frac{a_2^{\sigma_1+\sigma_2}}{(a_1-a_2)^{\sigma_1}}\right]e^{\pi(\sigma_1+\sigma_2)i} \qquad \gamma_2 = \frac{6\sigma_2}{1+3\sigma_2}.$$

Note that for $w \in (-a_1, -a_2)$, $\mathrm{Arg}(1/q_0^3) = -3\pi\sigma_1$ so the second term on the right of (4.39) is positive for $\sigma_1 > 1/3$, zero if $\sigma_1 = 1/3$, and negative otherwise. Thus assuming all other quantities to be $\mathcal{O}(1)$, the $w = -a_1$ corner will exponentially dominate the other if $\sigma_1 > 1/3$, whereas the second will dominate the first if $\sigma_1 < 1/3$.

The difference in the phases contributions between the two waves is given by $\Delta = \Psi_2 - \Psi_1$ from (4.29), or

$$\Delta = \frac{1}{\epsilon}\Im\left[\int_{-a_1}^{-a_2}\chi'\, dw\right] + \left[(6-3\gamma_2)\mathrm{Arg}(c_2) - (6-3\gamma_1)\mathrm{Arg}(c_1)\right] + \frac{\pi}{2}\left[\gamma_2 - \gamma_1\right] + \Im\left[3\int_{-a_1}^{-a_2}\frac{\mathscr{H}[\theta_1(\varphi)]}{q_0^3}\, d\varphi\right]. \tag{4.40}$$

In order to find the total wave amplitude of two sinusoidals of the form:

$$A_1\cos\left(\frac{w}{\epsilon}\right) + A_2\cos\left(\frac{w}{\epsilon} + \Delta\right),$$

we can show that this produces a single cosine wave with amplitude

$$A = \left| C\left\{ \cos\left[\tan^{-1}\left(\frac{D}{C}\right)\right] - \cos\left[\tan^{-1}\left(\frac{D}{C}\right) + \pi\right]\right\} \right.$$
$$\left. + D\left\{ \sin\left[\tan^{-1}\left(\frac{D}{C}\right)\right] - \sin\left[\tan^{-1}\left(\frac{D}{C}\right) + \pi\right]\right\} \right|,$$

where $C = A_1 + A_2 \cos\Delta$ and $D = -A_2 \sin\Delta$, and thus after simplification:

$$A = \frac{2(A_1^2 + A_2^2 + 2A_1A_2\cos\Delta)}{(A_1 + A_2\cos\Delta)\sqrt{1 + \left(\frac{A_2 \sin\Delta}{A_1 + A_2\cos\Delta}\right)^2}}.$$

4.5.1 Numerical vs. analytical results (full problem)

As discussed in the first part of our work, the numerical computation of the nonlinear stern problem for small values of ϵ is particularly difficult, and the culprit is the presence of the attachment singularity at $\phi = 0$, which causes numerical errors and produces a very small inner region which is difficult to resolve.

For hulls where the total deviation is more than $\pi/3$, and thus $\sigma_{N+1} > 1/3$, a very simple finite difference scheme based on the methods outlined in Vanden-Broeck & Tuck (1977) can be used, provided that we limit our search to waves larger than $\sim 10^{-4}$. Figure 4.5 provides an example of solutions found using this method. Hulls with total deviations less than $\pi/3$ require more elaborate treatments of the stagnation point singularity, and so we will instead focus on the former case.

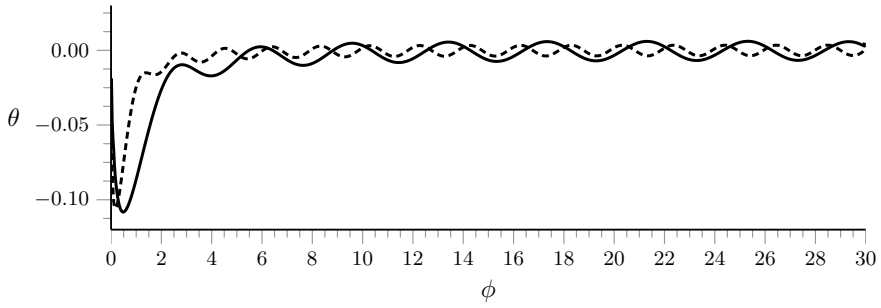

Figure 4.5: Solutions for the $[0.5, 0.125]$-Hull (dashed line) and $[0.25, 0.25]$-Hull (solid line) at $\epsilon = 2/3$ and $\epsilon = 1/3$, respectively. Both ships have corners set at $\alpha_1 = 0.8$ and $\alpha_2 = 0.2$. The solutions were computed using ALGORITHM A of Section 3.7.1 in the preceding chapter with $n = 1000$ and $\Delta\phi = 0.015$ for the former ship and $n = 2000$ and $\Delta\phi = 0.015$ for the latter.

As in the numerical work for the one-cornered ship, we can provide verification of our analytical predictions by comparing wave amplitudes over a range of Froude numbers. This is shown in Figure 4.6 for three 2-Hulls with their corners fixed at $a_1 = 0.8$ and $a_2 = 0.2$. Here, the match between numerical and asymptotic solutions is quite good, and, like the previous chapter, we remark that the results are applicable over a wide range of Froude numbers.

However, for certain hulls, we find that the convergence of the asymptotic prediction is slower (in the limit that $\epsilon \to 0$); the reason for this anomaly is easily seen by computing numerical solutions with a *fixed* values of ϵ and

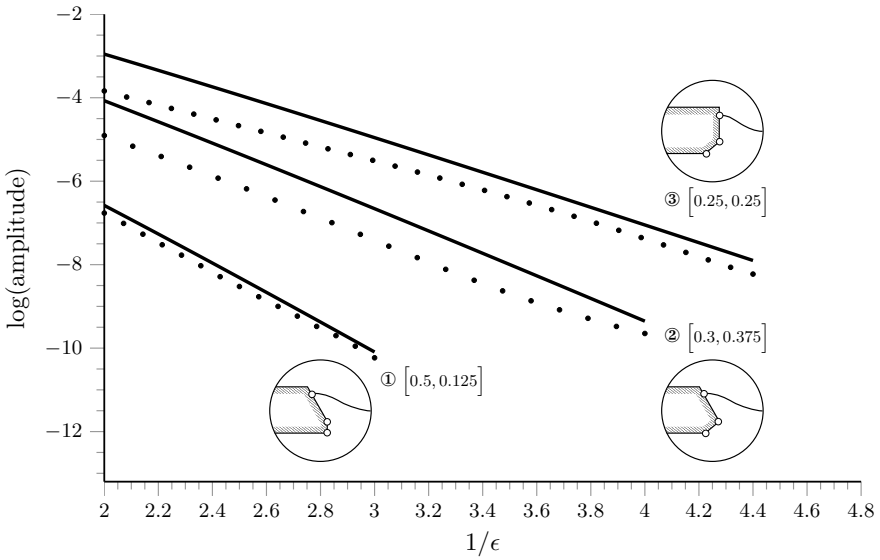

Figure 4.6: Numerical (dots) and asymptotic (solid) amplitudes of the downstream waves for a range of hull inclinations. In all cases, the corner points are fixed with $a_1 = 0.8$ and $a_2 = 0.2$. In the ship with $[0.3, 0.375]$, the slight raising of the last six points is a numerical artifact, and can be removed using a more careful treatment of the grid discretisation. The solutions were computed using ALGORITHM A of Section 3.7.1 in the preceding chapter. The parameters used were:
①: $n = 1000$, $\Delta\phi = 0.04$
②: $n = 1500$, $\Delta\phi = 0.03$
③: $n = 2000$, $\Delta\phi = 0.025$.

σ_i, but allowing the points a_1 and a_2 to vary. The wave amplitude for such a computation is shown in Figure 4.7. We see, then, that the asymptotic prediction is terrifically accurate when the corners are well separated, but diverges when the corners begin to approach each other. A uniform approximation would need to smoothly match with the one-cornered approximation at one end, and the (separated) two-cornered analysis at the other. Our final goal of this thesis will be to demonstrate how the asymptotic methodology can be changed to deal with ships containing closely-spaced corners.

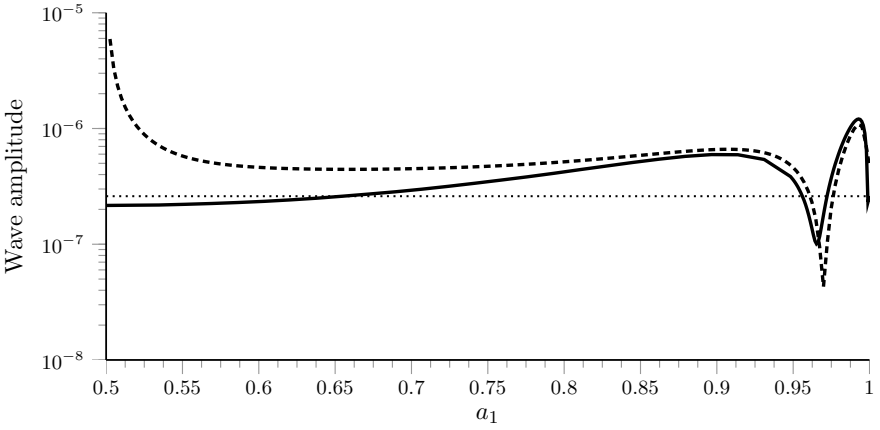

Figure 4.7: The numerical solution (solid) for the $[1/4, 1/4]$-Hull is plotted against the asymptotic approximation at $\epsilon = 0.15$ and $a_1 + a_2 = 1$. The two-cornered approximation (solid line) very accurately predicts the solution when the two corners are well separated, but is singular when $a_1, a_2 \approx 0.5$ near the left. Near this point, we will need to develop a uniform methodology which takes in account the fact that the relevant singularities are both found in the inner region. This solution was computed for the simplified nonlinear problem of Section 4.6.1 using the code of Table 4.1.

4.6 THE CLOSE-CORNERED APPROXIMATION FOR TWO-CORNERED SHIPS

In the inner problem analysis of Section 4.3.3, the crucial re-scaling of w near a singularity at $w = -a$ is

$$w + a \sim \mathcal{O}\left(\epsilon^{\frac{1}{1-3\alpha}}\right), \tag{4.41}$$

which can be predicted by setting $\epsilon q_1 \sim q_0$ or, in general, $\epsilon^n q_n \sim q_0$, and thus

$$\frac{\epsilon^n}{\chi^n} \sim \mathcal{O}(1).$$

Thus, if two (or more) singularities are spaced within a distance of (4.41) apart, then our previous asymptotic methodology breaks down.

4.6.1 The simplified non-linear problem

Although the full problem in eqns (4.5) to (4.6) is tractable using our methodology, we present a simpler problem which nevertheless illustrates the key ideas. The most important reason why we find it necessary to propose this simplification is that accurate numerical verification of the asymptotic analysis demands numerical precision of five or six digits—otherwise, the fine effects of adjusting the geometry are easily missed; this precision is only achievable for the simpler problem, which we now derive.

As we know, when the exponentially small terms are sought from (4.5), the integral term, $\mathscr{H}[\theta]$ serves to only change the amplitude coefficient of the downstream waves by a non-zero $\mathcal{O}(1)$ amount. If we return to the derivation of the late-orders ansatz, we see that $\mathscr{H}[\theta]$ was in fact subdominant in the analysis, as assumed in eqn (4.13). Moreover, it is again ignored when we proceed inwards to the analysis near the singularity.

In fact, in the final form of the free-surface waves, the only effect of $\mathscr{H}[\theta]$ is in (i) changing q_1 in (4.11), (ii) changing the computation of C in (4.23), and (iii) replacing the expression of Q_k in (4.17), valid everwhere, by its expression valid near the singularity.

Thus, we notice that salient features of the problem are still retained if we use $\log q \pm i\theta = \log q_s$ instead of (4.5), and this way we simplify the full problem in eqns (4.5) to (4.6) to a simpler nonlinear differential equation in q. Analytic continuation into the upper-half plane then gives

$$\epsilon q_0 q^3 \frac{dq}{dw} + \frac{i}{2}(q^2 - q_0^2) = 0. \tag{4.42}$$

Note that because of the simplified form, it is much more convenient to work under the substitution $\phi = q^2$, which gives

$$\phi - q_s^2 - i\epsilon q_s \phi \frac{d\phi}{dw} = 0. \tag{4.43}$$

The form of the far-field waves of this simplified problem (with well-separated corners) is now given by

$$q_{\text{exp},k} \sim \frac{2\pi\Omega_k(\sigma_k)}{\epsilon^{\gamma_k} q_0^5(w)} \left[\frac{|c_k|^{6-3\gamma_k}}{2(1+3\sigma_k)^{\gamma_k}}\right] \exp\left[-\frac{\Re[\chi_k]}{\epsilon}\right] \cos\left(-\frac{w}{\epsilon} + \Psi_k\right) \tag{4.44}$$

and

$$\Psi_k = -\frac{1}{\epsilon}\Im\left[\int_{-a_k}^{-a_1} \frac{d\chi}{dw}\, dw\right] + (6-3\gamma_k)\text{Arg}(c_k) + \frac{\pi}{2}\gamma_k, \tag{4.45}$$

instead of eqns (4.28) and (4.29). The reduction of the factor of 2 in eqn (4.44) occurs because in the new problem (4.42), we have already chosen to analytically continue into the upper-half w-plane, so there is no need for the addition of the complex conjugate solution.

```
a1 = 0.8; a2 = 0.2; % Location of corners
s1 = 1/4; s2 = 1/4; % Divergent angles
ep = 0.15;          % Epsilon

sigma = s1 + s2;    % Local behaviour near stagnation point
q0 = @(w) w.^sigma./(w+a1).^s1./(w+a2).^s2; % [s1, s2] ship

w0 = 1e-8;                              % First mesh point
wmax = 2000;                            % Last mesh point
w = @(s) s.^(1/sigma);                  % Stretched mesh
dwds = @(s) s.^(1/sigma-1)/sigma;
d = ([w0 wmax]).^(sigma);               % Domain
bc = w0^(sigma);                        % Assume q(w0) ~ w0^sigma

% Solve the differential equation
F = @(s,q) 0.5i*dwds(s)*(q.^2-q0(w(s))^2)/(ep*q0(w(s))*q^3);
opts = odeset('reltol', 1e-13, 'abstol', 1e-13);
[s,q] = ode113(F,d,bc,opts);
u = q-q0(w(s)); plot(w(s), real(u));
```

Table 4.1: MATLAB code for solving the simplified nonlinear problem of (4.42). This particular instance solves the $[1/4, 1/4]$-hull, with $a_1 = 0.8$, $a_2 = 0.2$, and $\epsilon = 0.15$ using MATLAB's `ode113` solver. The boundary condition is approximated by $q(w_0) = w_0^{1/2}$ with $w_0 = 10^{-8}$. Solutions in Figures 4.7 and 4.11 were computed using this same code, but with different values for the hull. Note that a more accurate solver would implement a special treatment of the flow near the stagnation point.

4.6.2 *The general methodology*

In this section, we will discuss the general methodology for developing the uniform asymptotics valid when two corners of a 2-Hull are sufficiently closely spaced so as to both lie a one inner region. However, this problem is a great deal more difficult than the usual assumptions of well-separateness of Section 4.3; the algebraic complexity is higher, and as such, we will only present the main ideas, leaving a detailed analysis for specific cases.

Suppose we begin by assuming that the inner region scaling for this new problem remains the same as for the original, well-separated analysis of Section 4.3, and thus given by eqn (4.41). We can then define positive integers ℓ and m such that

$$\frac{\ell}{m} \equiv 1 - 3\alpha,$$

where the ratio ℓ/m is irreducible. This approach is then only applicable for hull deviations $\pi\sigma$ for which σ is rational. We now propose an alternative hull shape described by

$$\begin{aligned} q_s &= \frac{w^{\sigma_1+\sigma_2}}{(w+a+\epsilon^{\frac{\ell}{m}}\beta)^{\sigma_1}(w+a-\epsilon^{\frac{\ell}{m}}\beta)^{\sigma_2}} \\ &= \left(\frac{w}{w+a}\right)^{\sigma_1+\sigma_2} \sum_{n=0}^{\infty} \epsilon^{\frac{\ell n}{m}} \left(\frac{\beta}{w+a}\right)^n f_n, \end{aligned} \tag{4.46}$$

where

$$f_n = f(n) = \frac{1}{\Gamma(\sigma_1)\Gamma(\sigma_2)} \sum_{m=0}^{n} (-1)^m \frac{\Gamma(\sigma_1+m)\Gamma(\sigma_2+n-m)}{\Gamma(m+1)\Gamma(n-m+1)},$$

and the shape of this hull is illustrated in Figure 4.8.

For the asymptotic expansion of eqn (4.43), then, we we will need to expand

$$\phi = \sum_{n=0}^{\infty} \epsilon^{\frac{n}{m}} \phi_n. \tag{4.47}$$

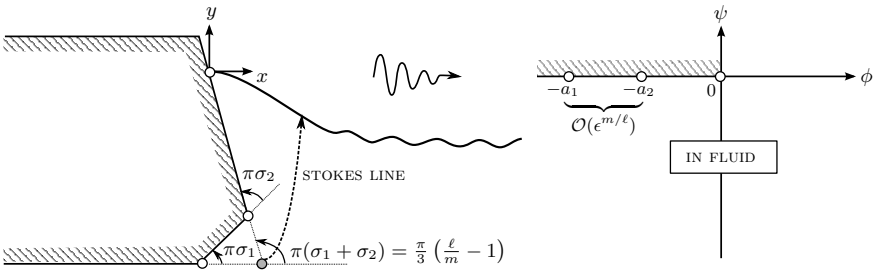

Figure 4.8: In the close-cornered analysis applied to a $[\sigma_1, \sigma_2]$-Hull, the corners are assumed to be located at the points $-a_1 = -(a + \epsilon^{m/\ell}\beta)$ and $-a_1 = -(a - \epsilon^{m/\ell}\beta)$. Away from the inner region, only the *merged* singularity at $w = -a$ is seen, and so only a single Stokes line appears. However, the inner analysis is changed due to both corners being in the same inner region.

With the expansions in powers of $1/m$, it is convenient to write

$$q_s = q_0 \sum_{n=0}^{\infty} \epsilon^{\frac{\ell}{m}} e_n,$$

where

$$e_n = \begin{cases} \left(\frac{\beta}{w+a}\right)^{\frac{n}{\ell}} f\left(\frac{n}{\ell}\right) & \text{if } \operatorname{mod}(n,\ell) = 0 \\ 0 & \text{if } \operatorname{mod}(n,\ell) \neq 0, \end{cases}$$

and we have also written

$$q_0 = \left(\frac{w}{w+a}\right)^{\sigma_1+\sigma_2}.$$

Initially, this problem seems similar to the situation studied in Combescot et al. (1988) and Chapman et al. (1999) for the Saffman-Taylor viscous fingering problem. If we follow the same methodology, then we would expect for the asymptotic expansion in (4.47) to split like so:

$$\begin{aligned} \phi = \sum_{n=0}^{\infty} \epsilon^n \phi_n = \sum_{n=0}^{\infty} \epsilon^{\frac{n}{m}} \phi_{mn} + \sum_{n=0}^{\infty} \epsilon^{\frac{n}{m}+\frac{1}{m}} \phi_{mn+1} \\ + \ldots + \sum_{n=0}^{\infty} \epsilon^{\frac{n}{m}+\frac{k}{m}} \phi_{mn+k} + \ldots + \sum_{n=0}^{\infty} \epsilon^{\frac{n}{m}+\frac{m-1}{m}} \phi_{mn+m-1}. \end{aligned} \tag{4.48}$$

For the viscous fingering problem, the early orders, ϕ_0, ϕ_1, ϕ_2, …are determined using all three terms of (4.43). However, the high-order terms, given by ϕ_{nm+k} for $k = 0, 1, \ldots, m-1$, are only coupled between terms $\mathcal{O}(\epsilon)$ apart. Because of this unique property at high orders, the late terms are still given by the same factorial over power ansatz of (4.12). Does the same simplification hold for our problem?

No, it does not, and the most direct way to see this is to perform the inner analysis *before* we look at the late-orders behaviour of the outer terms. In the inner region, we will define variables z and $\widehat{\phi}$ and re-scale, setting

$$w + a = \epsilon^{\ell/m}\eta = \epsilon^{\ell/m} X^{-\ell/m} z^{\ell} \tag{4.49}$$

$$\phi = c^2 (w+a)^{2\alpha} \widehat{\phi} \tag{4.50}$$

where the convention of using c, X, and α is consistent with the one introduced in Section 4.3.2. From (4.43), the inner equation then becomes

$$\left(\frac{2\alpha\ell}{m}\right) \frac{\widehat{q_s}\widehat{\phi}^2}{z^m} + \frac{1}{m}\frac{1}{z^{m-1}} \widehat{q_s}\widehat{\phi}\frac{d\widehat{\phi}}{dz} + \widehat{\phi} - \widehat{q_s}^2 = 0. \tag{4.51}$$

The expansion for $\widehat{q_s}$, from (4.46), will now be re-written as

$$\widehat{q_s} = \frac{(X^{-\ell/m} z^\ell)^{\sigma_1+\sigma_2}}{(z^\ell+\beta)^{\sigma_1}(z^\ell-\beta)^{\sigma_2}} = \sum_{n=0}^{\infty} \frac{\widehat{e_n}}{z_n},$$

with

$$\widehat{e_n} = \begin{cases} \beta^{n/\ell} X^{n/m} f\left(\frac{n}{\ell}\right) & \text{if } \mathrm{mod}(n,\ell) = 0 \\ 0 & \text{if } \mathrm{mod}(n,\ell) \neq 0 \end{cases}$$

Expanding

$$\widehat{\phi} = \sum_{n=0}^{\infty} \frac{A_n}{z^n}, \tag{4.52}$$

we have

$$A_0 = 1, \tag{4.53}$$

$$A_n = \sum_{j=0}^{n} \widehat{e}_j \widehat{e}_{n-j} \qquad \text{for } n < m, \tag{4.54}$$

and, at $\mathcal{O}(z^n)$ for $n \geq m$,

$$A_n = \sum_{j=0}^{n} \widehat{e}_j \widehat{e}_{n-j} + \sum_{j=0}^{n-m-k} \sum_{k=0}^{n-m} \left(\frac{j}{m} - \frac{2\alpha}{1-3\alpha} \right) \widehat{e}_k A_j A_{n-m-k-j}. \tag{4.55}$$

In the limit that $n \to \infty$, the correct ansatz to use for the late terms is

$$A_n \sim \Omega^{\mathrm{cc}} e^{i\tau} \Gamma\left(\frac{n}{m} + \gamma\right) \exp\left[\sum_{j=1}^{m-1} \mu_j n^{\frac{m-j}{m}} \right], \tag{4.56}$$

with $\gamma, \mu_j \in \mathbb{C}$, $\Omega^{\mathrm{cc}}, \tau \in \mathbb{R}$, and the 'cc' (for closed-corner) differentiates the pre-factor from that corresponding to the separated-corners analysis. Under this substitution, we can see that the series expansions of the various ratios are given by

$$\begin{array}{lcccccc}
\dfrac{A_{n-m}}{A_n} & \sim & \dfrac{c_{10}}{n} & + & \dfrac{c_{11}}{n^{\frac{m+1}{m}}} & + \ldots + & \dfrac{c_{1(m-1)}}{n^{\frac{2m-1}{m}}} + \dfrac{c_{1m}}{n^2} \\
\dfrac{A_{n-m-1}}{A_n} & \sim & & & \dfrac{c_{21}}{n^{\frac{m+1}{m}}} & + \ldots + & \dfrac{c_{2(m-1)}}{n^{\frac{2m-1}{m}}} + \dfrac{c_{2m}}{n^2} \\
\vdots & & & & & \ddots & & \vdots \\
\dfrac{A_{n-2m+1}}{A_n} & \sim & & & & \cdots & \dfrac{c_{(m-1)(m-1)}}{n^{\frac{2m-1}{m}}} + \dfrac{c_{(m-1)m}}{n^2} \\
\dfrac{A_{n-2m}}{A_n} & \sim & & & & \cdots & \dfrac{c_{mm}}{n^2},
\end{array}$$

where the factors c_{jk} are functions of μ_j and γ and in general, require the higher-order terms of Stirling's Approximation to the Gamma function.

Thus, when we search for the $n \to \infty$ limit, we will need to conserve the terms with factors of A_n and A_{n-m}, and terms of orders nA_{n-m} to nA_{n-2m}

which earlier corresponded to derivatives in $\widehat{\phi}$. Terms with other indices will be of lower order. The asymptotic process is then most easily understood by dividing eqn (4.55) by A_n and writing it as

$$1+\sum_{j=0}^{m}\left[\sum_{k=0}^{j}\left(\frac{-1}{m}\right)\widehat{e}_k A_{j-k}\right]\frac{nA_{n-m-j}}{A_n}+\left[\frac{(4\ell-m)\widehat{e}_0 A_0}{3m}\right]\frac{A_{n-m}}{A_n}+\ldots=0 \tag{4.57}$$

For this equation, the leading order behaviour at $\mathcal{O}(1)$ is automatically satisfied by the Gamma function. μ_1 is then determined at $\mathcal{O}(n^{\frac{-1}{m}})$, μ_2 is determined at $\mathcal{O}(n^{\frac{-2}{m}})$, and so on until μ_{m-1} is determined at $\mathcal{O}(n^{\frac{-(m-1)}{m}})$. Lastly, the constant γ is determined at $\mathcal{O}(\frac{1}{n})$. We would indeed expect the series in A_n to split:

$$\widehat{\phi}=\sum_{n=0}^{\infty}\frac{A_{nm}}{z^{nm}}+\sum_{n=0}^{\infty}\frac{A_{mn+1}}{z^{nm+1}}+\ldots+\sum_{n=0}^{\infty}\frac{A_{mn+k}}{z^{nm+k}}+\ldots+\sum_{n=0}^{\infty}\frac{A_{m(n+1)-1}}{z^{m(n+1)-1}}, \tag{4.58}$$

with, in general, m different ansatzes

$$A_{n+k}\sim\Omega_k^{\mathrm{cc}}e^{i\tau_k}\Gamma\left(\frac{n}{m}+\gamma+\frac{k}{m}\right)\exp\left[\sum_{j=1}^{m-1}\mu_j n^{\frac{m-j}{m}}\right]. \tag{4.59}$$

for $k=0,1,\ldots,m-1$, and for which the prefactor $\Omega_k e^{i\tau_k}$ with $\Omega_k,\tau_k\in\mathbb{R}$ can then be found by numerically solving the recurrence relation.

We are now in a position to return to the outer analysis. The early terms of the asymptotic expansion of (4.43) are

$$\begin{aligned}\phi_0 &= q_0^2,\\ \phi_n &= q_0^2\sum_{k=0}^{n}e_k e_{n-k} \qquad \text{for } n<m,\end{aligned}$$

and motivated by the form of the inner ansatz (4.56), the correct late-orders behaviour is likely to be

$$\phi_{n+k}\sim\frac{P_k(w)\Gamma\left(\frac{n}{m}+\gamma+\frac{k}{m}\right)\exp\left[\sum_{i=1}^{m-1}r_i(w)n^{\frac{m-i}{m}}\right]}{[\chi(w)]^{\frac{n}{m}+\gamma}}.$$

Substitution of this ansatz into the differential equation yields a similar procedure to that which we used for the inner equation, except that now, we wish to keep terms ϕ_n and ϕ_{n-m}, as well as derivatives ϕ'_{n-m} to ϕ'_{n-2m}. The relevant terms at $\mathcal{O}(\epsilon^{\frac{n}{m}})$ are then

$$\phi_n+\sum_{j=0}^{m}\left[\sum_{k=0}^{j}\Big(-iq_0\Big)e_k\phi_{j-k}\right]\phi'_{n-m-j}+\left[(-i)e_0\phi'_0\right]\phi_{n-m}+\ldots=0. \tag{4.60}$$

As $n\to\infty$, the leading-order terms are easy to see as they simply involve

$$\phi_n-i\phi'_{n-m}e_0\phi_0.$$

Thus the equation for χ remains the same:

$$\chi = \int_{-a}^{w} \frac{i}{q_0^3}\, d\varphi,$$

The subsequent orders each yield a first-order differential equation for $r_i(w)$, and for $P_k(w)$. In order to match with the form of the inner ansatz in (4.59), we then must have $r_i(-a) = \mu_i$. Once the inner limits of $r_i(w)$ is verified, the value of γ can be checked by setting $n = 0$ in the late-orders ansatz and matching its behaviour as $w \to -a$. If we assume that

$$P_k \sim \mathcal{O}(w+a)^{\kappa},$$

as $w \to -a$, and for some complex constant κ, then setting $n = 0$ and matching with $\phi_0 \sim c^2(w+a)^{2\alpha}$ gives

$$\kappa - 2\gamma = 2\alpha,$$

which will turn out to be the same γ computed directly from the inner analysis. The derivation of the late-order terms of the outer expansion, ϕ_n is important in the sense that it provides a connection between the inner analysis and the Stokes Smoothing procedure. However, beyond its function as a bridge between the two analyses, the actual values of $r_i(w)$ and $P_k(w)$ for all w are generally unimportant.

Once we have completely determined the form of the late-order terms of ϕ, we may now proceed to the Stokes Smoothing procedure. We begin by truncating the asymptotic expansion at $n = \mathcal{N}$:

$$\phi = \sum_{n=0}^{\mathcal{N}-m} \epsilon^{\frac{n}{m}} \phi_n + R_{\mathcal{N}}$$

and substitute the expression into eqn (4.43). This gives a linear equation in $R_{\mathcal{N}}$, as well as a single $\mathcal{O}(\epsilon^{\mathcal{N}/m})$ term:

$$\mathcal{L}(R_{\mathcal{N}};\epsilon) \sim \epsilon^{\mathcal{N}/m} i q_0 \phi_0 \phi'_{\mathcal{N}-m},$$

valid for large $\mathcal{N}$. The right-hand side can be replaced using the equivalent $\mathcal{O}(\epsilon^{\mathcal{N}/m})$ term:

$$\mathcal{L}(R_{\mathcal{N}};\epsilon) \sim \epsilon^{\mathcal{N}/m} \phi_{\mathcal{N}}, \tag{4.61}$$

where the relevant terms of the linear operator $\mathcal{L}$ are given by

$$\mathcal{L}(R_{\mathcal{N}};\epsilon) = R_{\mathcal{N}} + \sum_{j=0}^{m} \left[\sum_{k=0}^{j} \Big(-iq_0\Big) e_k \phi_{j-k} \right] \epsilon^{1+\frac{j}{m}} \frac{dR_{\mathcal{N}}}{dw} + \left[(-i) e_0 \phi_0' \right] \epsilon R_{\mathcal{N}} + \ldots = 0, \tag{4.62}$$

and at this point, the connection between the asymptotic process to determine the forms of A_n, ϕ_n, and $R_{\mathcal{N}}$ should be clear; Table 4.2 summarises this connection between the inner, outer, and Stokes Smoothing procedures.

Table 4.2: This table indicates which terms correspond to which orders in the asymptotic methodology of the inner region, the outer region, and the Stokes smoothing; in particular, it illustrates the correspondence between all three analyses. For the inner analysis, seeking the $n \to \infty$ limit for A_n involves equations in orders of $n^{-1/m}$; for the outer analysis, the $n \to \infty$ limit also involves equations in orders of $n^{-1/m}$; for the Stokes smoothing procedure, the exponential behaviour of R_N is determined by matching at orders in $\epsilon^{1/m}$. The equations at each order are not the same for all three analyses, but they share corresponding values near the inner region (between terms A_n and q_n) and near the Stokes line (between terms q_n and R_N).

REGION	FORM	FIRST	FIRST	SECOND	...	LAST	LAST
Inner	$\sum_n \frac{A_n}{z^n}$	A_n	nA_{n-m}	nA_{n-m-1}	...	nA_{n-2m}	A_{n-m}
Outer	$\sum_n \epsilon^{\frac{n}{m}} \phi_n$	ϕ_n	ϕ'_{n-m}	ϕ'_{n-m-1}	...	ϕ'_{n-2m}	ϕ_{n-m}
Stokes	$R_{\mathcal{N}} e^F$	$R_{\mathcal{N}}$	$\epsilon^{\frac{1}{m}} R'_{\mathcal{N}}$	$\epsilon^{\frac{2}{m}} R'_{\mathcal{N}}$	...	$\epsilon^{\frac{m-1}{m}} R'_{\mathcal{N}}$	$\epsilon R'_{\mathcal{N}}$

In order to solve the homogeneous equation $\mathcal{L} = 0$, we set

$$R_{\mathcal{N}} = \overline{P_k} \exp\Big[F(w)\Big] = \overline{P_k} \exp\left[\sum_{j=0}^{m-1} \frac{F_i(w)}{\epsilon^{\frac{j}{m}}}\right],$$

so that the first derivative is

$$\frac{dR_{\mathcal{N}}}{dw} = \left(\left[\sum_{j=0}^{m-1} \frac{F_i'(w)}{\epsilon^{\frac{j}{m}}}\right] \overline{P_k} + \overline{P_k}'\right) \exp\left[\sum_{j=0}^{m-1} \frac{F_i(w)}{\epsilon^{\frac{j}{m}}}\right].$$

Substitution into $\mathcal{L} = 0$ yields equations at orders $\mathcal{O}(1)$, $\mathcal{O}(\epsilon^{\frac{1}{m}})$, ..., $\mathcal{O}(\epsilon^{\frac{m-1}{m}})$, $\mathcal{O}(\epsilon)$, which determines F_0', F_1', ... F_{m-1}', and Q, each in turn.

Crucially, however, we notice that these equations only involve the *derivatives* of F. To solve the inhomogeneous equation, we multiply the homogeneous solution by the Stokes Smoothing factor $\mathcal{S}(w)$

$$R_{\mathcal{N}} = \mathcal{S}\overline{P_k} \exp\Big[F(w)\Big]$$

then substitute this expression into (4.61), giving

$$\epsilon\left[-iq_0^3\right] \frac{d\mathcal{S}}{dw} \overline{P_k} e^F \sim \epsilon^{\mathcal{N}/m} \phi_{\mathcal{N}},$$

where the bracketed factor corresponds to the $j = 0$ contribution from the summation in eqn (4.62). Remember that P_k is determined from the late-orders analysis and $\overline{P_k}$ from the Stokes Smoothing. However, the key is that at optimal truncation and near the Stokes line,

$$\overline{P_k}(w) \sim P_k(w),$$

and the reason for this is that

$$r_i(w) \sim F_i(w),$$

for w evaluated near the Stokes line. In this way, we can establish a relationship between the components of the final exponential given by $R_{\mathcal{N}}$, and the crucial numerical constant of the inner problem Ω_k, all related through the late-order terms r_i and P_k. In the next section, we will demonstrate this method in full detail for a particular stern configuration.

4.6.3 *Close-corners analysis for the ship with* $\sigma_1 + \sigma_2 = 1/3$

Derivation of all the components of the late-order terms for general ℓ and m can become an arbitrarily complicated task for arbitrary choices of the two corners. Indeed, a small (rational) perturbation of ℓ/m can produce an unseemly fraction, for which the series in (4.48) splits as indicated, but now, computation of each component of the analysis becomes virtually impossible to do by hand. It then seems that the methodology previously outlined is rather unstable to small perturbations of the geometry. In any case, in this section, we will explicitly show how the procedure is accomplished, from beginning to end, for the case of $\ell = 1$ and $m = 2$, which corresponds to the ship with $\sigma_1 + \sigma_2 = 1/3$:

$$q_s = \frac{w^{1/3}}{(w + a + \sqrt{\epsilon}\beta)^{\sigma_1}(w + a - \sqrt{\epsilon}\beta)^{\sigma_2}},$$

and the alternative useful forms of q_s are

$$q_s = q_0 \sum_{n=0}^{\infty} \epsilon^{\frac{n}{2}} \underbrace{\left(\frac{\beta}{w+a}\right)^n f_n}_{e_n} = q_0 \sum_{n=0}^{\infty} \frac{1}{z^n} \underbrace{\left(\beta^n X^{\frac{n}{2}} f_n\right)}_{\widehat{e_n}},$$

where $w + a = \epsilon^{1/2} X^{-1/2} z$ and $\chi \sim X(w + a)^2$ as $w \to -a$. The inner expansion of eqn (4.52) then requires the ansatz

$$A_n \sim \Omega_k^{\text{cc}} e^{i\tau_k} \Gamma\left(\frac{n}{2} + \gamma\right) \exp\left[\frac{\mu_1}{\sqrt{n}}\right],$$

with $k = 0, 1$. Once substituted into the recurrence relation for A_n in (4.55), the relevant terms are

$$\begin{aligned} 1 &- \left[\frac{\widehat{e}_0 A_0}{2}\right] \frac{n A_{n-2}}{A_n} - \left[\frac{\widehat{e}_0 A_1 + \widehat{e}_1 A_0}{2}\right] \frac{n A_{n-3}}{A_n} \\ &- \left[\frac{\widehat{e}_0 A_2 + \widehat{e}_1 A_1 + \widehat{e}_2 A_1}{2}\right] \frac{n A_{n-4}}{A_n} + \left[\frac{\widehat{e}_0 A_0}{3}\right] \frac{A_{n-2}}{A_n} + \ldots = 0, \end{aligned} \tag{4.63}$$

and expanding the ansatz gives

$$\begin{aligned} 1 &- \left[\frac{\widehat{e}_0 A_0}{2}\right] \left\{2 - \frac{2\mu_1}{\sqrt{n}} + \frac{4 - 4\gamma\mu_1^2}{n} + \mathcal{O}\left(\frac{1}{n^{\frac{3}{2}}}\right)\right\} \\ &\quad - \left[\frac{\widehat{e}_0 A_1 + \widehat{e}_1 A_0}{2}\right] \left\{\frac{2\sqrt{2}}{\sqrt{n}} - \frac{3\sqrt{2}\mu_1}{n} + \mathcal{O}\left(\frac{1}{n^{\frac{3}{2}}}\right)\right\} \\ &- \left[\frac{\widehat{e}_0 A_2 + \widehat{e}_1 A_1 + \widehat{e}_2 A_1}{2}\right] \left\{\frac{4}{n} + \mathcal{O}\left(\frac{1}{n^{\frac{3}{2}}}\right)\right\} + \left[\frac{\widehat{e}_0 A_0}{3}\right] \left\{\frac{2}{n} + \mathcal{O}\left(\frac{1}{n^{\frac{3}{2}}}\right)\right\} = 0. \end{aligned} \tag{4.64}$$

Setting $\widehat{e_0} = A_0 = 1$, then eqn (4.64) is satisfied trivially at $\mathcal{O}(1)$. Afterwards, the $\mathcal{O}(n^{-1/2})$ and $\mathcal{O}(1/n)$ terms give

$$\mu_1 = 3\sqrt{2}\widehat{e_1}, \tag{4.65}$$

$$\gamma = 1 - 6\widehat{e_1}^2 + 3\widehat{e_2}, \tag{4.66}$$

and setting $\widehat{e_1} = \beta\sqrt{X}f_1$ and $\widehat{e_2} = \beta^2 X f_2$ gives

$$\mu_1 = 3\sqrt{2X}\beta f_1, \tag{4.67}$$

$$\gamma = 1 + 3\beta^2 X\left[f_2 - 2f_1^2\right]. \tag{4.68}$$

With the correct form of A_n as $n \to \infty$, we can now compute the numerical values of Ω_1^{cc} and Ω_2^{cc}. In general, both values are non-zero, except in certain limiting cases that we shall discuss in Section 4.6.5.

We now proceed to the outer asymptotic expansion in eqn (4.47). The relevant terms at $\mathcal{O}(\epsilon^{n/2})$ are

$$\begin{aligned} &1 - iq_0\left[e_0\phi_0\right]\frac{\phi'_{n-2}}{\phi_n} - iq_0\left[e_0\phi_1 + e_1\phi_0\right]\frac{\phi'_{n-3}}{\phi_n} \\ &- iq_0\left[e_0\phi_2 + e_1\phi_1 + e_2\phi_1\right]\frac{\phi'_{n-4}}{\phi_n} - iq_0\left[e_0\phi_0\right]\frac{\phi_{n-2}}{\phi_n} + \ldots = 0. \end{aligned} \tag{4.69}$$

Substituting the ansatz of the form

$$\phi_n \sim \frac{P_k\Gamma\left(\frac{n}{2}+\gamma\right)\exp\left[\frac{r_1}{\sqrt{n}}\right]}{\chi^{\frac{n}{2}+\gamma}}, \tag{4.70}$$

into (4.69) and expanding the ratios gives

$$\begin{aligned} &1 - iq_0\left[e_0\phi_0\right]\left\{-\chi' + \frac{\chi' r_1 + 2\chi r_1'}{\sqrt{n}} + \left(\frac{4\chi P_k' - \chi' P_k r_1^2 - 4\chi P_k r_1 r_1'}{2P_k}\right)\frac{1}{n} + \mathcal{O}\left(\frac{1}{n^{\frac{3}{2}}}\right)\right\} \\ &\quad - iq_0\left[e_0\phi_1 + e_1\phi_0\right]\left\{-\frac{\sqrt{2\chi}\chi'}{\sqrt{n}} + \left(\frac{3\sqrt{\chi}\chi' r_1}{\sqrt{2}} + 2\sqrt{2}\chi^{3/2}r_1'\right)\frac{1}{n} + \mathcal{O}\left(\frac{1}{n^{\frac{3}{2}}}\right)\right\} \\ &- iq_0\left[e_0\phi_2 + e_1\phi_1 + e_2\phi_1\right]\left\{-\frac{2\chi\chi'}{n} + \mathcal{O}\left(\frac{1}{n^{\frac{3}{2}}}\right)\right\} - iq_0\left[e_0\phi_0\right]\left\{\frac{2\chi}{n} + \mathcal{O}\left(\frac{1}{n^{\frac{3}{2}}}\right)\right\} = 0. \end{aligned} \tag{4.71}$$

The low-order terms of (4.47) satisfy

$$\phi_0 = q_0^2, \tag{4.72}$$

$$\phi_n = q_0^2\sum_{k=0}^{n} e_k e_{n-k} \qquad \text{for } n < m, \tag{4.73}$$

$$\phi_m = q_0^2\sum_{k=0}^{m} e_k e_{n-k} + 2ie_0 q_0^4\frac{dq_0}{dw}, \tag{4.74}$$

and, used in conjunction with (4.71), give for the first three orders as $n \to \infty$:

$$\frac{d\chi}{dw} = \frac{i}{q_0^3}, \tag{4.75}$$

$$\frac{dr_1}{dw} = \frac{3ie_1}{\sqrt{2\chi}q_0^3} - \frac{ir_1}{2\chi q_0^3}, \tag{4.76}$$

$$\frac{P_k'}{P_k} = \frac{-4q_0'}{q_0} + \frac{1}{q_0^3}\left(-6ie_1^2 + 3ie_2 + \frac{3ie_1r_1}{2\sqrt{2\chi}} - \frac{ir_1^2}{4\chi q_0^3}\right). \tag{4.77}$$

Solving (4.75) subject to $\chi(-a) = 0$ gives

$$\chi(w) = a\pi + i\left[(w+a) + a\log\left|\frac{w}{a}\right|\right],$$

where we have made sure to select the branch of the logarithm which corresponds to analytic continuation into the upper-half w-plane. Next, (4.76) is solved for $r_1(w)$ subject to the condition from (4.67),

$$r_1(-a) = \mu_1 = 3\sqrt{2X}\beta f_1,$$

which gives

$$\begin{aligned} r_1(w) &= \frac{3\beta f_1}{\sqrt{2}}\left(\frac{\sqrt{i}\log\left(\frac{w}{-a}\right)}{\sqrt{(w+a) + a\log\left(\frac{w}{-a}\right)}}\right) \\ &= \mu_1 + \left[\frac{\sqrt{-i}\beta f_1}{2a^{3/2}}\right](w+a) + \mathcal{O}(w+a)^2. \end{aligned}$$

Turning to (4.77) and integrating, we also have

$$P_k = \frac{\Delta_k q_0^4(w^\bigstar)}{q_0^4(w)} \exp\left[\int_{w^\bigstar}^{w} \frac{1}{q_0^3}\left(-6ie_1^2 + 3ie_2 + \frac{3ie_1r_1}{2\sqrt{2\chi}} - \frac{ir_1^2}{4\chi q_0^3}\right) dw\right]$$

for some constant Δ_k and arbitrary point of integration $w = w^\bigstar$ for which the integral is defined. As $w \to -a$, the series expansions of each term of the expression then gives

$$P_k = \frac{\Delta_k}{c^4} W^\kappa \underbrace{q_0^4(w^\bigstar) \exp\left[\frac{3i\beta^2}{4a^2}\left\{4f_1^2 - 4f_2\right\}\right]}_{C} \left\{1 + \mathcal{O}(w+a)\right\} \sim \frac{\Delta_k}{c^4} W^\kappa C$$

where

$$\kappa = \frac{4}{3} + \frac{3i\beta^2}{a}\left[2f_1^2 - f_2\right].$$

Matching the $n = 0$ term then requires

$$\kappa - 2\gamma = 2\alpha = -\frac{2}{3},$$

and solving for γ gives

$$\gamma = 1 + 3X\beta^2\left[f_2 - 2f_1^2\right], \tag{4.78}$$

precisely the same as the value found from the inner analysis. This completes our derivation of the late terms of the asymptotic expansion, and the final step is to match the inner and outer expansions for the determination of Δ_k.

By Van Dyke's matching rule, taking the n^{th} term of the outer expansion, written in inner coordinates and keeping the first term,

$$\phi \xrightarrow{(n.t.o)} \epsilon^{\frac{n}{m}}\phi_n \sim \frac{P_k\Gamma(\frac{n}{m}+\gamma)e^{r_1 n^{1/2}}}{\chi^{\frac{n}{m}+\gamma}} \xrightarrow{(1.t.i)} \frac{\Delta_k C W^{2\alpha} e^{\frac{4}{3a}}\Gamma(\frac{n}{m}+\gamma)e^{\mu_1 n^{1/2}}}{c^4 X^\gamma z^n}$$

provides a match with the first term of the inner approximation, written in outer variables and re-expanded to n terms,

$$\phi = c^2 W^{2\alpha}\widehat{\phi} \xrightarrow{(1.t.i)} c^2 W^{2\alpha}\sum_{n=0}^{\infty}\frac{A_n}{z^n} \xrightarrow{(n.t.o)} c^2 W^{2\alpha}\frac{A_n}{z^n}.$$

Matching thus requires

$$\Delta_k = \frac{c^6 X^\gamma e^{\frac{-4}{3a}}}{C}\left[\lim_{n\to\infty}\frac{A_n}{\Gamma(\frac{n}{2}+\gamma)e^{\mu_1 n^{1/2}}}\right] = \frac{c^6 X^\gamma e^{\frac{-4}{3a}}}{C}\left[\Omega_k e^{i\tau_k}\right]. \tag{4.79}$$

By the definitions of c and X in Section 4.3.2, and also by the value of γ in (4.78), we have

$$\begin{aligned} c &= a^{1/3}e^{\frac{\pi i}{3}} \\ X &= \frac{i}{c^3(1-3\alpha)} = \frac{-i}{2a} \\ \gamma &= \gamma_1 + i\gamma_2 = 1 - i\frac{3\beta^2(f_2 - f_1^2)}{2a} \end{aligned}$$

and, in particular,

$$|\Delta_k| = \frac{\Omega_k^{cc}|c|^6|X|^{\gamma_1}\exp[\text{Arg}(X)\gamma_2]}{|C|} = \frac{\Omega_k^{cc}a}{2}\exp\left[\frac{3\pi\beta^2}{4a}(f_2 - f_1)\right].$$

Stokes smoothing

The Stokes line smoothing procedure is slightly complicated by the appearance of the exponential terms in the late-orders ansatz. We optimally truncate the expansion

$$\phi = \sum_{n=0}^{\mathcal{N}-2}\epsilon^{\frac{n}{2}}\phi_n + R_{\mathcal{N}},$$

which gives

$$\mathcal{L}(R_{\mathcal{N}};\epsilon) \sim \epsilon^{\mathcal{N}/2}\phi_{\mathcal{N}}, \tag{4.80}$$

with $\mathcal{L}$ given by

$$\mathcal{L}(R_{\mathcal{N}};\epsilon) = R_{\mathcal{N}} - iq_0\left[e_0\phi_0\right]\epsilon R'_{\mathcal{N}} - iq_0\left[e_0\phi_1 + e_1\phi_0\right]\epsilon^{3/2}R'_{\mathcal{N}}$$
$$- iq_0\left[e_0\phi_2 + e_1\phi_1 + e_2\phi_1\right]\epsilon^2 R'_{\mathcal{N}} - iq_0\left[e_0\phi_0\right]\epsilon R_{\mathcal{N}} + \ldots = 0. \quad (4.81)$$

The solution of the homogeneous equation is found by substituting

$$R_{\mathcal{N}} = \overline{P_k}\exp\left[F(w)\right] = \overline{P_k}\exp\left[\frac{F_0(w)}{\epsilon} + \frac{F_1(w)}{\sqrt{\epsilon}}\right], \quad (4.82)$$

into (4.81) and dividing by $R_{\mathcal{N}}$, giving

$$1 - iq_0\left[e_0\phi_0\right]\left[F'_0 + \sqrt{\epsilon}F'_1 + \epsilon\frac{\overline{P_k}'}{\overline{P_k}}\right] - iq_0\left[e_0\phi_1 + e_1\phi_0\right]\left[\sqrt{\epsilon}F'_0 + \epsilon F'_1 + \mathcal{O}(\epsilon^{\frac{3}{2}})\right]$$
$$- iq_0\left[e_0\phi_2 + e_1\phi_1 + e_2\phi_1\right]\left[\epsilon F'_0 + \mathcal{O}(\epsilon^{\frac{3}{2}})\right] - iq_0\left[e_0\phi_0\right]\epsilon = 0. \quad (4.83)$$

Solving at each order yields

$$F'_0 = -\frac{i}{q_0^3} = -\frac{d\chi}{dw}, \quad (4.84)$$
$$F'_1 = \frac{3ie_1}{q_0^3}, \quad (4.85)$$
$$\frac{\overline{P_k}'}{\overline{P_k}} = \frac{2iq'_0}{q_0^4} - \frac{3q'_0}{q_0} - \frac{6ie_1^2}{q_0^3} + \frac{3ie_2}{q_0^3}. \quad (4.86)$$

These expressions for F_0, F_1 and $\overline{P_k}$ are related to the limiting values of $-\chi$, μ_1, and P_k from the late-order ansatz (4.70) when evaluated near the Stokes lines.

In order to solve the inhomogeneous equation, we multiply (4.82) by the Stokes Smoothing parameter, so that $R_{\mathcal{N}} = A\overline{P_k}e^F$, and substitute into (4.80), giving

$$\epsilon iq_0^3\frac{dA}{dw}\overline{P_k}e^F \sim \epsilon^{\frac{\mathcal{N}}{2}}\frac{P_k\Gamma\left(\frac{\mathcal{N}}{2}+\gamma\right)e^{r_1 n^{\frac{1}{2}}}}{\chi^{\frac{\mathcal{N}}{2}+\gamma}}.$$

For this expression, we write the derivative in terms of χ so that

$$\frac{d}{dw} = \frac{d\chi}{dw}\frac{d}{d\chi} = \frac{i}{q_0^3}, \frac{d}{d\chi}$$

giving

$$-\epsilon\frac{dA}{d\chi}\left[\overline{P_k}e^{\frac{F_1}{\sqrt{\epsilon}}}\right] \sim \left[P_k e^{r_1\mathcal{N}^{\frac{1}{2}}}\right]\frac{\epsilon^{\frac{\mathcal{N}}{2}}\Gamma\left(\frac{\mathcal{N}}{2}+\gamma\right)e^{\frac{\chi}{\epsilon}}}{\chi^{\frac{\mathcal{N}}{2}+\gamma}}. \quad (4.87)$$

The optimal truncation point is found where adjacent terms in the asymptotic approximation are of the same size:

$$\frac{\epsilon^{\frac{\mathcal{N}+1}{2}}}{\epsilon^{\mathcal{N}}}\left|\frac{\phi_{\mathcal{N}+1}}{\phi_{\mathcal{N}}}\right| \sim 1,$$

or where

$$\mathcal{N} = \frac{2r}{\epsilon} + \rho, \tag{4.88}$$

with $\rho \in (0,1)$ as $\epsilon \to 0$. We can write $\chi = re^{i\nu}$ and thus (4.87) gives

$$\frac{dA}{d\chi} = \left(\frac{-ie^{-i\nu}}{r}\right)\frac{dA}{d\nu}.$$

Using Stirling's formula on the Gamma function then gives

$$-\epsilon\left(\frac{-ie^{-i\nu}}{r}\right)\frac{dA}{d\nu}\left[\overline{P_k}e^{\frac{F_1}{\sqrt{\epsilon}}}\right] \sim \left[P_k e^{r_1\mathcal{N}^{\frac{1}{2}}}\right]\frac{\sqrt{2\pi}r^{-\frac{1}{2}}e^{-\frac{\mathcal{N}}{2}}e^{\frac{\chi}{\epsilon}}}{\epsilon^{\gamma-\frac{1}{2}}(e^{i\nu})^{\frac{\mathcal{N}}{2}+\gamma}},$$

or

$$\frac{dA}{d\nu}\left[\overline{P_k}e^{\frac{F_1}{\sqrt{\epsilon}}}\right] \sim -\left[P_k e^{r_1\mathcal{N}^{\frac{1}{2}}}\right]\frac{\sqrt{2\pi}r^{\frac{1}{2}}e^{-\frac{\mathcal{N}}{2}}e^{i\nu}e^{\frac{\chi}{\epsilon}}i}{\epsilon^{\gamma-\frac{1}{2}}(e^{i\nu})^{\frac{\mathcal{N}}{2}+\gamma}}.$$

We must relate the two bracketed quantities near the Stokes line. The critical scaling near the Stokes line is still given by $\nu \sim \mathcal{O}(\sqrt{\epsilon})$ and so we set $\nu = \epsilon\overline{\nu}$. Then we can write (4.76) as

$$\frac{dr_1}{d\overline{\nu}} = \frac{3i\sqrt{\epsilon}e_1 r^{\frac{1}{2}}}{\sqrt{2}}\left\{1+\mathcal{O}(\sqrt{\epsilon})\right\} - \frac{i\sqrt{\epsilon}r_1}{2}$$

where e_1 is evaluated near the Stokes line, where it is simply $\mathcal{O}(1)$. The dominant balance involves the derivative term and the first term on the right-hand-side, giving

$$\frac{dF_1}{dw} \sim \sqrt{2r}\frac{dr_1}{dw}.$$

Thus if we insist that the constant of integration in computing F_1' is found by matching with the value of $r_1(w)$ near the Stokes line, then using (4.88) we have

$$e^{r_1\mathcal{N}^{1/2}} \sim e^{\frac{r_1\sqrt{2r}}{\sqrt{\epsilon}}} \sim e^{\frac{F_1}{\sqrt{\epsilon}}}.$$

Using a similar argument, it is shown that near the Stokes line, $\overline{P_k} \sim P_k$ and so requiring that the constant of integration in determining $\overline{P_k}$ must be such that it matches with P_k near the Stokes line, we have

$$\overline{P_k} = \frac{\Delta_k q_0^3(w^\bigstar)}{q_0^3(w)}\exp\left[\int_{w^\bigstar}^{w} i\left(\frac{2q_0'}{q_0^4} - \frac{6e_1^2}{q_0^3} + \frac{3e_2}{q_0^3}\right)\,d\varphi\right], \tag{4.89}$$

so that finally,

$$\overline{P_k}e^{\frac{F_1}{\sqrt{\epsilon}}} \sim P_k e^{r_1\mathcal{N}^{\frac{1}{2}}},$$

and we are left with

$$\frac{dA}{d\overline{\nu}} \sim -\frac{\sqrt{2\pi r}e^{-\frac{\mathcal{N}}{2}}e^{i\nu}ie^{\frac{\chi}{\epsilon}}}{\epsilon^{\gamma+\frac{1}{2}}(e^{i\nu})^{\frac{\mathcal{N}}{2}+\gamma}}$$

precisely the same expression as discovered in Section 4.3.2 and for which the details can be found in the previous chapters. Thus, the same switching-on mechanism is found, and the jump in the remainder is

$$\left[R_{\mathcal{N}}\right]_{+}^{-} \sim \frac{2\pi i}{\epsilon^{\gamma}}\overline{P_k}e^{F},$$

from upstream $(+)$ to downstream $(-)$.

4.6.4 Formulae for the close-cornered approximation

Note that in the simplified formulation of eqn (4.42), we had already fixed the analytic continuation into the upper-half w-plane, so the final solution q evaluated on the positive real w-axis is left as a complex number. It is more convenient to write the exponential in terms of q rather than ϕ, so

$$q_{\text{exp},\,k}^{\text{c.c}} \sim \frac{\pi i}{\epsilon^{\gamma} q_0}\overline{P_k}e^{F},$$

and if we are only interested in the real part, then

$$\Re\left(q_{\text{exp},\,k}^{\text{c.c}}\right) \sim \frac{\pi}{\epsilon^{\gamma} q_0}\Im\left[\overline{P_k}e^{F}\right].$$

Since from (4.82) to (4.86),

$$F(w) = \int_{-a}^{w}\left(-\frac{\chi'}{\epsilon} + \frac{F_1'}{\sqrt{\epsilon}}\right)\,d\varphi,$$

for w evaluated on the positive real axis, if we choose the contour of integration, first from $u = -a$ to $u = -\infty$ along the negative real axis, then from $u = \infty$ to $u = w$ along the positive real axis, then the only real contribution of $F(w)$ is from the residue contribution at infinity. By examining the series expansions of χ' and F_1', this can be shown to be

$$\Re\Big[F(w)\Big] = -\frac{3\pi a(\sigma_1+\sigma_2)}{\epsilon} + \frac{3\beta\pi(-\sigma_1+\sigma_2)}{\sqrt{\epsilon}},$$

for $w \in \mathbb{R}^{+}$. For the imaginary parts, we also have

$$\Im\Big[F(w)\Big] = \frac{w}{\epsilon} + \mathcal{O}\left(\frac{\log w}{\sqrt{\epsilon}}\right),$$

as $w \to \infty$ and $w \in \mathbb{R}^{+}$. Now turning to $\overline{P_k}$ in (4.89), we have

$$\overline{P_k} \sim \left|\frac{\Delta_k}{q_0^3(w)}\right| e^{i\text{Arg}(P_k)},$$

where

$$\text{Arg}(P_k) = \text{Arg}(\Delta_k) + \left(\frac{2q_0'}{q_0^4} - \frac{6e_1^2}{q_0^3} + \frac{3e_2}{q_0^3}\right),$$

and the bracketed quantities are entirely real for $w \in \mathbb{R}^+$. Thus as $w \to \infty$, we can expect that

$$q^{\text{c.c}}_{\text{exp},\,k} \sim \frac{\pi|\Delta_k|}{\epsilon^\gamma q_0^4} \exp\left[-\frac{3\pi a(\sigma_1+\sigma_2)}{\epsilon} + \frac{3\beta\pi(-\sigma_1+\sigma_2)}{\sqrt{\epsilon}}\right] \times \exp\left[i\left(\frac{w}{\epsilon} + \mathcal{O}\left(\frac{\log w}{\sqrt{\epsilon}}\right) + \text{Arg}(P_k)\right)\right], \quad (4.90)$$

and in particular, the magnitude of the amplitudes at $w = \infty$ is

$$\left|q^{\text{c.c}}_{\text{exp},\,k}\right| = \frac{\pi\Omega^{\text{cc}}_k a}{2\epsilon^\gamma} \exp\left[\frac{3\pi\beta^2}{8a}(f_2 - f_1)\right] \times \exp\left[-\frac{3\pi a(\sigma_1+\sigma_2)}{\epsilon} + \frac{3\beta\pi(-\sigma_1+\sigma_2)}{\sqrt{\epsilon}}\right]. \quad (4.91)$$

4.6.5 *Analysing the $\sigma_1 = 1/6$ and $\sigma_2 = 1/6$ ship*

We will now apply the formulae developed over the course of the previous sections to the $[\frac{1}{6}, \frac{1}{6}]$ ship. In addition to comparing the asymptotic predictions to numerical computations, the most important step is to verify that as $\beta \to 0$, the close-corner approximation tends to the one-cornered approximation, and as $\beta \to \infty$, the close-cornered approximation tends to the two-cornered approximation.

The symmetry of the $[\frac{1}{6}, \frac{1}{6}]$ ship helps reduce the expressions. In particular, $f_1 = 0$ and $f_2 = 1/6$, and this has the effect of setting $\Omega^{\text{cc}}_2 = 0$. Using (4.91), we have

$$\left|q^{\text{c.c}}_{\text{exp},\,1}\right| = \frac{\pi\Omega^{\text{cc}}_1 a}{2\epsilon} \exp\left[\frac{3\pi\beta^2}{8a}\right] \times \exp\left[-\frac{\pi a}{\epsilon}\right] \quad (4.92)$$

The 1-hull approximation with $\sigma_1 = 1/3$ has

$$q_s = q_0 = \left(\frac{w}{w+a}\right)^{1/3}$$

and from (4.44), then, we have

$$|q_{\text{exp},1}| \sim \frac{\Omega_k(\sigma_1)}{2\epsilon} \exp\left[-\frac{\pi a}{\epsilon}\right]. \quad (4.93)$$

Setting $\beta = 0$, then matching eqns (4.92) and (4.93) gives the requirement that

$$\Omega^{\text{cc}}_1\left(\frac{1}{6}, \frac{1}{6}\right) \to \Omega\left(\frac{1}{3}\right),$$

as $\beta \to 0$ and where we have included the values of σ_1 and σ_2 in Ω^{cc}_1 simply to remind us of the argument of the pre-factor. This limiting behaviour is shown in Figure 4.9 for the $a = 0.5$ ship where we see that indeed, the close-cornered approximation tends to the one-cornered approximation as $\beta \to 0$.

We now turn to the two-cornered approximation, for which the waves are given by (4.44). Here, we remind ourselves that

$$q_s = q_0 = \frac{w^{1/3}}{(w+a_1)^{1/6}(w+a_2)^{1/6}},$$

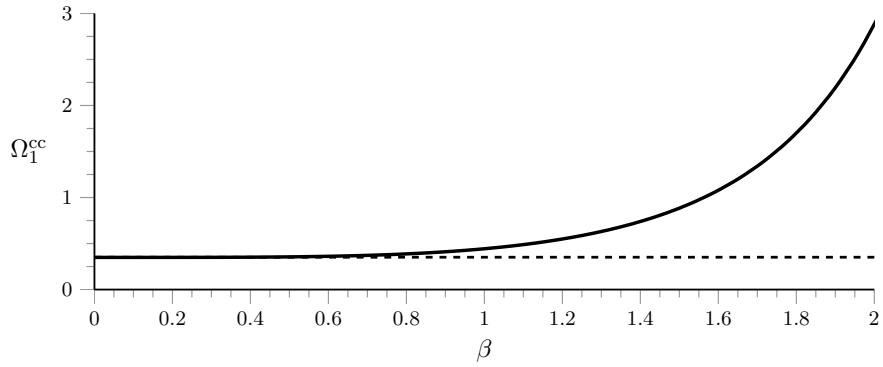

Figure 4.9: The solid curve is the prefactor $\Omega_1^{cc}(1/6, 1/6)$ for the close-cornered ship, with $a = 0.5$. As $\beta \to 0$ and the two corners coalesce, the prefactor approaches the same value as for the one-cornered ship, with $\Omega(1/3) \approx 0.351$ (shown dashed).

with $a_1 = a+\sqrt{\epsilon}\beta$ and $a_2 = a-\sqrt{\epsilon}\beta$. It is simple to check from the condition in (4.18) that there are no relevant Stokes lines emerging from the singularity at $w = -a_1$, and the waves are entirely generated by the singularity at $w = -a_2$. From (4.27), we have

$$\Re\Big[\chi_1\Big] = \pi a,$$

after using $a_1 + a_2 = 2a$; thus, the exponential of the second wave has an additional term, with

$$\Re\Big[\chi_2\Big] = \pi a + \Re\int_{-a_2}^{-a_1} \frac{i}{q_0^3}\, d\varphi.$$

Proceeding directly, we then have

$$\begin{aligned}\int_{-(a-\sqrt{\epsilon}\beta)}^{-(a+\sqrt{\epsilon}\beta)} \frac{i}{q_0^3}\, d\varphi = i\Bigg(&\frac{1}{2}(a_1+a_2)\log\Big[a_1+a_2+2w+2\sqrt{\varphi+a_1}\sqrt{\varphi+a_2}\Big]\\ &-\sqrt{a_1a_2}\log\Big[2a_1a_2+\varphi(a_1+a_2)+2\sqrt{a_1a_2}\sqrt{\varphi+a_1}\sqrt{\varphi+a_2}\Big]\\ &+\sqrt{\varphi+a_1}\sqrt{\varphi+a_2}+\sqrt{a_1a_2}\log\Big[(a_1a_2)^{3/2}\varphi\Big]\Bigg)\Bigg|_{-(a-\sqrt{\epsilon}\beta)}^{-(a+\sqrt{\epsilon}\beta)}\\ \sim -\frac{\pi\beta^2\epsilon}{2a} &+ \mathcal{O}(\epsilon^2).\end{aligned} \tag{4.94}$$

with all higher-orders entirely real. Thus, the wave from the second singularity has an additional exponential factor of $e^{\pi\beta^2/2a}$. The dominant contribution of the two-cornered approximation is then

$$\Big|q_{\text{exp, 2}}^{\text{c.c}}\Big| \sim \frac{2\pi|\Lambda_2|}{\epsilon^{\gamma_2}} \exp\left[\frac{\pi\beta^2}{2a}\right] \times \exp\Big[-\frac{\pi a}{\epsilon}\Big],$$

and using the values

$$\begin{aligned}\gamma_2 &= \frac{2}{3},\\ c_2 &= \frac{a^{\frac{1}{3}}}{(2\sqrt{\epsilon}\beta)^{\frac{1}{6}}}\exp\left[\frac{\pi i}{3}\right],\\ |\Lambda_2| &\sim \frac{\Omega_2 a^{\frac{4}{3}}}{\epsilon^{\frac{1}{3}}\beta^{\frac{2}{3}}2^{\frac{5}{3}}}\left(\frac{2}{3}\right)^{\frac{2}{3}},\end{aligned}$$

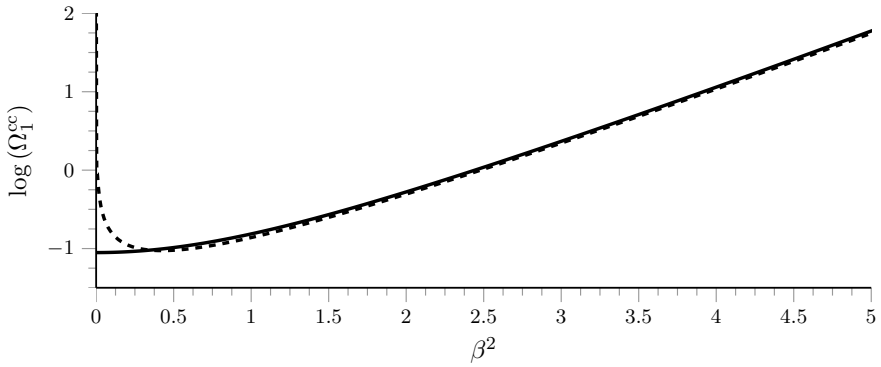

Figure 4.10: The solid curve is the pre-factor $\Omega_1^{cc}(1/6, 1/6)$ for the close-cornered ship, with $a = 0.5$. As $\beta \to \infty$ and the corners separate, the pre-factor approaches the dashed curve with $\Omega(1/6) \times 2a^{1/3}/(3\beta)^{\frac{2}{3}} \exp[\pi\beta^2/3a]$, corresponding to the 2-Hull with well separated corners.

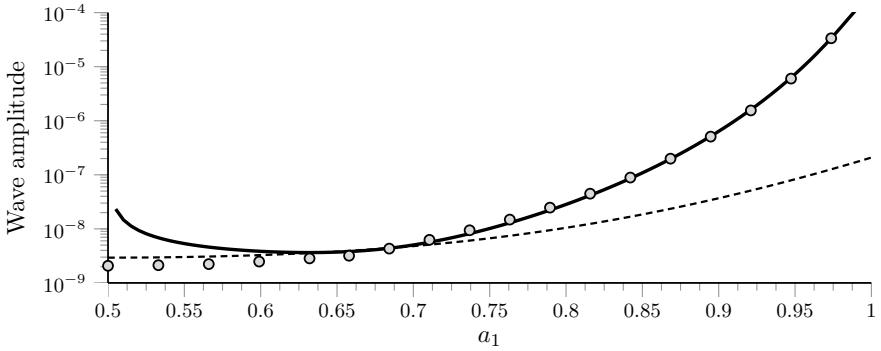

Figure 4.11: The numerical solution (nodes) for the $[1/6, 1/6]$-Hull versus the asymptotic approximations for $\epsilon = 0.075$ and $a_1 + a_2 = 1$. The two-cornered approximation (solid line) very accurately predicts the solution when the two corners are well separated, but is singular when $a_1, a_2 \approx 0.5$ near the left. Here, the solution is well approximated by the close-corners approximation (dashed). The computation was done using the code of Table 4.1.

the amplitude is

$$\left|q^{\text{c.c}}_{\text{exp, 2}}\right| \sim \frac{\pi\Omega_2 a^{\frac{4}{3}}}{\epsilon(3\beta)^{\frac{2}{3}}} \exp\left[\frac{\pi\beta^2}{2a}\right] \times \exp\left[-\frac{\pi a}{\epsilon}\right]. \tag{4.95}$$

Now returning to the close-cornered approximation in eqn (4.92), it can be shown that as $\beta \to \infty$, Ω_1^{cc} diverges exponentially. Thus in order to require a match between eqns (4.92) and (4.95), we need

$$\Omega_1^{cc}\left(\frac{1}{6}, \frac{1}{6}\right) \sim \Omega\left(\frac{1}{6}\right) \times \frac{2a^{1/3}}{(3\beta)^{\frac{2}{3}}} \exp\left[\frac{\pi\beta^2}{3a}\right]. \tag{4.96}$$

In Figure 4.10, we plot the natural logarithms of the left and right-hand sides of eqn (4.96) as a function of β^2 and indeed, the convergence between the two values is very fast.

The last and final result is shown in Figure 4.11; here, we compare the numerical and asymptotic approximations for the $[1/6, 1/6]$ ship. As expected, the two-cornered approximation of eqn (4.95) for the wave amplitude at infinity (which assumes well-separated corners) is a fine approximation, but only until the two corners coalesce at $a_1 = a_2 = 0.5$. At this point, the close-cornered approximation of eqn (4.92) provides a much better approximation.

4.7 DISCUSSION

Was it foolishly optimistic for us to have expected a simple and elegant answer to the question: *do waveless ships exist?*, applicable to the most general of multi-cornered ships?

In the end, we can offer several new insights into the study of ship-wave resistance: we can offer explicit formulae for the computation of waves given the shape of the ship's hull; we can offer simple interpretations of the production of such waves in terms of the crossing of Stokes lines and the Stokes Phenomenon; and perhaps most importantly, we can offer a methodology which, given specific ships, provides an intuitive and immediate understanding of its effect on the free-surface.

As applied mathematicians, then, we have gone as far as we are willing to go. What is the definitive, one-word answer to the conundrum of existence and non-existence? This question, dear reader, we leave to *you*.

FINAL REMARKS

5

The progress of nonlinear wave theory and exponential asymptotics will depend above all on sustaining that passion, and recruiting a new generation of the talented and opinionated [...] It can only offer fun to those who find the same sort of excitement in exponential asymptotics that others find in hot rods and rock climbing.

—JOHN BOYD, (1998)

Our work has tried to address two separate issues on the theory of free-surface flows: one completely new, on the subject of gravity-capillary waves, with no equivalent theory in the literature; the other, old, a question on the existence of waveless ship forms, posed again and again over the last forty years.

In general, the problem of gravity-capillary waves, while certainly not in its infancy, has proven to be formidable. Our contribution has been to suggest the theoretical existence of new classes of gravity-capillary waves, applicable for low-Froude, low-Bond flows over an obstruction. These new solutions include those already predicted by traditional linearised theory, but also suggests the existence of new classes of waves, waves which arise because of the inherent nonlinearity in the geometry of the problem. Do such waves truly exist? A discovery of such phenomena, in nature or in the digital world, would be a triumphant success for our theory, indeed.

Our second study, regarding the existence and non-existence of waveless ships, is one that has remained unanswered since the initial work of Vanden-Broeck & Tuck (1977). We have shown that a waveless, one-cornered ship cannot occur. For more complicated piecewise-linear hulls, our theory answers the question on a *per case* basis; a general theorem remains to be proven, but our hope is that the answers we have given are—at the very least—satisfactory to those naval engineers and applied mathematicians who, through the years, have taken an interest in the problem. Moreover, our theory goes *beyond* the question of existence and provides explicit formulae for the trailing waves of nonlinear ships.

Together, the marriage of these two issues is bound by the unifying theme of taking the low-Froude or low-Bond limit in order to study waves induced by nonlinear geometries. As we have seen, the machinery required for their study is *exponential asymptotics*, where ideas like asymptotic divergence, optimal truncation, Stokes lines, and the Stokes Phenomenon all play a key role in extracting the exponentially small waves which are so well hidden from regular asymptotic methodologies.

Understandably, these methods are not for the faint of heart, and the effort required to study these exponentially small effects can seem extraordinary at first glance. What does the future hold for the study of exponential asymptotics? Will it be possible to produce a complete gravity-capillary

theory for nonlinear, three-dimensional ships? Is such a goal even realistic, or is the complexity of such a problem forever beyond our grasp? These open questions, ripe for the eager and passionate researcher, is the subject of the next and final section of our thesis.

5.1 OPEN PROBLEMS

We have done our best to rank these problems in order of difficulty, beginning with the easiest, and concluding with the most difficult.

5.1.1 Do waveless ships exist? Part III: Bulbous ships

Naturally, our study of ship waves would be incomplete without a theory applicable for smooth hulls, with the eventual goal of addressing the well-known technique of using a bulb to reduce the wave resistance of a ship. In a sense, our work has *already* included such smooth geometries; take note that a piecewise-linear hull can always be replaced by one of the adjacent smooth streamlines of the flow. Then, the complex singularities remain in the same position, but now, the boundary of the ship is analytic. Thus, the waves for each piecewise-linear ship must correspond to the *same* waves as for an infinitude of smooth ships associated with the flow. However, in general, analytic continuation is an ill-posed process and small perturbations in the shape of a hull can have large effects on the associated singularities—a unified theory for arbitrary ship geometries will likely be difficult, if not downright impossible.

Perhaps, then, we should only consider specific classes of smooth ships. Ship waves associated with continuous geometries have been considered in the numerical work of Tuck & Vanden-Broeck (1984), Madurasinghe (1988), and Farrow & Tuck (1995), where there, the hulls are specified by piecewise-entire functions. For example, Farrow & Tuck (1995) consider the family of hulls given by

$$\theta = \begin{cases} 0 & \text{for } \phi \in (-\infty, -1) \\ A(\phi+1)(\phi+b) + \frac{\pi}{2}\frac{(\phi+1)}{(1-b)} & \text{for } \phi \in (-1, -b) \\ \frac{\pi}{2} & \text{for } \phi \in (-b, 0) \end{cases}$$

which, given parameters A and b, provides a ship consisting of a horizontal bottom and a vertical line, joined by a rounded section. $A > 0$ yields rounded corners and $A < 0$ yields bulbous sterns. The key is that if we restrict ourselves to classes of ships given by piecewise entire functions, then the complex singularities must be located at the points joining each piece. As a simpler example, we may consider the ship with

$$\theta = \begin{cases} 0 & \text{for } \phi \in (-\infty, -a_1) \\ \frac{\pi}{2}\left[1 + \frac{(\phi+a_2)}{(a_1-a_2)}\right] & \text{for } \phi \in (-a_1, -a_2) \\ \frac{\pi}{2} & \text{for } \phi \in (-a_2, 0), \end{cases} \tag{5.1}$$

which is similar to the vertically-faced one-cornered ships studied previously, but with a rounded edge. The leading-order rigid-body solution is then

$$q_0 = \sqrt{e}\left(\frac{w}{w+a_1}\right)^{\frac{1}{2}}\left(\frac{w+a_2}{w+a_1}\right)^{\frac{1}{2}\left(\frac{w+a_2}{a_1-a_2}\right)}, \tag{5.2}$$

where near the two singularities,

$$q_0 \sim A + (B + C\log W)W + \mathcal{O}(W^2), \tag{5.3}$$

with $W = w + a_1$, A, $C \neq 0$, and $B = 0$ for the a_1 singularity; and $W = w + a_2$, with A, B, and $C \neq 0$ for the a_2 singularity. The waves, then, originate from discontinuities in the *curvature* of the hull. Carrying out the exponential asymptotics on the simplified formulation of eqn (4.42), we discover to our surprise that the analysis is almost *easier* for this problem; here, the components of the late-orders ansatz can be computed *explicitly*:

$$q_n \sim \underbrace{\left[\frac{iA^9}{q_0^5(w)}\right]}_{Q}\Gamma(n-1)\times\underbrace{\left[\int_{w_0}^{w}\frac{i}{q_0^3}\,d\varphi\right]}_{\chi}^{-(n-1)} \tag{5.4}$$

with the form of the waves still given by $2\pi i\epsilon Q e^{-\chi/\epsilon}$. Then analysis of the Stokes lines shows that the relevant line emerges from $w = -a_2$; this is shown in Figure 5.1.

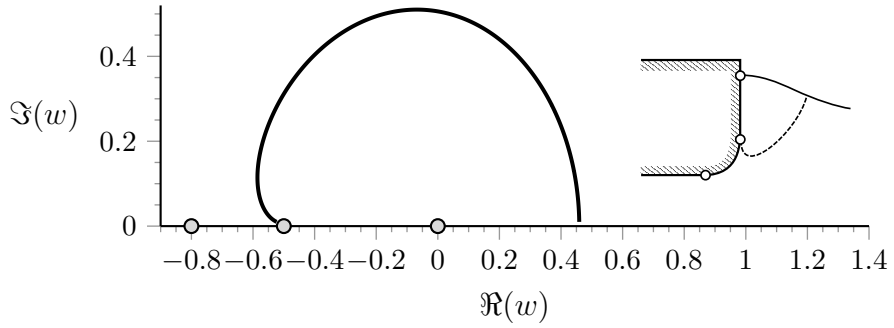

Figure 5.1: Stokes lines for the smoothed hull in eqn (5.1) with $a_1 = 0.8$ and $a_2 = 0.5$. The Stokes line leaves tangentially along the boundary, but later intersects the free-surface.

The analysis, however, is incomplete. A comparison between asymptotic and numerical solutions indicates that while the exponential scaling on the solution (5.4) is correct, the pre-factor is off by several orders of magnitude.

It seems the reason for this is due to the fact that adjusting the usual singularity from a power, to the weaker logarithmic singularity of eqn (5.3), induces a subtle change in the calculation—a change we have yet to account for. To resolve this apparent error, it may be necessary to first consider simpler (linear) problems with *beyond-all-order* terms, but which involve logarithmic singularities.

5.1.2 Parasitic capillary ripples

In (1958), Cox demonstrated the experimental existence of *parasitic capillary waves*—small ripples seen propagating near the crest of free gravity waves

(see Figure 5.2). Previous researchers initially believed that the ripples were predominantly caused by winds, but Cox's experiments showed that these small ripples are present even if the mean wind-speed is zero. In essence, their energy derives from the gravity waves themselves, rather than an external source.

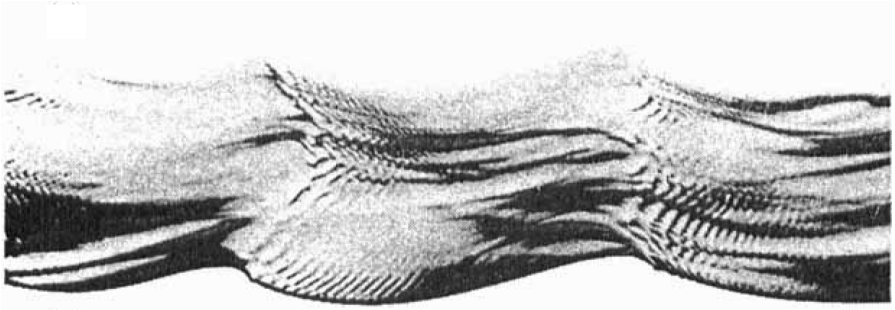

Figure 5.2: These waves were generated by a wind in a laboratory; the main action of the wind was to put energy into the gravity waves, steepening them to the point where the parasitic capillary ripples were generated (image from Longuet-Higgins 1995).

Analytical work on the parasitic capillary problem began with Longuet-Higgins (1963), although an update and improvement has been offered by the same author in Longuet-Higgins (1995). The essential idea underlying both studies is that near the crest of steep waves, the surface curvature is at maximum, and thus surface tension effects are localised in this region. Longuet-Higgins then assumes that the effect of the surface tension term can be approximated by a *known* pressure distribution, with for example, algebraically decaying tails away from the wave crest. A WKB approach then provides an analytical expression for the capillary ripples in terms of this approximate curvature.

We propose an improvement and more rigorous treatment of Longuet-Higgins' theory using the theory of exponential asymptotics. The idea is as follows: Grant (1973) has shown that for gravity waves less than the maximum height, there exist singularities in the analytic continuation of the free-surface. As the wave approaches its maximum height, where the crest forms a 120° angle, these singularities coalesce near the crest. These analytical observations have been confirmed by the numerical 'series improvement' analysis of Schwartz (1974) and Longuet-Higgins & Fox (1978) (Figure 5.3).

Figure 5.3: The leading-order gravity-wave solution with zero surface tension (hatched) contains singularities in the analytic continuation (figure from Longuet-Higgins & Fox (1978)). An asymptotic approximation in powers of the surface tension will consequently diverge, and exponentially small terms will be expected to be switched-on via the Stokes Phenomenon.

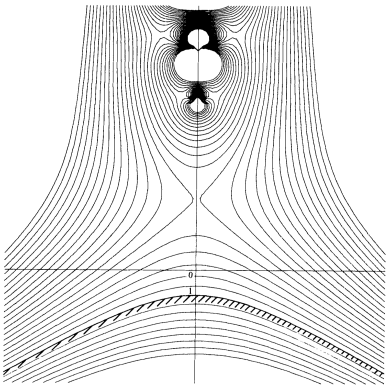

We may now expand the free surface elevation as

$$\eta(s) = \eta_0(s) + \epsilon\eta_1(s) + \dots,$$

where $\eta_0(s)$ is the base gravity wave, s is arc-length along the wave, and ϵ is a parameter indicating the amount of surface-tension. Due to the singularities in the analytic continuation, it is expected that as $\epsilon \to 0$, the series diverges and exponentially small terms (the parasitic capillary ripples) are turned on via the Stokes Phenomenon. The correct prediction of the waves will require knowledge of the solution near the singularities, as well as an optimal truncation of the divergent series.

With this standard methodology in mind, it seems possible that while the analysis of Longuet-Higgins is correct in spirit, the neglect of terms *up to optimal truncation* can have an $O(1)$ effect on the amplitude of the predicted capillary ripples. We predict that the difficulty in the full analysis will come from the fact that the exact Stokes' wave solution $\eta_0(s)$ can only be expressed using an infinite series with numerically-computed coefficients Schwartz (1974). However, there has been some recent progress in studying the properties of the complex singularities of the Stokes wave using numerical methods (Xie, 2009), and it may be possible to develop a *hybrid* analytical-numerical implementation of our methods in exponential asymptotics.

This is an important problem for several reasons. First, a proposed analysis of the ripples using standard tools in asymptotics beyond-all-orders will likely reveal more intricate details regarding the nature of gravity-capillary wave blockage (Shyu & Phillips, 1990) and other related phenomena. More importantly, the nature and properties of the Stokes wave singularity also has important implications for more general questions regarding the regularity and singularity-formations of the Navier-Stokes equations (Tanveer, 1991).

5.1.3 Accurate numerical computations of gravity-capillary waves

A great deal of literature already exists on the numerical computation of nonlinear two dimensional potential free-surface problems using a boundary-integral formulation (for a review, see Yeung 1982; Tsai & Yue 1996). Many of these approximations rely on the fact that the boundary integral can be truncated sufficiently far from the disturbance, where the error is exponentially small and the appropriate radiations conditions can be given by a relatively simple numerical condition. For example, we know from our work on the problems of Chapters 3 and 4 that numerical computations rely on a sufficiently large choice of L such that the integral can be truncated to

$$\log q(\xi) \approx -\frac{1}{\pi} \int_{-L}^{L} \frac{\theta(\xi')}{\xi' - \xi}\, d\xi'. \tag{5.5}$$

Afterwards, for gravity-only flows, the upstream radiation condition can simply be chosen to be $\theta = 0$, whereas truncation downstream generally has a negligible effect. However, there are many physical circumstances, such as the one depicted in Figure 5.4, where truncating the boundary integral and imposing upstream and downstream conditions is not as straightforward.

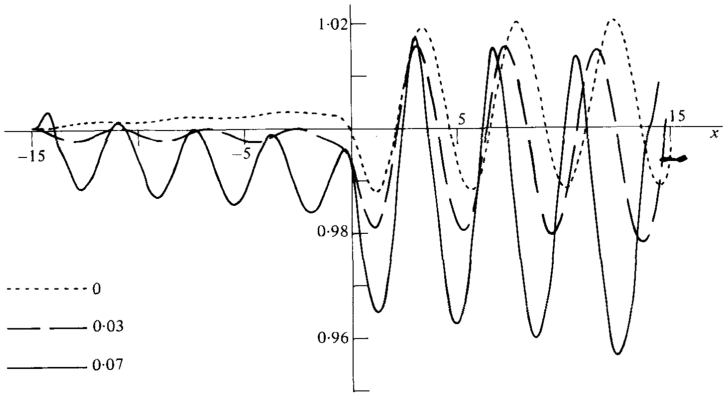

Figure 5.4: Forbes solved for the steady subcritical flow over a semi-circular cylinder including the effects of both gravity and surface tension (figure from Forbes (1983)). His treatment of the upstream (left) radiation condition was inadequate however, and the result were ill-resolved waves contradicting the predictions of linear theory. In general, no adequate solution has been offered for a numerical method which can properly resolve the upstream capillary waves.

Our interest is in the study of two cases in particular:

1. We know that as in low-Froude flows past a surface-piercing obstruction, the free-surface decays algebraically (and not exponentially) downstream, and thus it is no longer correct to truncate the boundary-integral and disregard the remainder. Of course, the waves are exponentially small, and it is unclear what are the effects of the downstream truncation on the numerical predictions.
2. In the computation of gravity-capillary waves past localised obstructions, as in Chapters 1 and 2, it is possible for capillary waves to appear upstream and gravity waves downstream. Then in contrast to the procedure for gravity-only flows, one cannot simply truncate the integral sufficiently far upstream, and some approximation must be made for the integral (5.5) from the neglected region from $-\infty$ to $-L$.

In the case of the first problem we ask whether there exist a better way to resolve free-surface solutions with waves on an infinite-domain using a boundary-integral formulation? For example, Boyd (1991b) has successfully used Chebyshev approximations supplemented by a radiation-basis function to solve the generalised solitary waves of the fifth-order KdV equation. However, the method is *ad-hoc*, does not make use of any theory assuring convergence, and has not been applied to the full water-wave equations.

In the case of the second problem, the only solution that seems have been offered is to approximate the free-surface upstream by a linear capillary wave, include this (known) upstream integral in the unknown truncated boundary-integral and require additional equations involving matching conditions on the first few mesh points Grandison & Vanden-Broeck (2006); this represents an improvement on the numerical work of Forbes (1983) (Figure 5.4). However, according to our preliminary numerics, the new methods by Grandison & Vanden-Broeck (2006) does not seem to be particularly robust.

A possible project, then, would be to develop numerical techniques for the resolution of both problems. One avenue we have considered is to supplement the numerical calculations with asymptotic predictions from the low-Froude, low-Bond regime given from Chapter 2. On a broader scale, however, this question of how to impose a numerical radiation condition for a general wave

problem has been a long-standing problem in the literature (Israeli & Orszag 1981, Yeung 1982, and Tsynkov 1998).

5.1.4 *Three-dimensional ship waves*

> *Does an asymptotic low-speed theory of [three-dimensional] thick ships really exist, and if so, what is its correct form?*
>
> —MARSHALL TULIN, (2005)

No one as yet managed to develop a non-trivial asymptotic theory for low-Froude flows past three-dimensional, full-bodied ships. As it concerns the literature, however, the seminal work for this problem likely belongs to Keller (1979), who sought to apply ray theory to its study (see Figure 5.5). Unfortunately, his analysis remains limited and in particular, he only derives practical formulae for the case of a *streamline* ship in the low-Froude limit (this is akin to our study of the small step problem in Chapter 1).

The singular nature of the low-Froude approximation and the resultant exponentially small waves have led to a great deal of confusion in the literature, and there are still many open questions regarding the validity and predictions of ray theory in this limit. It is unclear whether ray-theory is applicable near certain points of the hull-water intersection (Tulin, 1984; Eggers, 1990), unclear whether it is relevant to the understanding of bow divergent waves (Tulin, 1997), and even unclear what the correct linearization of the free-surface condition is under the approximation (Brandsma & Hermans, 1985).

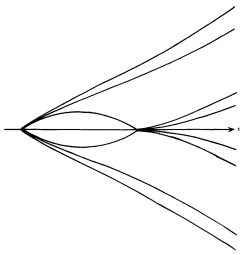

Figure 5.5: Keller's sketch of rays produced at the bow and stern of a ship moving with constant velocity (from Keller 1979). We believe a three-dimensional model should also incorporate rays that are produced by the immersed section of the ship's hull. These wave contributions should exponentially dominate those produced at the ship and free-surface interface.

Our work on the two-dimensional ship-wave problem has led to much greater understanding of the underlying causes of the free-surface waves in the low-Froude limit. For example, we now realize that in the case of stern flow, the dominant wave contribution derives not from the stagnation point between free-surface and ship, but rather from sharp changes in the hull's geometry. Thus, it would seem likely that a similar situation arises in a real full-bodied ship, and ray theory is still applicable in the examination of the resultant waves. In the case of bow flows, our work also demonstrates that the Stokes Phenomenon necessarily implies a breakdown of the low-Froude approximation near the ship—likely the indication that a correct model involves an overturning jet.

In the future, we suggest for a project to address the still-open question of low-speed theory in the context of three-dimensional ships. As a starting

point, this can be based on the ray-theory developed by Keller (1979), supplemented by more recent work on the Stokes Phenomenon applied to complex rays (Chapman et al., 1999; Chapman & Mortimer, 2005) and partial differential equations (Chapman & Mortimer, 2005), as well as the newfound understanding of the two-dimensional ship-wave problem presented in previous two chapters.

Earlier in this thesis, we pointed out the fact that the study of water waves and their interactions with floating bodies continues to drive a great portion of the research in the mathematical and engineering communities. Today, however, a great deal of this research is done from the perspective of computational and experimental fluid dynamics. Analytical developments in the study of water-body interactions seem to have stagnated, and it may be the case that some workers have simply given up, believing that such problems are beyond the outdated capabilities of pen and paper. Perhaps, then, the greatest contribution of this thesis, from the gravity-capillary theory of the first few chapters, to the waveless ships and open questions of the last, is to provide a small measure of hope—hope for mathematicians, hope for engineers, hope for researchers, both young and old; together, we may yet conquer the seas.

REFERENCES

Baba, E. (1976). Wave breaking resistance of ships. In *Proc. Int. Seminar on Wave Resistance, Tokyo*, (pp. 75–92).

Beale, J. T. (1991). Exact solitary water waves with capillary ripples at infinity. *Comm. Pure Appl. Math.*, *44*, 211–257.

Bender, C. M., & Orszag, S. A. (1978). *Advanced Mathematical Methods for Scientists and Engineers*. McGraw-Hill, Inc.

Benjamin, T. B. (1967). Instability of periodic wave trains in nonlinear dispersive systems. *Proc. Roy. Soc. Lond. A*, *299*, 59–75.

Benjamin, T. B., & Feir, J. E. (1967). The disintegration of wavetrains on deep water, part 1, theory. *J. Fluid Mech.*, *27*, 417–430.

Berk, H. L., Nevins, W. M., & Roberts, K. V. (1982). New stokes' line in wkb theory. *J. Math. Phys.*, *23*(6), 968–1002.

Berry, M. V. (1989). Uniform asymptotic smoothing of Stokes discontinuities. *Proc. Roy. Soc. London*, *A 422*, 7–21.

Boyd, J. P. (1991a). A comparison of numerical and analytical methods for the reduced wave equation with multiple spatial scales. *App. Num. Math.*, *7*, 453–479.

Boyd, J. P. (1991b). Weakly non-local solitons for capillary-gravity waves: the fifth-degree korteweg-de vries equation. *Phys. D*, *48*, 129–146.

Boyd, J. P. (1998). *Weakly nonlocal solitary waves and beyond-all-orders asymptotics*. Kluwer Academic Publishers.

Boyd, J. P. (1999). The Devil's invention: Asymptotics, superasymptotics and hyperasymptotics. *Acta Applicandae*, *56*, 1–98.

Brandsma, F. J., & Hermans, A. J. (1985). A quasi-linear free surface condition in slow ship theory. *Schiffstechnik Bd.*, *32*, 25–41.

Brockel, H. (1982). *The Yankee mariner and sea power: America's challenge of ocean space*, chap. Moving the World's Trade, (p. 186). University of Southern California Press.

Chapman, S. J. (1999). On the role of Stokes lines in the selection of Saffman-Taylor fingers with small surface tension. *Eur. J. Appl. Math.*, *10*(6), 513–534.

Chapman, S. J. (2002). Subcritical transition in channel flows. *J. Fluid Mech.*, *451*, 35–97.

Chapman, S. J., King, J. R., & Adams, K. L. (1998). Exponential asymptotics and Stokes lines in nonlinear ordinary differential equations. *Proc. R. Soc. Lond. A*, *454*, 2733–2755.

Chapman, S. J., Lawry, J. M. H., Ockendon, J. R., & Tew, R. H. (1999). On the theory of complex rays. *SIAM Rev.*, *41*(3), 417–509.

Chapman, S. J., & Mortimer, D. B. (2005). Exponential asymptotics and Stokes lines in a partial differential equation. *Proc. R. Soc. A*, *461*(2060), 2385–2421.

Chapman, S. J., & Vanden-Broeck, J.-M. (2002). Exponential asymptotics and capillary waves. *SIAM J. Appl. Math.*, *62 (6)*, 1872–1898.

Chapman, S. J., & Vanden-Broeck, J.-M. (2006). Exponential asymptotics and gravity waves. *J. Fluid Mech.*, *567*, 299–326.

Combescot, R., Hakim, V., Dombre, T., Pomeau, Y., & Pumir, A. (1986). Shape selection of Saffman-Taylor fingers. *Phys. Rev. A*, *56*(19), 2036–2039.

Combescot, R., Hakim, V., Dombre, T., Pomeau, Y., & Pumir, A. (1988). Analytic theory of the Saffman-Taylor fingers. *Phys. Rev. A*, *37*(4), 1270–1283.

Cox, C. S. (1958). Measurements of slopes of high-frequency wind waves. *J. Mar. Res.*, *16*, 199–225.

Crapper, G. D. (1957). An exact solution for progressive capillary waves of arbitrary amplitude. *J. Fluid Mech.*, *2*(6), 532–540.

Dagan, G., & Tulin, M. P. (1972). Two-dimensional free-surface gravity flow past blunt bodies. *J. Fluid Mech.*, *51 (3)*, 529–543.

Dawson, C. W. (1977). A practical computer method for solving ship-wave problems. In *2nd Int. Conf. Numerical Ship Hydrodynamics, Berkeley, USA*.

Debnath, L. (1994). *Nonlinear Water Waves*. Academic Press.

Dias, F., Menasce, D., & Vanden-Broeck, J.-M. (1996). Numerical study of capillary-gravity solitary waves. *Eur. J. Mech. B/Fluids*, *15 (1)*, 17–36.

Dias, F., & Vanden-Broeck, J.-M. (1993). Nonlinear bow flows with spray. *J. Fluid Mech.*, *255*, 91–102.

Dingle, R. B. (1973). *Asymptotic Expansions: Their Derivation and Interpretation*. Academic Press, London.

Eggers, K. (1981). Non-Kelvin dispersive waves around non-slender ships. *Schiffstechnik*, *28*, 223–251.

Eggers, K. (1990). On the breakdown of ship wave ray tracing near the bow. In *Proc. 5th International Workship on Water Waves and Floating Bodies (IWWWFB05)*, (pp. 66–70). Manchester, UK.

Europa (2009). The European Union's maritime transport policy for 2018. Press Release.

Farrow, D. E., & Tuck, E. O. (1995). Further studies of stern wavemaking. *J. Austral. Math. Soc. Ser. B*, *36*, 424–437.

Forbes, L. K. (1983). Free-surface flow over a semi-circular obstruction, including the influence of gravity and surface tension. *J. Fluid Mech.*, *127*, 283–297.

Gakhov, F. D. (1966). *Boundary Value Problems*. Pergamon Press Ltd.

Grandison, S., & Vanden-Broeck, J.-M. (2006). Truncation approximations for gravity-capillary free-surface flows. *J. Eng. Math.*, *54*, 89–97.

Grant, M. A. (1973). The singularity at the crest of a finite amplitude progressive stokes wave. *J. Fluid Mech.*, *59*, 257–262.

Grimshaw, R. (2010). *Asymptotic Methods in Fluid Mechanics: Survey and Recent Advances*, chap. Exponential Asymptotics and Generalized Solitary Waves, (pp. 71–120). SpringerWienNewYork.

Grimshaw, R., & Joshi, N. (1995). Weakly nonlocal solitary waves in a singularly perturbed Korteweg-de Vries equation. *SIAM J. Appl. Math.*, *55*, 124–135.

Hardy, G. H. (1949). *Divergent Series*. Clarendon Press, Oxford.

Harrison, W. J. (1909). The influence of viscosity and capillarity on waves of finite amplitude. *Proc. Lond. Math. Soc.*, *2*(7), 107.

Howls, C. J., Langman, P. J., & Daalhuis, A. B. O. (2004). On the higher-order Stokes Phenomenon. *Proc. R. Soc. Lond. A*, *460*, 2285–2303.

Hunter, J. K., & Scheurle, J. (1988). Existence of perturbed solitary wave solutions to a model equation for water waves. *Physica D*, *32*, 253–268.

Hunter, J. K., & Vanden-Broeck, J.-M. (1983). Solitary and periodic gravity-capillary waves of finite amplitude. *J. Fluid Mech.*, *134*, 205–219.

Israeli, M., & Orszag, S. A. (1981). Approximation of radiation boundary conditions. *J. Comp. Phys.*, *41*(115-135).

Kamesvara Rav, J. C. (1920). On ripples of finite amplitude. *Proc. Indian Ass. Cultiv. Sci*, *6*, 175.

Keller, J. B. (1979). The ray theory of ship waves and the class of streamlined ships. *J. Fluid Mech.*, *91*, 465–487.

King, A. C., & Bloor, M. I. G. (1987). Free-surface flow over a step. *J. Fluid. Mech.*, *182*, 193–208.

King, A. C., & Bloor, M. I. G. (1990). Free-surface flow of a stream obstructed by an arbitrary bed topography. *Q. J. Mech. appl. Math.*, *43*, 87–106.

Kinnersley, W. (1976). Exact large amplitude capillary waves on sheets of fluid. *J. Fluid Mech.*, *77*, 229–241.

Kline, M. (1972). *Mathematical Thought from Ancient to Modern Times*. Oxford University Press.

Kostyukov, A. A. (1968). *Theory of Ship Waves and Wave Resistance*. Iowa City: Effective Communication Inc.

Kotik, J., & Newman, D. J. (1964). A sequence of submerged dipole distributions whose wave resistance tends to zero. *J. Math. Mech.*, *13*, 693–700.

Krasovskii, Y. P. (1960). The theory of steady-state waves of finite amplitude. *Dokl. Akad. Nauk SSSR*, *130*, 1237–1240.

Kruskal, M. D., & Segur, H. (1991). Asymptotics beyond all orders in a model of crystal growth. *Stud. Appl. Math.*, *85*, 129–181.

Lamb, H. (1932). *Hydrodynamics*. Dover Publications.

Levi-Civita, T. (1925). Determination rigoureuse des ondes permanentes d'ampleur finie. *Math. Ann.*, *93*, 264–314.

Lighthill, M. J. (1965). Contributions to the theory of waves in nonlinear dispersive systems. *J. Inst. Maths. Applics.*, *1*, 1–28.

Longuet-Higgins, M. S. (1963). The generation of capillary waves by steep gravity waves. *J. Fluid Mech.*, *16*, 138–159.

Longuet-Higgins, M. S. (1995). Parasitic capillary waves: a direct calculation. *J. Fluid Mech.*, *301*, 79–107.

Longuet-Higgins, M. S., & Fox, M. J. H. (1978). Theory of the almost-highest wave: Part 2. matching and analytic extension. *J. Fluid Mech.*, *85*, 769–786.

Madurasinghe, M. A. D. (1988). Splashless ship bows with stagnant attachment. *J. Ship. Res.*, *32*(3), 194–202.

Madurasinghe, M. A. D., & Tuck, E. O. (1986). Ship bows with continuous and splashless flow attachment. *J. Austral. Math. Soc. Ser. B*, *27*(442-452).

Maleewong, M., Asavanant, J., & Grimshaw, R. (2005a). Free surface flow under gravity and surface tension due to an applied pressure distribution: I Bond number greater than one-third. *Theor. Comput. Fluid Dyn.*, *19*(4), 237–252.

Maleewong, M., Asavanant, J., & Grimshaw, R. (2005b). Free surface flow under gravity and surface tension due to an applied pressure distribution: II Bond number less than one-third. *Eur. J. Mech. B/Fluids*, *24*, 502–521.

Milne-Thomson, L. M. (1968). *Theoretical Hydrodynamics*. Courier Dover Publications.

Nakos, D. E. (1990). *Ship wave patterns and motions by a three-dimensional Rankine panel methods*. Ph.D. thesis, MIT, Cambridge, Mass., USA.

Nekrasov, A. I. (1921). On steady waves. *Izv. Ivanovo-Voznesensk Politekhn. Inst.*, *3*, 52.

Newman, J. N. (1976). Linearized wave resistance theory, Tokyo/Osaka, Society of Navel Architects Japan. In *International Seminar on Wave Resistance*.

Noble, B., & Beighton, S. (1980). Error estimates for three methods of evaluating Cauchy principal value integrals. *J. Inst. Maths Applics*, *26*, 431–446.

Ogilvie, T. F. (1968). Wave resistance: The low speed limit. Tech. rep., Michigan University, Ann Arbor.

Olde Daalhuis, A. B., Chapman, S. J., King, J. R., Ockendon, J. R., & Tew, R. H. (1995). Stokes Phenomenon and matched asymptotic expansions. *SIAM J. Appl. Math.*, *55(6)*, 1469–1483.

Pomeau, Y., Ramani, A., & Grammaticos, B. (1988). Structural stability of the Korteweg-de Vries solitons under a singular perturbation. *Physica D*, *31*, 127–134.

Sir Raleigh, W. (1829). *The Works of Sir Walter Raleigh*. Oxford: The University Press.

Raven, H. C. (1996). *A solution method for the nonlinear ship wave resistance problem*. Ph.D. thesis, Delft University of Technology.

Lord Rayleigh (1883). The form of standing waves on the surface of running water. *Proc. Lond. Math. Soc.*, *15*, 69–78.

Russell, J. S. (1844). Report on waves. In J. Murray (Ed.) *14th meeting of the British Association for the Advancement of Science*, (pp. 311–390). London: BAAS.

Schooley, A. H. (1960). Double, triple, and higher-order dimples in the profiles of wind-generated water waves in the capillary-gravity transition region. *J. Geophys. Res.*, *65*, 4075–4079.

Schwartz, L. W. (1974). Computer extension and analytic continuation of stokes' expansion for gravity waves. *J. Fluid Mech.*, *62*, 553–578.

Schwartz, L. W., & Vanden-Broeck, J.-M. (1979). Numerical solution of the exact equations for capillary-gravity waves. *J. Fluid. Mech.*, *95*, 119–139.

Shyu, J.-H., & Phillips, O. M. (1990). The blockage of gravity and capillary waves by longer waves and currents. *J. Fluid Mech.*, *217*, 115–141.

Stieltjes, T. J. (1886). Recherches sur quelques series semiconvergentes. *Ann. Sci. école norm. sup.*, *3*, 201–258.

Stoker, J. (1957). *Water waves*. Interscience Publishers, Inc.

Stokes, G. G. (1847a). On the numerical calculation of a class of definite integrals and infinite series. *Trans. Camb. Phil. Soc.*, *9*, 379–407.

Stokes, G. G. (1847b). On the theory of oscillatory waves. *Trans. Camb. Philos. Soc.*, *8*, 441–455.

Stokes, G. G. (1864). On the discontinuity of arbitrary constants which appear in divergent developments. *Trans. Camb. Phil. Soc.*, *10*, 106–128.

Stokes, G. G. (1880). Appendices and supplement to a paper on the theory of oscillatory waves. In *Mathematical and Physical Papers, vol. 1*. Cambridge University Press.

Stokes, G. G. (1902). On the discontinuity of arbitrary constants that appear as multiples of semi-convergent series. *Acta. Math. Stockholm*, *26*, 393–397.

Sun, S. M. (1991). Existence of a generalized solitary wave solution for water with positive bond number less than 1/3. *J. Math. Anal. Appl.*, *156*, 471–504.

Tanveer, S. (1991). Singularities in water waves and rayleigh-taylor instablity. *Proc. R. Soc. Lond. A*, *435*, 137–158.

Thomson, S. W. B. K. (1871). Hydrokinetic solutions and observations. *Phil. Mag.*, *42*(4), 374.

Toland, J. F. (1996). Stokes waves. *Topol. Method. Nonl. An.*, *7*, 1–48.

Trinh, P. H. (2010). *Asymptotic Methods in Fluid Mechanics: Survey and Recent Advances*, chap. Exponential Asymptotics and Stokes Line Smoothing for Generalized Solitary Waves, (pp. 121–126). SpringerWienNewYork.

Trinh, P. H., Chapman, S. J., & Vanden-Broeck, J.-M. (2010). The existence and non-existence of waveless ships. In *Proceedings 25th International Workshop on Water Waves and Floating Bodies*. Harbin, China: Harbin Engineering University.

Tsai, W.-T., & Yue, D. K. P. (1996). Computation of nonlinear free-surface flows. *Annu. Rev. Fluid Mech.*, *28*, 249–278.

Tsynkov, S. V. (1998). Numerical solutions of problems on unbounded domains: A review. *App. Num. Math.*, *27*(4), 465–532.

Tuck, E., & Roberts, A. (1997). Bow-like free surfaces under gravity. *Phil. Trans. R. Soc. Lond. A*, *355*, 655–677.

Tuck, E. O. (1991a). Ship-hydrodynamic free-surface problems without waves. *J. Ship Res.*, *35*(4), 277–287.

Tuck, E. O. (1991b). Waveless solutions of wave equations. In *Proceedings 6th International Workshop on Water Waves and Floating Bodies*. Wood's Hole, Mass.: M.I.T.

Tuck, E. O. (1994). The planing splash. In M. Ohkusu (Ed.) *Proc. 9th Int. Workshop on Water Waves and Floating Bodies*. Kyushu University, Japan.

Tuck, E. O., & Vanden-Broeck, J.-M. (1984). Splashless bow flows in two-dimensions. In *Proc. 15th Symp. Naval Hydrodynamics*. Hamburg, Germany: National Academy Press.

Tulin, M. P. (1984). Surface waves from the ray point of view. In *Proc. 15th Symp. Naval Hydrodynamics*, (pp. 9–19). Hamburg, Germany: National Academy Press.

Tulin, M. P. (1997). Divergent bow waves. In *Proc. 21st Symp. on Naval Hydrodynamics*, (pp. 661–679). Trondheim, Norway: National Academy Press.

Tulin, M. P. (2005). Reminiscences and reflections: Ship waves, 1950-2000. *J. Ship Res.*, *49*(4), 238–246.

Van Dyke, M. (1975). *Perturbation Methods in Fluid Mechanics: By Milton Van Dyke. Annotated Ed*. Parabolic Press.

Vanden-Broeck, J.-M. (1980). Nonlinear stern waves. *J. Fluid Mech.*, *96*(3), 603–611.

Vanden-Broeck, J.-M. (2002). Wilton ripples generated by a moving pressure distribution. *J. Fluid Mech.*, *451*, 193–201.

Vanden-Broeck, J.-M., & Dias, F. (1992). Gravity-capillary solitary waves in water of infinite depth and related free-surface flows. *J. Fluid Mech.*, *240*, 549–557.

Vanden-Broeck, J.-M., & Tuck, E. O. (1977). Computation of near-bow or stern flows using series expansion in the Froude numbers. In *2nd International Conference on Numerical Ship Hydrodynamics*. Berkeley, California: University of California, Berkeley.

Vanden-Broeck, J.-M., & Tuck, E. O. (1994). Flow near the intersection of a free surface with a vertical wall. *SIAM J. Appl. Math.*, *54*(1), 1–13.

Wehausen, J. V., & Laitone, E. V. (1960). Surface waves. In *Encyclopedia of Physics*, vol. IX. Springer-Verlag.

Whitham, G. B. (1967). Nonlinear dispersion of water waves. *J. Fluid Mech.*, *27*, 399–412.

Wilton, J. R. (1915). On ripples. *Phil. Mag.*, *29*, 688–700.

Xie, C. (2009). *Singularities in the Unphysical Complex Plane for Deep Water Waves*. Ph.D. thesis, Ohio State University.

Xie, X., & Tanveer, S. (2002). Analyticity and nonexistence of classical steady Hele-Shaw fingers. *Commun. Pur. Appl. Math.*, *56*(3), 353–402.

Yeung, R. W. (1982). Numerical methods in free-surface flows. *Ann. Rev. Fluid Mech.*, *14*, 395–442.

Yeung, R. W. (1991). *Mathematical Approaches in Hydrodynamics*, chap. Nonlinear Bow and Stern Waves – Inviscid and Viscous Solutions, (pp. 349–369). SIAM.